REPUBLIQUE DU CAMEROUN
Paix-Travail-Patrie
****
UNIVERSITE DE YAOUNDÉ I
****
CENTRE DE RECHERCHE ET DE FORMATION
DOCTORALE EN SCIENCES, TECHNOLOGIES
ET GEOSCIENCES
****
UNITE DE RECHERCHE ET DE FORMATION
DOCTORALE EN PHYSIQUES ET APPLICATIONS
****
B.P 812 Yaoundé
Email: crfd_stg@uy1.uninet.cm

REPUBLIC OF CAMEROON
Peace-Work-Fatherland
****
THE UNIVERSITY OF YAOUNDÉ I
****
POSTGRADUATE SCHOOL OF SCIENCES, TECHNOLOGY AND GEOSCIENCES
****
RESEARCH AND POSTGRADUATE TRAINING UNIT FOR PHYSICS AND APPLICATIONS
****
P.O. Box 812 Yaoundé
Email: crfd_stg@uy1.uninet.cm

DYNAMICS OF ROTATIONAL ELECTROMECHANICAL SYSTEMS SUBJECTED TO THE ACTION OF MAGNETS: THEORY AND EXPERIMENT

Thesis Submitted and defended for the award of Doctorat/ PhD in Physics

Speciality: Mechanics, Materials and Structures

By

KOUAM TAGNE Roland Fidèle

Master in Physics

Registration Number: 12W1308

Under the supervision of

WOAFO Paul

Professor
University of Yaoundé 1

Year 2025

UNIVERSITÉ DE YAOUNDE I
THE UNIVERSITY OF YAOUNDE I

FACULTÉ DES SCIENCES
FACULTY OF SCIENCES

DÉPARTEMENT DE PHYSIQUE
DEPARTMENT OF PHYSICS

ATTESTATION DE CORRECTION DE LA THÈSE DE DOCTORAT/Ph.D

Nous, Professeur **NANA NBENDJO Blaise Roméo** et Professeur **ESSIMBI ZOBO Bernard**, respectivement Examinateur et Président du jury de la Thèse de Doctorat/Ph.D de Monsieur **KOUAM TAGNE Roland Fidèle**, Matricule **12W1308**, préparée sous la direction du Professeur **WOAFO Paul** (Université de Yaoundé 1) intitulée : «**Dynamics of rotational electromechanical systems subjected to the action of magnets: theory and experiment**», soutenue le lundi, **20 Janvier 2025**, en vue de l'obtention du grade de Docteur/PhD en Physique, Spécialité **Mécanique, Matériaux et Structures,** option **Mécanique Fondamentale et Systèmes Complexes** attestons que toutes les corrections demandées par le jury de soutenance ont été effectuées.

En foi de quoi, la présente attestation lui est délivrée pour servir et valoir ce que de droit.

Fait à Yaoundé, le 28 MARS 2025

Examinateur	Le Président du jury	Le Chef de Département de Physique
Pr. NANA NBENDJO B. R.	Pr. ESSIMBI ZOBO B.	Pr. NDJAKA Jean-Marie B.

UNIVERSITE DE YAOUNDE I ★ FACULTE DES SCIENCES ★ DEPARTEMENT DE PHYSIQUE
Le Chef de Département

DEPARTMENT OF PHYSICS

Dynamics of rotational electromechanical systems subjected to the action of magnets: theory and experiment

Thesis

Submitted and defended for the award of

Doctorat/ PhD in Physics

Specialty: Mechanics, materials and structures

Option: Fundamental mechanics and complex systems

by

KOUAM TAGNE Roland Fidèle

Registration Number:**12W1308**

MASTER DEGREE in Physics

supervised by

WOAFO Paul

Professor

Year 2025

International Journal of Bifurcation and Chaos, Vol. 33, No. 5 (2023) 2350052 (14 pages)

DOI: 10.1142/S0218127423500529

Dynamics of the Rotating Arm of an Electromechanical System Subjected to the Action of Circularly Placed Magnets: Numerical Study and Experiment

R. Kouam Tagne and P. Woafo*
Laboratory of Modelling and Simulation in Engineering, Biomimetics and Prototypes, Faculty of Science, University of Yaoundé I, P. O. Box 812, Yaoundé, Cameroon
**Laboratory of Products Development and Entrepreneurship, Institut Supérieur de l'Innovation et de Technologie, P. O. Box 8210, Yaoundé, Cameroon*
**pwoafo1@yahoo.fr*

J. Awrejcewicz
Department of Automation, Biomechanics, and Mechatronics, Lodz University of Technology, 1/15 Stefanowski St. (Building A22), Lodz, 90-924, Poland

Received September 6, 2022; Revised March 7, 2023

This paper considers the experimental and numerical study of an electromechanical arm powered by a DC motor and subjected to the action of permanent magnets. The magnetic torques arise from permanent magnets mounted at the free end of the arm and along a circle. The electrical subsystem is powered by two forms of input signal (DC and AC voltage sources). For each case, we determine the condition for complete rotation of the mechanical arm versus the parameters of the system such as the arm length, the number of magnets, and the frequency of the external signal. The nonlinear dynamics of the system is examined by means of time-histories, bifurcation diagrams, Lyapunov exponents and phase portraits. Chaotic and periodic dynamics are detected numerically and confirmed experimentally.

Keywords: Electromechanical system; magnetic torque; array of magnets; nonlinear dynamics; chaos.

1. Introduction

Resulting from nonlinearities due to the material properties, to the geometry, to magnetic components or to boundary conditions, chaotic dynamics is omnipresent in nature. It is found in various systems such as chemical reactions, lasers, neural networks, internet communication networks, fluid flow, population growth in species, engineering systems, social and economic systems, etc. In many cases, chaos can be seen as dangerous or destructive and is thus avoided [Akinlar *et al.*, 2020; Mahmoud *et al.*, 2020; Kakmeni *et al.*, 2004; Nana Nbendjo & Woafo, 2007; Rajagopal *et al.*, 2017; Yamapi *et al.*, 2007; Shaohua *et al.*, 2022]. But, chaos also presents positive implications in diverse systems such as mechanical engineering systems

*Author for correspondence

and telecommunication [Awrejcewicz *et al.*, 2008; Kouam Tagne *et al.*, 2021; Tsapla Fotsa & Woafo, 2016; Kumar *et al.*, 2017; Chatterjee *et al.*, 2018; Nana *et al.*, 2017; Ge *et al.*, 2004; Wojna *et al.*, 2018; Zhu & Ishitobi, 1999; Moon *et al.*, 1993; Kemajou *et al.*, 2022; Kitio & Woafo, 2010; Xizhe *et al.*, 2017; Nana *et al.*, 2018].

Electromechanical systems are widely used in different branches of engineering [Kemajou *et al.*, 2022; Kitio & Woafo, 2010; Xizhe *et al.*, 2017; Ana *et al.*, 2010; Tcheutchoua & Woafo, 2013; Polczynski *et al.*, 2019; Belato *et al.*, 2001; Kazmierczak *et al.*, 2013, 2015]. They transform electrical energy into mechanical actions and vice versa via magnetic, piezoelectric and capacitive couplings. In the quest for increasing the efficiency of some industrial and home devices such as vibrating sieves, industrial mixers and industrial shakers, nonlinear phenomena have been analyzed in those systems with the nonlinear components natural to the systems or introduced in the systems. These nonlinear components can be present in the mechanical part (material, geometric or inertial nonlinearities), in the electrical circuit (nonlinear inductor, nonlinear capacitor, nonlinear resistance) and in the coupling between the mechanical and electrical parts [Kitio & Woafo, 2010]. Most of the time, nonlinearities are built using electronic components for low power systems. The low power is in practice used to command the motion of very light mechanical arms or micro arms in micro robots and for other micro actuations. At the macroscopic level where the power necessary to set parts into chaotic motion is high, one needs to use some other solutions, specifically found with electrical components. This is for instance the case of electrical circuit having hysteretic iron-core. Inserted in an electric circuit, it is able to generate high amplitude chaotic signals. This has been used recently to power a model of electromechanical sieve [Kemajou *et al.*, 2022]. Another way is to use magnets to generate the nonlinearity and then work with linear electrical systems. This is for instance the example considered in [Kouam Tagne *et al.*, 2021] where the authors introduced permanent magnets in the mechanical part to provide complex phenomenon. In the same line, Polczynski *et al.* [2019] investigated two pendulums with magnets embedded in a variable magnetic field. The magnetic interaction originates from permanent magnets, mounted at free ends of the pendulums, and current-powered air coils placed underneath. The authors proved that the two-pendulum system is able to display regions of chaotic and regular motions. The authors in [Polczynski *et al.*, 2021] studied both experimentally and analytically the model described by [Polczynski *et al.*, 2019] with a new rational approximation of the magnetic torque which helps to use mathematical methods to get a deep understanding of the influence of the magnetic field. In particular, the resonant phenomena, and periodic and chaotic regimes were studied. In [Wijata *et al.*, 2021], the authors analyzed theoretically and numerically a single magnetic pendulum system in which the magnetic interaction is between the magnet placed at the end of the pendulum and an electrical coil powered by a pulsating rectangular current signal. The system shows different periodic one-side oscillations as well as chaotic and multi-periodic behaviors for various values of the electric current frequency. The same magnetic oscillator was studied by Skurativskyi *et al.* [2022] using averaging methods and numerical simulation. The results were compared with the experimental data.

The aim of this paper is to present, construct, conduct mathematical modeling, and study numerically and experimentally a nonlinear electromechanical system made of a mechanical arm having a permanent magnet at one end. This magnetized end interacts with a set of N-magnets placed along a circle. This is an extension of the work carried out in [Kouam Tagne *et al.*, 2021]. The many magnets will regularly generate a sort of periodic multistable potential. One of the main outputs of this work is the physical realization of the model and its experimental study. The paper is organized as follows. In Sec. 2, the physical description and the mathematical model of the system are given. In Sec. 3, the effects of some parameters on the behavior of the system are presented using the numerical simulation. Bifurcation diagrams and Lyapunov exponents are obtained in Sec. 4. Section 5 is devoted to experimental investigation and comparison between simulations and experimental results. The conclusion is given in Sec. 6.

2. Physical Description and Mathematical Modeling

2.1. *Physical description*

The rotating electromechanical system is presented in Fig. 1. It is constituted of two main parts: an

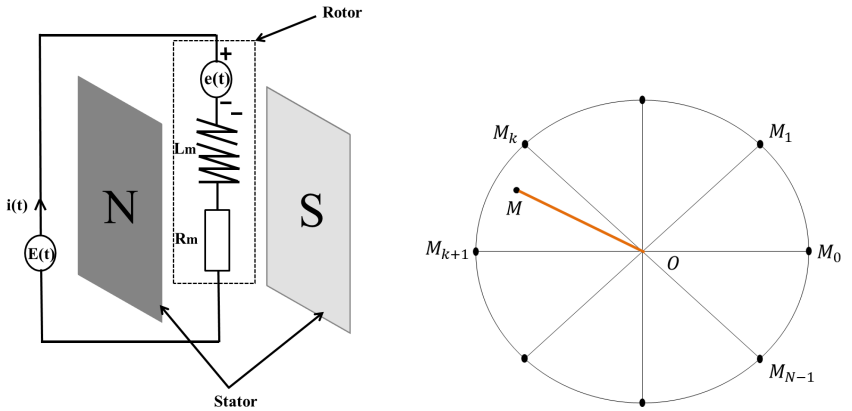

(a) (b)

Fig. 1. Schematic representation of (a) the equivalent of the electric part and (b) the electromechanical arm with magnets.

electrical one and a mechanical one. The electrical subsystem is made of a DC motor powered by a generator. This part is seen as a resistor, an inductance and a power supply mounted in series [see Fig. 1(a)]. As for the mechanical part, it is a pendulum (OM) having a neodymium magnet at the end M [Fig. 1(b)]. This magnet interacts with a set of magnets at points M_k arranged periodically along a circle and creating repulsive forces. The angle between two consecutive magnets is 2ϕ. The axis of rotation is the motor shaft axis. The other end of the arm is attached to the shaft.

2.2. *Mathematical modeling*

This section concerns the mathematical modeling process of the considered system. The governing differential equation of motion is derived using Newton's second law of rotational motion. This equation takes the following form:

$$J_m \frac{d^2\theta}{dt^2} = \Gamma_d + \Gamma_M + \Gamma, \tag{1}$$

where $J_m = (m_0 + \frac{m}{3})l^2$ is the total moment of inertia relative to the rotation axis of the arm with the fixed magnet. m and m_0 represent the mass of the arm and that of the magnet M respectively. θ is the angular coordinate relative to a reference line (the horizontal line); Γ_d is the damping torque; Γ_M is the resulting magnetic torque; Γ is the DC motor torque.

The damping torque has the following expression:

$$\Gamma_d = -\beta_m \frac{d\theta}{dt}, \tag{2}$$

where β_m is the damping coefficient. The DC motor torque is assumed to be proportional to the current i passing through the windings of the rotor. Then if K_C is the electromechanical coupling of the motor, this torque can be defined as follows:

$$\Gamma = K_C i. \tag{3}$$

Finally, the term Γ_M is the total external torque created by the magnetic interaction between the magnets. In the model, we consider the action of all magnets. The kth magnet M_k produces on the arm (point M) the following magnetic torque [Tesso *et al.*, 2022]:

$$\Gamma_{M_k/M} = \frac{\mu_0 q_1 q_2}{4\pi R} \frac{\delta \sin(\theta - 2k\phi)}{[1 + \delta^2 - 2\delta\cos(\theta - 2k\phi)]^{\frac{3}{2}}}, \tag{4}$$

where μ_0 is the permeability of the vacuum, q_1 is the pole strength of the magnet M and q_2 is the pole strength of magnets M_k. R is the distance between the point O and the position of the fixed magnets. $\delta = \frac{l}{R}$ is the dimensionless length of the mechanical arm. The total magnetic torque is then:

$$\Gamma_M = \sum_{K=0}^{N-1} \Gamma_{M_k/M} \tag{5}$$

with N the number of magnets.

Combining Eqs. (2), (3) and (5) leads to the first differential equation of the system

$$J_m \frac{d^2\theta}{dt^2} + \beta_m \frac{d\theta}{dt} + \frac{\mu_0 q_1 q_2}{4\pi R} g(\theta) = K_C i. \tag{6}$$

The nonlinear function $g(\theta)$ is defined as follows:

$$g(\theta) = -\sum_{k=0}^{N-1} \frac{\delta \sin(\theta - 2k\phi)}{[1 + \delta^2 - 2\delta\cos(\theta - 2k\phi)]^{\frac{3}{2}}}. \tag{7}$$

Applying the Kirchhoff's voltage law to the electrical part of the DC motor, the electric part is described by the following differential equation:

$$L_m \frac{di}{dt} + R_m i + e(t) = E(t). \tag{8}$$

The back electromotive force expression is:

$$e(t) = K_C \frac{d\theta}{dt} \cos\theta. \tag{9}$$

L_m and R_m are respectively the inductance and resistance of the windings of the motor. $E(t)$ is the input voltage.

Equations (6) and (8) take the following dimensionless form:

$$\ddot{y} + \lambda_m \dot{y} + \gamma g(\theta_0 y) = \varepsilon_m x, \tag{10}$$

$$\dot{x} + \lambda_e x + \varepsilon_e \dot{y} \cos(\theta_0 y) = u(t), \tag{11}$$

with the following dimensionless variables:

$$x = \frac{i}{I_0}, \quad y = \frac{\theta}{\theta_0}, \quad \tau = \omega_0 t \tag{12}$$

and dimensionless coefficients:

$$\lambda_m = \frac{\beta_m}{J_m \omega_0}, \quad \gamma = \frac{\mu_0 q_1 q_2}{4\pi R J_m \omega_0^2 \theta_0},$$

$$\varepsilon_m = \frac{K_C I_0}{J_m \omega_0^2 \theta_0}, \quad \varepsilon_e = \frac{K_C \theta_0}{L I_0}, \tag{13}$$

$$u(t) = \frac{E(t)}{L\omega_0 I_0}, \quad \lambda_e = \frac{R}{L\omega_0}, \quad \Omega = \frac{\omega}{\omega_0}.$$

The values of the physical parameters are given in Table 1.

Table 1. Values of the physical parameters of the electromechanical system.

Physical Parameter	Value	Physical Parameter	Value
l	variable	L_m	92×10^{-2} H
R	11.25 cm	K_C	42×10^{-3} Nm/A
m	16.80 g	β_m	0.50×10^{-3} Ns
m_0	2.50 g	θ_0	2π
q_1	20.46 Am	ω_0	$50\,\text{rad} \cdot \text{s}^{-1}$
q^2	43.76 Am	I_0	1 A
R_m	10.71 Ω		

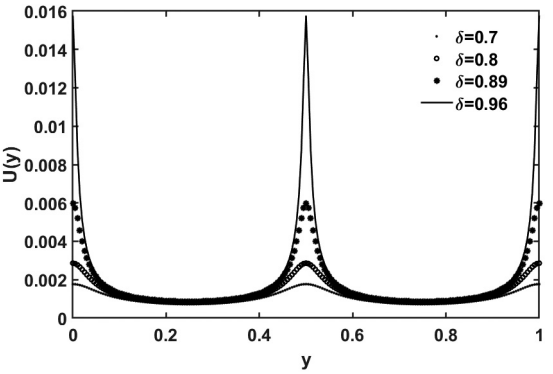

(a)

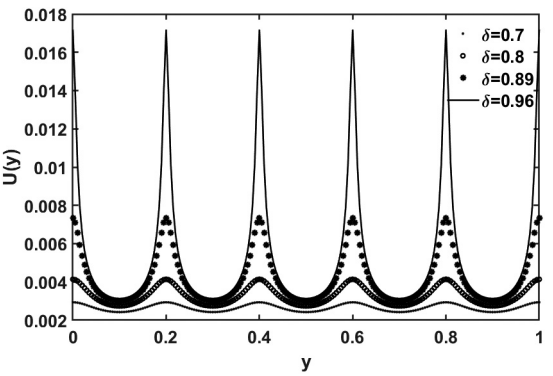

(b)

Fig. 2. Potential energy of the system versus the angular displacement: (a) for $N = 2$ magnets and (b) for $N = 5$ magnets.

2.3. *Potential energy*

The potential energy associated with the system of Eq. (6) is:

$$U = \gamma \sum_{k=0}^{N-1} \frac{1}{[1 + \delta^2 - 2\delta \cos(\theta - 2k\phi)]^{\frac{1}{2}}}. \tag{14}$$

Figure 2 presents some potential curves for different values of the parameter δ and the number of magnets N. These curves have been plotted for one period ($y = 1$) and for $N = 2$ magnets and $N = 5$ magnets. It shows two wells for $N = 2$ and five wells for $N = 5$. The stable equilibrium points are between two consecutive magnets. We also notice that the depth of the wells increases with the parameter δ.

3. Numerical Simulation

An important phenomenon to investigate is to find the condition for which the arm can cross

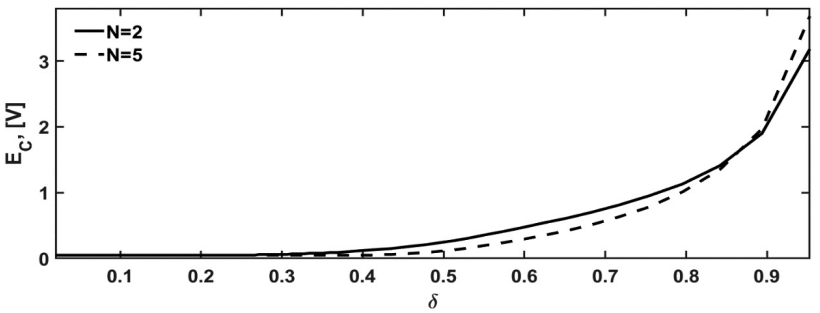

Fig. 3. Critical value of the voltage for complete rotation versus the parameter δ.

the potential barrier and undergo large amplitude motion leading, for instance, to complete rotation. For this purpose, we look for the critical value E_c of the external amplitude voltage above which complete rotation takes place. Two different forms of input signal have been considered: DC and AC voltage sources. The condition for complete rotation is written as follows $y_{\max} > 1$. The fourth order Runge–Kutta method is used to solve the differential Eqs. (10) and (11).

3.1. *Critical values in DC voltage case*

3.1.1. *Effects of the dimensionless length δ*

Figure 3 presents the critical voltage values versus the dimensionless length for $N = 2$ magnets (solid line) and $N = 5$ magnets (dotted line). One finds that E_c increases with the arm length. In the interval [0; 0.27], one needs the same energy to perform a complete rotation for both numbers of magnets. But in the interval [0.27; 0.88], more energy is required for two magnets while for the interval [0.88; 0.96], less energy is required for two magnets than for five magnets.

3.1.2. *Effects of the number of magnets N*

We have also analyzed the effects of the number of magnets on the critical voltage. As shown in Fig. 4, the voltage required to make a complete rotation is larger for $\delta = 0.96$ than for $\delta = 0.80$. This is due to the fact that for large values of δ, the repulsive forces are more accentuated and therefore more energy is needed to perform a full turn. In addition, for $\delta = 0.80$, we note a decrease of this voltage with the number of magnets while for $\delta = 0.96$, it increases until reaching a maximum value at $N = 5$ then decreases with N.

When complete rotation takes place, the arm rotation velocity shows a sort of NT-periodic oscillations where N is the number of magnets (see Fig. 5). This reflects the different accelerations produced by the repulsion created by the fixed magnets as they approach the magnet attached to the arm end.

3.2. *Critical values in the AC voltage case*

This subsection is devoted to find the condition for complete rotation when the electromechanical system is powered by a sinusoidal voltage.

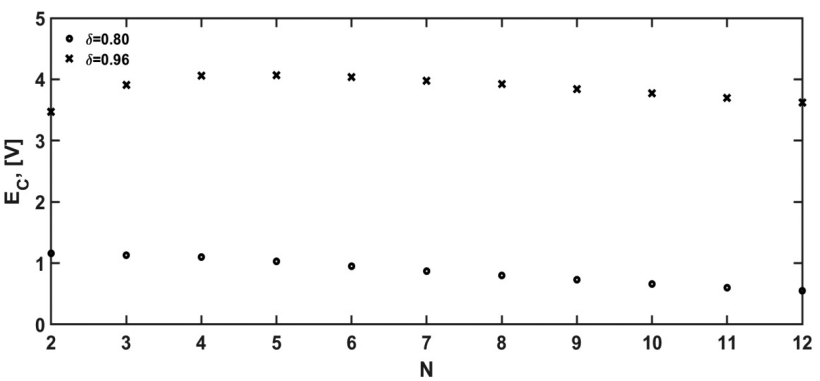

Fig. 4. Critical value of the voltage for complete rotation versus the number of magnets N.

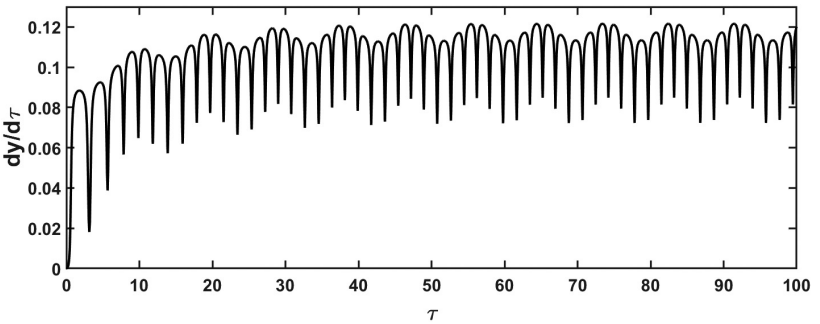

Fig. 5. Time-histories of the rotational velocity for $N = 5$ magnets, $\delta = 0.96$ when the arm performs complete rotation for $E = 4.5\,\mathrm{V}$.

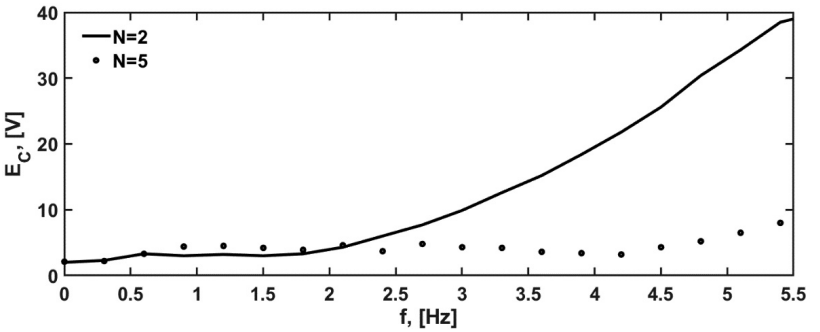

Fig. 6. Critical value of the sinusoidal voltage amplitude for complete rotation versus the frequency of the generator.

3.2.1. *Critical values versus the frequency of external voltage*

In Fig. 6, the critical values of the amplitude of the sinusoidal voltage is plotted versus its frequency for two and five magnets. When the frequency lies between 0.1 Hz and 0.6 Hz, the critical values are the same. But, much more voltage amplitude is needed in the range 0.6 Hz to 2.2 for $N = 5$ magnets than for $N = 2$ magnets. As the excitation frequency is increased more, the critical voltage amplitude is less for $N = 5$ magnets than for $N = 2$ magnets.

In order to confirm the curves displayed in Fig. 6, the time-histories of the angular displacement of the arm have been presented for two points belonging to the two regions separated by the curve (case for $N = 2$ magnets) (Fig. 7). The arm angular displacement presents oscillations with amplitude less than 1 for the region under the curve and greater than 1 for the region above the curve.

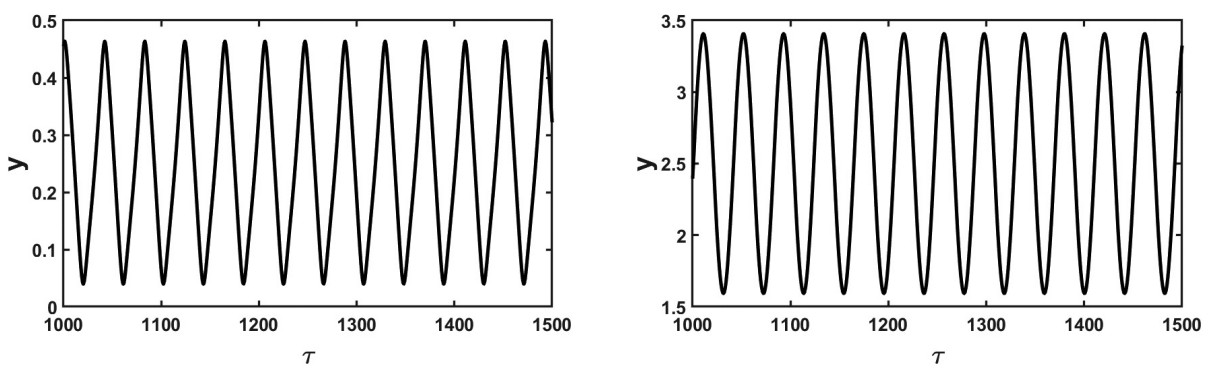

(a) (b)

Fig. 7. Time-histories of the angular displacement for $N = 2$ magnets. (a) For an input voltage lower than the critical value ($E_m = 4.5\,\mathrm{V}$) and (b) for an input voltage higher than the critical value ($E_m = 5\,\mathrm{V}$) and for $f = 1.2\,\mathrm{Hz}$.

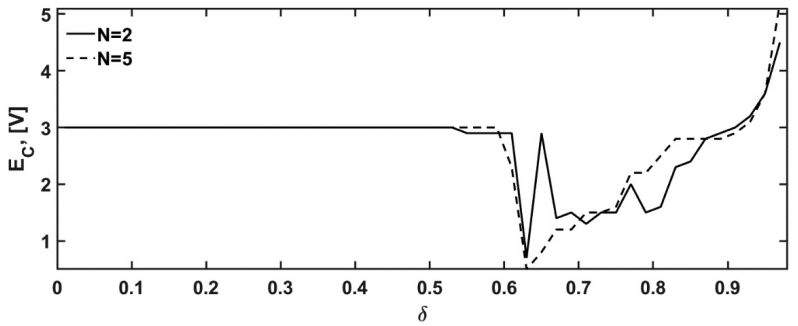

Fig. 8. Critical value of the amplitude of the sinusoidal voltage for complete rotation versus the parameter δ.

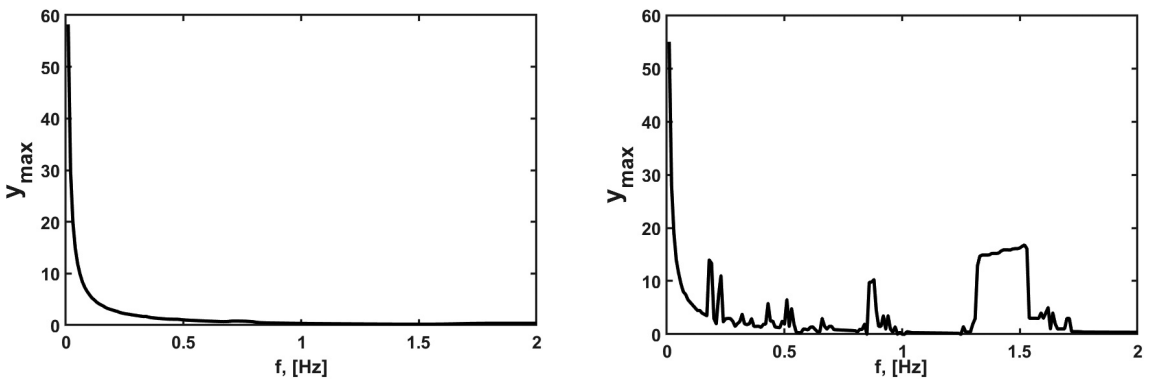

(a) (b)

Fig. 9. Maximum amplitude of the rotation angle versus the frequency of the sinusoidal voltage for $E = 3\,\mathrm{V}$, (a) for $\delta = 0.3$ and (b) for $\delta = 0.8$.

3.2.2. *Critical values versus the dimensionless length δ*

Figure 8 presents the critical value of the sinusoidal voltage amplitude when the arm length varies. One finds the same critical values for the dimensionless length belonging to the interval [0; 0.55] for two and five magnets. But, in the range [0.55; 0.98], one obtains an alternation between the two curves. Furthermore, abrupt drops are observed at $\delta = 0.53$ for $N = 2$ and at $\delta = 0.61$ for $N = 5$. This can be justified by the presence of several resonance peaks in the system for large values of δ as it can be seen in Fig. 9 which presents the oscillation amplitude versus the frequency.

3.2.3. *Critical amplitude of voltage versus the number of magnets*

As in the case of DC current, the critical voltages are higher for $\delta = 0.96$. For $\delta = 0.96$, this critical voltages are constant as the number of magnets varies while for $\delta = 0.80$, it increases and reaches a maximum at $N = 6$. Then, it decreases to reach its

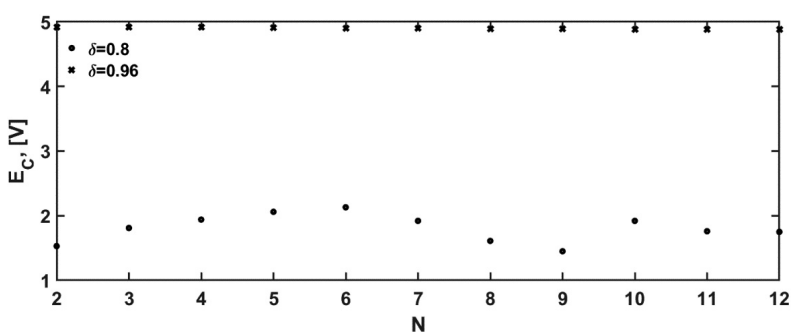

Fig. 10. Critical value of the amplitude of the sinusoidal voltage for complete rotation versus the number of magnets N.

minimum at $N = 9$. Thereafter, it takes another relative maximal value at $N = 10$ and then decreases with the number of magnets (see Fig. 10).

4. Bifurcation Diagrams and Lyapunov Exponents

To fully characterize the dynamical behaviors of the systems, the bifurcation diagrams and Lyapunov exponents are plotted both for DC and AC voltage sources. The value $\delta = 0.83$ is used. It corresponds to the arm length $l = 9.3\,\text{cm}$ which is used later for the experimental investigation.

4.1. *Bifurcation diagram in case of the DC voltage source*

Figure 11 shows that by varying the value of the DC voltage, two types of behaviors occur. The first one corresponds to the state where there is no oscillation or no motion. After a transient motion, the system evolves to a fixed state where the current and angular velocities are equal to 0 while the angular displacement attains a fixed value depending on the initial conditions. The second type of motion corresponds to the state where the angular displacement increases continuously as a function of time while the angular velocity oscillates around a fixed non null value. The transition between these two dynamics is observed at $E = 1.98\,\text{V}$ for $N = 2$ magnets and at $E = 2.07\,\text{V}$ for $N = 5$ magnets. These values represent the critical voltages for complete rotation at the corresponding numbers of magnets.

4.2. *Bifurcation diagram in case of the AC voltage source*

4.2.1. *Bifurcation diagram versus the amplitude E_m of the AC voltage*

First, we have plotted the bifurcation diagram of the mechanical displacement y versus the amplitude

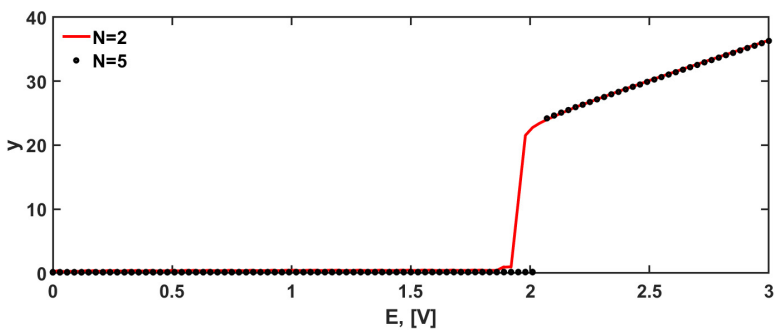

Fig. 11. Bifurcation diagram versus the DC voltage E when there are two magnets (full line) and five magnets (line with large dots).

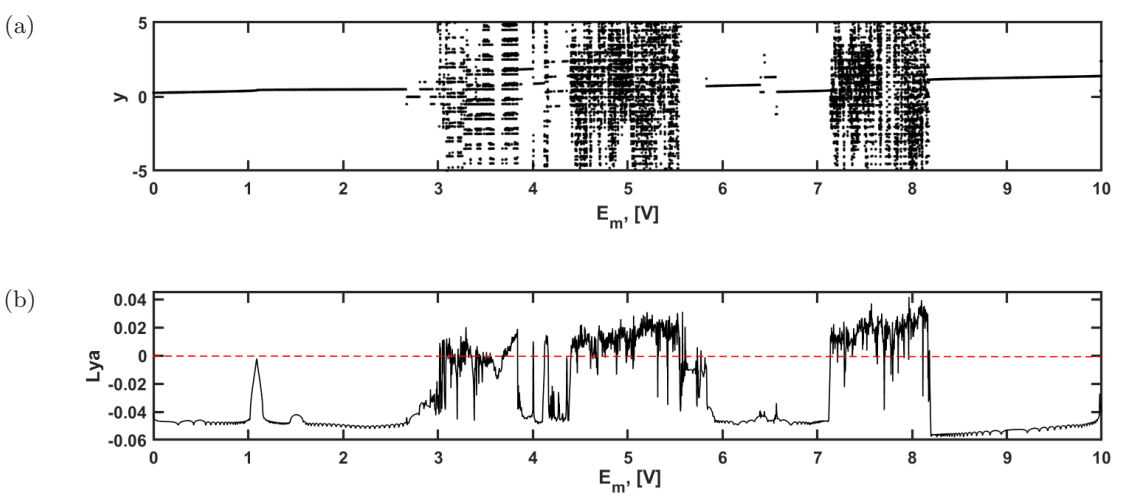

Fig. 12. (a) Bifurcation diagram and (b) variation of the Lyapunov exponent, both as function of the amplitude of the external generator E_m for $f = 1.2\,\text{Hz}$ and $N = 2$ magnets.

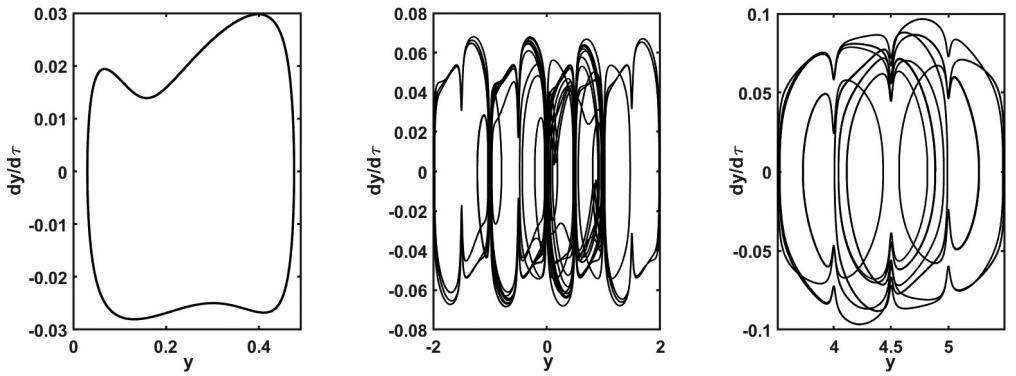

(a) (b) (c)

Fig. 13. Phase portraits of the mechanical subsystem when $f = 1.2\,\text{Hz}$ and $N = 2$ magnets; (a) $E_m = 2.0\,\text{V}$, (b) $E_m = 3.1\,\text{V}$ and (c) $E_m = 5.0\,\text{V}$.

E_m of the sinusoidal voltage source for $f = 1.2\,\text{Hz}$. The diagram for $N = 2$ magnets is presented in Fig. 12(a) while Fig. 12(b) presents the corresponding Lyapunov exponent. Periodic motion starts when $E_m = 0.1\,\text{V}$ and continues until 2.9 V. With the amplitude between 2.9 and 5.8 V, the system response exhibits an alternation of periodic and chaotic motions. The system response comes into a periodic motion when the amplitude lies between 5.8 and 7.2 V, and returns to an alternation of periodic and chaotic motions when $7.8\,\text{V} \leq E_m \leq 8.2\,\text{V}$. As the excitation amplitude increases further, the system undergoes periodic oscillation. Some examples of phase portraits are plotted in Fig. 13.

For $N = 5$ magnets, the dynamical response is almost the same (see Fig. 14). But here, chaos occurs for higher values of the voltage amplitude.

4.2.2. *Bifurcation diagram versus the frequency f of the AC voltage*

Now considering the frequency as the control parameter, the amplitude of the external source is kept constant at $E_m = 5.0\,\text{V}$. Figure 15 presents the bifurcation diagram of the arm displacement y for $N = 2$ magnets for $0.1\,\text{Hz} \leq f \leq 5\,\text{Hz}$. Periodic and chaotic oscillations are also present as the frequency varies. As in the case of the bifurcation

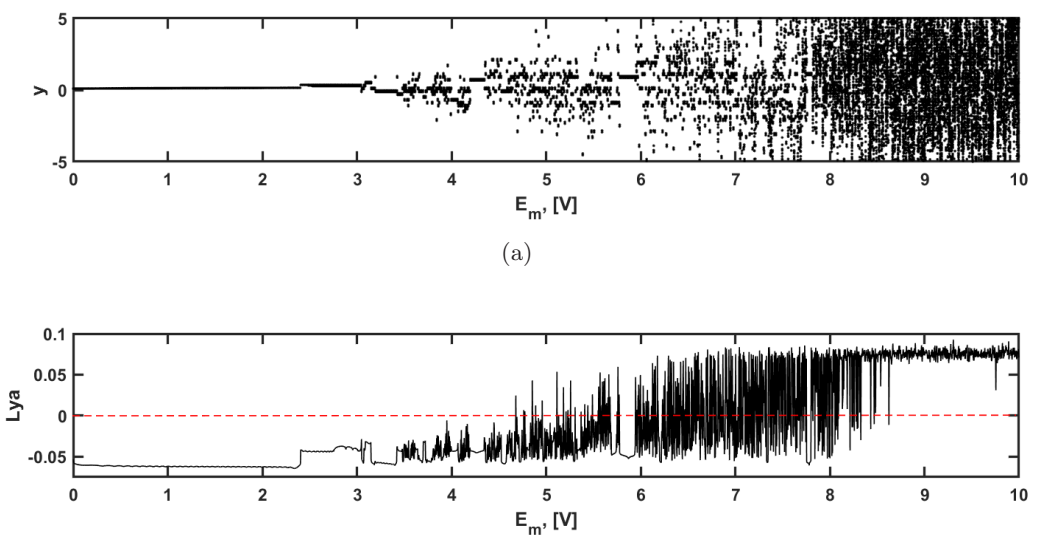

(a)

(b)

Fig. 14. (a) Bifurcation diagram as function of the amplitude of the external generator E_m for $f = 1.2\,\text{Hz}$ and $N = 5$ magnets and (b) the corresponding variation of the Lyapunov exponent.

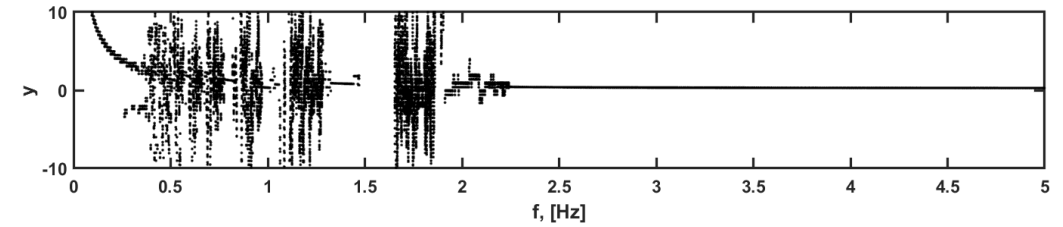

(a)

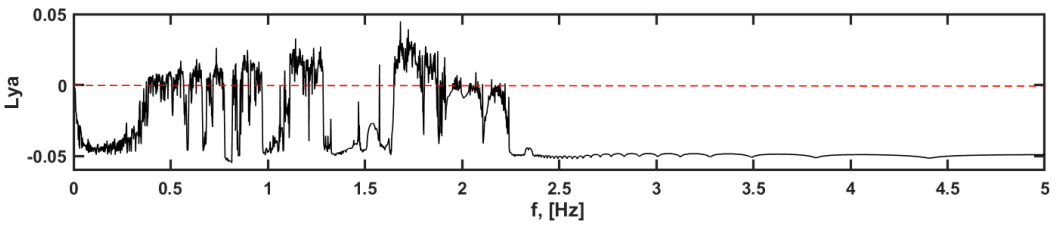

(b)

Fig. 15. (a) Bifurcation diagram and (b) the corresponding Lyapunov exponent as function of the excitation frequency f for $E_m = 5.0\,\mathrm{V}$ and $N = 2$ magnets.

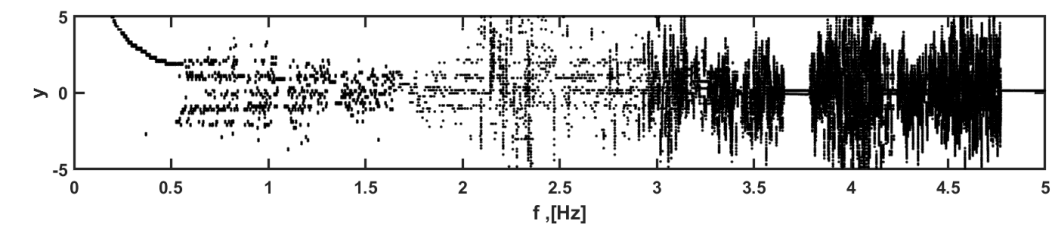

(a)

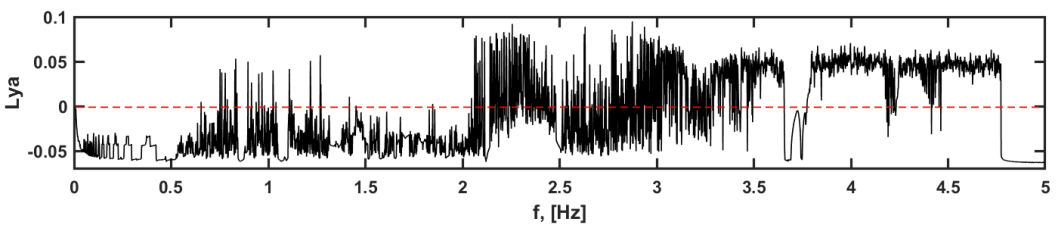

(b)

Fig. 16. (a) Bifurcation diagram and (b) the corresponding Lyapunov exponent as function of the excitation frequency f for $E_m = 5.0\,\mathrm{V}$ and $N = 5$ magnets.

diagram versus the voltage amplitude, the chaotic behavior, for $N = 5$ magnets, starts for higher values of the frequency (Fig. 16).

5. Experiment

5.1. *Experimental setup*

Figure 17 displays the experimental setup of the physical model described and studied theoretically in the previous sections. A voltage generator powers a low-power DC motor. The motor shaft supports a rigid iron rod which moves in the horizontal plane. The results of the experiment are presented only in the case of the system powered by the low frequency generator.

At the end of the arm, a neodymium magnet is fixed and interacts with two other magnets symmetrically positioned on a circle. The time,

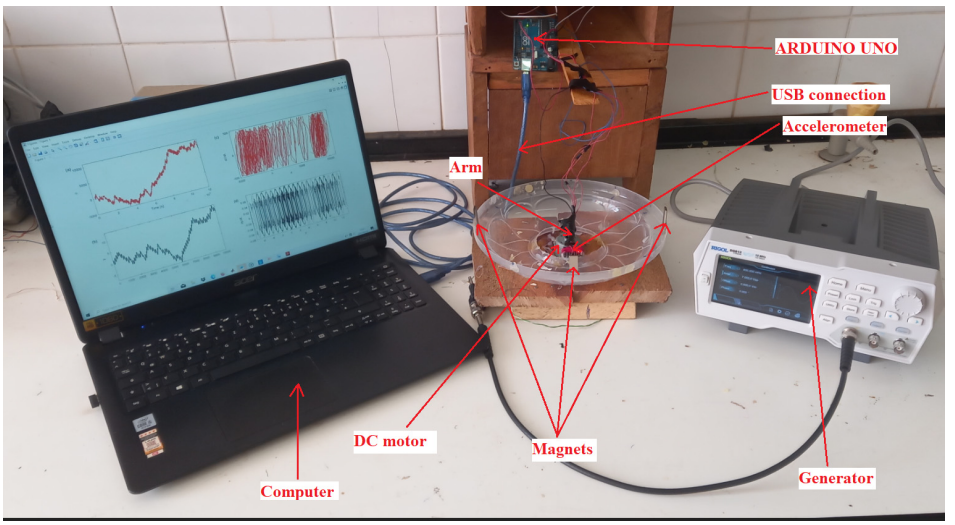

Fig. 17. Experimental setup.

the angle and the angular velocity are recorded in the computer using an accelerometer MPU 6050 through an ARDUINO UNO microcontroller.

5.2. *Experimental versus numerical results*

Figure 18 compares the experimental and numerical results in terms of time-histories and phase portraits when the amplitude of the external excitation is $E_m = 1.92\,\mathrm{V}$ and the frequency is $f = 1.2\,\mathrm{Hz}$. As it appears, the system leads to regular dynamics. The coincidence of the numerical and experimental results is clearly visible. The same agreement is visible in Figs. 19 and 20 where chaotic behaviors are presented. Let us however mention that the agreement here should be understood considering the shapes of the responses instead of considering

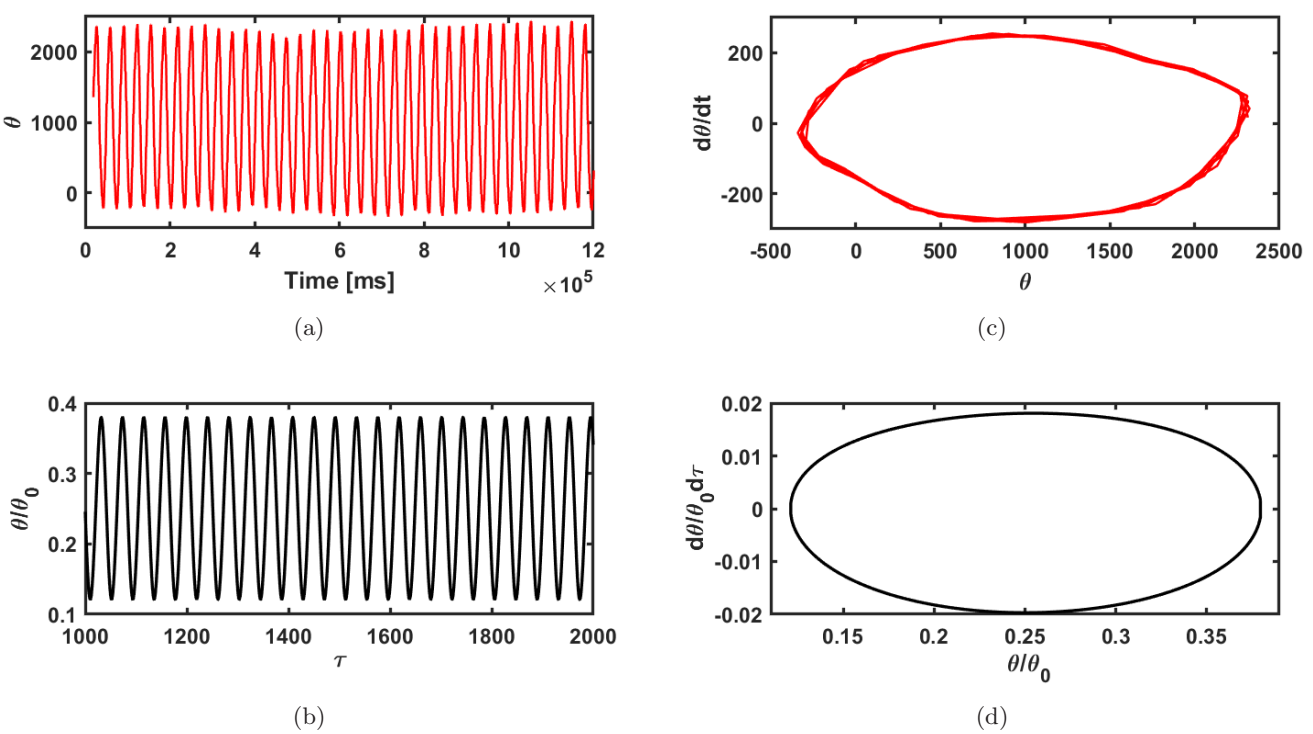

Fig. 18. Time-histories of the mechanical response and phase portraits (a), (c) experimentally obtained and (b), (d) numerical simulation results for $E_m = 1.92\,\mathrm{V}$, $f = 1.2\,\mathrm{Hz}$ and $N = 2$ magnets.

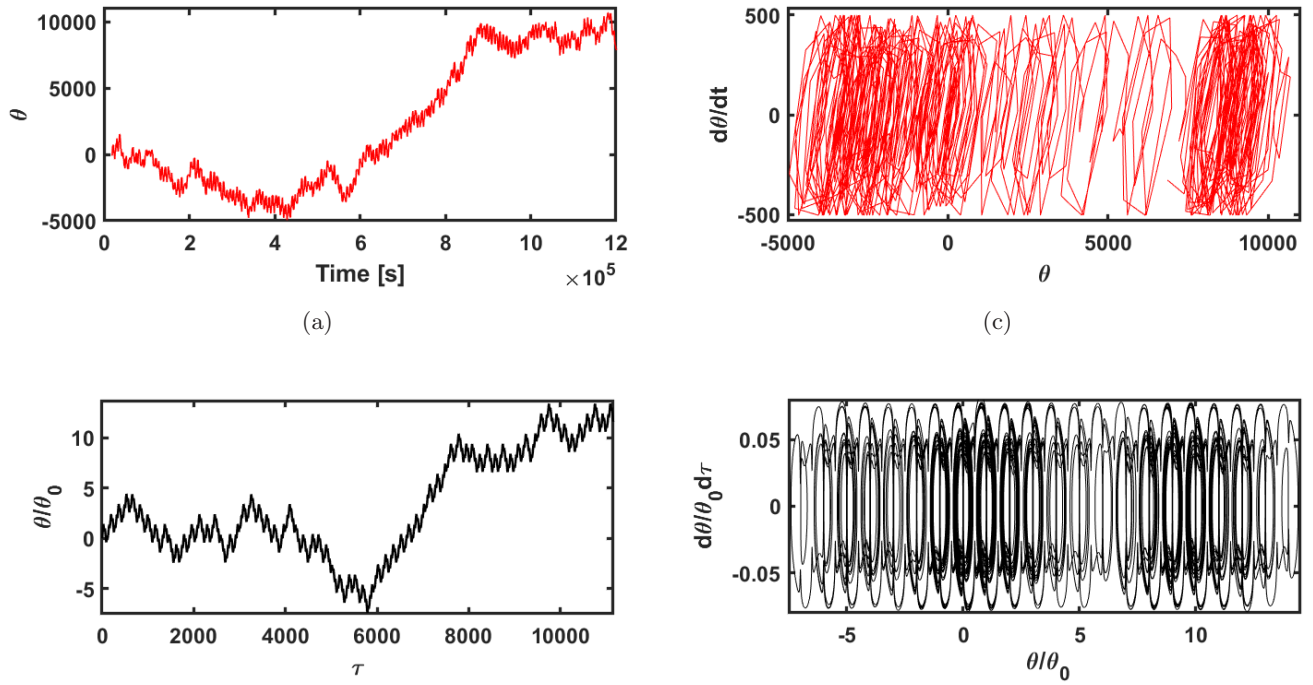

(a) (c) (b) (d)

Fig. 19. Time-histories of the mechanical response and phase portraits (a), (c) experimentally obtained and (b), (d) numerical simulation results for $E_m = 4.0\,\mathrm{V}$, $f = 1.2\,\mathrm{Hz}$ and $N = 2$ magnets.

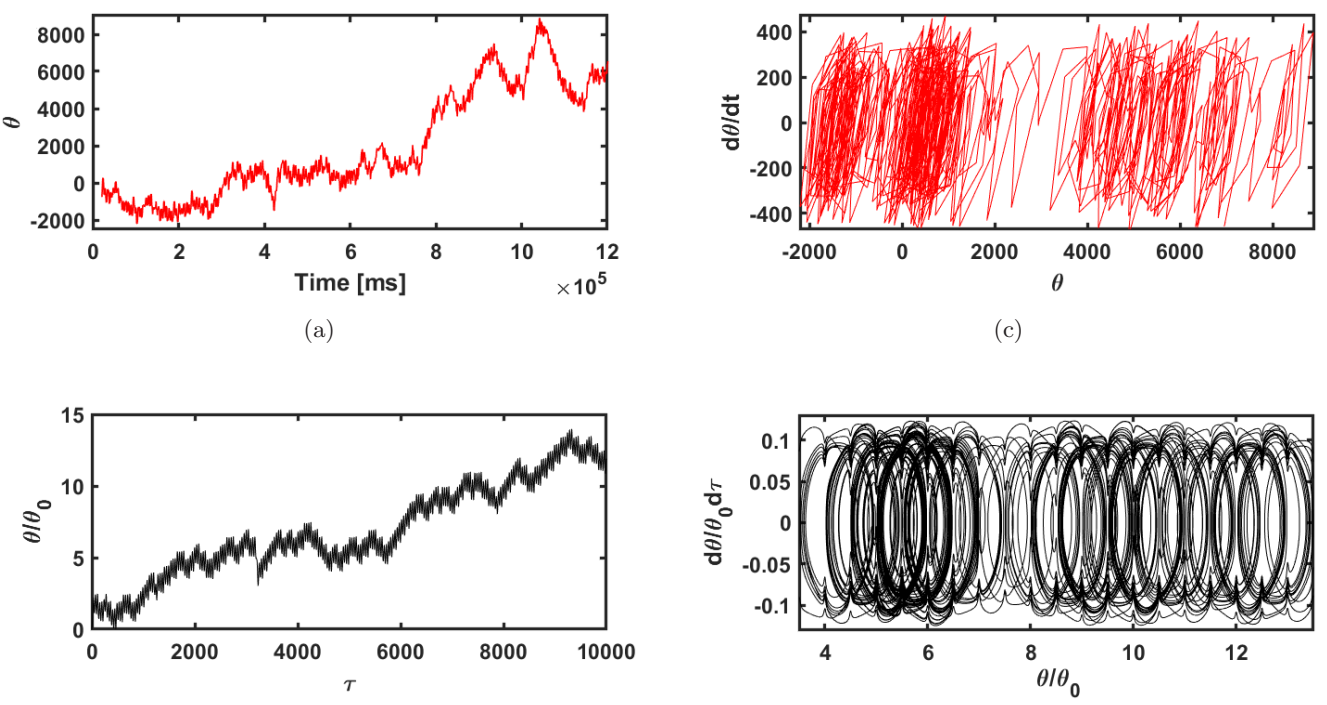

(a) (c) (b) (d)

Fig. 20. Time-histories of the mechanical response and phase portraits (a), (c) experimentally obtained and (b), (d) numerical simulation results for $E_m = 7.2\,\mathrm{V}$, $f = 1.2\,\mathrm{Hz}$ and $N = 2$ magnets.

the amplitudes of the responses since some differences are observed because of the difficulty of measuring the exact values of some physical parameters.

6. Conclusion

This paper has considered the dynamics of a rotating electromechanical arm subjected to nonlinear magnetic torques due to a series of magnets aligned periodically along a circle in front of which a rigid arm fixed on a motor axis rotates with another magnet at its end. The magnetic potential energy curves were presented displaying the number of wells equivalent to the number of magnets. The critical voltage for which the mechanical arm undergoes a complete rotation was determined for the DC and AC input voltages. The results have shown that, for a DC voltage lower than the critical value, the mechanical arm undergoes damped oscillations and then stabilizes at an equilibrium position. When the voltage is above the critical value, the arm displacement increases continuously with time (performing complete rotation) while the angular velocity oscillates showing frequency proportional to the number of magnets. When the motor is powered by a sinusoidal voltage, the arm displays angular oscillations with amplitude larger than one turn for large values of the voltage amplitude. The regions of chaotic and periodic motions were obtained through the bifurcation diagrams and the corresponding Lyapunov exponent. The theoretical results have been confirmed by an experiment conducted on a setup constructed in the laboratory. The model considered in this work can be used to mechanically study some phenomena encountered in condensed matter physics such as a particle moving in periodic potential with variable shape and in the study of the resistively capacitance shunted Josephson junctions [McCumber, 1968].

Acknowledgment

This work has been supported by the Polish National Science Centre, Poland under the Grant OPUS 18 No. 2019/35/B/ ST8/00980.

References

Akinlar, M. A., Tchier, F. & Inc, M. [2020] "Chaos control and solutions of fractional-order Malkus waterwheel model," *Chaos Solit. Fract.* **135**, 109746.

Ana, R. K., José, M. B., Jorge, L. P. & Fábio, R. C. [2010] "The nonlinear dynamics of a vibrating systemmodeled by an inverted pendulum, with an electrodynamics shaker," *Conf. Dynamics, Control and Their Applications*, Brazil, 7–11 June 2010.

Awrejcewicz, J., Supe, B., Kudra, G., Wasilewski, G. & Olejnik, P. [2008] "Numerical and experimental study of regular and chaotic motion of triple physical pendulum," *Int. J. Bifurcation and Chaos* **18**, 2883–2915.

Belato, D., Weber, H. I., Balthazar, J. M. & Mook, D. T. [2001] "Chaotic vibrations of a nonideal electromechanical system," *Int. J. Solids Struct.* **38**, 1699–1706.

Chatterjee, M., Mohamed, A. & Almehmadi, F. [2018] "Secure freespace communication, turbulence mitigation, and other applications using acousto-optic chaos," *Appl. Opt.* **57**, 1–13.

Ge, Z. M., Cheng, J. M. & Chen, Y. S. [2004] "Chaos anticontrol and synchronization of three time scales brushless DC motor system," *Chaos Solit. Fract.* **22**, 1165–1182.

Kakmeni, F., Bowong, S., Tchawoua, C. & Kaptouom, E. [2004] "Dynamics and chaos control in nonlinear electrostatic transducers," *Chaos Solit. Fract.* **21**, 1093–1108.

Kazmierczak, M., Kudra, G., Awrejcewicz, J. & Wasilewski, G. [2013] "Numerical and experimental investigation of bifurcational dynamics of an electromechanical system consisting of a physical pendulum and DC motor," *Dynamical Systems-Applications* (TU Lodz Press, Lodz), pp. 49–58.

Kazmierczak, M., Kudra, G., Awrejcewicz, J. & Wasilewski, G. [2015] "Mathematical modeling, numerical simulations and experimental verification of bifurcation dynamics of a pendulum driven by a DC motor," *Eur. J. Phys.* **36**, 1–13.

Kemajou, I., Nana, B. & Woafo, P. [2022] "Dynamics of the electromechanical sieve with hysteretic iron-core inductor," *Nonlin. Dyn.* **110**, 237–255.

Kitio, K. & Woafo, P. [2010] "Experimental realization and simulations a self-sustained macro electromechanical system," *Mech. Res. Commun.* **37**, 106–110.

Kouam Tagne, R. F., Tsapla Fotsa, R. & Woafo, P. [2021] "Dynamics of a DC motor-driving arm with a circular periodic potential and DC/AC voltage input," *Int. J. Bifurcation and Chaos* **31**, 2150178-1–132.

Kumar, G., Kumar, T., Kumar, M. & Shovan, B. [2017] "Observer design for semilinear descriptor systems with applications to chaos-based secure communication," *Int. J. Appl. Comput. Math.* **3**, 1313–1324.

Mahmoud, E. E., Trikha, P., Jahanzaib, L. S. & Almaghrabi, O. A. [2020] "Dynamical analysis and chaos control of the fractional chaotic ecological model," *Chaos Solit. Fract.* **141**, 110348.

McCumber, D. E. [1968] "Effect of AC Impedance on DC voltage–current characteristics of superconductor weak-link junctions," *J. Appl. Phys.* **39**, 3113–3118.

Moon, F. C., Cusumano, J. & Holmes, P. J. [1993] "Evidence for homoclinic orbits as a precursor to chaos in a magnetic pendulum," *Physica D* **24**, 383–390.

Nana, B., Yamgoué, S. B., Tchitnga, R. & Woafo, P. [2017] "Dynamics of a pendulum driven by a DC motor and magnetically controlled," *Chaos Solit. Fract.* **104**, 18–27.

Nana, B., Yamgoué, S. B., Tchitnga, R. & Woafo, P. [2018] "Nonlinear dynamics of a sinusoidally driven lever in repulsive magnetic fields," *Nonlin. Dyn.* **91**, 55–66.

Nana Nbendjo, B. R. & Woafo, P. [2007] "Active control with delay of horseshoes chaos using piezoelectric absorber on a buckled beam under parametric excitation," *Chaos Solit. Fract.* **32**, 73–79.

Polczynski, K., Wijata, A., Awrejcewicz, J. & Wasilewski, G. [2019] "Numerical and experimental study of dynamics of two pendulums under a magnetic field," *J. Syst. Contr. Engin.* **233**, 441–453.

Polczynski, K., Skurativskyi, S., Bednarek, M. & Awrejcewicz, J. [2021] "Nonlinear oscillations of coupled pendulums subjected to an external magnetic stimulus," *Mech. Syst. Sign. Process.* **154**, 107560.

Rajagopal, K., Vaidyanathan, S., Karthikeyan, A. & Duraisamy, P. [2017] "Dynamic analysis and chaos suppression in a fractional order brushless DC motor," *Electr. Engin.* **99**, 721–733.

Shaohua, L., Huanhuan, M., Fengyun, L. & Hassen, M. O. [2022] "Dynamical analysis and chaos control of MEMS resonators by using the analog circuit," *Nonlin. Dyn.* **108**, 97–112.

Skurativskyi, S., Polczyński, K., Wojna, M. & Awrejcewicz, J. [2022] "Quantifying periodic, multiperiodic, hidden and unstable regimes of a magnetic pendulum via semi-analytical, numerical and experimental methods," *J. Sound Vib.* **524**, 116710.

Tcheutchoua, F. D. O. & Woafo, P. [2013] "Generation of complex phenomena in a simple electromechanical system using the feedback control," *Commun. Nonlin. Sci. Numer. Simulat.* **18**, 209–218.

Tesso, P. C. W., Kouam Tagne, R. & Woafo, P. [2022] "Energy harvesting from a micro-system with circular bistable potential due to magnets," *Int. J. Bifurcation and Chaos* **32**, 2250039-1–16.

Tsapla Fotsa, R. & Woafo, P. [2016] "Chaos in a new bistable rotating electromechanical system," *Chaos Solit. Fract.* **93**, 48–57.

Wijata, A., Polczynski, K. & Awrejcewicz, J. [2021] "Theoretical and numerical analysis of regular one-side oscillations in a single pendulum system driven by a magnetic field," *Mech. Syst. Sign. Process.* **150**, 107229.

Wojna, M., Wijata, A., Wasilewski, G. & Awrejcewicz, J. [2018] "Numerical and experimental study of a double physical pendulum with magnetic interaction," *J. Sound Vib.* **430**, 214–230.

Xizhe, Z., Sajid, I.,Yanhe, Z., Xinyu, L. & Jie, Z. [2017] "Applications of chaotic dynamics in robotics," *Int. J. Adv. Robot. Syst.* **13**, 1–7.

Yamapi, R., Nana Nbendjo, B. R. & Enjieu Kadji, H. G. [2007] "Dynamics and active control of motion of a driven multi-limit-cycle van der Pol oscillator," *Int. J. Bifurcation and Chaos* **17**, 1343–1354.

Zhu, Q. & Ishitobi, M. [1999] "Experimental study of chaos in a driven triple pendulum," *J. Sound Vib.* **227**, 230–238.

International Journal of Bifurcation and Chaos, Vol. 33, No. 5 (2023) 2350052 (14 pages)

DOI: 10.1142/S0218127423500529

Dynamics of the Rotating Arm of an Electromechanical System Subjected to the Action of Circularly Placed Magnets: Numerical Study and Experiment

R. Kouam Tagne and P. Woafo*
Laboratory of Modelling and Simulation in Engineering, Biomimetics and Prototypes, Faculty of Science, University of Yaoundé I, P. O. Box 812, Yaoundé, Cameroon
**Laboratory of Products Development and Entrepreneurship, Institut Supérieur de l'Innovation et de Technologie, P. O. Box 8210, Yaoundé, Cameroon*
**pwoafo1@yahoo.fr*

J. Awrejcewicz
Department of Automation, Biomechanics, and Mechatronics, Lodz University of Technology, 1/15 Stefanowski St. (Building A22), Lodz, 90-924, Poland

Received September 6, 2022; Revised March 7, 2023

This paper considers the experimental and numerical study of an electromechanical arm powered by a DC motor and subjected to the action of permanent magnets. The magnetic torques arise from permanent magnets mounted at the free end of the arm and along a circle. The electrical subsystem is powered by two forms of input signal (DC and AC voltage sources). For each case, we determine the condition for complete rotation of the mechanical arm versus the parameters of the system such as the arm length, the number of magnets, and the frequency of the external signal. The nonlinear dynamics of the system is examined by means of time-histories, bifurcation diagrams, Lyapunov exponents and phase portraits. Chaotic and periodic dynamics are detected numerically and confirmed experimentally.

Keywords: Electromechanical system; magnetic torque; array of magnets; nonlinear dynamics; chaos.

1. Introduction

Resulting from nonlinearities due to the material properties, to the geometry, to magnetic components or to boundary conditions, chaotic dynamics is omnipresent in nature. It is found in various systems such as chemical reactions, lasers, neural networks, internet communication networks, fluid flow, population growth in species, engineering systems, social and economic systems, etc. In many cases, chaos can be seen as dangerous or destructive and is thus avoided [Akinlar *et al.*, 2020; Mahmoud *et al.*, 2020; Kakmeni *et al.*, 2004; Nana Nbendjo & Woafo, 2007; Rajagopal *et al.*, 2017; Yamapi *et al.*, 2007; Shaohua *et al.*, 2022]. But, chaos also presents positive implications in diverse systems such as mechanical engineering systems

*Author for correspondence

and telecommunication [Awrejcewicz *et al.*, 2008; Kouam Tagne *et al.*, 2021; Tsapla Fotsa & Woafo, 2016; Kumar *et al.*, 2017; Chatterjee *et al.*, 2018; Nana *et al.*, 2017; Ge *et al.*, 2004; Wojna *et al.*, 2018; Zhu & Ishitobi, 1999; Moon *et al.*, 1993; Kemajou *et al.*, 2022; Kitio & Woafo, 2010; Xizhe *et al.*, 2017; Nana *et al.*, 2018].

Electromechanical systems are widely used in different branches of engineering [Kemajou *et al.*, 2022; Kitio & Woafo, 2010; Xizhe *et al.*, 2017; Ana *et al.*, 2010; Tcheutchoua & Woafo, 2013; Polczynski *et al.*, 2019; Belato *et al.*, 2001; Kazmierczak *et al.*, 2013, 2015]. They transform electrical energy into mechanical actions and vice versa via magnetic, piezoelectric and capacitive couplings. In the quest for increasing the efficiency of some industrial and home devices such as vibrating sieves, industrial mixers and industrial shakers, nonlinear phenomena have been analyzed in those systems with the nonlinear components natural to the systems or introduced in the systems. These nonlinear components can be present in the mechanical part (material, geometric or inertial nonlinearities), in the electrical circuit (nonlinear inductor, nonlinear capacitor, nonlinear resistance) and in the coupling between the mechanical and electrical parts [Kitio & Woafo, 2010]. Most of the time, nonlinearities are built using electronic components for low power systems. The low power is in practice used to command the motion of very light mechanical arms or micro arms in micro robots and for other micro actuations. At the macroscopic level where the power necessary to set parts into chaotic motion is high, one needs to use some other solutions, specifically found with electrical components. This is for instance the case of electrical circuit having hysteretic iron-core. Inserted in an electric circuit, it is able to generate high amplitude chaotic signals. This has been used recently to power a model of electromechanical sieve [Kemajou *et al.*, 2022]. Another way is to use magnets to generate the nonlinearity and then work with linear electrical systems. This is for instance the example considered in [Kouam Tagne *et al.*, 2021] where the authors introduced permanent magnets in the mechanical part to provide complex phenomenon. In the same line, Polczynski *et al.* [2019] investigated two pendulums with magnets embedded in a variable magnetic field. The magnetic interaction originates from permanent magnets, mounted at free ends of the pendulums, and current-powered air coils placed underneath. The authors proved that the two-pendulum system is able to display regions of chaotic and regular motions. The authors in [Polczynski *et al.*, 2021] studied both experimentally and analytically the model described by [Polczynski *et al.*, 2019] with a new rational approximation of the magnetic torque which helps to use mathematical methods to get a deep understanding of the influence of the magnetic field. In particular, the resonant phenomena, and periodic and chaotic regimes were studied. In [Wijata *et al.*, 2021], the authors analyzed theoretically and numerically a single magnetic pendulum system in which the magnetic interaction is between the magnet placed at the end of the pendulum and an electrical coil powered by a pulsating rectangular current signal. The system shows different periodic one-side oscillations as well as chaotic and multi-periodic behaviors for various values of the electric current frequency. The same magnetic oscillator was studied by Skurativskyi *et al.* [2022] using averaging methods and numerical simulation. The results were compared with the experimental data.

The aim of this paper is to present, construct, conduct mathematical modeling, and study numerically and experimentally a nonlinear electromechanical system made of a mechanical arm having a permanent magnet at one end. This magnetized end interacts with a set of N-magnets placed along a circle. This is an extension of the work carried out in [Kouam Tagne *et al.*, 2021]. The many magnets will regularly generate a sort of periodic multistable potential. One of the main outputs of this work is the physical realization of the model and its experimental study. The paper is organized as follows. In Sec. 2, the physical description and the mathematical model of the system are given. In Sec. 3, the effects of some parameters on the behavior of the system are presented using the numerical simulation. Bifurcation diagrams and Lyapunov exponents are obtained in Sec. 4. Section 5 is devoted to experimental investigation and comparison between simulations and experimental results. The conclusion is given in Sec. 6.

2. Physical Description and Mathematical Modeling

2.1. *Physical description*

The rotating electromechanical system is presented in Fig. 1. It is constituted of two main parts: an

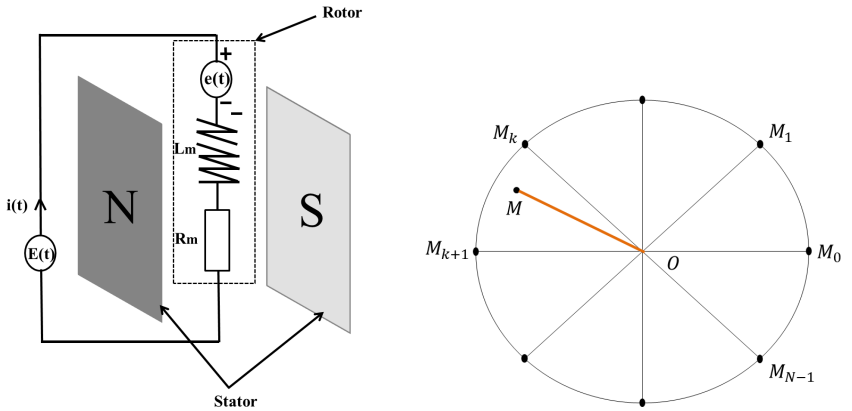

(a) (b)

Fig. 1. Schematic representation of (a) the equivalent of the electric part and (b) the electromechanical arm with magnets.

electrical one and a mechanical one. The electrical subsystem is made of a DC motor powered by a generator. This part is seen as a resistor, an inductance and a power supply mounted in series [see Fig. 1(a)]. As for the mechanical part, it is a pendulum (OM) having a neodymium magnet at the end M [Fig. 1(b)]. This magnet interacts with a set of magnets at points M_k arranged periodically along a circle and creating repulsive forces. The angle between two consecutive magnets is 2ϕ. The axis of rotation is the motor shaft axis. The other end of the arm is attached to the shaft.

2.2. *Mathematical modeling*

This section concerns the mathematical modeling process of the considered system. The governing differential equation of motion is derived using Newton's second law of rotational motion. This equation takes the following form:

$$J_m \frac{d^2\theta}{dt^2} = \Gamma_d + \Gamma_M + \Gamma, \tag{1}$$

where $J_m = (m_0 + \frac{m}{3})l^2$ is the total moment of inertia relative to the rotation axis of the arm with the fixed magnet. m and m_0 represent the mass of the arm and that of the magnet M respectively. θ is the angular coordinate relative to a reference line (the horizontal line); Γ_d is the damping torque; Γ_M is the resulting magnetic torque; Γ is the DC motor torque.

The damping torque has the following expression:

$$\Gamma_d = -\beta_m \frac{d\theta}{dt}, \tag{2}$$

where β_m is the damping coefficient. The DC motor torque is assumed to be proportional to the current i passing through the windings of the rotor. Then if K_C is the electromechanical coupling of the motor, this torque can be defined as follows:

$$\Gamma = K_C i. \tag{3}$$

Finally, the term Γ_M is the total external torque created by the magnetic interaction between the magnets. In the model, we consider the action of all magnets. The kth magnet M_k produces on the arm (point M) the following magnetic torque [Tesso *et al.*, 2022]:

$$\Gamma_{M_k/M} = \frac{\mu_0 q_1 q_2}{4\pi R} \frac{\delta \sin(\theta - 2k\phi)}{[1 + \delta^2 - 2\delta\cos(\theta - 2k\phi)]^{\frac{3}{2}}}, \tag{4}$$

where μ_0 is the permeability of the vacuum, q_1 is the pole strength of the magnet M and q_2 is the pole strength of magnets M_k. R is the distance between the point O and the position of the fixed magnets. $\delta = \frac{l}{R}$ is the dimensionless length of the mechanical arm. The total magnetic torque is then:

$$\Gamma_M = \sum_{K=0}^{N-1} \Gamma_{M_k/M} \tag{5}$$

with N the number of magnets.

Combining Eqs. (2), (3) and (5) leads to the first differential equation of the system

$$J_m \frac{d^2\theta}{dt^2} + \beta_m \frac{d\theta}{dt} + \frac{\mu_0 q_1 q_2}{4\pi R} g(\theta) = K_C i. \tag{6}$$

The nonlinear function $g(\theta)$ is defined as follows:

$$g(\theta) = -\sum_{k=0}^{N-1} \frac{\delta \sin(\theta - 2k\phi)}{[1 + \delta^2 - 2\delta\cos(\theta - 2k\phi)]^{\frac{3}{2}}}. \tag{7}$$

Applying the Kirchhoff's voltage law to the electrical part of the DC motor, the electric part is described by the following differential equation:

$$L_m \frac{di}{dt} + R_m i + e(t) = E(t). \tag{8}$$

The back electromotive force expression is:

$$e(t) = K_C \frac{d\theta}{dt} \cos\theta. \tag{9}$$

L_m and R_m are respectively the inductance and resistance of the windings of the motor. $E(t)$ is the input voltage.

Equations (6) and (8) take the following dimensionless form:

$$\ddot{y} + \lambda_m \dot{y} + \gamma g(\theta_0 y) = \varepsilon_m x, \tag{10}$$

$$\dot{x} + \lambda_e x + \varepsilon_e \dot{y} \cos(\theta_0 y) = u(t), \tag{11}$$

with the following dimensionless variables:

$$x = \frac{i}{I_0}, \quad y = \frac{\theta}{\theta_0}, \quad \tau = \omega_0 t \tag{12}$$

and dimensionless coefficients:

$$\lambda_m = \frac{\beta_m}{J_m \omega_0}, \quad \gamma = \frac{\mu_0 q_1 q_2}{4\pi R J_m \omega_0^2 \theta_0},$$

$$\varepsilon_m = \frac{K_C I_0}{J_m \omega_0^2 \theta_0}, \quad \varepsilon_e = \frac{K_C \theta_0}{L I_0}, \tag{13}$$

$$u(t) = \frac{E(t)}{L\omega_0 I_0}, \quad \lambda_e = \frac{R}{L\omega_0}, \quad \Omega = \frac{\omega}{\omega_0}.$$

The values of the physical parameters are given in Table 1.

Table 1. Values of the physical parameters of the electromechanical system.

Physical Parameter	Value	Physical Parameter	Value
l	variable	L_m	92×10^{-2} H
R	11.25 cm	K_C	42×10^{-3} Nm/A
m	16.80 g	β_m	0.50×10^{-3} Ns
m_0	2.50 g	θ_0	2π
q_1	20.46 Am	ω_0	$50\,\text{rad} \cdot \text{s}^{-1}$
q^2	43.76 Am	I_0	1 A
R_m	10.71 Ω		

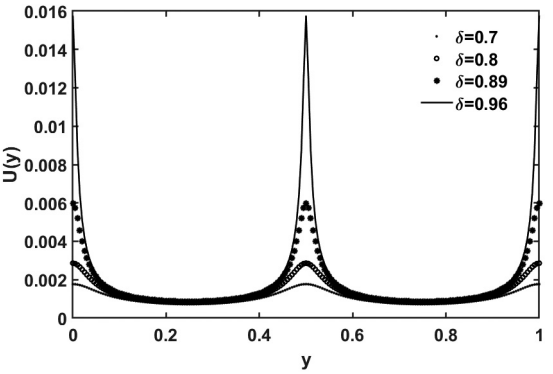

(a)

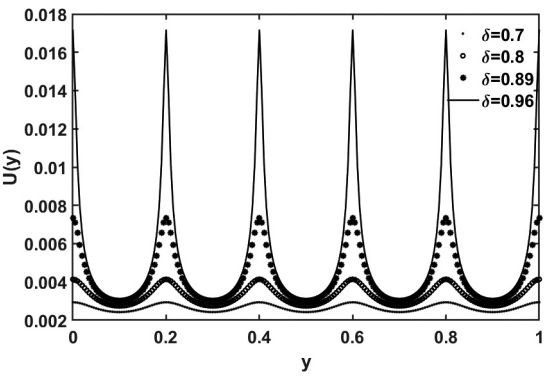

(b)

Fig. 2. Potential energy of the system versus the angular displacement: (a) for $N = 2$ magnets and (b) for $N = 5$ magnets.

2.3. *Potential energy*

The potential energy associated with the system of Eq. (6) is:

$$U = \gamma \sum_{k=0}^{N-1} \frac{1}{[1 + \delta^2 - 2\delta \cos(\theta - 2k\phi)]^{\frac{1}{2}}}. \tag{14}$$

Figure 2 presents some potential curves for different values of the parameter δ and the number of magnets N. These curves have been plotted for one period ($y = 1$) and for $N = 2$ magnets and $N = 5$ magnets. It shows two wells for $N = 2$ and five wells for $N = 5$. The stable equilibrium points are between two consecutive magnets. We also notice that the depth of the wells increases with the parameter δ.

3. Numerical Simulation

An important phenomenon to investigate is to find the condition for which the arm can cross

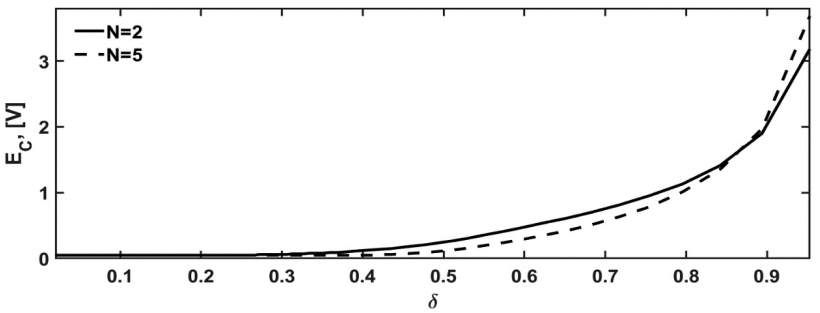

Fig. 3. Critical value of the voltage for complete rotation versus the parameter δ.

the potential barrier and undergo large amplitude motion leading, for instance, to complete rotation. For this purpose, we look for the critical value E_c of the external amplitude voltage above which complete rotation takes place. Two different forms of input signal have been considered: DC and AC voltage sources. The condition for complete rotation is written as follows $y_{\max} > 1$. The fourth order Runge–Kutta method is used to solve the differential Eqs. (10) and (11).

3.1. *Critical values in DC voltage case*

3.1.1. *Effects of the dimensionless length δ*

Figure 3 presents the critical voltage values versus the dimensionless length for $N = 2$ magnets (solid line) and $N = 5$ magnets (dotted line). One finds that E_c increases with the arm length. In the interval [0; 0.27], one needs the same energy to perform a complete rotation for both numbers of magnets. But in the interval [0.27; 0.88], more energy is required for two magnets while for the interval [0.88; 0.96], less energy is required for two magnets than for five magnets.

3.1.2. *Effects of the number of magnets N*

We have also analyzed the effects of the number of magnets on the critical voltage. As shown in Fig. 4, the voltage required to make a complete rotation is larger for $\delta = 0.96$ than for $\delta = 0.80$. This is due to the fact that for large values of δ, the repulsive forces are more accentuated and therefore more energy is needed to perform a full turn. In addition, for $\delta = 0.80$, we note a decrease of this voltage with the number of magnets while for $\delta = 0.96$, it increases until reaching a maximum value at $N = 5$ then decreases with N.

When complete rotation takes place, the arm rotation velocity shows a sort of NT-periodic oscillations where N is the number of magnets (see Fig. 5). This reflects the different accelerations produced by the repulsion created by the fixed magnets as they approach the magnet attached to the arm end.

3.2. *Critical values in the AC voltage case*

This subsection is devoted to find the condition for complete rotation when the electromechanical system is powered by a sinusoidal voltage.

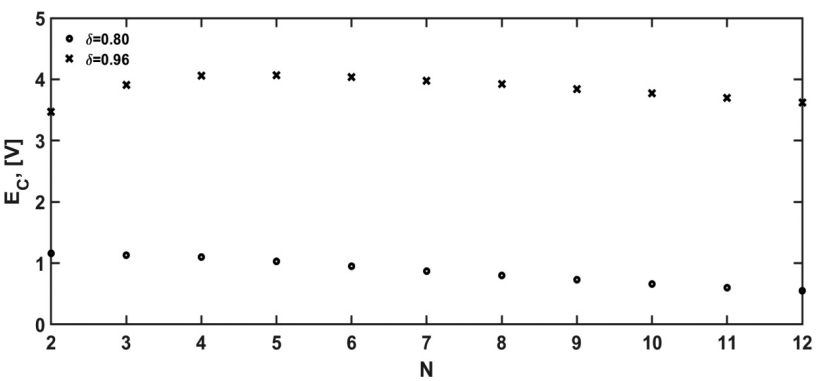

Fig. 4. Critical value of the voltage for complete rotation versus the number of magnets N.

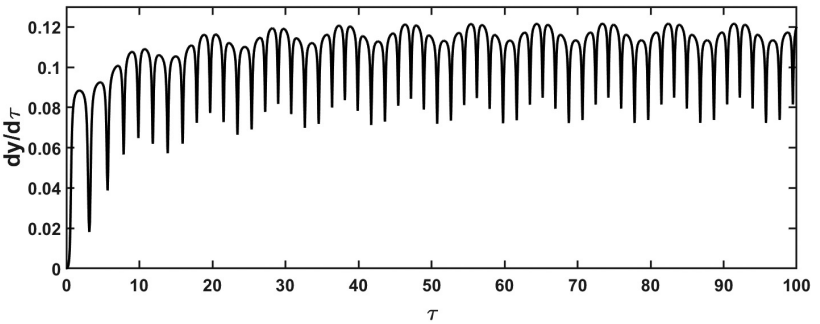

Fig. 5. Time-histories of the rotational velocity for $N = 5$ magnets, $\delta = 0.96$ when the arm performs complete rotation for $E = 4.5\,\mathrm{V}$.

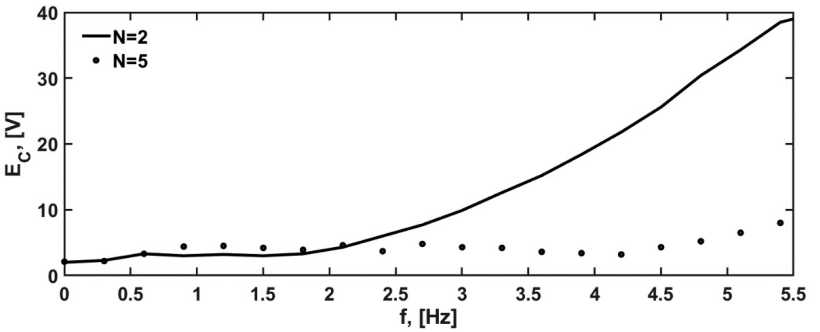

Fig. 6. Critical value of the sinusoidal voltage amplitude for complete rotation versus the frequency of the generator.

3.2.1. *Critical values versus the frequency of external voltage*

In Fig. 6, the critical values of the amplitude of the sinusoidal voltage is plotted versus its frequency for two and five magnets. When the frequency lies between 0.1 Hz and 0.6 Hz, the critical values are the same. But, much more voltage amplitude is needed in the range 0.6 Hz to 2.2 for $N = 5$ magnets than for $N = 2$ magnets. As the excitation frequency is increased more, the critical voltage amplitude is less for $N = 5$ magnets than for $N = 2$ magnets.

In order to confirm the curves displayed in Fig. 6, the time-histories of the angular displacement of the arm have been presented for two points belonging to the two regions separated by the curve (case for $N = 2$ magnets) (Fig. 7). The arm angular displacement presents oscillations with amplitude less than 1 for the region under the curve and greater than 1 for the region above the curve.

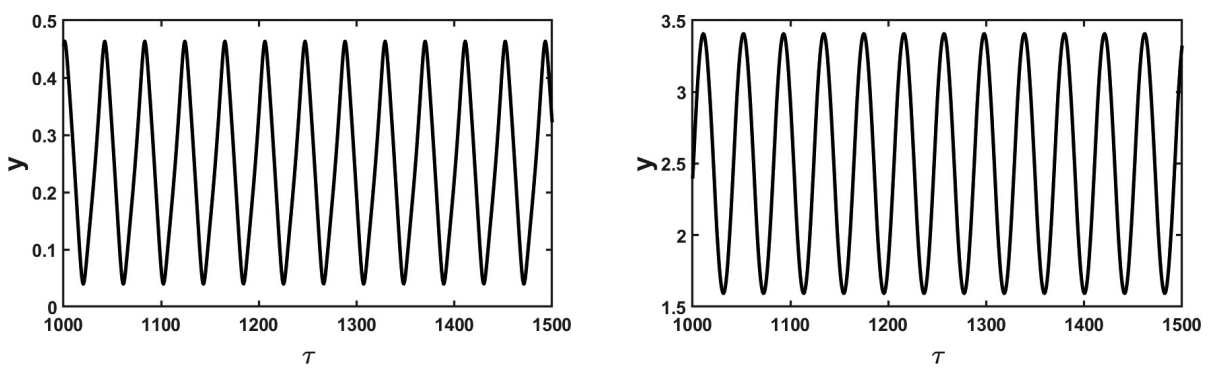

(a) (b)

Fig. 7. Time-histories of the angular displacement for $N = 2$ magnets. (a) For an input voltage lower than the critical value ($E_m = 4.5\,\mathrm{V}$) and (b) for an input voltage higher than the critical value ($E_m = 5\,\mathrm{V}$) and for $f = 1.2\,\mathrm{Hz}$.

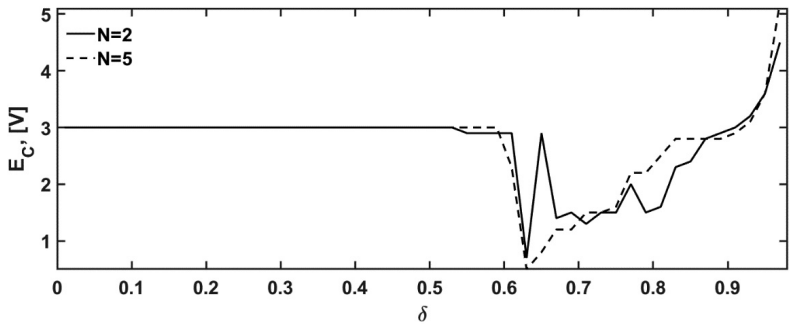

Fig. 8. Critical value of the amplitude of the sinusoidal voltage for complete rotation versus the parameter δ.

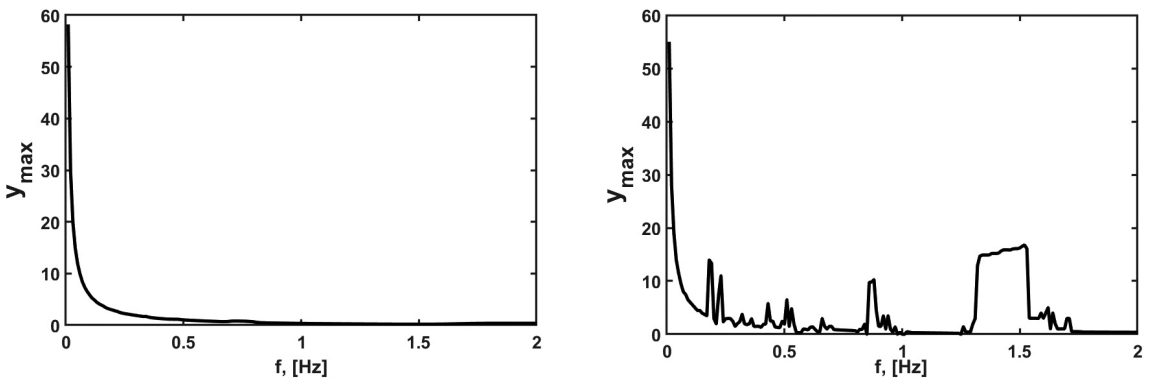

(a) (b)

Fig. 9. Maximum amplitude of the rotation angle versus the frequency of the sinusoidal voltage for $E = 3\,\mathrm{V}$, (a) for $\delta = 0.3$ and (b) for $\delta = 0.8$.

3.2.2. *Critical values versus the dimensionless length δ*

Figure 8 presents the critical value of the sinusoidal voltage amplitude when the arm length varies. One finds the same critical values for the dimensionless length belonging to the interval [0; 0.55] for two and five magnets. But, in the range [0.55; 0.98], one obtains an alternation between the two curves. Furthermore, abrupt drops are observed at $\delta = 0.53$ for $N = 2$ and at $\delta = 0.61$ for $N = 5$. This can be justified by the presence of several resonance peaks in the system for large values of δ as it can be seen in Fig. 9 which presents the oscillation amplitude versus the frequency.

3.2.3. *Critical amplitude of voltage versus the number of magnets*

As in the case of DC current, the critical voltages are higher for $\delta = 0.96$. For $\delta = 0.96$, this critical voltages are constant as the number of magnets varies while for $\delta = 0.80$, it increases and reaches a maximum at $N = 6$. Then, it decreases to reach its

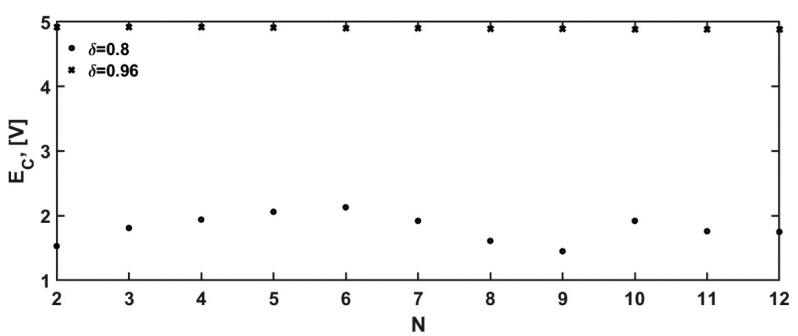

Fig. 10. Critical value of the amplitude of the sinusoidal voltage for complete rotation versus the number of magnets N.

minimum at $N = 9$. Thereafter, it takes another relative maximal value at $N = 10$ and then decreases with the number of magnets (see Fig. 10).

4. Bifurcation Diagrams and Lyapunov Exponents

To fully characterize the dynamical behaviors of the systems, the bifurcation diagrams and Lyapunov exponents are plotted both for DC and AC voltage sources. The value $\delta = 0.83$ is used. It corresponds to the arm length $l = 9.3\,\text{cm}$ which is used later for the experimental investigation.

4.1. *Bifurcation diagram in case of the DC voltage source*

Figure 11 shows that by varying the value of the DC voltage, two types of behaviors occur. The first one corresponds to the state where there is no oscillation or no motion. After a transient motion, the system evolves to a fixed state where the current and angular velocities are equal to 0 while the angular displacement attains a fixed value depending on the initial conditions. The second type of motion corresponds to the state where the angular displacement increases continuously as a function of time while the angular velocity oscillates around a fixed non null value. The transition between these two dynamics is observed at $E = 1.98\,\text{V}$ for $N = 2$ magnets and at $E = 2.07\,\text{V}$ for $N = 5$ magnets. These values represent the critical voltages for complete rotation at the corresponding numbers of magnets.

4.2. *Bifurcation diagram in case of the AC voltage source*

4.2.1. *Bifurcation diagram versus the amplitude E_m of the AC voltage*

First, we have plotted the bifurcation diagram of the mechanical displacement y versus the amplitude

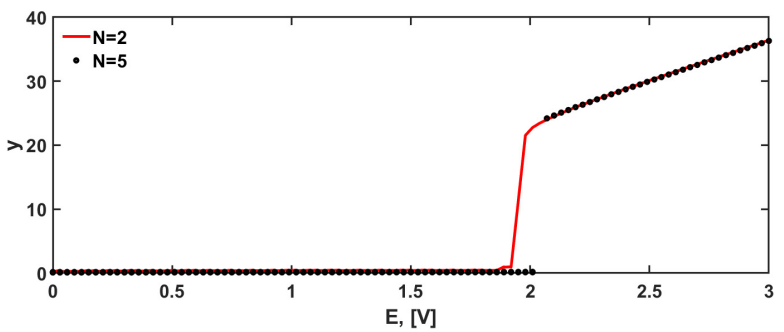

Fig. 11. Bifurcation diagram versus the DC voltage E when there are two magnets (full line) and five magnets (line with large dots).

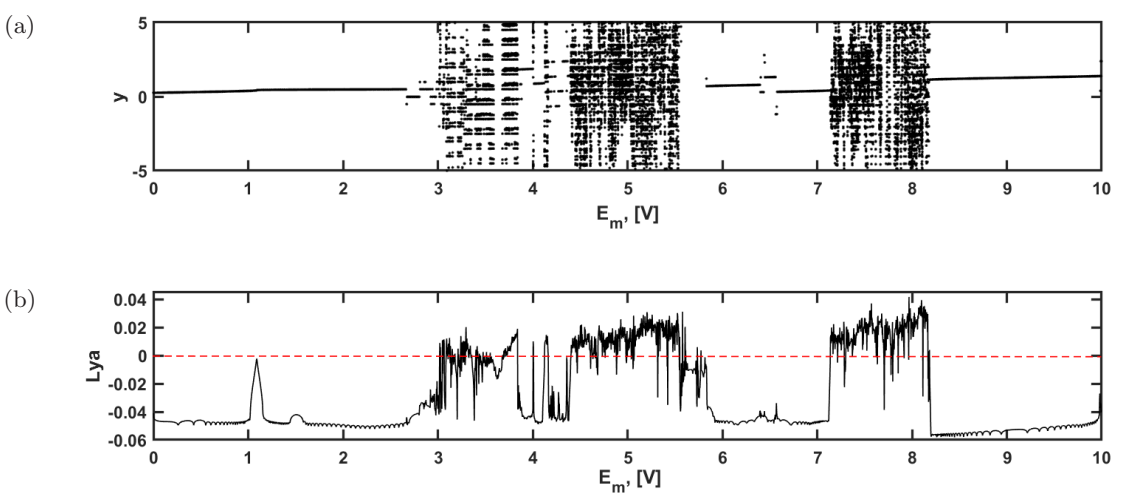

Fig. 12. (a) Bifurcation diagram and (b) variation of the Lyapunov exponent, both as function of the amplitude of the external generator E_m for $f = 1.2\,\text{Hz}$ and $N = 2$ magnets.

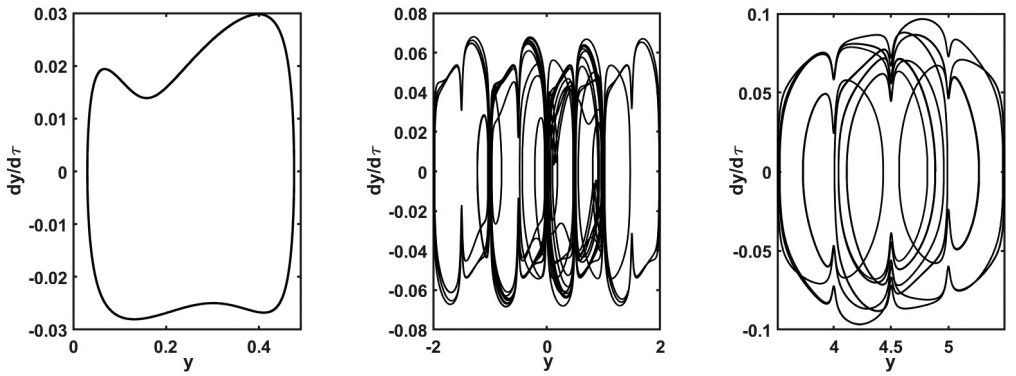

(a) (b) (c)

Fig. 13. Phase portraits of the mechanical subsystem when $f = 1.2\,\text{Hz}$ and $N = 2$ magnets; (a) $E_m = 2.0\,\text{V}$, (b) $E_m = 3.1\,\text{V}$ and (c) $E_m = 5.0\,\text{V}$.

E_m of the sinusoidal voltage source for $f = 1.2\,\text{Hz}$. The diagram for $N = 2$ magnets is presented in Fig. 12(a) while Fig. 12(b) presents the corresponding Lyapunov exponent. Periodic motion starts when $E_m = 0.1\,\text{V}$ and continues until 2.9 V. With the amplitude between 2.9 and 5.8 V, the system response exhibits an alternation of periodic and chaotic motions. The system response comes into a periodic motion when the amplitude lies between 5.8 and 7.2 V, and returns to an alternation of periodic and chaotic motions when $7.8\,\text{V} \leq E_m \leq 8.2\,\text{V}$. As the excitation amplitude increases further, the system undergoes periodic oscillation. Some examples of phase portraits are plotted in Fig. 13.

For $N = 5$ magnets, the dynamical response is almost the same (see Fig. 14). But here, chaos occurs for higher values of the voltage amplitude.

4.2.2. *Bifurcation diagram versus the frequency f of the AC voltage*

Now considering the frequency as the control parameter, the amplitude of the external source is kept constant at $E_m = 5.0\,\text{V}$. Figure 15 presents the bifurcation diagram of the arm displacement y for $N = 2$ magnets for $0.1\,\text{Hz} \leq f \leq 5\,\text{Hz}$. Periodic and chaotic oscillations are also present as the frequency varies. As in the case of the bifurcation

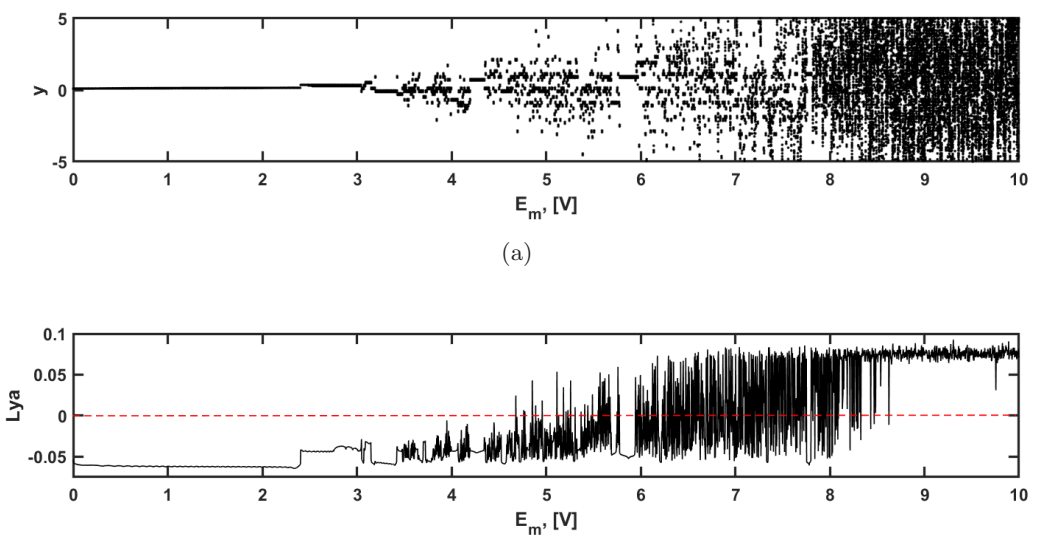

(a)

(b)

Fig. 14. (a) Bifurcation diagram as function of the amplitude of the external generator E_m for $f = 1.2\,\text{Hz}$ and $N = 5$ magnets and (b) the corresponding variation of the Lyapunov exponent.

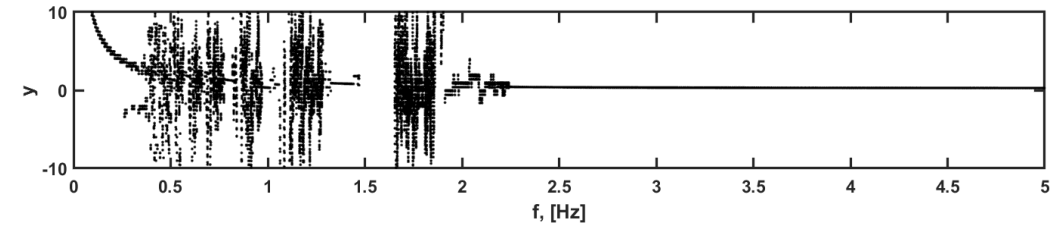

(a)

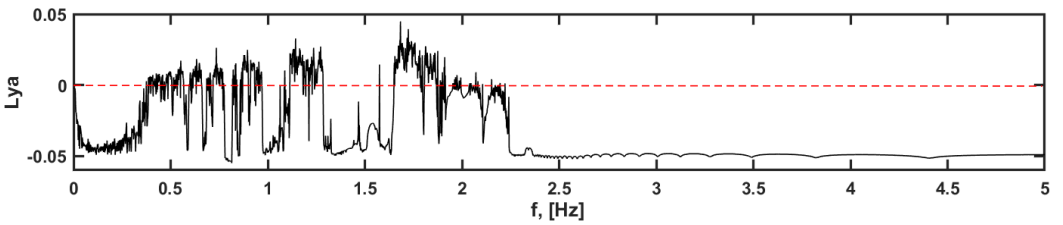

(b)

Fig. 15. (a) Bifurcation diagram and (b) the corresponding Lyapunov exponent as function of the excitation frequency f for $E_m = 5.0\,\mathrm{V}$ and $N = 2$ magnets.

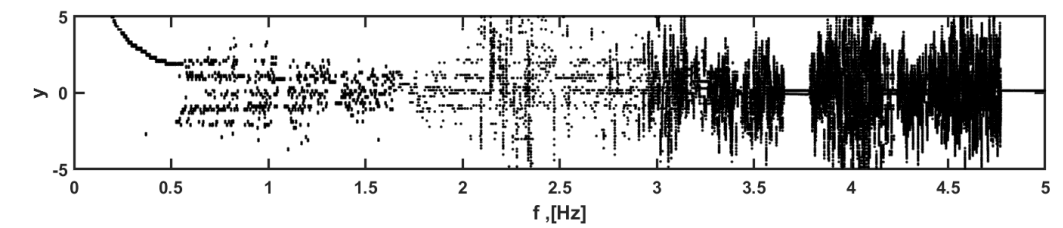

(a)

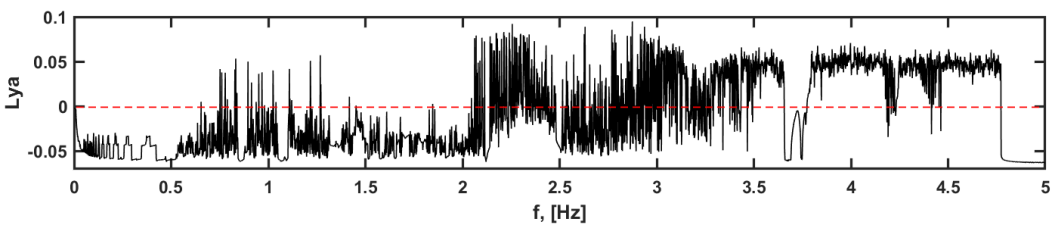

(b)

Fig. 16. (a) Bifurcation diagram and (b) the corresponding Lyapunov exponent as function of the excitation frequency f for $E_m = 5.0\,\mathrm{V}$ and $N = 5$ magnets.

diagram versus the voltage amplitude, the chaotic behavior, for $N = 5$ magnets, starts for higher values of the frequency (Fig. 16).

5. Experiment

5.1. *Experimental setup*

Figure 17 displays the experimental setup of the physical model described and studied theoretically in the previous sections. A voltage generator powers a low-power DC motor. The motor shaft supports a rigid iron rod which moves in the horizontal plane. The results of the experiment are presented only in the case of the system powered by the low frequency generator.

At the end of the arm, a neodymium magnet is fixed and interacts with two other magnets symmetrically positioned on a circle. The time,

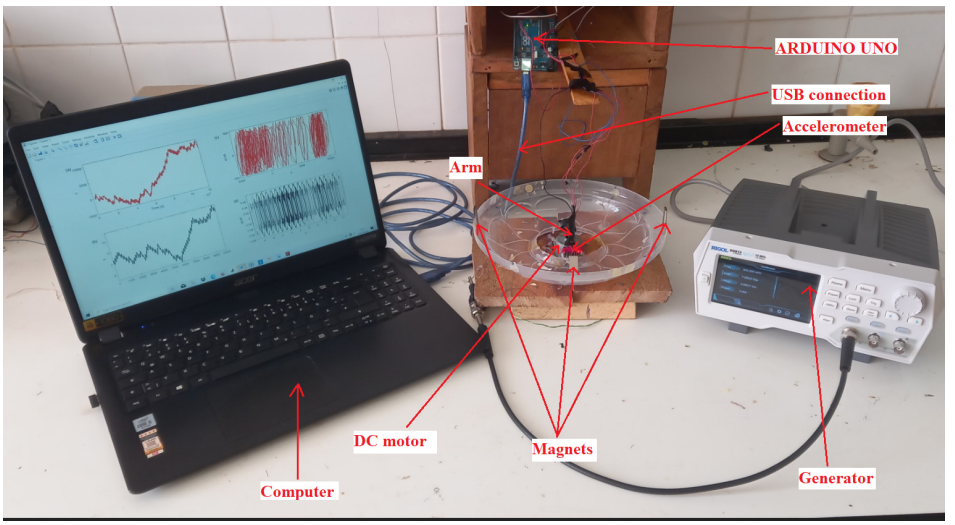

Fig. 17. Experimental setup.

the angle and the angular velocity are recorded in the computer using an accelerometer MPU 6050 through an ARDUINO UNO microcontroller.

5.2. *Experimental versus numerical results*

Figure 18 compares the experimental and numerical results in terms of time-histories and phase portraits when the amplitude of the external excitation is $E_m = 1.92\,\mathrm{V}$ and the frequency is $f = 1.2\,\mathrm{Hz}$. As it appears, the system leads to regular dynamics. The coincidence of the numerical and experimental results is clearly visible. The same agreement is visible in Figs. 19 and 20 where chaotic behaviors are presented. Let us however mention that the agreement here should be understood considering the shapes of the responses instead of considering

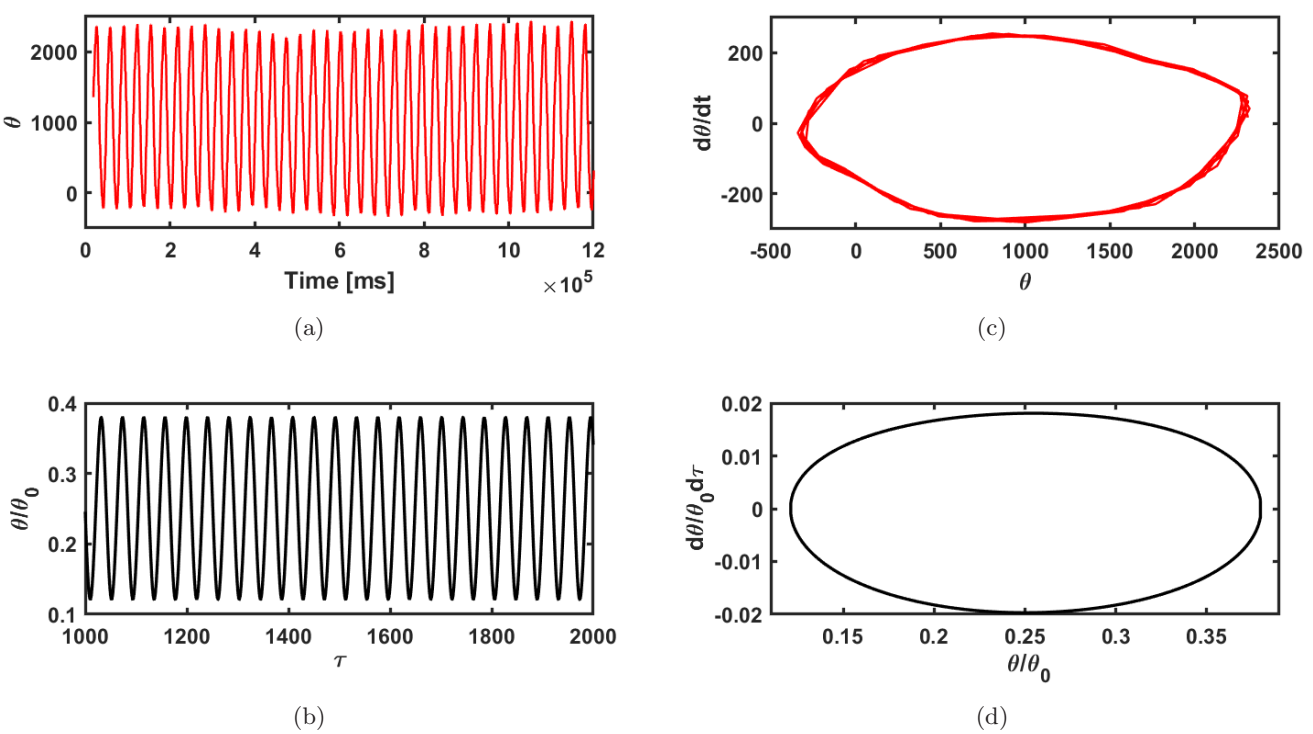

Fig. 18. Time-histories of the mechanical response and phase portraits (a), (c) experimentally obtained and (b), (d) numerical simulation results for $E_m = 1.92\,\mathrm{V}$, $f = 1.2\,\mathrm{Hz}$ and $N = 2$ magnets.

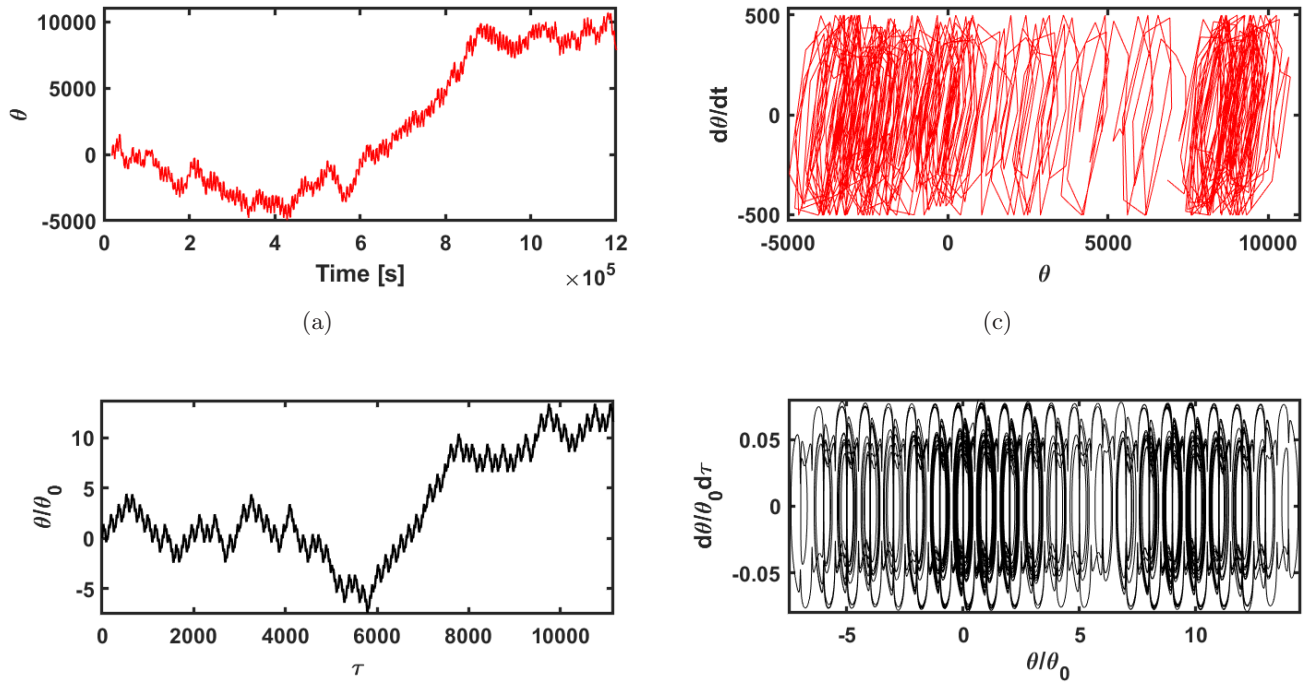

(a) (c) (b) (d)

Fig. 19. Time-histories of the mechanical response and phase portraits (a), (c) experimentally obtained and (b), (d) numerical simulation results for $E_m = 4.0\,\mathrm{V}$, $f = 1.2\,\mathrm{Hz}$ and $N = 2$ magnets.

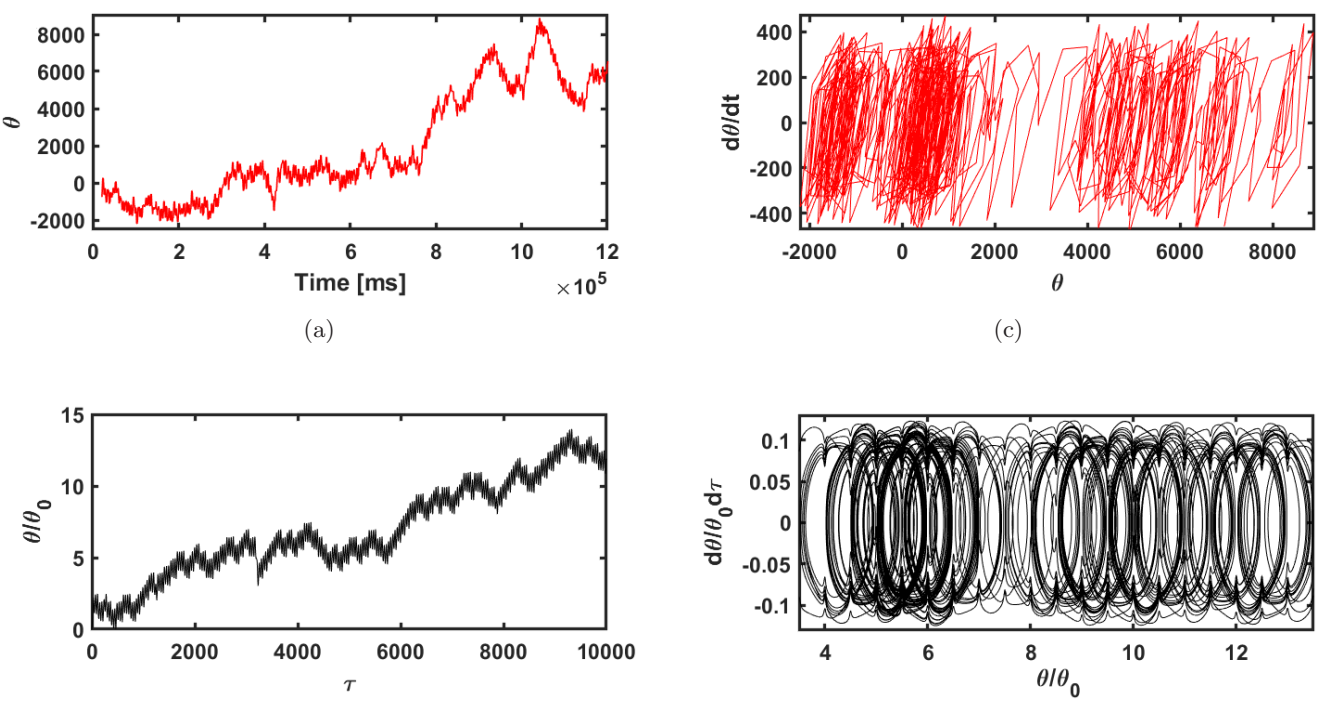

(a) (c) (b) (d)

Fig. 20. Time-histories of the mechanical response and phase portraits (a), (c) experimentally obtained and (b), (d) numerical simulation results for $E_m = 7.2\,\mathrm{V}$, $f = 1.2\,\mathrm{Hz}$ and $N = 2$ magnets.

the amplitudes of the responses since some differences are observed because of the difficulty of measuring the exact values of some physical parameters.

6. Conclusion

This paper has considered the dynamics of a rotating electromechanical arm subjected to nonlinear magnetic torques due to a series of magnets aligned periodically along a circle in front of which a rigid arm fixed on a motor axis rotates with another magnet at its end. The magnetic potential energy curves were presented displaying the number of wells equivalent to the number of magnets. The critical voltage for which the mechanical arm undergoes a complete rotation was determined for the DC and AC input voltages. The results have shown that, for a DC voltage lower than the critical value, the mechanical arm undergoes damped oscillations and then stabilizes at an equilibrium position. When the voltage is above the critical value, the arm displacement increases continuously with time (performing complete rotation) while the angular velocity oscillates showing frequency proportional to the number of magnets. When the motor is powered by a sinusoidal voltage, the arm displays angular oscillations with amplitude larger than one turn for large values of the voltage amplitude. The regions of chaotic and periodic motions were obtained through the bifurcation diagrams and the corresponding Lyapunov exponent. The theoretical results have been confirmed by an experiment conducted on a setup constructed in the laboratory. The model considered in this work can be used to mechanically study some phenomena encountered in condensed matter physics such as a particle moving in periodic potential with variable shape and in the study of the resistively capacitance shunted Josephson junctions [McCumber, 1968].

Acknowledgment

This work has been supported by the Polish National Science Centre, Poland under the Grant OPUS 18 No. 2019/35/B/ ST8/00980.

References

Akinlar, M. A., Tchier, F. & Inc, M. [2020] "Chaos control and solutions of fractional-order Malkus waterwheel model," *Chaos Solit. Fract.* **135**, 109746.

Ana, R. K., José, M. B., Jorge, L. P. & Fábio, R. C. [2010] "The nonlinear dynamics of a vibrating systemmodeled by an inverted pendulum, with an electrodynamics shaker," *Conf. Dynamics, Control and Their Applications*, Brazil, 7–11 June 2010.

Awrejcewicz, J., Supe, B., Kudra, G., Wasilewski, G. & Olejnik, P. [2008] "Numerical and experimental study of regular and chaotic motion of triple physical pendulum," *Int. J. Bifurcation and Chaos* **18**, 2883–2915.

Belato, D., Weber, H. I., Balthazar, J. M. & Mook, D. T. [2001] "Chaotic vibrations of a nonideal electromechanical system," *Int. J. Solids Struct.* **38**, 1699–1706.

Chatterjee, M., Mohamed, A. & Almehmadi, F. [2018] "Secure freespace communication, turbulence mitigation, and other applications using acousto-optic chaos," *Appl. Opt.* **57**, 1–13.

Ge, Z. M., Cheng, J. M. & Chen, Y. S. [2004] "Chaos anticontrol and synchronization of three time scales brushless DC motor system," *Chaos Solit. Fract.* **22**, 1165–1182.

Kakmeni, F., Bowong, S., Tchawoua, C. & Kaptouom, E. [2004] "Dynamics and chaos control in nonlinear electrostatic transducers," *Chaos Solit. Fract.* **21**, 1093–1108.

Kazmierczak, M., Kudra, G., Awrejcewicz, J. & Wasilewski, G. [2013] "Numerical and experimental investigation of bifurcational dynamics of an electromechanical system consisting of a physical pendulum and DC motor," *Dynamical Systems-Applications* (TU Lodz Press, Lodz), pp. 49–58.

Kazmierczak, M., Kudra, G., Awrejcewicz, J. & Wasilewski, G. [2015] "Mathematical modeling, numerical simulations and experimental verification of bifurcation dynamics of a pendulum driven by a DC motor," *Eur. J. Phys.* **36**, 1–13.

Kemajou, I., Nana, B. & Woafo, P. [2022] "Dynamics of the electromechanical sieve with hysteretic iron-core inductor," *Nonlin. Dyn.* **110**, 237–255.

Kitio, K. & Woafo, P. [2010] "Experimental realization and simulations a self-sustained macro electromechanical system," *Mech. Res. Commun.* **37**, 106–110.

Kouam Tagne, R. F., Tsapla Fotsa, R. & Woafo, P. [2021] "Dynamics of a DC motor-driving arm with a circular periodic potential and DC/AC voltage input," *Int. J. Bifurcation and Chaos* **31**, 2150178-1–132.

Kumar, G., Kumar, T., Kumar, M. & Shovan, B. [2017] "Observer design for semilinear descriptor systems with applications to chaos-based secure communication," *Int. J. Appl. Comput. Math.* **3**, 1313–1324.

Mahmoud, E. E., Trikha, P., Jahanzaib, L. S. & Almaghrabi, O. A. [2020] "Dynamical analysis and chaos control of the fractional chaotic ecological model," *Chaos Solit. Fract.* **141**, 110348.

McCumber, D. E. [1968] "Effect of AC Impedance on DC voltage–current characteristics of superconductor weak-link junctions," *J. Appl. Phys.* **39**, 3113–3118.

Moon, F. C., Cusumano, J. & Holmes, P. J. [1993] "Evidence for homoclinic orbits as a precursor to chaos in a magnetic pendulum," *Physica D* **24**, 383–390.

Nana, B., Yamgoué, S. B., Tchitnga, R. & Woafo, P. [2017] "Dynamics of a pendulum driven by a DC motor and magnetically controlled," *Chaos Solit. Fract.* **104**, 18–27.

Nana, B., Yamgoué, S. B., Tchitnga, R. & Woafo, P. [2018] "Nonlinear dynamics of a sinusoidally driven lever in repulsive magnetic fields," *Nonlin. Dyn.* **91**, 55–66.

Nana Nbendjo, B. R. & Woafo, P. [2007] "Active control with delay of horseshoes chaos using piezoelectric absorber on a buckled beam under parametric excitation," *Chaos Solit. Fract.* **32**, 73–79.

Polczynski, K., Wijata, A., Awrejcewicz, J. & Wasilewski, G. [2019] "Numerical and experimental study of dynamics of two pendulums under a magnetic field," *J. Syst. Contr. Engin.* **233**, 441–453.

Polczynski, K., Skurativskyi, S., Bednarek, M. & Awrejcewicz, J. [2021] "Nonlinear oscillations of coupled pendulums subjected to an external magnetic stimulus," *Mech. Syst. Sign. Process.* **154**, 107560.

Rajagopal, K., Vaidyanathan, S., Karthikeyan, A. & Duraisamy, P. [2017] "Dynamic analysis and chaos suppression in a fractional order brushless DC motor," *Electr. Engin.* **99**, 721–733.

Shaohua, L., Huanhuan, M., Fengyun, L. & Hassen, M. O. [2022] "Dynamical analysis and chaos control of MEMS resonators by using the analog circuit," *Nonlin. Dyn.* **108**, 97–112.

Skurativskyi, S., Polczyński, K., Wojna, M. & Awrejcewicz, J. [2022] "Quantifying periodic, multiperiodic, hidden and unstable regimes of a magnetic pendulum via semi-analytical, numerical and experimental methods," *J. Sound Vib.* **524**, 116710.

Tcheutchoua, F. D. O. & Woafo, P. [2013] "Generation of complex phenomena in a simple electromechanical system using the feedback control," *Commun. Nonlin. Sci. Numer. Simulat.* **18**, 209–218.

Tesso, P. C. W., Kouam Tagne, R. & Woafo, P. [2022] "Energy harvesting from a micro-system with circular bistable potential due to magnets," *Int. J. Bifurcation and Chaos* **32**, 2250039-1–16.

Tsapla Fotsa, R. & Woafo, P. [2016] "Chaos in a new bistable rotating electromechanical system," *Chaos Solit. Fract.* **93**, 48–57.

Wijata, A., Polczynski, K. & Awrejcewicz, J. [2021] "Theoretical and numerical analysis of regular one-side oscillations in a single pendulum system driven by a magnetic field," *Mech. Syst. Sign. Process.* **150**, 107229.

Wojna, M., Wijata, A., Wasilewski, G. & Awrejcewicz, J. [2018] "Numerical and experimental study of a double physical pendulum with magnetic interaction," *J. Sound Vib.* **430**, 214–230.

Xizhe, Z., Sajid, I.,Yanhe, Z., Xinyu, L. & Jie, Z. [2017] "Applications of chaotic dynamics in robotics," *Int. J. Adv. Robot. Syst.* **13**, 1–7.

Yamapi, R., Nana Nbendjo, B. R. & Enjieu Kadji, H. G. [2007] "Dynamics and active control of motion of a driven multi-limit-cycle van der Pol oscillator," *Int. J. Bifurcation and Chaos* **17**, 1343–1354.

Zhu, Q. & Ishitobi, M. [1999] "Experimental study of chaos in a driven triple pendulum," *J. Sound Vib.* **227**, 230–238.

International Journal of Bifurcation and Chaos, Vol. 31, No. 12 (2021) 2150178 (19 pages)

DOI: 10.1142/S0218127421501789

Dynamics of a DC Motor-Driving Arm with a Circular Periodic Potential and DC/AC Voltage Input

R. F. Kouam Tagne*, R. Tsapla Fotsa†,‡ and P. Woafo*
*Laboratory of Modelling and Simulation in Engineering, Biomimetics and Prototypes, Faculty of Science, University of Yaoundé I, P. O. Box 812, Yaoundé-Cameroon
†Mechanical Engineering Department, College of Technology, University of Buea, P. O. Box 63 Buea, South West Region, Republic of Cameroon
‡rtsapla@yahoo.com

Received December 11, 2020; Revised May 17, 2021

In this paper, we investigate the dynamics of an electromechanical system consisting of a DC motor-driving arm within a circular periodic potential created by three permanent magnets. Two configurations of the circular potential appear when one varies the positions of the magnets and the length of the DC motor, respectively. Two different forms of input signal are used: DC and AC voltage sources. For each case, conditions under which the mechanical arm can perform a complete rotation are obtained. Under the DC voltage excitation, the arm oscillates and then is stabilized at an equilibrium position for a DC voltage lower than a critical value E_C. When the DC voltage is higher than the critical value E_C, the arm performs large amplitude motions (complete rotation). Submitted to an AC voltage with amplitude lower than a critical value, the mechanical arm exhibits sinusoidal oscillations around the equilibrium position 0 with amplitudes less than one turn. Angular oscillations with amplitudes greater than one turn are observed when the voltage amplitude is higher than the critical value. Bifurcation diagrams show that the simple system can enter chaotic regime with the amplitudes of angular oscillations varying erratically from small to high values.

Keywords: DC motor arm; chaos; bifurcation; circular potential; magnet.

1. Introduction

Electromechanics is an interdisciplinary research area at the interface of mechanics and electricity. It crosses traditional engineering boundaries. In recent years, considerable efforts have been devoted to the investigation of electromechanical machines, which can help and assist humans in their daily activities and keep everyone safe through several types of motions such as translational, pendulum and rotary motions or the combination of two of these types of motions. [Moon *et al.*, 1993; Lyshevski, 2009; Zhu & Ishitobi, 1999; Jang & Jeon, 2000; Gao & Chau, 2002; Haan, 2006; Yamapi, 2006; Johan, 2005; Kitio Kwuimy & Woafo, 2007; Yamapi & Woafo, 2008; Kitio Kwuimy & Woafo, 2008; Awrejcewicz *et al.*, 2008; Aline & Marcelo, 2009; Yang & Jing, 2009; Kazmierczak *et al.*, 2013; Tcheutchoua Fossi & Woafo, 2013; Avanço *et al.*, 2014; Lin & Xuemei, 2014; Notué & Woafo, 2014; Kazmierczak *et al.*, 2015; Coronel *et al.*, 2016;

‡Author for correspondence

Tsapla & Woafo, 2016; Nana *et al.*, 2017, 2018; Wojna *et al.*, 2018].

Among several types of actuation principles or components, electrical motors have gained particular attention [Chen *et al.*, 2020; Singh *et al.*, 2019; Qi & Hu, 2017; Ge *et al.*, 2004; Ge & Cheng, 2005; Diyi *et al.*, 2012; Tsapla & Woafo, 2016; Nana *et al.*, 2017]. They are used to actuate mechanical arms leading to several types of dynamical behaviors such as constant rotational speed, oscillations and chaos.

In [Nana *et al.*, 2017], the authors conducted theoretical and experimental investigations of an electromechanical system consisting of an horizontal lever fixed at the axis of a DC motor with the ends of the lever submitted to the repulsive forces of two magnets placed symmetrically. Because of the nonlinear potential generated by the magnets, several types of nonlinear phenomena were observed such as hysteresis, jump and chaos. The study has been extended considering a vertical lever [Nana *et al.*, 2018], and the authors also demonstrated theoretically and experimentally the generation of different nonlinear phenomena when the physical parameters are suitably chosen.

Thanks to the different potential energy configurations generated by the magnets placed in an appropriate manner, and the types of dynamical states generated because of the magnets presence and their possible applications (for instance, in sieving processes), it is of special interest to extend the use of magnets in other electromechanical systems. In this paper, we consider an horizontal mechanical arm fixed on a DC motor axis and which can thus rotate with the motor axis. But, unlike the classical configuration in which the arm can undergo simple rotation, two magnets are disposed symmetrical around the circular trajectory so that the arm is subjected to a circular and periodic potential energy inside which it rotates. The dynamical behaviors are analyzed considering first the motor powered by a DC voltage and then powered by an AC voltage. An image of this system can be seen as that of a particle moving inside a periodic potential and submitted to the action of constant force or to that of a sinusoidal force. This image is well known in the context of particle diffusion in atomic lattices or on metallic surfaces [Gomer, 1990; Braum & Kivshar, 1998; Woafo *et al.*, 1997].

The paper is organized as follows. Section 2 deals with the modeling of the DC motor arm in a circular potential and its mathematical and numerical analyses when a DC voltage powers the system. Section 3 considers the dynamics when the system is submitted to the action of an AC voltage and comes out with different dynamical behaviors and bifurcation diagrams. Section 4 concludes this paper.

2. DC Motor Arm in a Circular Periodic Potential Submitted to a Constant Voltage Source

2.1. *Creation of the circular periodic potential*

2.1.1. *The system*

The system considered in this paper is shown in Fig. 1(a). It consists of three main parts. The first part is a DC motor understood as a device converting the electrical energy to the mechanical one. The electrical motor is with permanent magnet, resistance R_i and inductance L_i. The rotor has two windings: one with the blue cable carries electrical current to produce a mechanical torque while the winding with purple cable is used to measure the back electromotive force (f.e.m) in case of experiment. The f.e.m is related to the rotation velocity of the mechanical arm. The second part is a one-degree of freedom mechanical arm welded to the shaft of the electrical motor. The third part consists of three permanent and identical magnets located at points M, A and B [see Fig. 1(b)]. The magnets A and B produce magnetic forces ($\mathbf{F}_{A/M}, \mathbf{F}_{B/M}$) on magnet M. The positions of the magnets A and B are measured by the angle ϕ made by the lines OA and OB with the horizontal line. The only damping force that the model contains is inside the motor and it is characterized by a simple viscous damping function. Since the arm is undergoing horizontal motions, the effect of the gravitational force is not included. The input voltage is provided either by a DC generator or by a low frequency generator and is represented by $u(t)$. The angular displacement of the mechanical arm is the coordinate $\theta(t)$ relative to a reference line (the horizontal line).

2.1.2. *Mathematical modeling*

Applying Kirchhoff's voltage laws to the electrical part of the DC motor, we find that the electric part of the model is described by the following

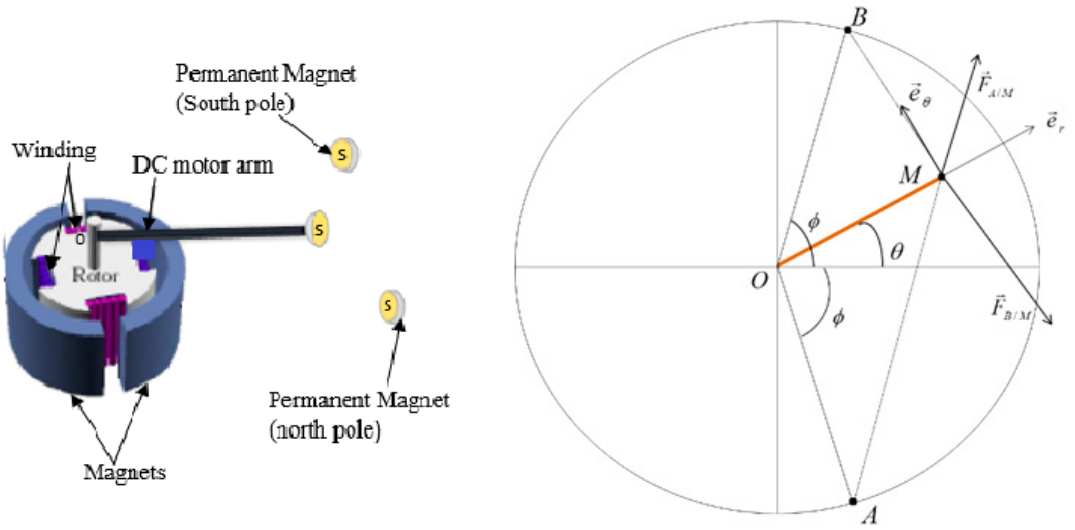

(a) (b)

Fig. 1. (a) Schematic representation of the DC motor arm and (b) geometric representation of the magnetic forces acting on DC motor arm (in red).

differential equation [Nana *et al.*, 2017]:

$$L_i\frac{di}{dt} + R_i i + e(t) = u(t) \tag{1}$$

$u(t)$ is the input voltage and i is the current through the winding. $e(t)$ is the back electromotive force. L_i, R_i and $e(t)$ are defined by the following expressions:

$$\begin{aligned} L_i &= \frac{\mu_0\mu_r N^2 hD}{l_g}; \quad R_i = \frac{8\varphi(h+D)N}{\pi d^2}; \\ e(t) &= hDB_m N\frac{d\theta}{dt}\cos\theta \end{aligned} \tag{2}$$

μ_0 is the permeability of the vacuum, h and D represent the height and diameter of the rotor respectively, B_m is the magnetic induction intensity and N is the number of turns.

Applying the Newton's second law of motion to the rotational motion, and taking into account the Laplace force, it is found that the mechanical part is governed by the following equation:

$$J_m\frac{d^2\theta}{dt^2} + \beta_m\frac{d\theta}{dt} + \frac{\mu_0 q_1 q_2}{4\pi R}f(\theta) = hDB_m N i, \tag{3}$$

where $J_m = (m_0 + \frac{m}{3})l^2$ is the total moment of inertia of the mechanical arm with the fixed magnet. m and l represent the mass and the length of the mechanical arm, respectively. m_0 is the mass of the magnet M. β_m is the damping coefficient, q_1 is the pole strength of the magnet M and q_2 is the pole strength of magnets A and B. R is the distance between the focus O and the position of fixed magnets. The nonlinear function $f(\theta)$ comes from the repulsive interactions between magnets and is expressed as:

$$\begin{aligned} f(\theta) = &-\frac{\delta\sin(\theta+\phi)}{[1+\delta^2-2\delta\cos(\theta+\phi)]^{\frac{3}{2}}} \\ &-\frac{\delta\sin(\theta-\phi)}{[1+\delta^2-2\delta\cos(\theta-\phi)]^{\frac{3}{2}}}, \end{aligned} \tag{4}$$

where ϕ is the angle formed between the equilibrium position (horizontal line) and the position of a magnet and $\delta = \frac{l}{R}$ is the dimensionless length of the mechanical arm.

Let us introduce the following dimensionless variables:

$$x = \frac{i}{I_0}; \quad y = \frac{\theta}{\theta_0}; \quad \tau = \omega_0 t. \tag{5}$$

Equations (1) and (3) take the following dimensionless form:

$$\ddot{y} + \lambda_m\dot{y} + \gamma f(\theta_0 y) = \varepsilon_m x, \tag{6}$$

$$\dot{x} + \lambda_e x + \varepsilon_e\dot{y}\cos(\theta_0 y) = E(t), \tag{7}$$

where the dots refer to the derivative with respect to the dimensionless time τ given above. The nondimensional coefficients are defined as:

$$\lambda_m = \frac{\beta_m}{J_m\omega_0}; \quad \gamma = \frac{\mu_0 q_1 q_2}{4\pi R J_m\omega_0^2\theta_0};$$

Table 1. Values of the physical parameters of the electromechanical system.

Parameter	Value	Parameter	Value
B_m	0.73 T	N	20
μ_r	985	h	9.85 cm
d	0.15 mm	β_m	0.2×10^{-3} Ns
q_1	43.76 Am	m_0	16.67 g
q_2	43.76 Am	m	5.13 g
D	8.12 cm	I_0	1 A
l_g	5.0 mm	ω_0	$50\,\mathrm{rad}\cdot\mathrm{s}^{-1}$
φ	$1.72 \times 10^{-8}\,\Omega$m	R	15.96 cm

$$\varepsilon_m = \frac{hDB_mNI_0}{J_m\omega_0^2\theta_0}; \quad \varepsilon_e = \frac{hDB_mN\theta_0}{LI_0};$$
$$E(t) = \frac{u(t)}{L\omega_0 I_0}; \quad \lambda_e = \frac{R}{L\omega_0}. \tag{8}$$

The values of the physical and geometrical parameters used in this study are summarised in Table 1.

2.2. *Equilibrium points and their stability*

The potential energy associated with Eq. (3) is:

$$U(\theta) = \gamma\left[\frac{1}{[1+\delta^2-2\delta\cos(\theta+\phi)]^{\frac{1}{2}}} + \frac{1}{[1+\delta^2-2\delta\cos(\theta-\phi)]^{\frac{1}{2}}}\right]. \tag{9}$$

Using the Taylor expansion formula, the potential energy can be approximated by the following expression:

$$U(\theta) = \frac{\gamma}{\delta_1}\left[2 + \frac{A}{2}(2\cos(\theta)\cos(\phi)) + \frac{3A^2}{8}(1+\cos(2\phi)\cos(2\theta))\right], \tag{10}$$

where $\delta_1 = \sqrt{1+\delta^2}$ and $A = \frac{2\delta}{\delta_1^2}$.

The derivative of Eq. (10) is:

$$\frac{dU}{d\theta} = \frac{\gamma}{\delta_1}\left[-A\cos(\phi)\sin(\theta) - \frac{3A^2}{4}\cos(2\phi)\sin(2\theta)\right]. \tag{11}$$

By looking at the zeros of the derivative of the potential [Eq. (11)], one finds the following equilibrium points:

$$\begin{cases}\theta_1 = 0,\\ \theta_2 = \pi.\end{cases} \tag{12}$$

Let us calculate the second derivative of the potential at the points $\theta = 0$ and $\theta = \pi$.

One obtains

$$\frac{d^2U}{d\theta^2}(0) = \frac{2\gamma\delta}{(1+\delta^2-2\delta\cos(\phi))^{\frac{3}{2}}} \times\left[\frac{3\delta\sin^2(\phi)}{(1+\delta^2-2\delta\cos(\phi))} - \cos(\phi)\right], \tag{13}$$

$$\frac{d^2U}{d\theta^2}(\pi) = \frac{2\gamma\delta}{(1+\delta^2+2\delta\cos(\phi))^{\frac{3}{2}}} \times\left[\frac{3\delta\sin^2(\phi)}{(1+\delta^2+2\delta\cos(\phi))} + \cos(\phi)\right]. \tag{14}$$

A point is said to be stable if the second derivative is positive. Otherwise, it is unstable. From Eq. (13), one finds that depending on the $(\delta;\phi)$, $\theta = 0$ can be stable or unstable. It is stable (respectively unstable) under the following respective conditions

$$\frac{3\delta\sin^2(\phi)}{(1+\delta^2-2\delta\cos(\phi))} < \cos(\phi), \tag{15}$$

$$\frac{3\delta\sin^2(\phi)}{(1+\delta^2-2\delta\cos(\phi))} > \cos(\phi). \tag{16}$$

From Eq. (14), it appears that the point $\theta = \pi$ is unconditionally stable since the second derivative of the potential is positive. Figure 2 shows the potential energy configurations over two periods for two couples of parameters: $(\delta = 0.1; \phi = \frac{3\pi}{8})$ and $(\delta = 0.9; \phi = \frac{\pi}{8})$. These pairs of parameters meet the criteria (15) and (16), respectively. According to these shapes, the potential is 2π-periodic with the angular displacement. In the first configuration [Fig. 2(a)], the potential presents two equilibrium points: one unstable ($\theta = 0$) and one stable ($\theta = \pi$) (modulo 2π). The second configuration [Fig. 2(b)] shows four equilibrium points, among which two are stable ($\theta = 0$ and $\theta = \pi$) and two unstable at magnets' positions ($\theta = -\phi$ and $\theta = \phi$).

For small values of the parameter δ, the interactions between the magnets are weak, the dynamical

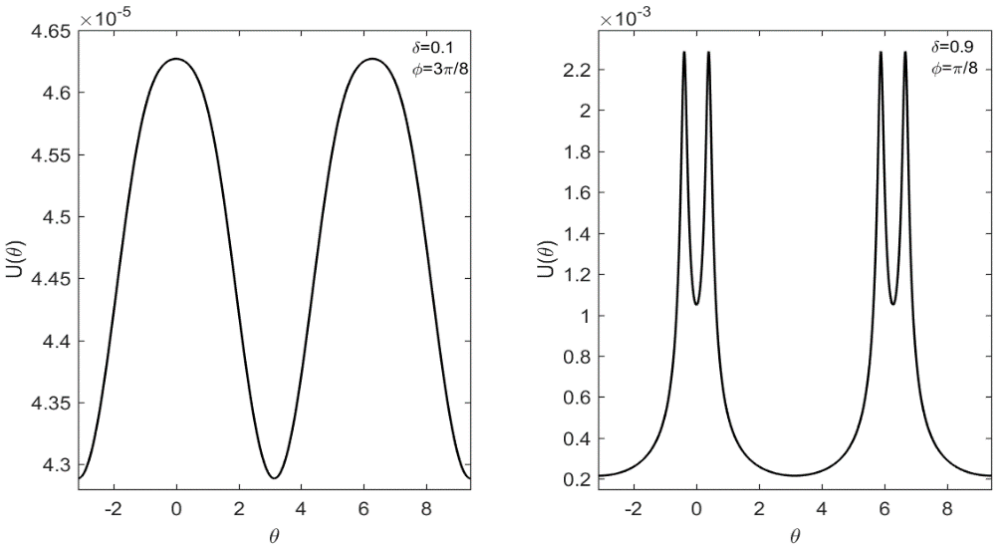

(a) (b)

Fig. 2. Different configurations of the potential energy.

behavior is less complex. Consequently, for the rest of the work, we consider the case where δ is high. Specifically, we use the couple $(\delta = 0.9; \phi = \frac{\pi}{8})$. The next section is dedicated to the response of the system when it is powered by a DC voltage source.

2.3. *Dynamical behavior under DC voltage source*

An important phenomenon to analyze in this case is to find out the condition for which the arm can mitigate the potential barrier and undergo large amplitude motion leading to complete rotation. For this purpose, we look for the critical value E_c of the DC potential above which a complete rotation takes place. Two subconfigurations of the potential are taken into account: The first for which the motion is around its stable focus $\theta = 0$ and the second, around its stable focus $\theta = \pi$. We carry out the numerical simulation with the initial condition $x = 0$; $y = 0$; $\dot{y} = 0$, in the first case and $x = 0$; $y = 0.5$; $\dot{y} = 0$, for the second. The fourth order Runge–Kutta method is used to solve the differential Eqs. (6) and (7). The condition for complete rotation is written as follows:

$$y_{\max} > 1. \tag{17}$$

With the parameters used here, the critical value above which complete rotation takes place is $E_c = 4.71077 \times 10^{-2}$ for the first configuration and $E_c = 7.5 \times 10^{-4}$ for the second configuration.

Figures 3 and 4 present the time histories of the current, angular displacement and rotational velocity for the two configurations when the DC voltage is lower than the critical value E_C. Figure 3 indicates that the current, angular displacement and rotational velocity oscillate and then stabilize at the dimensionless values $x = 0.266$; $y = 0.041$; $\dot{y} = 0$ respectively. In Fig. 4, as above, we observe that the current, angular displacement and rotational velocity oscillate and then stabilize at the dimensionless values $x = 4.188 \cdot 10^{-3}$; $y = 0.0$; $\dot{y} = 0$. This highlights the fact that these points represent the new equilibrium positions in the presence of the DC voltage.

The dynamical response of the system is also explored when the DC voltage is higher than the critical value E_C. Figure 5 presents the angular displacement and rotational velocity for dimensionless voltage equal to $E = 4.71076 \times 10^{-2}$. The current oscillates around the equilibrium point $x = 0.266$, the angular displacement increases with the time while the angular velocity starts to increase and then oscillates around a fixed value. Figure 6 shows that the current oscillates around the equilibrium value $x = 4.188 \times 10^{-3}$, and the angular displacement first increases slightly, then decreases after some time and finally increases to large values. The angular velocity oscillates around a constant value different to zero. Due to the nonlinearity, the angular displacement curves present small amplitude ripples due to the oscillating behavior of the rotation velocity.

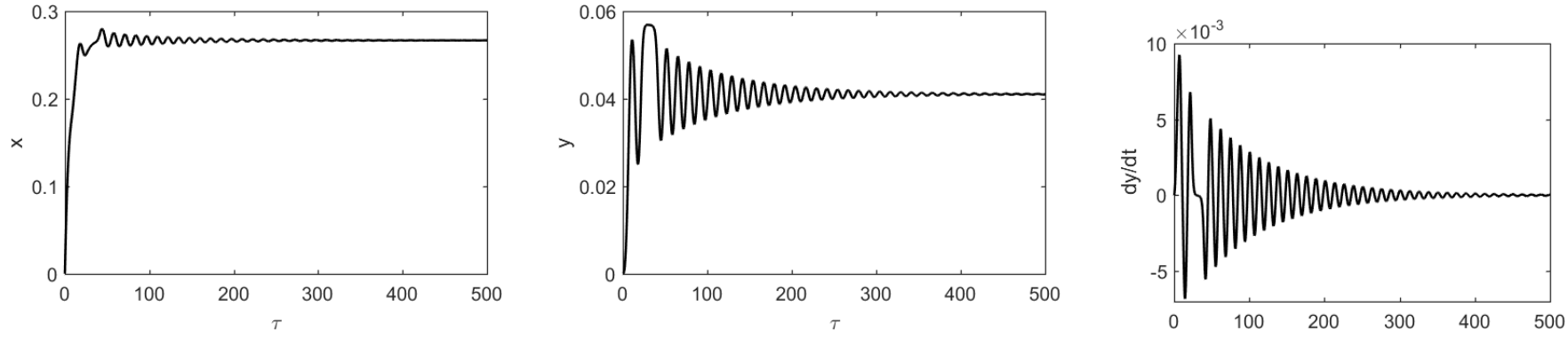

(a) (b) (c)

Fig. 3. Time history of the (a) current, (b) angular displacement and (c) rotational velocity for subconfiguration of stable equilibrium point at $\theta = 0$ when the arm cannot perform complete rotation for $E = 4.71076 \times 10^{-2}$.

2150178-6

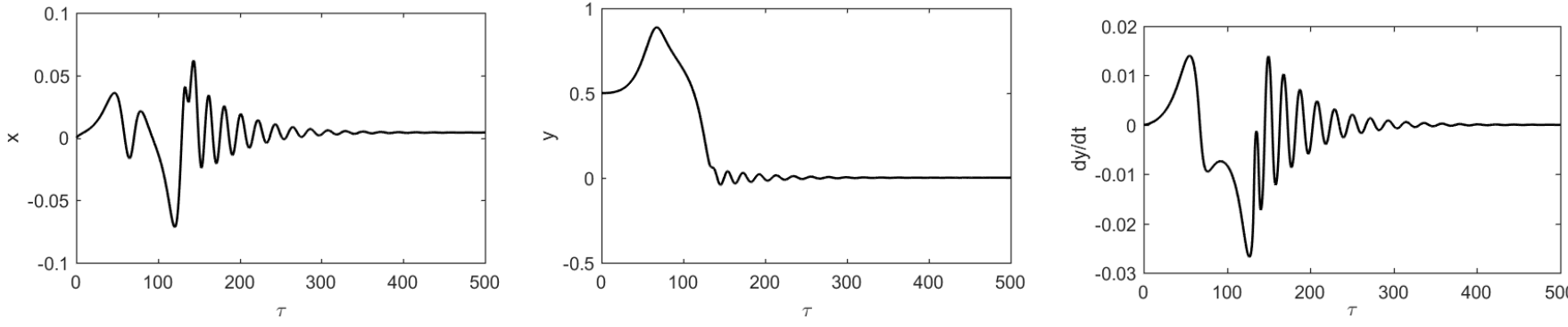

(a) (b) (c)

Fig. 4. Time history of the (a) current, (b) angular displacement and (c) rotational velocity for subconfiguration of stable equilibrium point is $\theta = \pi$ when the device cannot perform complete rotation for $E = 7.4 \times 10^{-4}$.

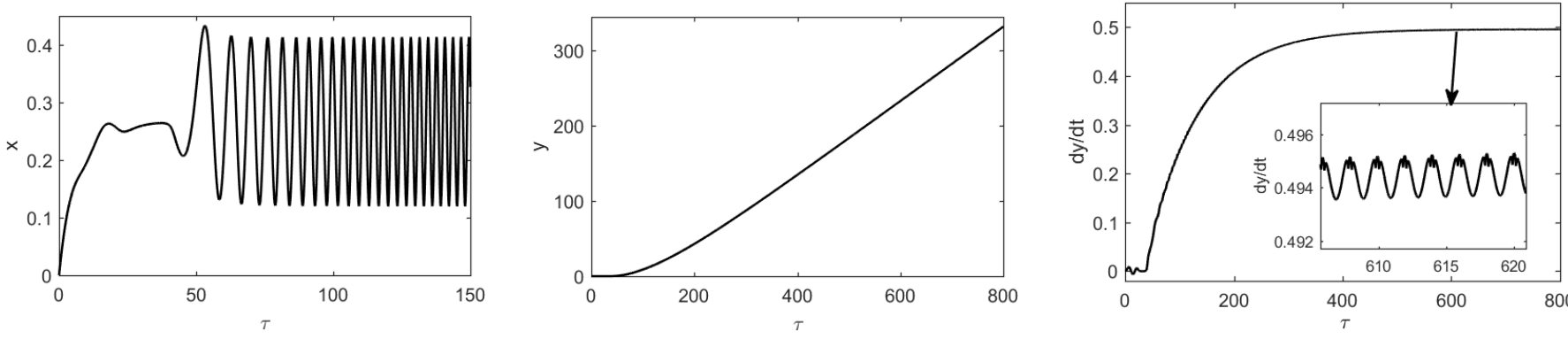

(a) (b) (c)

Fig. 5. Time history of the (a) current, (b) angular displacement and (c) rotational velocity for subconfiguration of stable equilibrium point at $\theta = 0$ when the arm performs complete rotation for $E = 4.71077 \times 10^{-2}$.

2150178-7

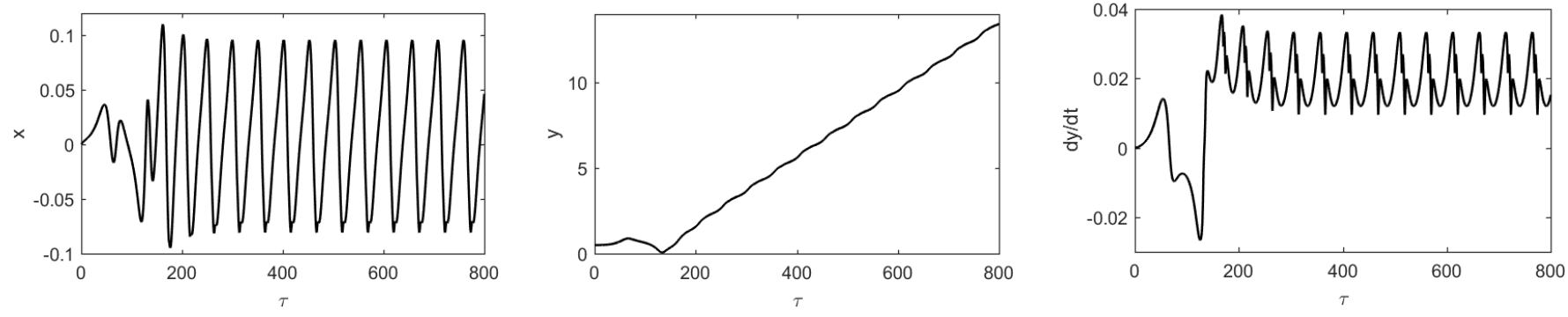

(a) (b) (c)

Fig. 6. Time history of the (a) current, (b) angular displacement and (c) rotational velocity for the subconfiguration of stable equilibrium point at $\theta = \pi$ when the arm performs complete rotation for $E = 7.9 \times 10^{-4}$.

3. DC Motor Arm in a Circular Periodic Potential Submitted to AC Voltage

3.1. *Linear oscillations around stable equilibrium points*

We first look for the amplitudes of linear oscillations around the equilibrium points $\theta = 0$ and $\theta = \pi$. For the oscillations around the stable equilibrium point $\theta = 0$, we take $\cos(\theta) = 1$ and the nonlinear function given by Eq. (4) can be linearized using the Taylor expansion formula and thus gives:

$$f(\theta) = c\theta \tag{18}$$

with

$$c = \frac{2\delta}{(1+\delta^2-2\delta\cos(\phi))^{\frac{3}{2}}} \times \left[\frac{3\delta\sin^2(\phi)}{(1+\delta^2-2\delta\cos(\phi))} - \cos(\phi)\right].$$

Equations (6) and (7) can thus be written as:

$$\ddot{y} + \lambda_m\dot{y} + \gamma c\theta_0 y = \varepsilon_m x, \tag{19}$$

$$\dot{x} + \lambda_e x + \varepsilon_e\dot{y} = E\sin(\Omega\tau). \tag{20}$$

The harmonic balance method is used to solve Eqs. (19) and (20) to find the sinusoidal approximations of the electrical current and angular displacement. So, the expressions of the electrical current and the angular displacement can be written as:

$$x = A_1\cos(\Omega\tau) + A_2\sin(\Omega\tau), \tag{21}$$

$$y = B_1\cos(\Omega\tau) + B_2\sin(\Omega\tau). \tag{22}$$

Let us set

$$A = \sqrt{A_1^2 + A_2^2} \quad \text{and} \quad B = \sqrt{B_1^2 + B_2^2}$$

the maximal amplitude of current and the maximal amplitude of the mechanical displacement. Inserting Eqs. (21) and (22) into Eqs. (19) and (20) and after some mathematical manipulations, one obtains that A and B are given as follows:

$$B = \frac{\varepsilon_m E}{\sqrt{[-\Omega(-\Omega^2+\gamma c) - \lambda_e\lambda_m\Omega - \varepsilon_e\varepsilon_m\Omega]^2 + [\lambda_e(-\Omega^2+\gamma c) - \Omega^2\lambda_m]^2}}, \tag{23}$$

$$A = \frac{\sqrt{[(-\Omega^2+\gamma c)^2 + \lambda_m^2\Omega^2]}}{\varepsilon_m}B. \tag{24}$$

Figures 7(a) and 7(b) show both the amplitude response of the mechanical part and electrical part. The amplitude of the current displays two peaks: an anti-resonant peak and a resonant peak, while the mechanical displacement presents a resonant behavior.

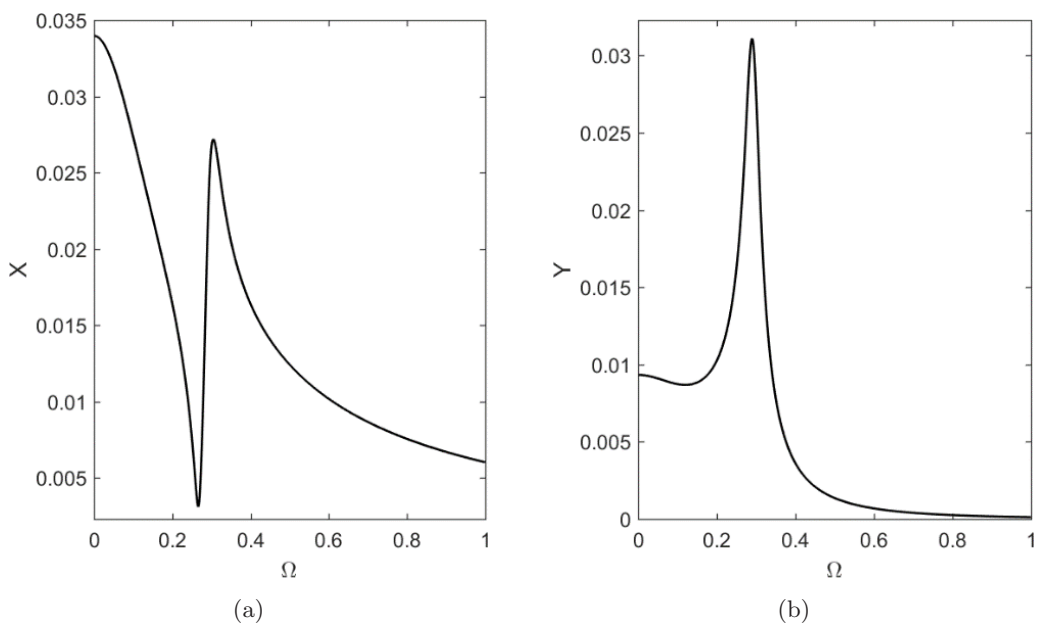

(a) (b)

Fig. 7. (a) Amplitude of the current x and (b) amplitude of angle y versus the parameter Ω around stable equilibrium point $\theta = 0$ for $E = 6 \cdot 10^{-3}$.

For oscillations around, $\theta = \pi$, we assume that $\theta = \pi + \alpha$, where α is very small compared to π and $\cos(\theta) = -1$. The linearization of the nonlinear function gives:

$$f(\theta) = c_1(\theta - \pi), \tag{25}$$

where

$$c_1 = \frac{2\delta}{(1+\delta^2+2\delta\cos(\phi))^{\frac{3}{2}}} \times \left[\frac{3\delta\sin^2(\phi)}{(1+\delta^2+2\delta\cos(\phi))} + \cos(\phi)\right].$$

Equations (6) and (7) thus become:

$$\ddot{\zeta} + \lambda_m\dot{\zeta} + \gamma c_1\theta_0\zeta = \varepsilon_m x, \tag{26}$$

$$\dot{x} + \lambda_e x - \varepsilon_e\dot{\zeta} = E\sin(\Omega\tau), \tag{27}$$

where $\zeta = \frac{\alpha}{\theta_0}$.

The expressions of the electrical current and the angular displacement can be written as:

$$x = C_1\cos(\Omega\tau) + C_2\sin(\Omega\tau), \tag{28}$$

$$\zeta = D_1\cos(\Omega\tau) + D_2\sin(\Omega\tau). \tag{29}$$

The amplitude of the current and that of the mechanical displacement are given as:

$$D = \frac{\varepsilon_m E}{\sqrt{[-\Omega(-\Omega^2+\gamma c_1) - \lambda_e\lambda_m\Omega + \varepsilon_e\varepsilon_m\Omega]^2 + [\lambda_e(-\Omega^2+\gamma c_1) - \Omega^2\lambda_m]^2}},$$
$$C = \frac{\sqrt{[(-\Omega^2+\gamma c_1)^2 + \lambda_m^2\Omega^2]}}{\varepsilon_m}D, \tag{30}$$

where

$$C = \sqrt{C_1^2 + C_2^2} \quad \text{and} \quad D = \sqrt{D_1^2 + D_2^2}.$$

As shown in Figs. 8(a) and 8(b), the amplitude of the current presents two peaks: an antiresonant peak and a resonant one, while the amplitude of angular displacement decreases when the frequency increases.

3.2. *Conditions for complete rotation in case of AC excitations*

Another point to study is the condition for complete rotation when a sinusoidal voltage powers the electromechanical system. The same criterion [Eq. (18)] considered in Sec. 2.3 is used. Figure 9 displays E_C versus Ω for the two configurations. The domain

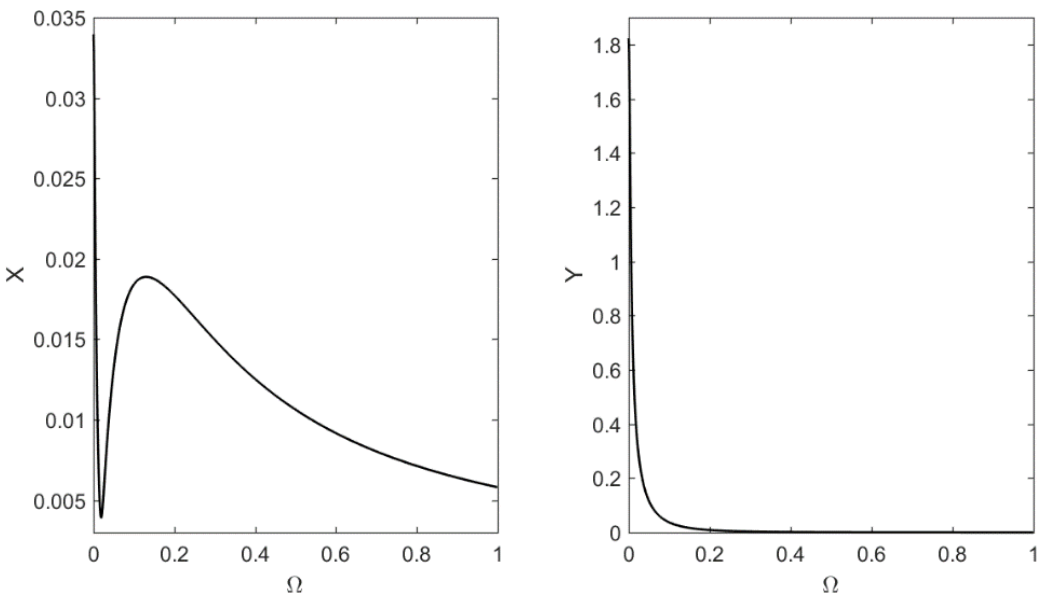

(a) (b)

Fig. 8. (a) Amplitude of current x and (b) amplitude of angle y versus the parameter Ω around stable equilibrium point $\theta = \pi$ for $E = 6 \cdot 10^{-3}$.

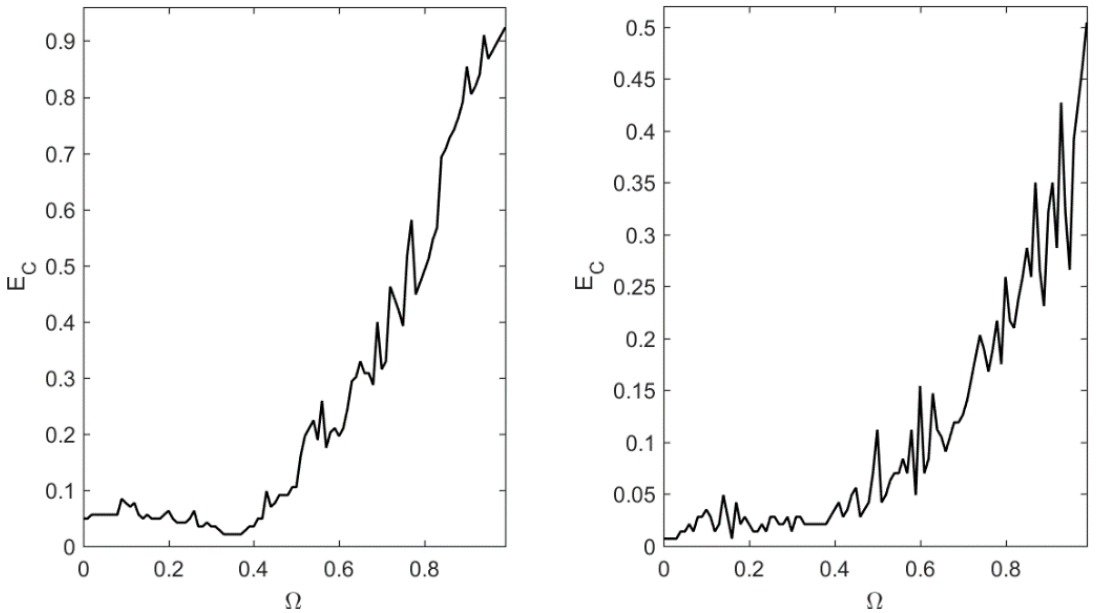

(a) (b)

Fig. 9. Numerical boundary criterion for complete rotation for the arm starting at (a) the equilibrium angle $\theta = 0$ and (b) the equilibrium angle $\theta = \pi$.

located below each curve is where the dimensionless amplitude of the vibration of the mechanical arm is less than 1 (meaning no complete rotation). Complete rotations are observed for values of E above the curves. It is found that E_C increases with the frequency. It is also observed that when the arm moves from the equilibrium point $\theta = 0$, more energy is needed to make the arm undergo complete rotation.

Figure 10(b) presents the time history of the angular displacement for the amplitude of vibration less than 1 for the subconfiguration of stable equilibrium point at $\theta = 0$. The arm oscillates with a perfect sinusoidal shape around the equilibrium

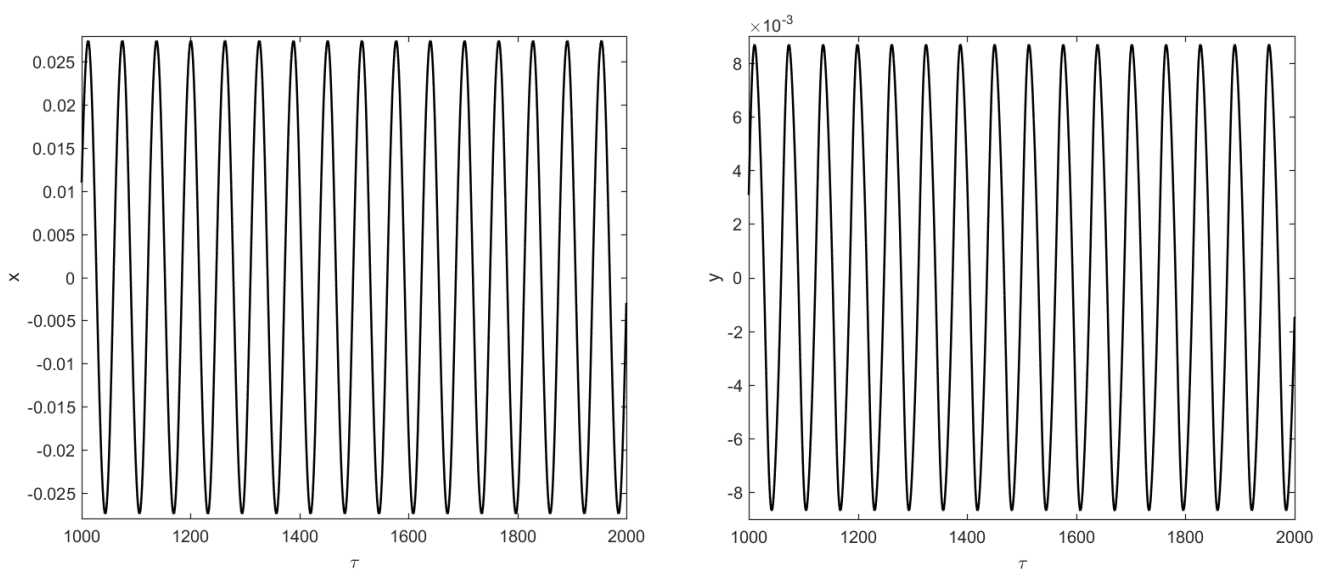

(a) (b)

Fig. 10. Time histories of (a) the current and (b) the angular displacement for the subconfiguration of stable equilibrium point at $\theta = 0$ (with $\Omega = 0.1$ and $E = 6 \times 10^{-3}$).

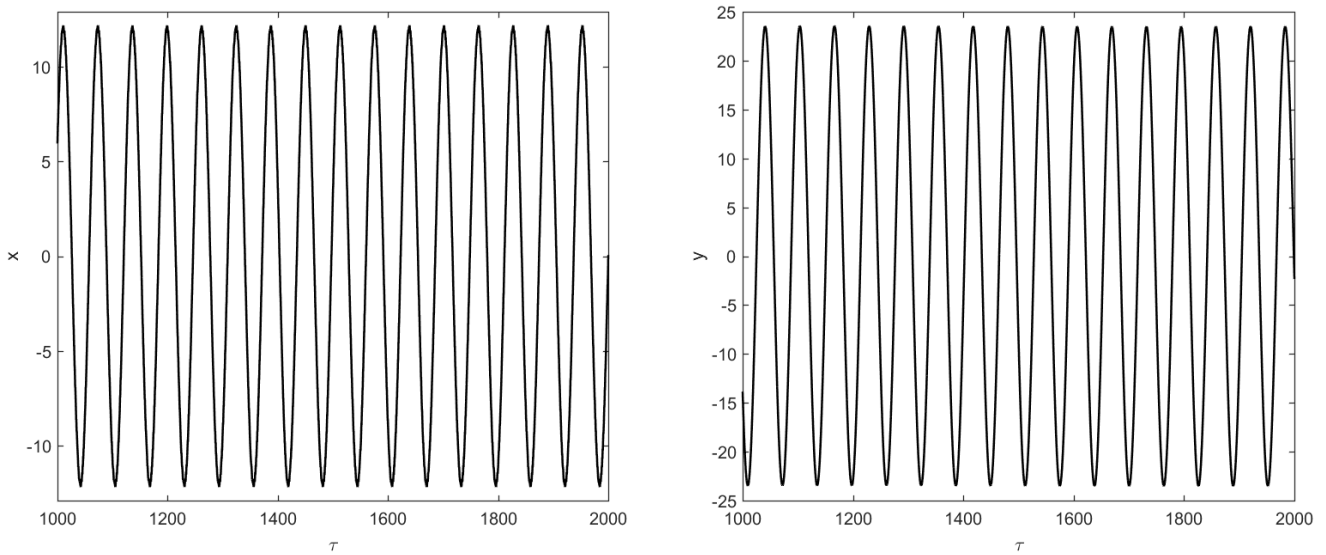

(a) (b)

Fig. 11. Time histories of (a) the current and (b) the angular displacement for the subconfiguration of stable equilibrium point $\theta = 0$ (with $\Omega = 0.1$ and $E = 2.45$).

position. For the subconfiguration of stable equilibrium point at $\theta = \pi$, we have also plotted in Fig. 12(b) the response of mechanical part. As in Fig. 10(b), it shows sinusoidal shape around 0 with amplitude less than one (1) turn.

Figure 11(b) shows the time history of the angular displacement for the subconfiguration of stable equilibrium point $\theta = 0$, for the amplitude of sinusoidal voltage higher than the critical value. One observes that the mechanical arm presents sinusoidal oscillations in this case with amplitude of 23 turns. This means that the arm rotates 23 turns in the forward direction; then turns back to the stable position and continues in the reverse side until 23 turns before returning back and so on. The same work has been done for the other subconfiguration; it is found that the arm performs sinusoidal oscillations with amplitude of 25 turns [see Fig. 13(b)].

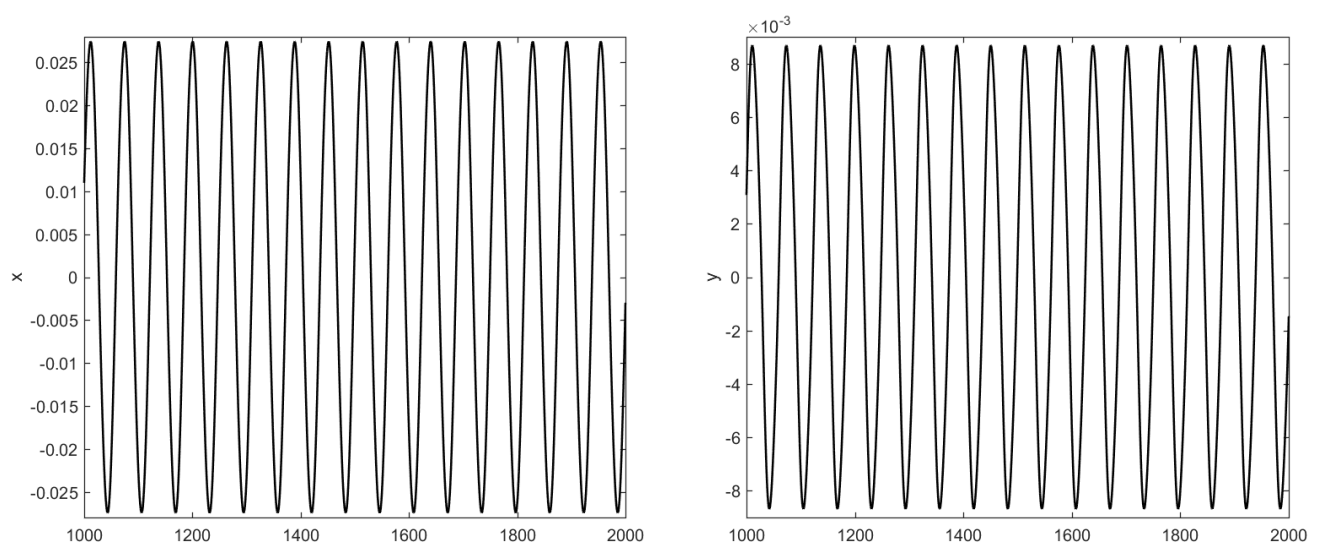

(a) (b)

Fig. 12. Time histories of (a) the current and (b) the angular displacement for the subconfiguration of stable equilibrium point $\theta = \pi$ (with $\Omega = 0.1$ and $E = 6 \times 10^{-3}$).

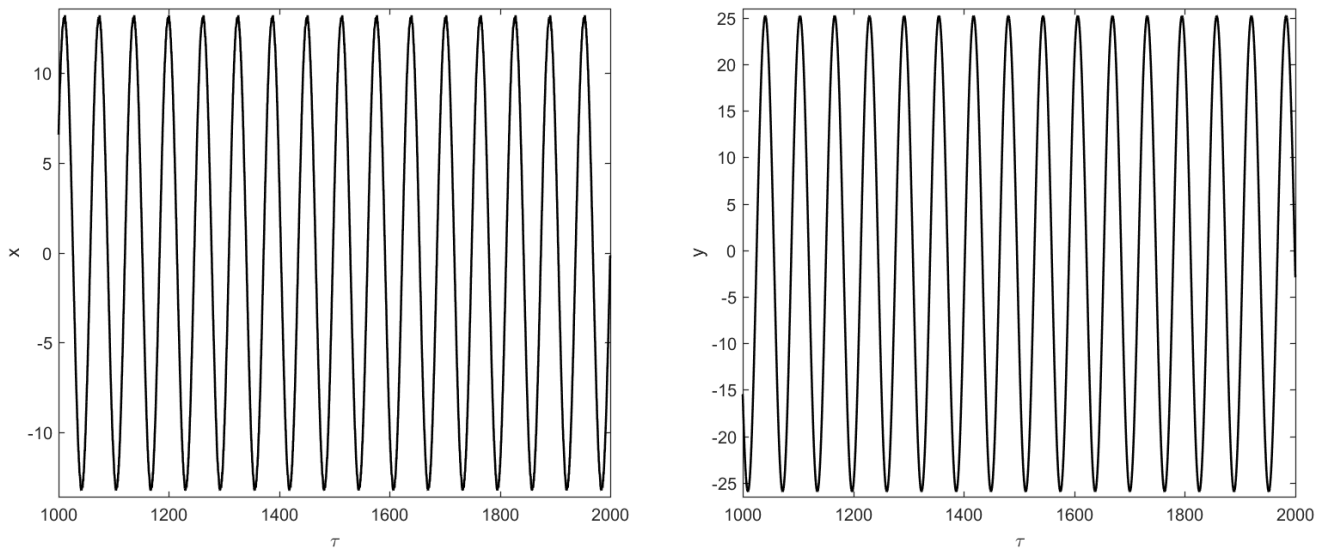

(a) (b)

Fig. 13. Time histories of (a) the current and (b) the angular displacement for the subconfiguration of stable equilibrium point $\theta = \pi$ (with $\Omega = 0.1$ and $E = 2.67$).

Figures 10(a), 11(a), 12(a) and 13(a) display the response of the electrical part of the system. These curves show that the current x oscillates like the angular displacement y.

3.3. *Bifurcation diagrams*

In order to fully characterize the dynamical behavior of the system, bifurcation diagrams have been obtained from the numerical simulation taking the amplitude of the sinusoidal excitation as the control parameter. Considering $\theta = 0$ as the initial condition, the bifurcation diagram is presented in Fig. 14 along with the largest Lyapunov exponent, while in Fig. 15, examples of time traces and phase portraits are represent. It is found that the system moves from regular (periodic oscillation to chaotic dynamics). From the variation of the Lyapunov exponent, one finds that the system is very sensitive to the variation of the voltage amplitude since points of positive Lyapunov exponent alternate erratically with points of negative Lyapunov exponent in some ranges of the sinusoidal voltage amplitude.

Figures 15(a) and 15(c) also present two examples of time history of the angular displacement, one for periodic oscillations and the other one for chaotic oscillations. Figures 15(b) and 15(d) display the corresponding phase portraits.

To characterize more the system, we have also obtained the bifurcation diagram for the subconfiguration where the stable equilibrium point is $\theta = \pi$. This is presented in Fig. 16, which looks similar to Fig. 14. Here, the chaotic behavior occurs for smaller values of the voltage amplitude. Figures 17(a) and 17(b) show time histories while Figs. 17(c) and 17(d) present the corresponding phase portrait of the angular displacement for different values of E. These curves present respectively periodic and chaotic behaviors. Because of the fact that the angular displacement is not bounded, but decreases with chaotic ripples [Fig. 15(d)], the phase portrait looks different to what is always observed. This is specific for this system since for some values of the parameters, the angular displacement y makes more than one turn before returning back while the angular velocity dy/dt oscillates around 0. This specific shape is also visible in Fig. 19(b).

3.4. *Amplitude response curves*

To plot the amplitude response curves versus the frequency, one needs to have the frequency domain where the system shows periodic behavior (in order to avoid plotting a curve in a domain where the system undergoes chaotic dynamics). In this respect, the bifurcation diagram is plotted versus the frequency. An example is presented in Fig. 18 when the motion starts at $\theta = 0$. One finds that periodic motion of the system starts when $\Omega = 0.01$ and continues until 0.231. For the frequency between 0.231 and 0.408, the system response exhibits an alternation of periodic and chaotic behaviors (see

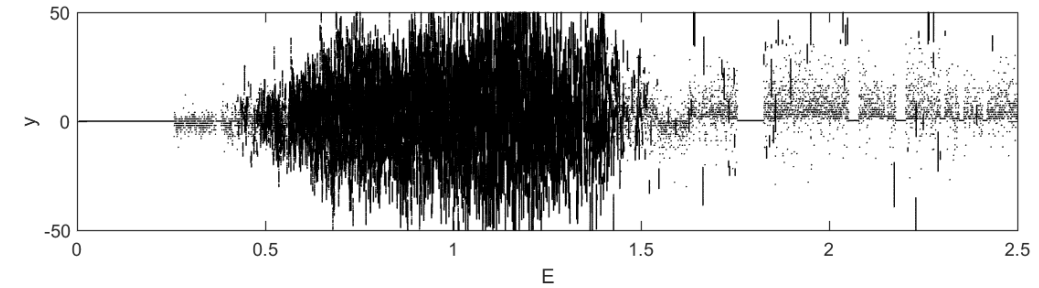

(a)

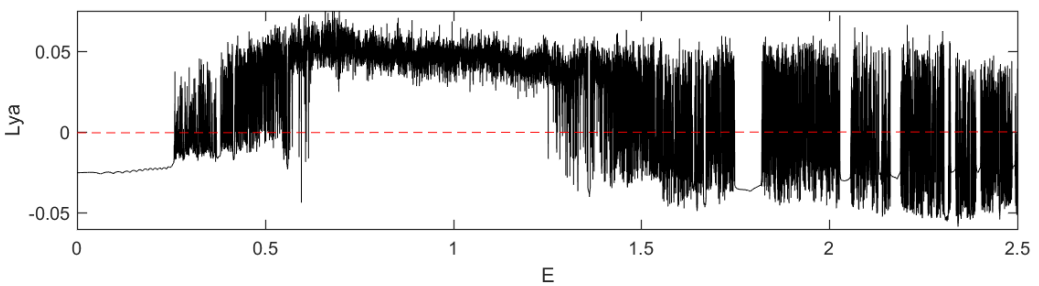

(b)

Fig. 14. (a) Bifurcation diagram and (b) Lyapunov exponent versus the amplitude E for the subconfiguration of stable equilibrium point $\theta = 0$ with $\Omega = 0.66$.

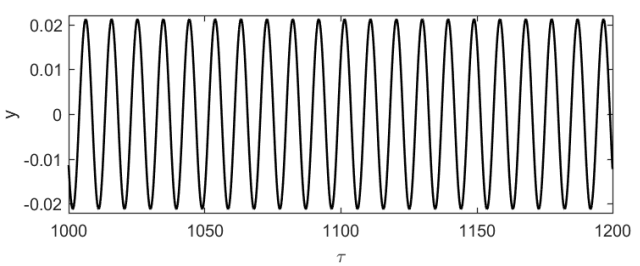

(a)

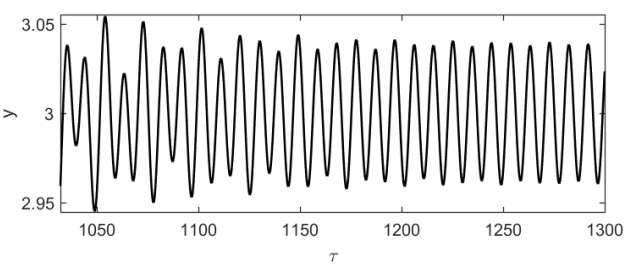

(b)

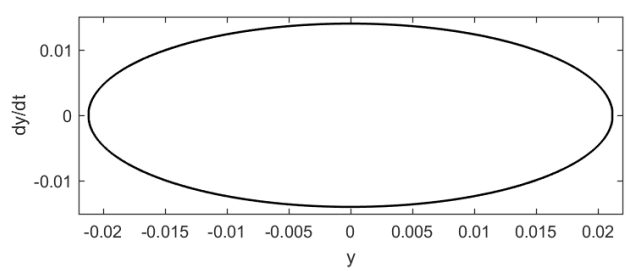

(c)

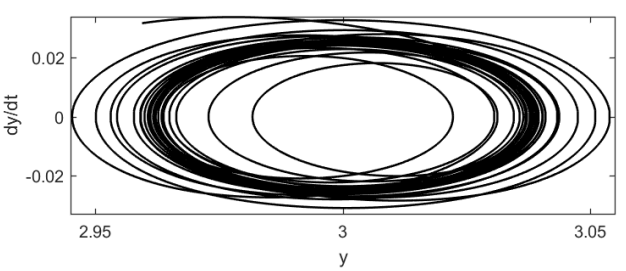

(d)

Fig. 15. (a) and (c) Time histories and corresponding phase portraits of the angular displacement showing periodic motion with $E = 0.25$ and (b) and (d) chaotic oscillations with $E = 0.42$ for $\Omega = 0.66$, for the subconfiguration of stable equilibrium point $\theta = 0$.

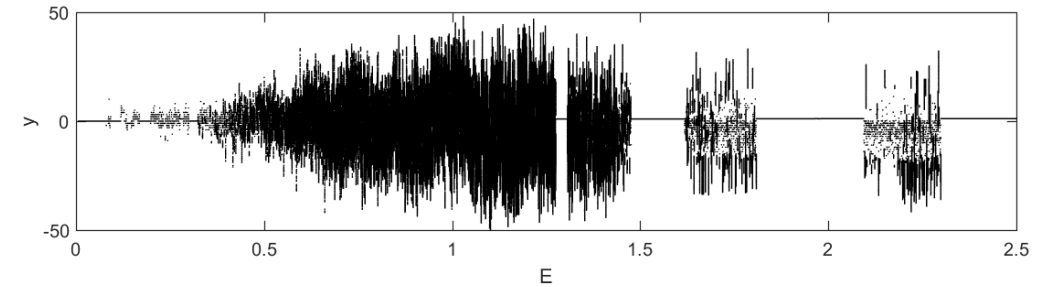

(a)

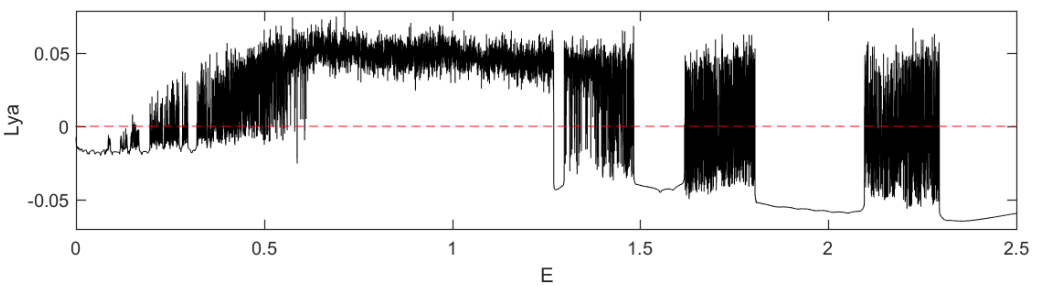

(b)

Fig. 16. (a) Bifurcation diagram and (b) Lyapunov exponent versus the amplitude E of the AC voltage for the subconfiguration of stable equilibrium point at $\theta = \pi$ with $\Omega = 0.66$.

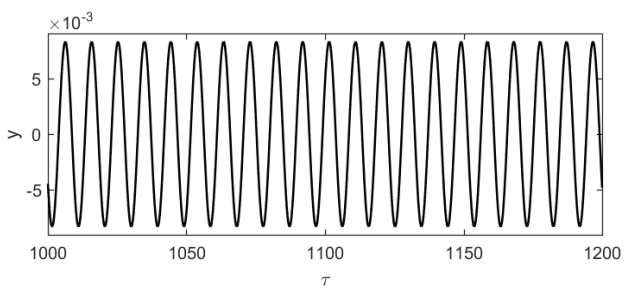

(a)

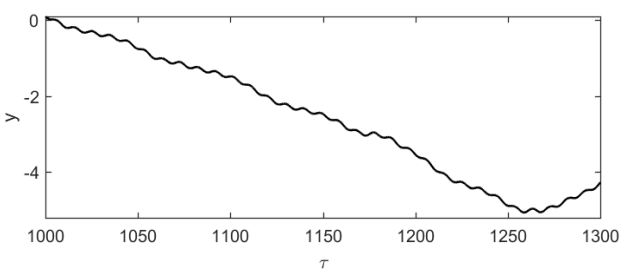

(b)

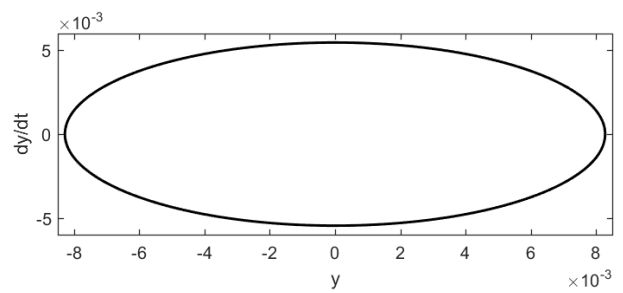

(c)

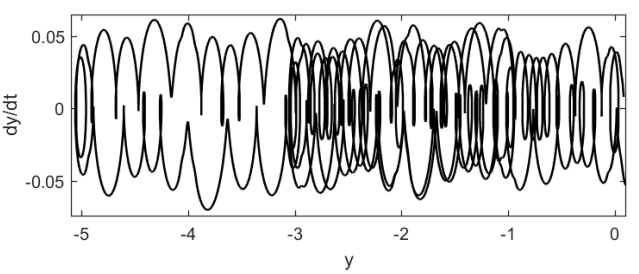

(d)

Fig. 17. (a) and (c) Time histories and corresponding phase portraits of the angular displacement showing periodic motion with $E = 0.10$ and (b) and (d) chaotic oscillations with $E = 0.66$ for $\Omega = 0.66$ and for the subconfiguration of stable equilibrium point at $\theta = \pi$.

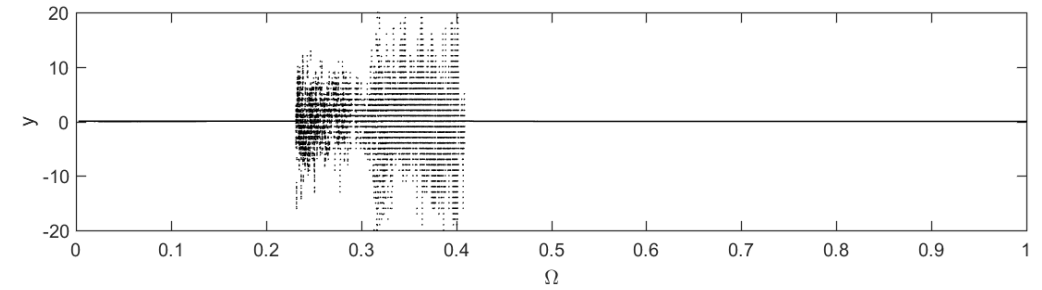

(a)

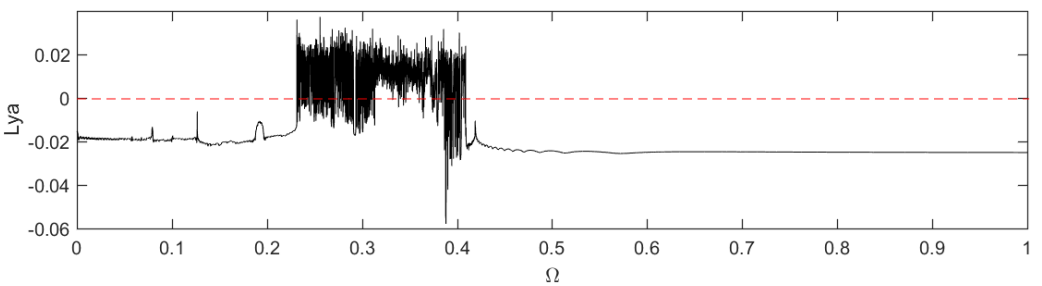

(b)

Fig. 18. (a) Bifurcation diagram and (b) Lyapunov exponent versus the frequency Ω for the subconfiguration of stable equilibrium point at $\theta = 0$ with $E = 4 \cdot 10^{-2}$.

the phase portraits of Fig. 19). As the excitation frequency increases, the system undergoes periodic oscillations.

In Fig. 20, we have plotted the frequency response curve in the frequency domain where the system presents periodic oscillations. One observes that the amplitude of the current and that of the amplitude of the mechanical displacement decrease when the frequency increases.

The same analysis is done for the subconfiguration where the motion starts at $\theta = \pi$. In this case, the system response presents an alternation of

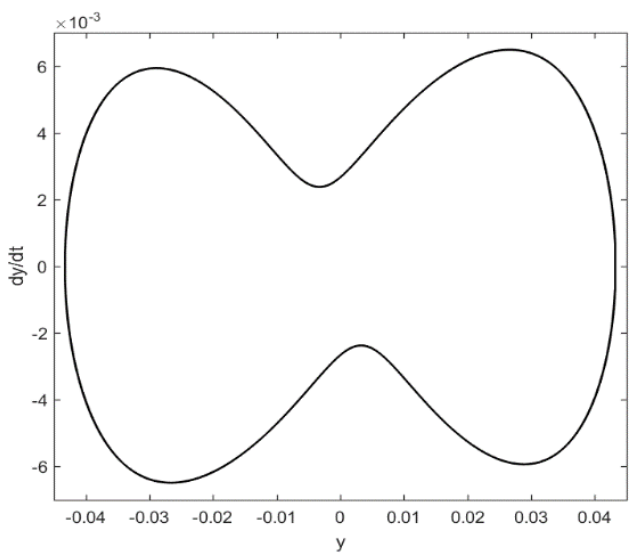

(a)

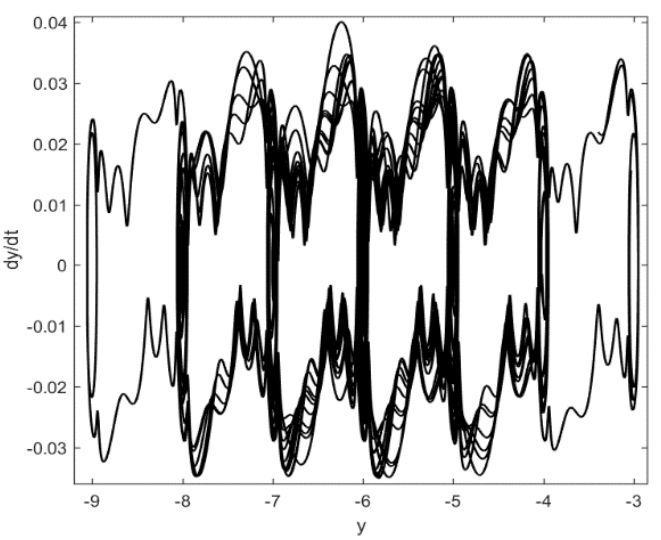

(b)

Fig. 19. Phase portrait of the angular displacement with (a) $\Omega = 0.15$ and (b) $\Omega = 0.35$.

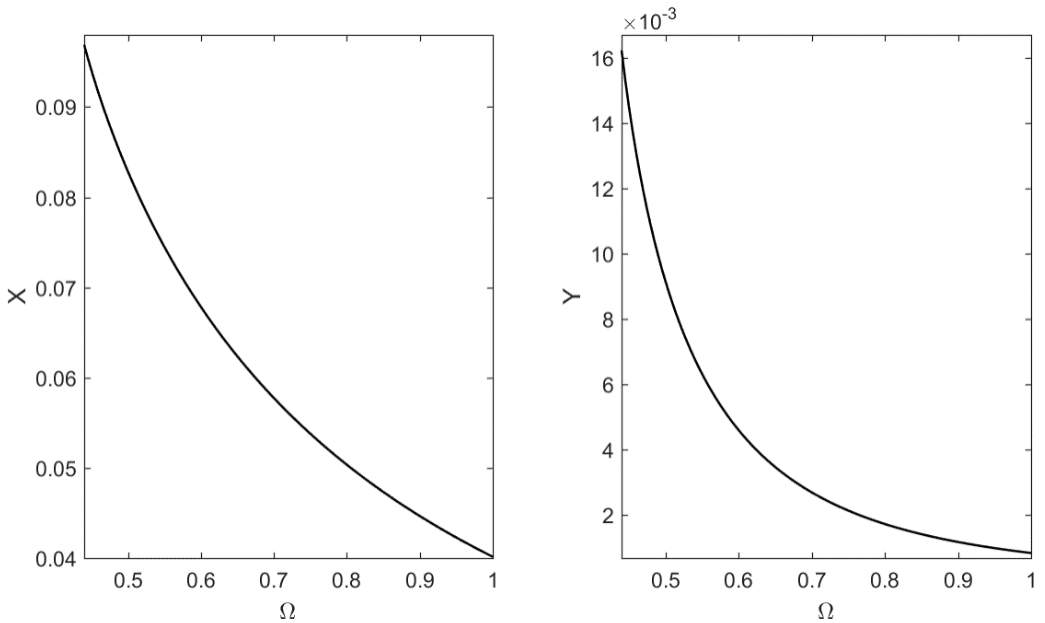

(a) (b)

Fig. 20. Amplitude of (a) the current x and (b) angular displacement versus the parameter Ω with $E = 4 \cdot 10^{-2}$ for the subconfiguration of stable equilibrium point at $\theta = 0$.

periodic and chaotic behaviors when Ω lies between 0.01 and 0.439 and is periodic until $\Omega = 1$ (see Figs. 21 and 22).

Because of the fact that the arm can oscillate around 0, 1 and 2, we have plotted in Fig. 23, the maximal value (not the amplitude as in the sense of amplitude of sinusoidal oscillations) attained by the current and the angular displacement versus the frequency. The current amplitude decreases with the frequency. However, the angular displacement

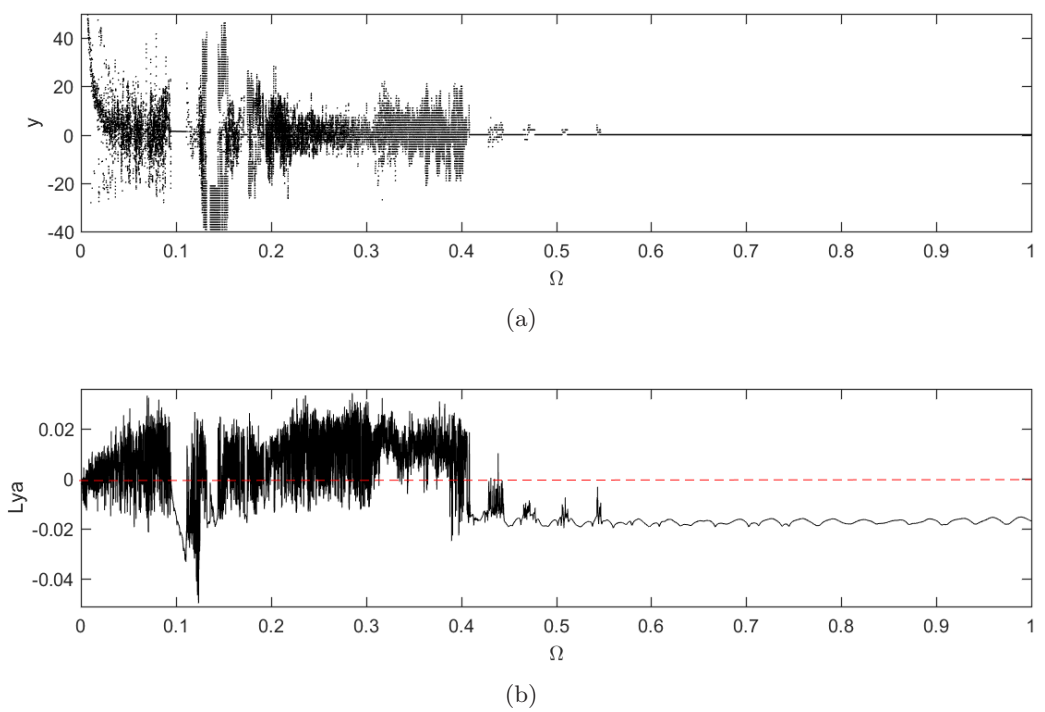

(a)

(b)

Fig. 21. (a) Bifurcation diagram and (b) Lyapunov exponent versus the parameter Ω for the subconfiguration of stable equilibrium point at $\theta = \pi$ with $E = 4 \cdot 10^{-2}$.

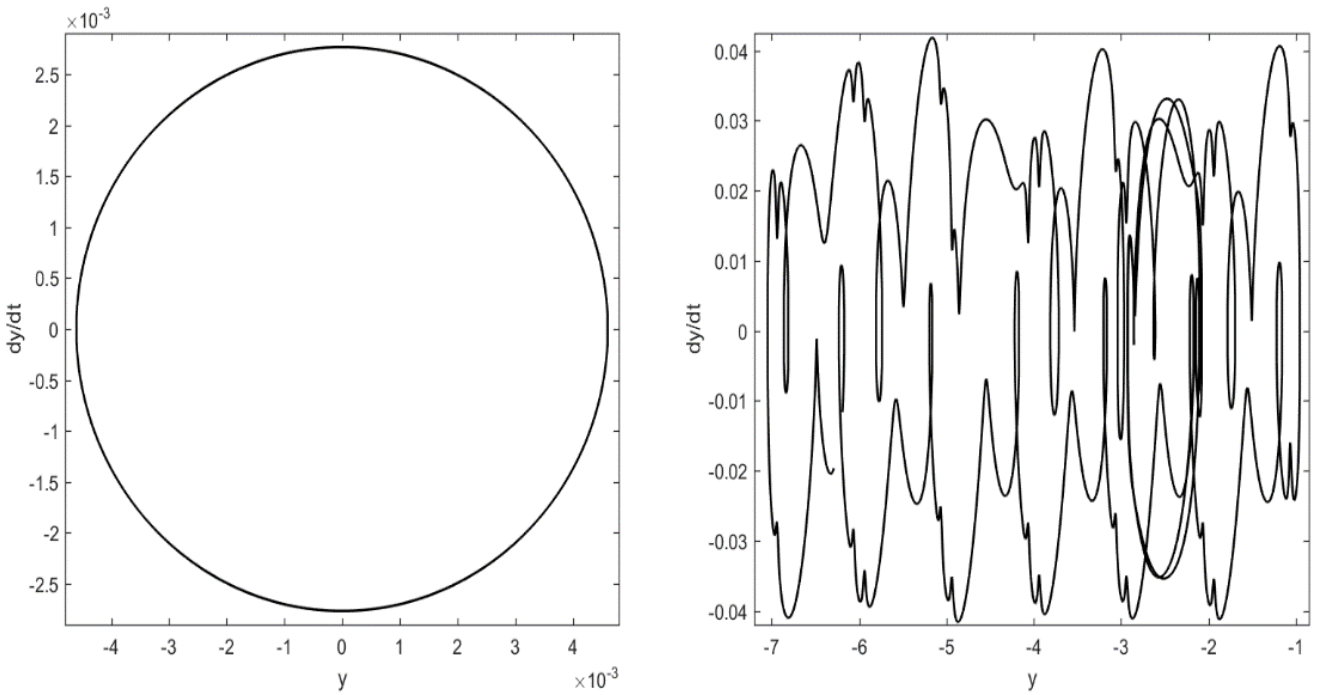

(a) (b)

Fig. 22. Phase portrait of the angular displacement with (a) $\Omega = 0.6$ and (b) $\Omega = 0.2$.

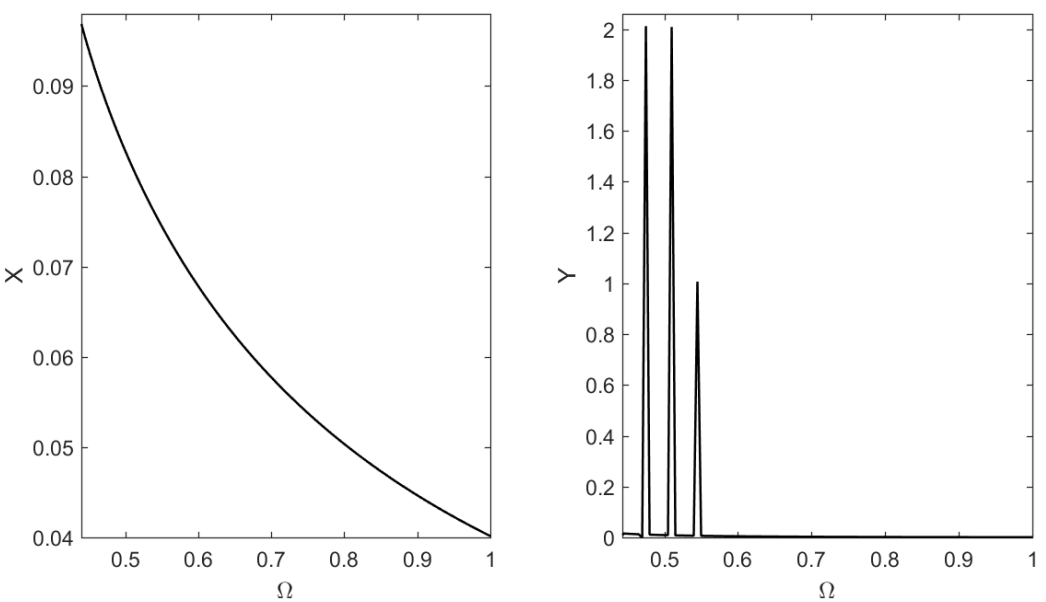

(a) (b)

Fig. 23. Amplitude of (a) current x and (b) the mechanical displacement y versus the parameter Ω for $E = 4 \cdot 10^{-2}$ in the subconfiguration of stable equilibrium point at $\theta = \pi$.

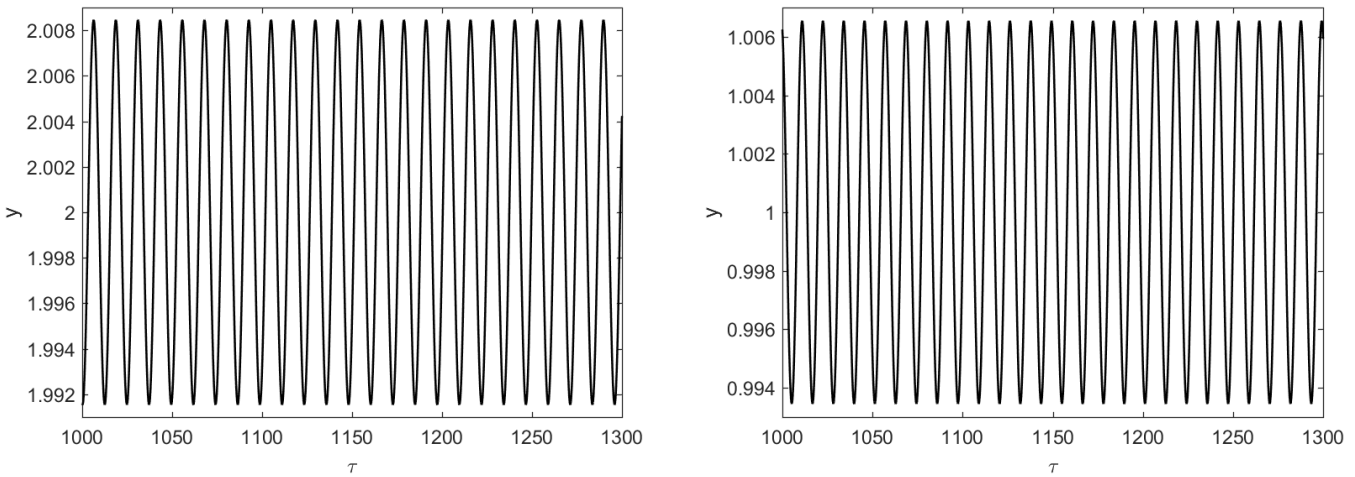

(a) (b)

Fig. 24. (a) Oscillations around 2 for the peak at $\Omega = 0.51$ and (b) oscillations around 1 for the peak at $\Omega = 0.545$.

shows some special features indicating oscillations around 0, oscillations around 1 and around 2 for some selected values of the frequency corresponding to the peaks in Fig. 23. The oscillations at those frequencies are presented in Fig. 24.

4. Conclusion

We have studied the dynamical behavior of a mechanical arm fixed on the axis of a DC motor and moving in a circular potential generated by three permanent magnets. Equilibrium points of the potential and their stability have been established. The potential energy displays two configurations. The first one presents two equilibrium points: one unstable ($\theta = 0$) and one stable ($\theta = \pi$) (modulo 2π). The second presents four equilibrium points, among which two are stable ($\theta = 0$ and $\theta = \pi$) and two are unstable corresponding to the magnets' positions ($\theta = -\phi$ In addition, $\theta = \phi$). Dynamical responses of the system have been analyzed for two cases: when it is powered by DC and AC voltage sources. A numerical estimation of the critical parameters for which the mechanical arm undergoes a complete rotation has been obtained. The results have shown that for voltage lower than a critical value, the mechanical arm oscillates and then stabilizes at the equilibrium position in the case of DC voltage while in the case of AC voltage, the arm exhibits oscillations with amplitude less than one turn. When the voltage amplitude is higher than the critical value, the mechanical arm undergoes large amplitude motion (complete rotation) for DC voltage source and displays angular oscillations with amplitude greater than one turn for the AC source. The bifurcation diagrams have shown that the system exhibits chaotic dynamics.

In the future works, we will consider other configurations where the two poles of magnets are used. Moreover, the case of several magnets (more than two) arranged along a circle will be explored as a type of energy harvesters. Added to that, it will be interesting to conduct experimental investigations.

References

Aline, S. P. & Marcelo, A. S. [2009] "Controlling chaos in a nonlinear pendulum using an extended time-delayed feedback control method," *Chaos Solit. Fract.* **42**, 2981–2988.

Avanço, R. H., Navarro, H. A., Brasil, R. M. & Balthazar, J. M. [2014] "Nonlinear dynamics of a pendulum excited by a crank-shaft-slider mechanism," *ASME 2014 Int. Mech. Engin. Congr. Exp.*, Vol. 4B, Dynamics, Vibration and Control, Montreal, Quebec, Canada.

Awrejcewicz, J., Supe, B., Kudra, G., Wasilewski, G. & Olejnik, P. [2008] "Numerical and experimental study of regular and chaotic motion of triple physical pendulum," *Int. J. Bifurcation and Chaos* **18**, 2883–2915.

Braum, O. M. & Kivshar, Y. S. [1998] "Nonlinear dynamics of the Frenkel–Kontorowa model," *Phys. Rep.* **306**, 1–108.

Chen, X., Han, S., Li, J. & Sun, S. [2020] "Chaos suppression for coupled electromechanical torsional vibrations in a high-speed permanent magnet synchronous motor driven system via multitime delayed feedback control," *Int. J. Bifurcation and Chaos* **30**, 2050128-1–13.

Coronel, E. A., Gomez-Aguilar, J. F., Lopez-Lopez, M. G., Alvarado-Martínez, V. M. & Guerrero-Ramírez, G. V. [2016] "Triple pendulum model involving fractional derivatives with different kernels," *Chaos Solit. Fract.* **91**, 248–261.

Diyi, C., Peng, S. & Xiaoyi, M. [2012] "Control and synchronization of chaos in an induction motor system," *Int. J. Innov. Comput. Inform. Contr.* **8**, 7237–7248.

Gao, Y. & Chau, T. K. [2002] "Chaotification of permanent-magnet synchronous motor drives using time-delay feedback," *Proc. Industrial Electronics Conf.* **1**, 762–766.

Ge, Z. M., Cheng, J. M. & Chen, Y. S. [2004] "Chaos anticontrol and synchronization of three time scales brushless DC motor system," *Chaos Solit. Fract.* **22**, 1165–1182.

Ge, Z. M. & Cheng, J. W. [2005] "Chaos synchronization and parameter identification of three time scales brushless DC motor system," *Chaos Solit. Fract.* **24**, 597–616.

Gomer, R. [1990] "Diffusion of adsorbates on metallic surfaces," *Rep. Prog. Phys.* **53**, 917–1002.

Haan, S. [2006] "NEMS-emerging products and applications of nano-electromechanical systems," *Nanotechnol. Perceptions* **2**, 267–275.

Jang, J. O. & Jeon, G. J. [2000] "A parallel neurocontroller for DC motors containing nonlinear friction," *Neurocomputing* **30**, 233–248.

Johan, J. [2005] *Introduction to Robotics Mechanics and Control*, 3rd edition (Prentice Hall), pp. 109–114.

Kazmierczak, M., Kudra, G., Awrejcewicz, J. & Wasilewski, G. [2013] "Numerical and experimental investigation of bifurcational dynamics of an electromechanical system consisting of a physical pendulum and DC motor," *Dynamical Systems — Applications* (TU of Lodz Press, Lodz.), pp. 49–58.

Kazmierczak, M., Kudra, G., Awrejcewicz, J. & Wasilewski, G. [2015] "Mathematical modeling, numerical simulations and experimental verification of bifurcation dynamics of a pendulum driven by a DC motor," *Eur. J. Phys.* **36**, 1–13.

Kitio Kwuimy, C. A. & Woafo, P. [2007] "Dynamics of a self-sustained electromechanical system with flexible arm and cubic coupling," *Commun. Nonlin. Sci. Numer. Simul.* **12**, 1504–1517.

Kitio Kwuimy, C. A. & Woafo, P. [2008] "Dynamics, chaos and synchronization of self-sustained electromechanical systems with clamped-free flexible arm," *Nonlin. Dyn.* **53**, 201–214.

Lin, L. & Xuemei, L. [2014] "Existence of quasi-periodic solutions of the real pendulum equation," *Chaos Solit. Fract.* **63**, 23–33.

Lyshevski, L. E. [2009] "Nonlinear control of mechatronic systems with permanent magnet DC motors," *Mechatronics* **9**, 539–552.

Moon, F. C., Cusumano, J. & Holmes, P. J. [1993] "Evidence for homoclinic orbits as a precursor to chaos in a magnetic pendulum," *Physica D* **24**, 383–390.

Nana, B., Yamgoué, S. B., Tchitnga, R. & Woafo, P. [2017] "Dynamics of a pendulum driven by a DC motor and magnetically controlled," *Chaos Solit. Fract.* **104**, 18–27.

Nana, B., Yamgoué, S. B., Tchitnga, R. & Woafo, P. [2018] "Nonlinear dynamics of a sinusoidally driven lever in repulsive magnetic fields," *Nonlin. Dyn.* **91**, 55–66.

Notué, K. A. & Woafo, P. [2014] "Effects of springs on a pendulum electromechanical energy harvester," *Theor. Appl. Mech. Lett.* **4**, 2–7.

Qi, G. & Hu, J. [2017] "Force analysis and energy operation of chaotic system of permanent-magnet synchronous motor," *Int. J. Bifurcation and Chaos* **27**, 1750216-1–18.

Singh, J. P., Roy, B. K. & Kuznetsov, N. V. [2019] "Multistability and hidden attractors in the dynamics of permanent magnet synchronous motor," *Int. J. Bifurcation and Chaos* **29**, 1950056-1–17.

Tcheutchoua Fossi, D. O. & Woafo, P. [2013] "Generation of complex phenomena in a simple electromechanical system using the feedback control," *Commun. Nonlin. Sci. Numer. Simulat.* **18**, 209–218.

Tsapla, F. R. & Woafo, P. [2016] "Chaos in a new bistable rotating electromechanical system," *Chaos Solit. Fract.* **93**, 48–57.

Woafo, P., Kofane, T. C. & Bokosah, A. S. [1997] "Soliton mechanism of surface diffusion with a deformable substrate potential," *Phys. Scripta* **56**, 655–660.

Wojna, M., Wijata, A., Wasilewski, G. & Awrejcewicz, J. [2018] "Numerical and experimental study of a double physical pendulum with magnetic interaction," *J. Sound Vibr.* **430**, 214–230.

Yamapi, R. [2006] "Dynamics of an electromechanical damping device with magnetic coupling," *Commun. Nonlin. Sci. Numer. Simul.* **11**, 907–921.

Yamapi, R. & Woafo, P. [2008] *Nonlinear Electromechanical Devices*: *Dynamics and Synchronization in Mechanical Vibrations*: *Measurement*, *Effects and Control*, ed. Sapri, R. C. (Nova Publishers).

Yang, J. & Jing, Z. [2009] "Controlling chaos in a pendulum equation with ultra-subharmonic resonances," *Chaos Solit. Fract.* **42**, 1214–1226.

Zhu, Q. & Ishitobi, M. [1999] "Experimental study of chaos in a driven triple pendulum," *J. Sound Vibr.* **227**, 230–238.

Dedications

I dedicate this work to my **parents** who have always believed in me and have encouraged me to go far.

Acknowledgements

First of all, I would like to thank the Lord Almighty for the strength given every day to accomplish this thesis. It is also an opportunity to thank all those who have contributed in any way to the development of this work. I think particularly to:

- **Professor WOAFO Paul,** my PhD supervisor who has given me the opportunity to join his research laboratory, to present my investigation work during laboratory seminars and some conferences that he organized and that helped me to improve the quality of this work. I also thank him for the encouragements, advice, orientations, and supports in all aspects of this research and during the writing of this thesis.
- **Professor Jean-Marie Bienvenu NDJAKA,** the Head of the Department of Physics, Faculty of Science, UYI and all **the teaching staff** and **personnel of the Department of Physics** for their valuable teachings and their fruitful advice from my first year of undergrad at the University until now.
- To All the members of **jury** for the examination of this thesis.
- **Professor ESSIMBI ZOBO Bernard,** Professor at the University of Yaounde I, Faculty of Science for his encouragement and his support.
- **Professor NANA NBENDJO Blaise,** Professor at the University of Yaounde I, Faculty of Science for his availability and his advice.

- To **Dr. TSAPLA FOTSA Rolande** for her scientific assistance and her availability during a part of this work.

- To **Dr. TCHAKOUNTE Hyacinthe** for teaching me some experimental technics and quick response to my inquiries.

- All my elders of the Laboratory in Modelling and Simulation in Engineering and Biomimetics and Prototypes (LaMSEBP) who supported this work with their knowledge: **Professor SIFEU TAKOUGANG KINGNI**, **Dr. CHAMGOUE André, Dr. NWAGOUM Peguy, Dr. THEPI Raoul, Dr. SIMO DOMGUIA, Dr. TCHAKUI Murielle, Dr. FANKEM Raissa and Dr. TALLA Francis**.

- All My labmates and PhD students with whom I share wonderful moments and particularly: **Dr. MBOU SOH Guy, Dr. YOUMBI FOUEGO Dorota, Dr. ESSAMBA MAH Ursule, Dr. NGATCHA TANLY Nelly, Dr. MONKAM Ibriss Joel, Dr. MBOYO Réné, TEMGOUA Pavel, KOUNCHIE Prosper, AMBASSA Armel, Mrs NFOPA Nikèse** and **FOFOU Ruth** for fruitful interactions during the seminars and my presentations at the LaMSEBP.

- All the scientific organizations in which I have been involved and for the different financial support they provided to the group to carry out activities in secondary schools, universities and conferences that helped me to flourish scientifically during my PhD Studies notably **the Optical Society** (OSA),**the Society of Photonics, Instrumentation and Engineering**(SPIE), **the Institute of Electronics, Electricity and Engineering** (IEEE) **CPS student Chapter**.

- My friends **Dr. NDJAWA YOMI pavel, OUANDJI KAMDOUM Magloire** and **MOIHAMETTE FOUAPOUAGNIGNI**, for their moral support, assistance, and encouragements.

- The great family of **CPP Notre Dame du Perpétuel Secours** for their encouragement and their spiritual support.

- My parents **Mr. KOUAM Pierre** and **Mrs. MONOUO Nicole** for their love, advice, encouragement, support in every way and particularly for their prayers to God to see this thesis achieved.

- Father **Abbé MANI Michel** for his moral and spiritual support.

- My brothers and sisters **KOUAM Murielle Sandra, KOUAM KOUAM Ulrich, KOUAM GUIADEM Francisca** and **MALIEDJE KOUAM Pamela** who always believed in me and supported me in different ways.

Contents

List of abbreviations

A: Ampère

AC: Alternative Current

DC: Direct Current

EMS: ElectroMechanical System

FORTRAN: FORmula TRANslator

Hz: Hertz

MaEMS: Macro ElectroMechanical System

MATLAB: MATrix LABoratry

MRI: Magnetic Resonance Imaging

NODE: Nonlinear Ordinary Differential Equations

ODE: Ordinary Differential Equations

RK4: Fourth-order Runge-Kutta

T: Tesla

USB: Universal Serial Bus

V: Volt

List of Tables

List of Figures

Abstract

This thesis deals with the dynamics of rotating electromechanical systems subjected to the action of potential wells generated by permanent magnets. Two models are considered. The first, in which arm with magnet at the free end, is immersed in a potential created by two permanent magnets, and the second where the arm (with a magnet at the free end) is embedded in a magnetic field generated by several magnets arranged in a circle. In each case, the electrical subsystem is supplied with two forms of input signal (DC and AC voltage sources). Following a schematic representation and the detailed description of each prototype, the mathematical models are written, and appropriate theoretical and experimental methods are used to investigate their dynamical behaviors. The following main results are obtained:

- The obtained magnetic potential shapes change with the parameters of the system such as: the length of the arm, the positions, and the number of magnets.

- The condition of a full rotation of the rotating arm versus the parameters of systems is determined. Under the DC voltage excitation, the arm oscillates and then stabilizes at an equilibrium position for a DC voltage below a critical value . When the DC voltage is higher than the critical value , the arm performs large amplitude motions (complete rotation). Submitted to an AC voltage with amplitude lower than a critical value, the mechanical arm exhibits sinusoidal oscillations around the equilibrium position with an amplitude less than 2π. Angular oscillations with an

amplitude greater than one revolution (360°) are observed when the voltage amplitude is greater than the critical value. These correspond to rotation oscillations.

- Chaotic and periodic dynamics are numerically detected and experimentally confirmed.

Keywords: Electromechanical systems, rotational arm, magnetic potential, nonlinear dynamics, chaos, rotation oscillations.

Résumé

Cette thèse traite de la dynamique des systèmes électromécaniques rotatifs soumis à l'action des puits de potentiel générés par des aimants permanents. Deux modèles sont considérés. Le premier dans lequel le bras avec un aimant à l'extrémité libre, est sujet à un potentiel créé par deux aimants permanents, et le second où le bras (avec un aimant à l'extrémité libre) est sujet à un champ magnétique généré par plusieurs aimants disposés périodiquement le long d'un cercle. Dans chaque cas, la partie électrique est alimentée par deux formes de signaux d'entrée (sources de tension continue et alternative). Après une représentation schématique et une description détaillée de chaque prototype, les modèles mathématiques sont établis et des méthodes théoriques et expérimentales appropriées sont utilisées pour étudier leurs comportements dynamiques. Les principaux résultats suivants ont été obtenus :

- Les formes du potentiel magnétique obtenues changent en fonction des paramètres du système tels que la longueur du bras, les positions et le nombre d'aimants.
- La condition pour une rotation complète du bras mécanique en fonction des paramètres des systèmes est déterminée. Sous l'excitation de la tension continue, le bras oscille puis se stabilise à une position d'équilibre pour une tension continue inférieure à la valeur critique. Lorsque la tension continue est supérieure à la valeur critique, le bras effectue des mouvements de grande amplitude (rotation complète). Soumis à une tension alternative d'amplitude inférieure à la valeur critique, le bras mécanique présente des oscillations sinusoïdales autour de la position d'équilibre avec une am-

plitude inférieure à 360°. Des oscillations angulaires d'une amplitude supérieure à 2π sont observées lorsque l'amplitude de la tension est supérieure à la valeur critique. Ce sont des rotations oscillatoires.

- Les dynamiques chaotiques et périodiques sont détectées numériquement et confirmées expérimentalement.

Mots-clés: Système électromécanique, bras rotatif, potentiel magnétique, dynamiques non-linéaires, chaos, rotations oscillatoires.

GENERAL INTRODUCTION

The magnetic field is a region of space in which magnetic forces occur. It can essentially be created from permanent magnets and electromagnets generating attractive/repulsive forces between the interacting objects [1, 2]. It is used in everyday life. The most popular application, where the magnetic field plays a key role, is exhibited by major types of electric motors including induction motors, stepper motors, and linear motors [3, 4]. Electric motors are characterized by high efficiency, high stall torque, and a high power-to-mass ratio, and hence, they attract interest in engineering-oriented research and beyond.

Technological progress yielded the fabrication of mechatronic or electromechanical devices such as active magnetic bearings and magnetic suspensions. To eliminate dangerous increases in the vibration amplitude when a critical frequency had been exceeded in rotating systems, auxiliary magnetic bearings are added. Magnetic suspensions are used in magnetically levitated vehicles for high-speed transportation of people and goods. They have many advantages including no contact, no friction, no dirt, and no lubrication effects. The mentioned advantages have helped build dirty-free factories and to solve numerous outer-space tasks [5–7]. Nowadays, we are increasingly witnessing the design and implementation of magnetic and electromagnetic springs due to the possibility of adjusting their stiffness unlike mechanical springs [8–12], offering applications in the production of vibration isolators [12].

Pendulum systems are one of the most popular objects in physics and were studied many times in terms of different kinds of excitation sources. Different configurations can

be found in the literature including plane or spatial, single or multiple, and sometimes parametrically excited pendulums [13–18]. Physicists are particularly interested in such dynamical systems, because, despite their relatively simple structure, they can exhibit almost all aspects of nonlinear dynamics (Oscillation, bifurcation, and chaos) [13–17,19–31]. Actual devices made of pendulums are technologically complex, sometimes they interact with magnetic and electric fields to generate mechanical energy with a high level of efficiency. Analyzing and understanding the behavior of such systems is crucial for the effective design and control of more complex mechanical systems with many degrees of freedom. Because of the importance of this topic, many researchers have investigated numerically, analytically and experimentally physical pendulums with magnetic interactions. One of the first scientists that analyzed such a system was Bethenod [32,33]. Subsequently, other studies have been carried out, such as the work done by Kraftmakher [34, 35], who investigated the pendulum behavior in the electromagnetic field produced by two magnets placed on opposite sides of the pendulum$'s$ rod at different distances from the point of the rotation. The external magnetic field drove the pendulum motion and could be used to modify the torque. In another paper, Wojna et al. [36] analyzed numerically and experimentally the behavior of a system containing a double physical pendulum with two permanent magnets forced by alternating magnetic fields coming from the coils. They presented extended bifurcation diagrams for different frequencies of excitation signal as a control parameter, obtained both experimentally and numerically. Polczyński et al. [37,38] described the behavior of a two-degree-of-freedom system consisting of two pendulums with magnets and elastic element coupling their pivots. Tests were conducted both numerically and experimentally. Moon et al [39] presented a permanent magnet rotor in crossed steady and time-varying magnetic fields. Experimental and theoretical investigations show that homoclinic orbits in a Poincaré map associated with a phase portrait flow are precursors of chaotic motion.

On the other hand, magneto-electro-mechanical pendulum-type systems are widespread in technical applications such as space exploration, robotic, servo-motor construction and fabrication, manufacturing estimation, control and automation, sensor [24–30, 40]. Investigations of these systems can be an essential challenge due to the presence of strong nonlinearities. The fine effects related to the details of the interaction description and mutual influence of force fields can appear in experiments. Nana et al [27, 28] studied both theoretically and experimentally an electromechanical system composed of a physical pendulum with repulsive magnets and a DC motor. They demonstrated that the device exhibits several types of nonlinear phenomena such as hysteresis, jump, and chaos.

Magnetic pendulums might be also used as an energy harvesting system [41–45]. An interesting fact from the demonstration is that the presence of magnets in energy harvesting systems is a source of optimization since it can lead to high power gain, and also facilitate the capture of energy on a large frequency spectrum. A double pendulum system with a magnet moving in the vicinity of electric coils [43] has shown that harvested power increases when the system motion undergoes a chaotic regime. Malaji et al. [44] reported that the harvesting capabilities may be enhanced by finding the optimal initial conditions in a harvester consisting of two torsionally coupled pendulums. Moreover, for other similar pendula systems [45], they observed that nonlinear responses improve individual harvester performance due to the adding mechanical coupling to the system which had only a magnetic one.

As we indicated before, in the investigation of the dynamics of mechanical and electromechanical systems within magnetic potential, several models have been developed and studied. In some cases, experimental realization has been carried out. It has come that these devices can exhibit all aspects of nonlinear behaviors such as amplitude jumps, hysteresis, chaos etc. The main purpose of our contribution to study the dynamics of nonlinear electromechanical systems

made of an arm possessing a magnet at one end and immersed in a circular trajectory on which magnets are positioned. Pendulum-like lever arms, rigid or flexible pendulum-like slender member, pendulum-like robots arms and mechanical manipulators are increasingly employed in industries. The dynamics of this system is investigated both theoretically and experimentally. In the theoretical aspect of our investigation, we use Newtonian physics and Kirchhoff laws to derive the equations of motion that describe the dynamics of the system. From these equations, amplitude response, condition for full rotation, bifurcation diagrams, time-histories and phase space plots are constructed. One of the main output of this thesis is the experimental investigation which demonstrated the complex dynamics of the horizontal magnetic pendulum.

This thesis is divided in three chapters. In chapter one, we briefly present some generalities on magnetic fields and their applications in everyday life. After that, research results on mechanical and electromechanical systems subjected to magnetic potential are presented. We end this chapter by highlighting the problem to be solved in this thesis. In chapter two, we present the physical descriptions of the systems analysed in this thesis and the methodology used. We describe the mathematical and numerical tools use to solve NODEs. Finally, experimental procedure is presented. In chapter three, the results are presented and we end with a general conclusion.

CHAPTER I

LITTERATURE REVIEW

1.1 Introduction

The goal of this chapter is to present magneto-electro-mechanical pendulum-type systems and some applications in everyday life then the main recent research results on the dynamics of such systems. At the end we come out with the problem analyzed in the thesis. In section I.2, the generalities of magnetic field and their applications are presented. Section I.3 is devoted to the presentation of research results on dynamics of mechanical systems in potential generated by magnets. Research results on rotational electromechanical systems in action within the magnetic field are presented in section I.4. Section I.5 will give more details on the problems to be solved in this thesis. The last section is dedicated to the conclusion.

1.2 Generalities on magnetic field

Magnetism has always been a phenomenon which has aroused interest in humans. According to the historical sources [46, 47], the magnetic phenomenon was documented for the first time in the ancient Greek by Thales of Miletus (about 585B.C.). Since that moment, many scientists have observed and written about magnetic attraction and repulsion. Many applications were developed, like the magnetic compass, which improved the navigation routes possibilities. It was not until the XIX century when the Danish physicist and chemist Hans Christian Œrsted [48] discovered that electric currents were able to create

disturbances in magnets. That was the first time that a connection between electricity and magnetic fields was discover. Since that moment, many other scientists in the following decades were going to develop the fundaments of electromagnetism. The magnetic field is generally produced by two main sources, namely electromagnets and permanent magnets.

1.2.1 Electromagnets

1.2.1.1 Definition

An electromagnet is a reluctant system that generates a magnetic induction that can create a force. This force is used to move a part of the magnetic circuit and thus drive a mechanical assembly. The importance of the study of electromagnets is considerable in electrical engineering. Coils are frequently used as passive magnetic components in electrical machines (transformers, alternators, asynchronous machines and direct current machines) requiring the use of magnetic materials. Generally, an electromagnet consists of two parts: the first, fixed, supports the winding that creates the magneto-motive force, and the second mobile, completes the deformable magnetic circuit. The deformation is carried out in such a way that the flux is as great as possible, by reducing the overall reluctance of the magnetic circuit [49–52].

1.2.1.2 Constitution of an electromagnet

An electromagnet is a device designed to exert attractive forces (or torques) on a ferromagnetic part to transmit a translational or rotational movement to it. Its magnetic circuit, which can be deformed, generally consists of a fixed yoke, surrounded by one or more magnetiying coils and a moving armature. When the coil is energized, the moving armature moves so that the flux is as high as possible, reducing the overall reluctance of the magnetic circuit [53–57].

First of all, the operation of an electromagnet is associated with the creation of a

variable magnetic field, thanks to the supply of electric current; we have a coil behaving like a magnet around which a magnetic field prevails. A magnet has the property of attracting elements containing iron. It has two ends: the North and the South Pole. Two identical poles repel each other and two poles in opposite directions attract each other [1]. Magnets, therefore act on each other through forces of attraction and repulsion represented by magnetic lines of force.

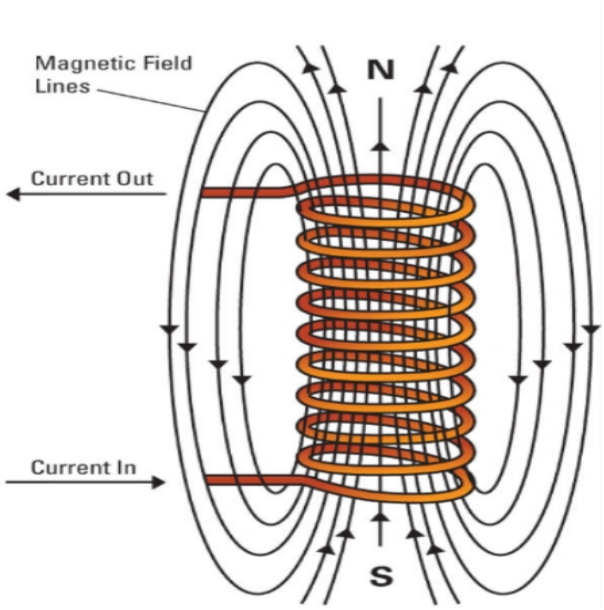

Figure 1.1: *Magnetic field lines in an Electromagnet* [57].

1.2.1.3 Principle of the electromagnet

Unlike permanent magnets, they are driven by the presence of a current When the electromagnet is supplied with current, the magnetic field created is channeled through the magnetic circuit. The power of an electromagnet is proportional to its number of turns (windings of copper wire around the magnetic circuit). The greater the number of turns, the more powerful the electromagnet becomes: it is the principle of the electromagnet that has made it possible to use electricity to transmit information instantly from a distance. The magnetic field is a force resulting from the displacement of charges; these magnets

create the magnetic field. Each point in a region of space in which a magnetic field exists is associated with a magnetic field vector B, which is characterized by specific properties of the electromagnet.

1.2.1.4 Physical characteristics of electromagnets

- **Geometrical characteristics**

  Depending on the application, electromagnets can take different forms. Mainly, electromagnets can be divided into four categories [1, 56].

  U-shaped electromagnets (Fig 1.2.a): In these electromagnets the core is U-shaped. The moving armature completes the magnetic circuit. In this category, electromagnets are distinguished by the shape of the armature, which can be flat, flap, plunging or rotating. To minimize eddy current losses, ferromagnetic parts can be made of laminated material.

  E-shaped electromagnets (Fig 1.2.b): In these electromagnets the core is E-shaped. The moving armature can be flat or plunging.

  Plunging core electromagnets (Fig 1.2.c): it consists of a coil and a core engaged at the entrance to the coil. The passage of current causes the core to be drawn in. The core sinks several centimeters inside the coil.

  Cylindrical electromagnets(Fig 1.2.d): these electromagnets are cylindrical in shape and have a flat armature or a plunging core. In this category of electromagnets, the winding is completely housed in the magnetic circuit, resulting in a robust structure. This shape does not lend itself to laminating the magnetic circuit, which is usually made of ferrite (rotor).

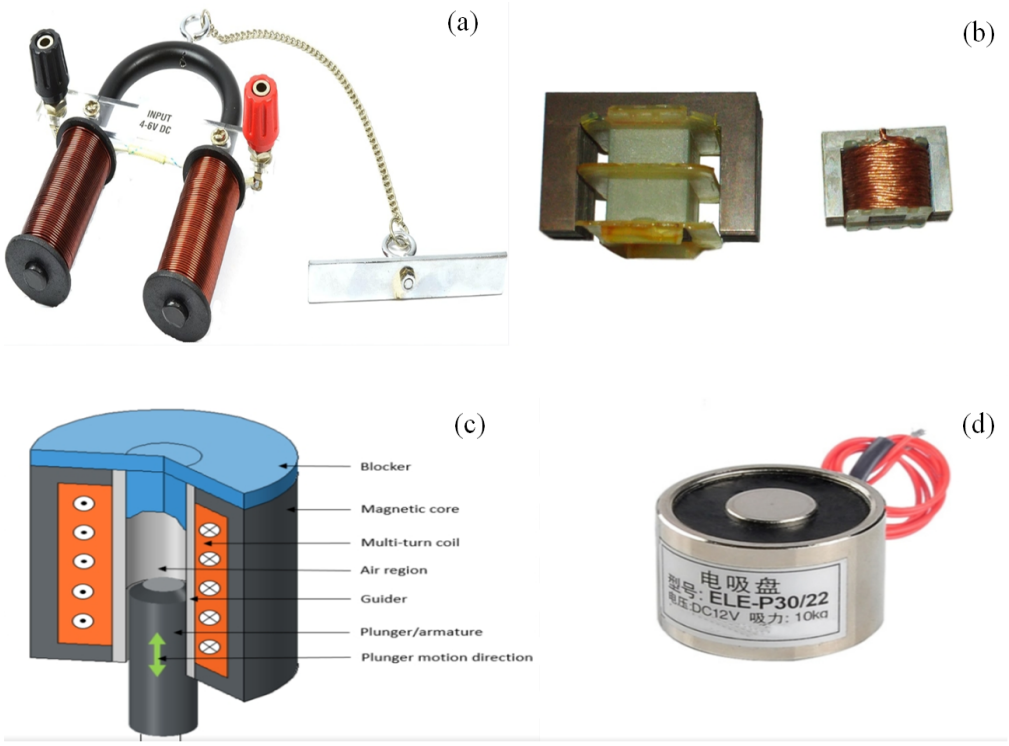

Figure 1.2: *Different forms of electromagnets* [1, 56].

- **Electrical characteristics**

  Control solenoids are defined by closing and opening sequences of the supply circuit. The resulting movement can be straight or rotary and the control can be described as single or multiple. In single control solenoids, the movement can only take place in a certain direction. This type of electromagnet is used, for example, in the cutting of sheet metal or plastic films. Intermediate positions of the armature, which are achieved by electronic control, give the electromagnet other types of functions (e.g. fluid flow control tool). Multi-control solenoids allow the armature to move in one direction or the other. This is for example the case with electromagnetic sewing machines.

1.2.2 Permanent magnets

Permanent magnets are ferromagnetic object which, when magnetised, retain a certain magnetic state, the most noticeable effect of which is to attract a piece of iron. These have only really developed since the 1930s. New types have been discovered, synthesised and industrialised, with performances such that applications have multiplied in many fields, from the automobile to electro-acoustics, from watchmaking to the mining industry, from household appliances to toys, etc. Permanent magnets are increasingly used in planar actuators [58–65].

1.2.2.1 Magnetism

Magnetism is an invisible force, acting at a distance, created by natural or artificial magnets. Natural magnets are bodies capable of attracting pieces of iron or filings. When a piece of iron is rubbed against an elongated piece of steel, an artificial magnet is created.

Not all bodies are attracted to a magnet. Those that are, called ferromagnetic bodies. Every magnet has a north and a south pole. If you break one magnet in half, you get two magnets, each with its own north and south poles. It is therefore impossible to isolate the north pole of a magnet from its south pole.

Some objects called magnets generate magnetic fields, the Earth itself is a giant magnet. The needle of a compass is a magnet, under the effect of the earth's magnetic field, it points (approximately) in the north-south direction. The end of the needle that points north is called the South Pole. This can be represented by magnetic field lines. These lines leave the magnet near the North Pole and re-enter the magnet near the South Pole [60, 65].

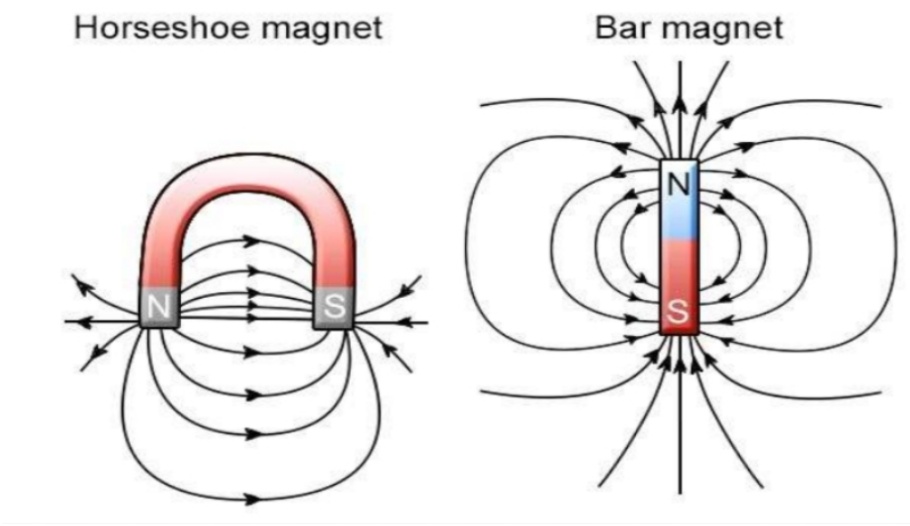

Figure 1.3: *Magnetic field lines in permanent magnets* [66].

1.2.2.2 Different types of permanent magnets

There are four families of permanent magnets. These are the:

- **Alnico permanent magnets**

  Permanent magnets were originally made from steel or chrome-cobalt. In the 1935s, people began to investigate iron-aluminium, nickel, cobalt and, copper alloys. These molten or sintered alloys are known as ticonal or alnico. They are very little used today because of the presence of cobalt (very expensive) and their modest magnetic properties.

- **Ferrites magnets**

  Ferrite magnets, or ceramic magnets, are still widely used. They have a maximum energy product of up to about 4.3 MGOe. Ferrite is the cheapest magnetic material and has a high corrosion resistance, which eliminates the need for coating. Ferrite magnets can be produced both isotropically and anisotropically and the maximum operating temperature is 225°C. Ferrite is a chemical composition, composed of ceramic material with iron oxide (Fe_2O_3) as the main component, supplemented by Strontium.

- **Samarium-Cobalt Permanent Magnets**

  Samarium-cobalt permanent magnets were discovered in the 1960s. These magnets have a much better magnetic performance than the two previous families, especially in terms of temperature resistance, but their cost is a major drawback. Cobalt is an expensive and strategic material, and its reserves are concentrated in a small number of countries. Samarium is one of the most expensive rare earths.

- **Neodymium-iron-boron permanent magnets**

  A neodymium magnet (Nd-Fe-B magnet) is a permanent magnet composed of an alloy of neodymium, iron, and boron ($Nd_2Fe_{14}B$) to form a tetragonal crystal system. Developed in 1982 by General Motors and Sumitomo Special Metals, neodymium magnets are the strongest permanent magnets available on the market, also described as a "rare earth magnet", is the strongest and most powerful magnetic material. Nowadays, Nd-Fe-B is the most popular and widely used magnetic alloy.

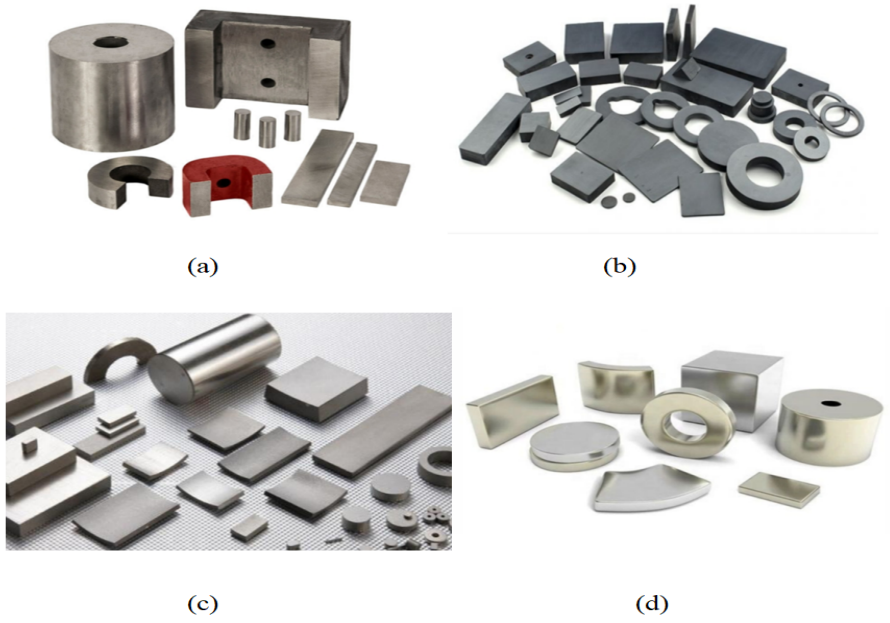

Figure 1.4: *(a) Alnico; (b) Ferrites; (c) Samarium-Cobalt and (d) Neodymium magnets* [56, 67].

1.2.3 Various applications and use of Magnets

Due to their magnetic properties, magnets are used in many ways in everyday life. For example, magnets are used in the compass, in electric motors, in medical imaging tools, and other applications [68–70].

- We might be using computers in our day-to-day lives but never wondered about the presence of a magnet inside it. Magnetic elements on a hard disk help to represent computer data, which is later read by the computer to extract information.
- Magnets are used inside Televisions, sound speakers, and radios. The small coil of wire and a magnet inside a speaker transforms the electronic signal into sound vibrations.
- Mechanical energy is converted into electric energy in a generator by using magnets. In contrast, other kinds of motors use magnets to change electric energy to Mechanical energy.
- Electrically charged magnets can help cranes to move large metal pieces
- We often use a pocket compass to find out directions when we are on a trek. The pocket compass uses a magnetic needle to point north.
- The dark strip on the back of debit and credit cards is magnetic and is used to store data like a computer's hard drives.
- At home, you use magnets when you stick a paper on the refrigerator in order to remember something. Attaching a magnetic bottle opener to the fridge can come in handy.
- Magnetic Resonance Imaging (MRI) machines are used to create an image of the bone structure, organs, and tissues. Even magnets are used to cure cancer.

- It is also used in food processing industries for separating small metallic pieces from grain etc.
- Magnets can help collect all the nails which are scattered on the ground after repair job.

1.3 Mechanical systems in potential generated by magnets

In recent years, nonlinear mechanical systems have received remarkable attention. Different forms of nonlinearly pendulums have been presented. Some studies investigated non-magnetic oscillators which present material, geometric or inertial nonlinearities [13, 15, 18, 71–75]. Other studies have focused on magnetic oscillators including magnetic pendulums [32–39, 76].

Magnetic interaction among magnets is a form of nonlinearity which is introduced into many systems. Researchers use analytical, numerical, and experimental tools to analyse the time evolution characteristics of these systems in several configurations.

1.3.1 Asymmetric magnetic pendulum under the action of a tilted excitation

Kitio et al. [76] studied the effect of tilted harmonic excitation and of parametric damping on the chaotic dynamic in an asymmetric magnetic pendulum. The Melnikov method is used to derive a criterion for transition to non-periodic motion in terms of the Gauss Hyper-geometric function. The regular and fractal shapes of the basin of attraction are used to validate the Melnikov predictions. In the absence of parametric damping, the results show that an increase of the tilt angle of the excitation causes the lower bound

for horseshoes chaos to increase and produces a singularity at the vertical position of the excitation. The authors also show that the presence of parametric damping without a periodic fluctuation can enhance or suppress horseshoes chaos while parametric damping with a periodic fluctuation can increase the region of regular motions significantly (See figure 1.5).

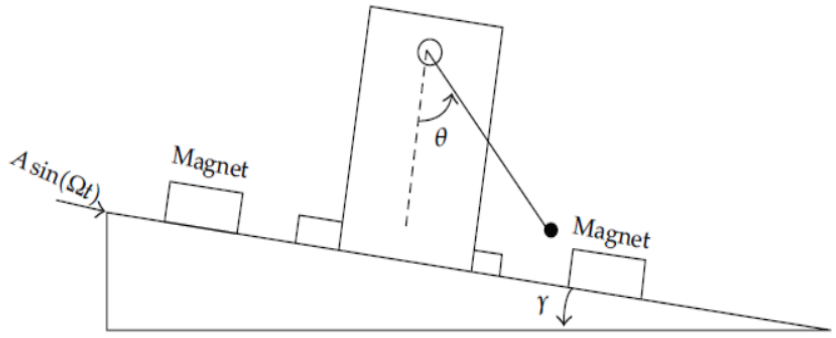

Figure 1.5: *Schematic representation of the pendulum* [76].

1.3.2 Double pendulum with magnetic interaction

Wojna et al [36] investigated numerically and experimentally the dynamics of a double physical pendulum with magnetic interaction. The authors first focused on mathematical modelling, numerical simulations, experimental measurements, and in particular on novel magnetic interaction modelling. System parameters are identified by matching the output signals from experiments and numerical solutions to the developed mathematical model governed by a strongly non-linear set of two second order ODEs including the friction and the magnetic interaction torques. The bifurcation diagrams have shown that the system exhibits periodic and chaotic dynamics. The authors have secondly illustrated the good agreement between the numerical simulation and experimental measurement (See figure 1.6).

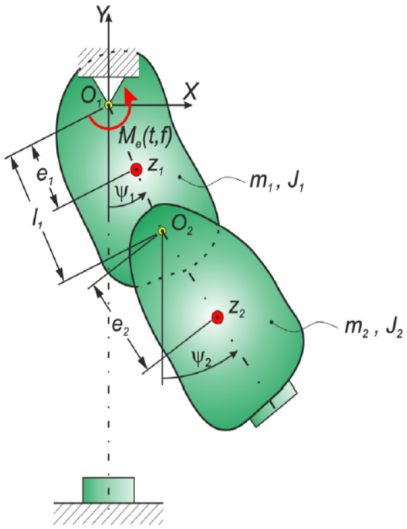

Figure 1.6: *Schematic representation of the pendulum* [36].

1.3.3 Coupled magnetic pendulums

Polczyński et al [37] studied a two-degree-of-freedom system consisting of two pendulums with magnets embedded in a variable magnetic field. Pivots of the pendulums are coupled by an elastic element. The magnetic interaction originates from permanent magnets, mounted at the free ends of the pendulums and current-powered air coils underneath. A novel model for the magnetic force has been proposed and verified experimentally. Time series, bifurcation diagrams, phase portraits, and Poincaré sections have been employed to examine the non-linear dynamics of the device. The results of this work have shown regions of chaotic and regular motion predicted numerically and justified experimentally. Multiperiodic motion and coexisting solutions are detected, and pictures in basins of their attraction are reported, among others.

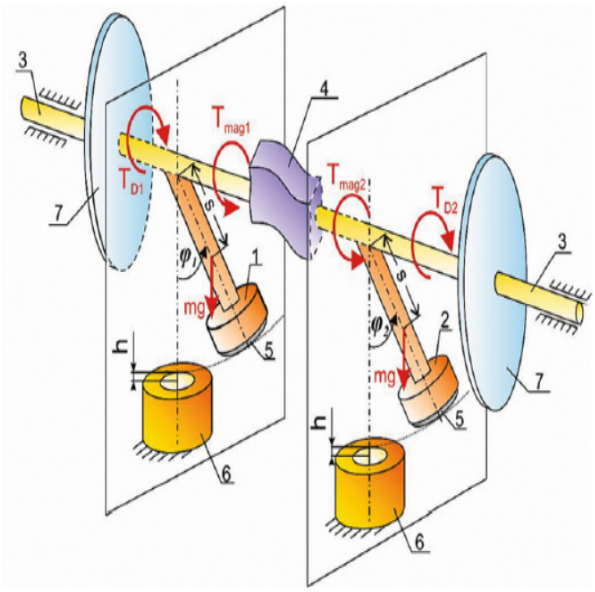

Figure 1.7: *Physical model. 1: pendulum; 2: pendulum; 3: pivot; 4: elastic element; 5: neodymium magnet; 6: air-core coil; 7: wheel.* [37].

1.3.4 Permanent magnet rotor in crossed magnetic field

Moon et al [39] found experimentally and theoretically critical values of magnetic torque and forcing frequency for chaotic oscillation of a permanent magnet rotor in crossed steady and time-varying magnetic fields. The experimental data shows good agreement between the criterion for homoclinic orbits using Melnikov theory and experimental values of torque and frequency at which strange attractors occurs. The fractal nature of the strange attractor is revealed by a Poincaré map triggered by the angular position of the rotor. The authors also used numerical simulations of the model and showed a good agreement with the theoretical and experimental criteria for chaos to appear in the system.

1.3.5 Magnetic pendulum excited by an electromagnet

Skurativskyi et al [94] have been used averaging methods and numerical simulation to study a single magnetic pendulum system in which the magnetic interaction is between the magnet placed at the end of the pendulum and an electrical coil powered by a pulsating

rectangular current signal. The mathematical model of the pendulum was represented by the non-autonomous ordinary nonlinear differential equation. The saw-tooth functions have been proposed by the authors to approximate highly nonlinear features possessed by the amplitude and phase shift of system solutions.

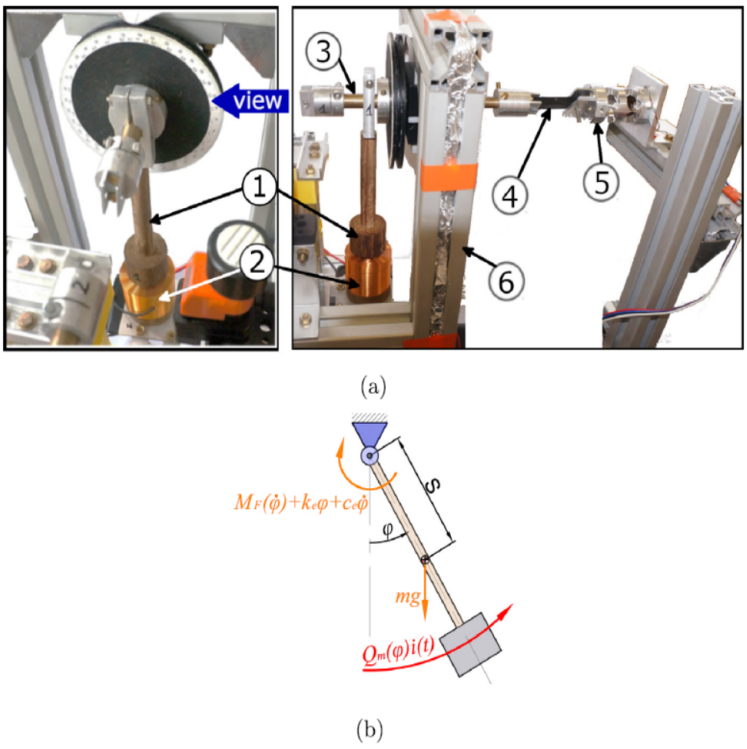

Figure 1.8: *Experimental set-up of a magnetic pendulum (a). (1): the pendulum with a magnet, (2): an electric coil, (3): a shaft, (4): a torsional spring, (5): a fixed base, (6): a frame; and its physical model (b).* [94].

1.4 Electromechanical systems with magnets-induced potential

An electromechanical system is a composite system formed by interconnecting mechanical and electrical parts. The central element in this interconnection is the conversion of mechanical energy into electrical energy, and vice versa. When it is supplied electrically,

it produces a mechanical motion (actuator). Reciprocally, it delivers a voltage when it is excited mechanically (generator). Electromechanical systems are found in many areas: manufacturing, communication, and energy production. Electromechanical transducers are pervasive in modern life, they include microphones, loudspeakers, electrical motors, magnetic suspensions, capacitive accelerometers, and also sensors and actuators [77–82]. Among those devices, we can find rotational and pendulum electromechanical systems.

1.4.1 Rotational electromechanical systems

Rotational electromechanical systems are complete rotating energy-transforming electromechanical motion devices that convert energy. We distinguish two main classes: motors which transform electrical energy into mechanical torque and generators which convert mechanical energy into electrical signal. They are generally consisting of two parts: the stator which is fixed and the rotor which moves. The stator establishes the magnetic excitation through the supplied winding or simply permanent magnets. Then, the interaction between the electrical current that flows the rotor windings and this magnetic interaction from the stator causes the rotor to move around its axis with respect to the Faraday's law. On the other hand, the rotating motion of the moving part within magnetic fields generated by the fixed part gives rise to an induced current according to Lorentz's law. Thanks to the fact that they are capable to operate in a large power range (from microwatt power to gigawatt power), rotational electromechanical systems are widely used in many domains [83]. Gensets, power generation stations, AC/DC motors, and dynamos are some applications of these systems.

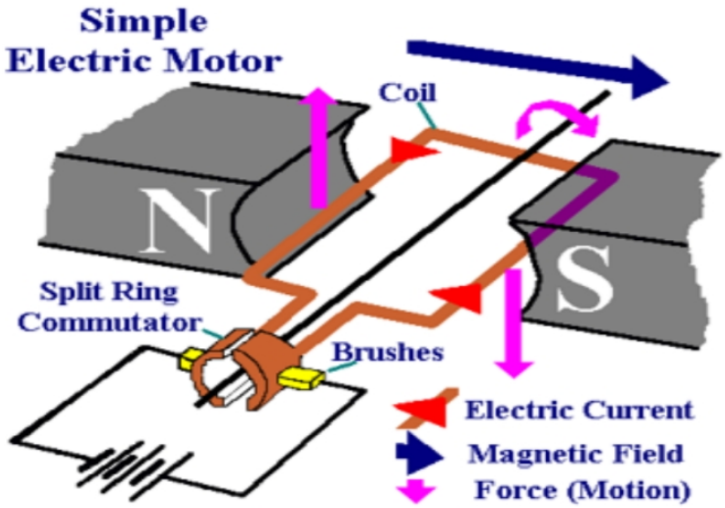

Figure 1.9: *Principle of conversion of electrical energy into mechanical energy: case of rotating electrical motor* [84].

1.4.2 Electromechanical pendulums

Pendulums are physical objet that attracted the attention of many researchers in their different configurations. They are used in modelling all kinds of phenomena related to oscillations, bifurcations and chaos. This is because many oscillatory problems may be reduced in some way to the equations of the pendulum. From the technological point of view, the pendulum arm is one of the fundamental elements of an engineering structure. It finds uses in varied structural applications. Moreover, structures like helicopter rotor blades, spacecraft antennae, flexible satellites, airplane wings, gun barrels, robot arms, mechanical manipulators, high-rise buildings, long-span bridges, and subsystems of more complex structures can be modeled as a rigid or flexible pendulum-like slender member. Therefore, studying the dynamical response, both analytically and numerically, of this simple structural component under various loading conditions would help in understanding and explaining the behavior of more complex, real structures under similar loading [85].

An electromechanical pendulum system is obtained when a mechanical pendulum system is coupled magnetically to a RL/RLC circuit [86, 87] or an electric motor [27, 28]

in order to produce a controllable motion or electricity. Sometimes magnets are added to many Macro-Electromechanical devices to provide more complex dynamics such as chaos in the case of the study of the motion and to increase the energy harvesting performance and broaden the effective harvesting frequency range. For example:

- Nana et al [28] investigated the dynamics of an EMS consisting of a DC motor, a physical pendulum-like lever arm with repulsive magnets. The author investigations show that both periodic and chaotic behaviors are observed, depending on the frequency and amplitude of the driver and the distance between the two magnets. Amplitude jumps, hysteresis and bistable states occur for a range of frequencies near the natural frequency of the physical system are also observed. (See figure 1.10)

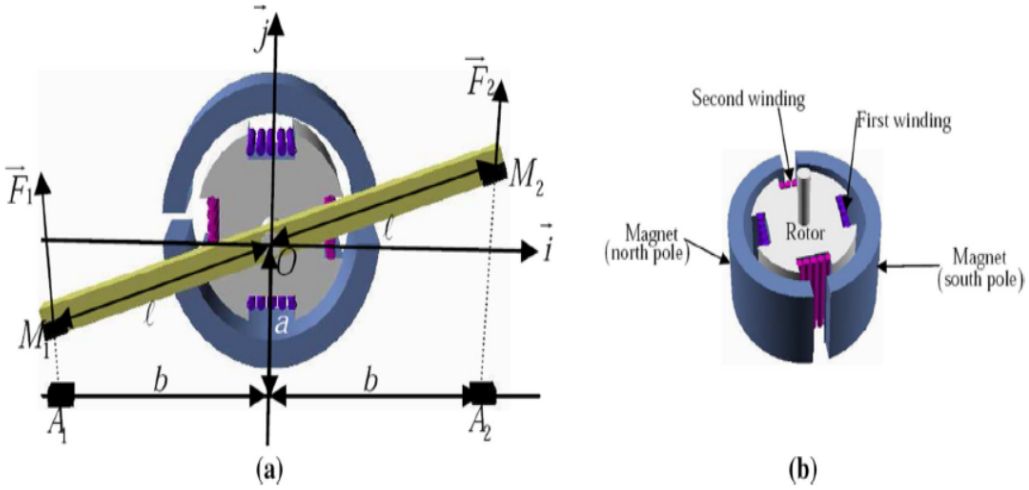

Figure 1.10: *(a) Completed physical system and (b) diagram of a permanent magnet electric motor* [28].

- Tesso et al [41] analyzed an energy harvesting system made of a beam possessing a magnet at one end and moving in a circular trajectory on which two magnets are diametrically positioned. Two types of excitation have been considered: the first one acts when the beam is passing inside an angular opening and the second one is a time periodic external excitation. The authors have presented and discussed the

generated mechanical potential energy due to the magnets. The conditions on the external excitation amplitude to obtain a complete rotation are obtained versus some parameters of the system and the types of motion which take place are presented. In addition, they have found that the power value increases with the magnetic strength when the magnets have strengths of the same sign. This showing an interesting result since it indicates the increase of power generated than to the presence of the magnets.

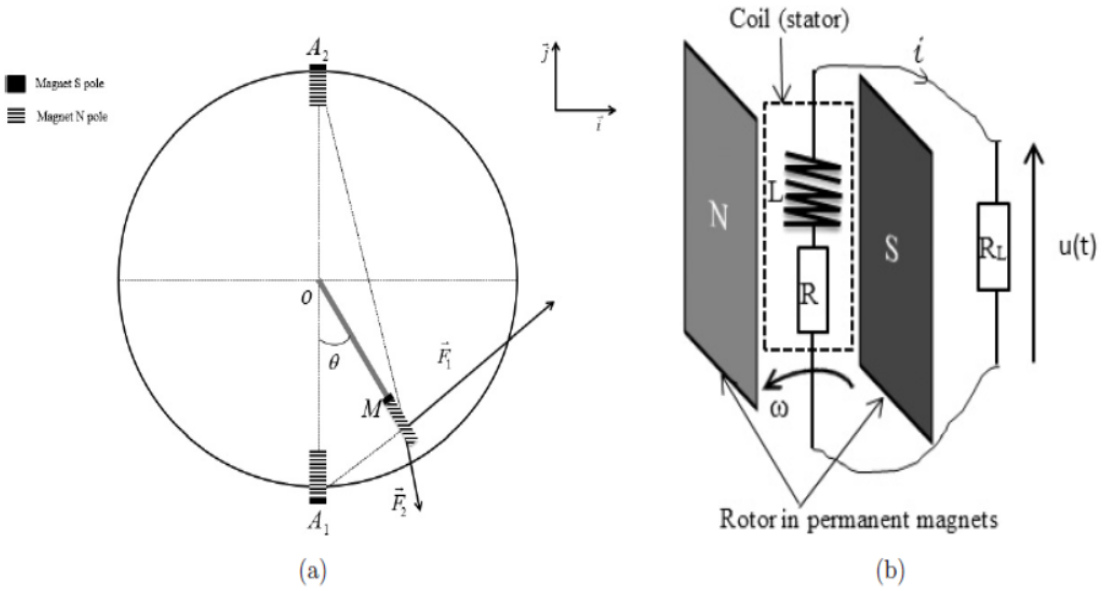

Figure 1.11: *Schematic representation of the electromechanical system* [41].

- Tsapla et al [26] studied the dynamics of an EMS consisting of an induction motor activating a rotating rigid arm and moving inside a bistable potential due to the presence of three permanent magnets. The numerical results both in the absence and in the presence of magnets are compared. In the presence of magnets, the authors have shown that the system presents periodic and dissipative chaotic dynamics. The Melnikov method is also used to derive the conditions for the appearance of Hamiltonian chaos by approximating the global potential energy to a bistable quartic potential.

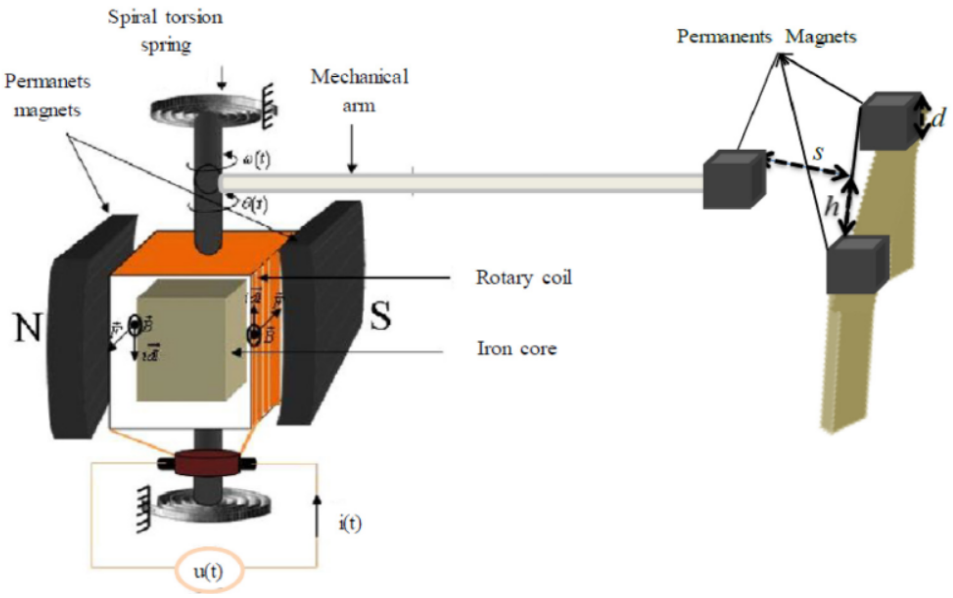

Figure 1.12: *Schematic representation of the electromechanical system* [26].

1.5 Problem statement of the work

Electromechanical systems are widely used in different branches of engineering [88–94]. They transform electrical energy into mechanical actions and vice versa via magnetic, piezoelectric, and capacitive couplings. Nonlinearities in an electromechanical system are often introduced in these systems because they could increase the efficiency of some industrial and home devices such as vibrating sieves, industrial mixers, and industrial shakers. Nonlinearities can appear either on the mechanical part, the electrical part, or on the coupling between the mechanical and electrical parts [89]. Nonlinearities appearing on mechanical components are particularly due to the inherent functioning of the structure as the stretching effects, the stiffness of a soft spring, and the boundary conditions on the structure. Nonlinearities on electrical components can be due for instance by diodes, capacitors, resistors, or inductors which have nonlinear characters. In practice, electronic components deliver low power and it is difficult to have mechanical components with nonlinear characteristics. Consequently, the chaotification technique which consists to introduce nonlinear electronic components in the EMS is limited to low power devices (e.g.,

micro arms in micro robots and for other micro actuation). At the macroscopic level where the power necessary to set parts into chaotic motion is high (MaEMS for example), one needs to use some other solutions, specifically found with electrical components. This is for instance the case of electrical circuit having a hysteretic iron-core. Inserted in an electric circuit, it can generate high amplitude chaotic signals. This has been used recently to power a model of an electromechanical sieve [88]. Another way is to use magnets to generate the nonlinearity and then work with linear electrical systems [26–30, 36–39, 92–95]. **The aim of this thesis is to present, construct, conduct mathematical modelling, and study mathematically, numerically, and experimentally a rotating electromechanical subjected to the action of a bistable potential generated by two magnets on the one hand and on the other hand, potential generated by several magnets regularly placed along a circle.**

1.6 Conclusion

In this chapter, we have provided background on magnetic fields and thier applications in everyday life. The recent research results on mechanical and electromechanical systems moving in magnetic potentials have been also presented. Finally, the problem to be solved in the thesis has been stated. In the next chapter, we will focus on the methodology used in this work.

CHAPTER II

METHODOLOGY

2.1 Introduction

In this chapter, we present the two models of EMS studied in this thesis, the theoretical methods used to solve NODEs and the experimental procedure. Theoretical methods concern both mathematical and numerical methods for NODEs describing the systems investigated in this work. The linear stability analysis for ODEs and the principle of harmonic balance used to obtain the analytical solutions of the systems of NODEs are presented in section 2.4. The fourth-order Runge-Kutta (RK4) algorithm, time histories diagrams, phase portraits diagrams, bifurcation diagrams, and Lyapunov exponent used to characterize the dynamical states of the systems are developed in section 2.5. Section 2.6 presents the experimental procedure and the last section is devoted to the conclusion.

2.2 Electromechanical device with two magnets

2.2.1 Description

Let us consider Figure 2.1 giving a schematic representation of the device and the magnetic forces acting on the arm. It consists of three main parts. The first part is a DC motor understood as a device converting the electrical energy to the mechanical one. The electrical motor is with permanent magnet, resistance R_i and inductance L_i. The rotor has two windings: one with the blue cable carries electrical current to produce a mechanical

torque while the winding with purple cable is used to measure the back electromotive force (f.e.m) in case of experiment. The f.e.m. is related to the rotation velocity of the mechanical arm [27, 28]. The second part is a one-degree of freedom mechanical arm welded to the shaft of the electrical motor. The third part consists of three permanent and identical magnets located at points M, A, and B (see Figure 2.1 (b)). The magnets A and B produce magnetic forces $(\vec{F}_{A/M}, \vec{F}_{B/M})$ on magnet M. The positions of the magnets A and B are measured by the angle ϕ made by the lines OA and OB with the horizontal line. The only damping force that the model contains is inside the motor and it is characterized by a simple viscous damping function. Since the arm is undergoing horizontal motions, the effect of the gravitational force is not included. The input voltage is either provided by a DC generator or a low frequency generator and is represented by $u(t)$. The angular displacement of the mechanical arm is the coordinate relative to a reference line (the horizontal line).

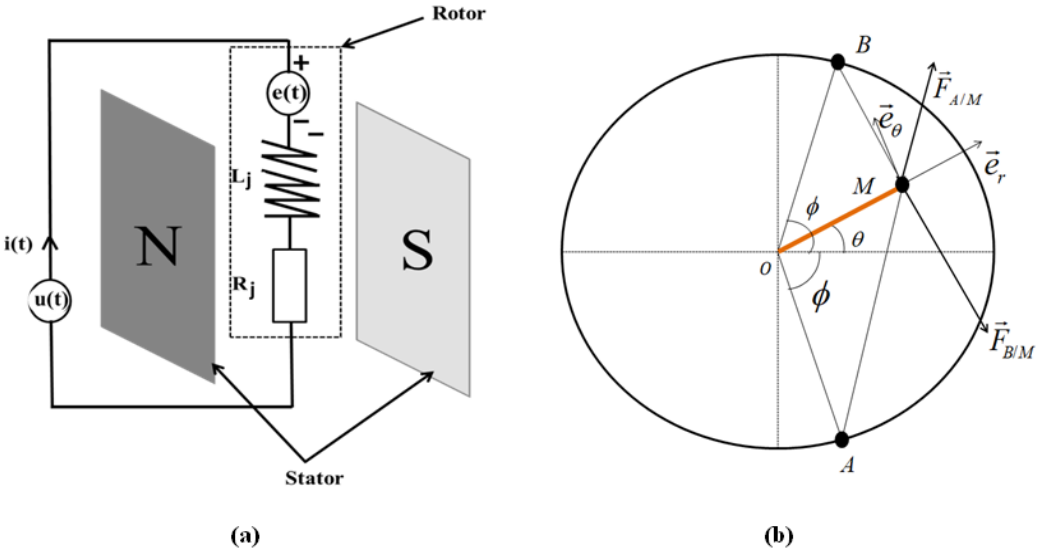

Figure 2.1: *(a) Schematic representation of the DC motor arm, (b) geometric representation of the magnetic forces acting on DC motor arm (in red).*

2.2.2 Mathematical modelling

Applying Kirchhoff's voltage laws to the electrical part of the DC motor, we find that the electric part of the model is described by the following differential equation:

$$L_j \frac{di}{dt} + R_j i + e(t) = u(t), \tag{2.1}$$

where $u(t)$ is the input voltage and i is the current through the winding. $e(t)$ is the back electromotive force. L_j, R_j and $e(t)$ are defined by the following expressions:

$$L_j = \frac{\mu_0 \mu_r N^2 h D}{l_g}; R_j = \frac{8\varphi(h+D)N}{\pi d^2}; e(t) = hDB_m N \frac{d\theta}{dt}\cos\theta, [27, 28] \tag{2.2}$$

where μ_0 is the permeability of the vacuum, h and D represent the height and diameter of the rotor respectively, B_m is the magnetic induction intensity and N is the number of turns.

Applying the Newton's second law of motion to the rotational motion, and taking into account the Laplace force, it is found that the mechanical part is governed by the following equation:

$$J_m \frac{d^2\theta}{dt^2} + \beta_m \frac{d\theta}{dt} + \frac{\mu_0 q_1 q_2}{4\pi R} f(\theta) = hDB_m N i, \tag{2.3}$$

where $J_m = (m_0 + \frac{m}{3})l^2$ is the total moment of inertia of the mechanical arm with the fixed magnet. m and l represent the mass and the length of the mechanical arm respectively. m_0 is the mass of the magnet M. β_m is the damping coefficient, q_1 is the pole strength of the magnet M and q_2 is the pole strength of magnets A and B. R is the distance between the focus O and the position of fixed magnets. The nonlinear function $f(\theta)$ comes from the repulsive interactions between magnets and is expressed as:

$$f(\theta) = -\frac{\delta \sin(\theta+\phi)}{[1+\delta^2 - 2\delta\cos(\theta+\phi)]^{\frac{3}{2}}} - \frac{\delta \sin(\theta-\phi)}{[1+\delta^2 - 2\delta\cos(\theta-\phi)]^{\frac{3}{2}}}, \tag{2.4}$$

where ϕ is the angle formed between the equilibrium position (horizontal line) and the position of a magnet and $\delta = \frac{l}{R}$ is the dimensionless length of the mechanical arm. Let us introduce the following dimensionless variables:

$$x = \frac{i}{I_0}; y = \frac{\theta}{\theta_0}; \tau = \omega_0 t. \tag{2.5}$$

Equations (2.1) and (2.3) take the following dimensionless form:

$$\ddot{y} + \lambda_m \dot{y} + \gamma f(\theta_0 y) = \varepsilon_m x, \tag{2.6}$$

$$\dot{x} + \lambda_e x + \varepsilon_e \dot{y} \cos(\theta_0 y) = E(t), \tag{2.7}$$

where the dots refer to the derivative with respect to the dimensionless time given above. The non-dimensional coefficients are defined as:

$$\lambda_m = \frac{\beta_m}{J_m \omega_0}; \gamma = \frac{\mu_0 q_1 q_2}{4\pi R J_m \omega_0^2 \theta_0}; \varepsilon_m = \frac{hDB_m N I_0}{J_m \omega_0^2 \theta_0}; \varepsilon_e = \frac{hDB_m N \theta_0}{L I_0}; E(t) = \frac{u(t)}{L\omega_0 I_0}; \lambda_e = \frac{R}{L\omega_0}. \tag{2.8}$$

The values of the physical and geometrical parameters used in this study are summarised in Table 2.1.

Table 2.1: *Values of the physical parameters of the first electromechanical system.*

Parameters	**Value**	**Parameters**	**Value**
B_m	0.73 T	N	20
μ_r	985	h	9.85 cm
d	0.15 mm	β_m	$0.2 * 10^{-3}$ Ns
q_1	43.76 Am	m_0	16.67 g
q_2	43.76 Am	m	5.13 g
D	8.12 cm	I_0	1 A
l_g	5.0 mm	ω_0	50 $rad.s^{-1}$
φ	$1.72 * 10^{-8}$ Ωm	R	15.96 cm

2.3 Case of the system with several magnets arranged periodically along a circle

2.3.1 Description

Figures 2.2 (a) and (b) show the schematic representation of the rotating electromechanical system. It is constituted of two main parts: an electrical one and a mechanical one. The electrical subsystem is made of a DC Motor powered by a generator, the whole seen as a resistor, an inductance and a power supply mounted in series (see Fig 2.2 a). As for the mechanical part, it considered physical pendulum system presented in Fig 2.2 b. The stand is equipped with the pendulum (OM), which has a neodymium magnet at the end M of the arm. This magnet interacts with a set of magnets at points M_k arranged periodically along a circle and creating repulsive forces. The angle between two consecutives of them is 2ϕ. The axis of rotation has coincided with the shaft axis. The other end of the arm is attached to the shaft.

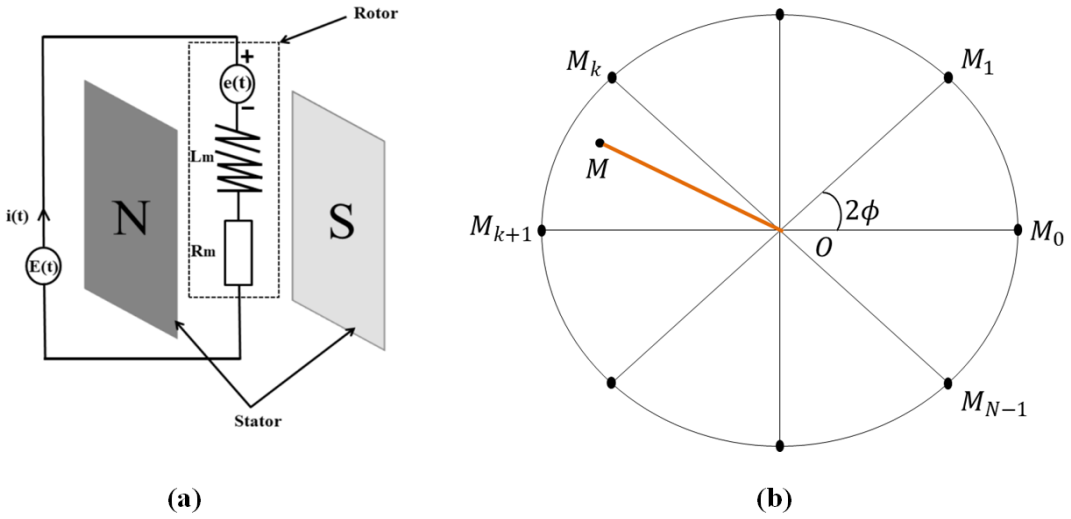

Figure 2.2: *Schematic representation of (a) the electric part and (b) the mechanical arm with magnets.*

2.3.2 Equations of motion

The governing differential equations will be derived by the use of the Newton's second law of motion, which for the analysed system takes the following form:

$$J_m \frac{d^2\theta}{dt^2} = \Gamma_d + \Gamma_M + \Gamma, \tag{2.9}$$

where $J_m = (m_0 + m/3)l^2$ is the total moment of inertia of the arm with the fixed magnet. m and m_0 represent the mass of the arm and the mass of the magnet M respectively. θ is the angular coordinate relative to a reference line (the horizontal line); Γ_d is the damping torque; Γ_M is the resulting magnetic torque; Γ is DC motor torque.

The damping torque is governed by the following formula:

$$\Gamma_d = -\beta_m \frac{d\theta}{dt}, \tag{2.10}$$

with β_m is the damping coefficient.

The DC motor torque is assumed to be proportional to the current passing through the windings of the rotor, i. Then if K_C is the electromechanical coupling of the motor, this torque can be defined as follows:

$$\Gamma = K_C i, \tag{2.11}$$

Finally, the terms Γ_M describe external torques responsible for the magnetic interaction between the magnets. In the model, we consider the action of all magnets. The $k-th$ magnet M_k produces on the arm (point M) the following magnetic torque [41].

$$\Gamma_{M_k/M} = \frac{\mu_0 q_1 q_2}{4\pi R} \frac{\delta \sin(\theta - 2k\phi)}{[1 + \delta^2 - 2\delta\cos(\theta - 2k\phi)]^{\frac{3}{2}}}, \tag{2.12}$$

where μ_0 is the permeability of the vacuum, q_1 is the pole strength of the magnet M and q_2 is the pole strength of magnets M_k. R is the distance between the focus O and the position of fixed magnets, $\delta = \frac{l}{R}$, the dimensionless length of the mechanical arm. The total magnetic torque is then:

$$\Gamma_M = \sum_{K=0}^{N-1} \Gamma_{M_k/M}, \tag{2.13}$$

with N the number of magnets.

Combining Eqs. (2.10), (2.11), and (2.13) leads to the first differential equation of the system:

$$J_m \frac{d^2\theta}{dt^2} + \beta_m \frac{d\theta}{dt} + \frac{\mu_0 q_1 q_2}{4\pi R} g(\theta) = K_C i, \tag{2.14}$$

The nonlinear function $g(\theta)$ is defined as follows:

$$g(\theta) = -\sum_{k=0}^{N-1} \frac{\delta \sin(\theta - 2k\phi)}{[1 + \delta^2 - 2\delta\cos(\theta - 2k\phi)]^{\frac{3}{2}}}. \tag{2.15}$$

Applying Kirchhoff's voltage law to the electrical part of the DC motor, we find that the electric part of the model is described by the following differential equation:

$$L_m \frac{di}{dt} + R_m i + e(t) = E(t), \tag{2.16}$$

The back electromotive force expression is:

$$e(t) = K_C \frac{d\theta}{dt} \cos\theta. \tag{2.17}$$

L_m and R_m respectively the inductance and resistance of the windings of the motor. $u(t)$ is the input voltage.

Equations (2.14) and (2.16) take the following dimensionless form:

$$\ddot{y} + \lambda_m \dot{y} + \gamma g(\theta_0 y) = \varepsilon_m x, \tag{2.18}$$

$$\dot{x} + \lambda_e x + \varepsilon_e \dot{y} \cos(\theta_0 y) = u(t), \tag{2.19}$$

using the following dimensionless variables:

$$x = \frac{i}{I_0}, y = \frac{\theta}{\theta_0}, \tau = \omega_0 t. \tag{2.20}$$

and dimensionless coefficients defined as :

$$\lambda_m = \frac{\beta_m}{J_m\omega_0}, \gamma = \frac{\mu_0 q_1 q_2}{4\pi R J_m \omega_0^2 \theta_0}, \varepsilon_m = \frac{K_C I_0}{J_m \omega_0^2 \theta_0}, \varepsilon_e = \frac{K_C \theta_0}{L I_0}, u(t) = \frac{E(t)}{L\omega_0 I_0}, \lambda_e = \frac{R}{L\omega_0}, \Omega = \frac{\omega}{\omega_0}. \tag{2.21}$$

The values of the physical parameters are given in Table 2.2.

Table 2.2: *Values of the physical parameters of the second electromechanical system.*

Physical parameter	**Value**	**Physical parameter**	**Value**
l	*variable*	L_m	$92 * 10^{-2}\ H$
R	$11.25\,cm$	K_C	$42 * 10^{-3}\ Nm/A$
m	$16.80\ g$	β_m	$0.50 * 10^{-3}\ Ns$
m_0	$2.50\ g$	θ_0	2π
q_1	$20.46\ Am$	ω_0	$50\,rad.s^{-1}$
q_2	$43.76\ Am$	I_0	$1\ A$

2.4 Mathematical formalisms

2.4.1 Linear stability analysis of ordinary differential equations

This subsection concern with the description of the method which permit to characterize the stability of the steady-state solutions or fixed points. To this end let us consider a given set of autonomous ODEs of first order, written in the vector form:

$$\frac{dX(t)}{dt} = F(X(t), \mu) \tag{2.22}$$

where $X(t) = (x_1(t), x_2(t), ..., x_n(t))$ is the vector of the dynamical variables of the system, a set of parameters μ and $F = (F_1, F_2..., F_n)$ is a differentiable vector function.

Suppose that X_0 is the steady state or fixe point. The linear stability analysis is based on analysing the time-dependent trajectory of a system slightly perturbed from a steady state X_0. Therefore, the solution $X(t)$ can be represented as a sum of the steady state X_0 and a small perturbation $\delta Y(t)$:

$$Y(t) = Y_0 + \delta Y(t) \tag{2.23}$$

Inserting (2.23) in (2.22) and linearizing around the steady state X_0 leads to the variational equation for the variable $\delta X(t)$.

$$\frac{d\delta X(t)}{dt} = J\delta X(t) \tag{2.24}$$

where J, the matrix of the partial derivatives is called the Jacobian matrix. The eigenvalues of the linear system of the equation (2.24) can be found from the characteristic equation of the system:

$$\det(\lambda I - J) = 0 \tag{2.25}$$

where I is the unit matrix and λ are the eigenvalues of the system (2.25) and roots of the characteristic equation. The stability of the steady state X_0 is determined by the eigenvalues of the system (2.25), as follows:

- If the eigenvalues of the Jacobian matrix all have real parts less than zero, then the steady state is stable;
- If at least one of the eigenvalues of the Jacobian matrix has real part greater than zero, then the steady state is unstable.

2.4.2 Principle of harmonic balance methods

The harmonic balance method is a technique applied to approximate oscillatory solution of a NODE submitted to a sinusoidal excitation. in the literature, it is one of the

most commonly used method for investigating nonlinear systems [96,97]. Let consider the following differential equation:

$$\ddot{x} + x = \varepsilon f(x, \dot{x}, t), \tag{2.26}$$

where the dot over x refers to differentiation with respect to time t the function $f(x, \dot{x}, t)$ contains explicitly the time t. The harmonic solution of this equation is expressed in the form:

$$x\,(t) = A_1 \cos(\Omega t) + A_2 \sin(\Omega t)\,, \tag{2.27}$$

where $A = \sqrt{A_1^2 + A_2^2}$ is the maximal amplitude of oscillations. Replacing equation (2.27) into equation (2.26) and equating separately the coefficient of sine and cosine terms, which have the same harmonics, one obtains (neglecting harmonics order greater than one) a system of algebraic equations which are the amplitude equations. This procedure is the basic principle of harmonic balance. It will be used in chapter III to obtain the amplitude and frequency response curves of the electromechanical devices with rotating arm.

2.5 Numerical methods

2.5.1 Fourth-order Runge-Kutta method for first-order differential equations

NODEs are solved analytically considering some assumption to obtain approximate solutions. In contrast, numerical method proposes solutions which are closed with the experiment. In this thesis, fourth order Runge-Kutta (RK4) is utilized for numerical resolution. Fortran 95, with Matlab and Maple software are also used as programming languages. RK4 numerical method is widely used because of its stability. It combines trapezium

numerical integration and Simpson methods. Let us consider the first order differential equation:

$$\frac{dy}{dt} = f(t, y), \tag{2.28}$$

with $y(t_0) = y_0$. This equation can also be under a vectoral form (and being vectors). The aim of the RK4 method is to find solutions after each time step h, the next solution as a function of the previous one. This method stipulates that:

$$y(t+h) = y(t) + \frac{1}{6}(L_1 + 2L_2 + 2L_3 + L_4), \tag{2.29}$$

where

$$\begin{aligned} &L_1 = hf[t, y(t)]; L_2 = hf\left[t + \tfrac{h}{2}, y(t) + \tfrac{L_1}{2}\right]; \\ &L_3 = hf\left[t + \tfrac{h}{2}, y(t) + \tfrac{L_2}{2}\right]; L_4 = hf[t + h, y(t) + L_3]. \end{aligned} \tag{2.30}$$

This procedure needs in its iteration only the initial value $y(t_0) = y_0$, to calculate all the other values taken by the function y at other times separated by the time step h.

2.5.2 Fourth-order Runge-Kutta method for m-order differential equations

In the case of m-order differential equation, we have:

$$\begin{cases} \frac{d^m y}{dt^m} = f_m\left(t, y, \frac{dy}{dt}, \frac{d^2y}{dt^2}..., \frac{d^{m-1}y}{dt^{m-1}}\right) \\ \frac{d^k y}{dt^k}(t_0) = y_0^{(k)} \end{cases} \tag{2.31}$$

with successive variables change, the equation (2.10) can be written under the following

form:

$$\begin{cases} \frac{d^0y}{dt^0} = u_0 = y = f_0(t, u_0, u_1, u_2..., u_{m-1}) \\ \frac{dy}{dt} = \frac{du_0}{dt} = u_1 = f_1(t, u_0, u_1, u_2..., u_{m-1}) \\ \frac{d^2y}{dt^2} = \frac{du_1}{dt} = u_2 = f_2(t, u_0, u_1, u_2..., u_{m-1}) \\ \vdots \\ \frac{d^{m-1}y}{dt^{m-1}} = \frac{du_{m-2}}{dt} = u_{m-1} = f_{m-1}(t, u_0, u_1, u_2..., u_{m-1}) \\ \frac{d^my}{dt^m} = \frac{du_{m-1}}{dt} = u_m = f_m(t, u_0, u_1, u_2..., u_{m-1}) \\ \frac{d^ky}{dt^k}(t_0) = u_k(t_0) = y_0^{(k)}, k \in \{1, 2, 3, ..., m-1\} \end{cases} \tag{2.32}$$

with this, general vectoral and form iterations can be performed to determine all the values of y and its derivatives at different time separated by the time step h using:

$$u_k(t+h) = u_k(t) + \frac{1}{6}\left(L_1^k + 2L_2^k + 2L_3^k + L_4^k\right) \tag{2.33}$$

where

$$\begin{aligned} L_1^k &= hf_k\left[t, u_0(t), u_1(t), u_2(t) ..., u_{m-1}(t)\right]; \\ L_2^k &= hf_k\left[t + \tfrac{h}{2}, u_0(t) + \tfrac{L_1^0}{2}, u_1(t) + \tfrac{L_1^1}{2}, u_2(t) + \tfrac{L_1^2}{2} ..., u_{m-1}(t) + \tfrac{L_1^{m-1}}{2}\right]; \\ L_3^k &= hf_k\left[t + \tfrac{h}{2}, u_0(t) + \tfrac{L_2^0}{2}, u_1(t) + \tfrac{L_2^1}{2}, u_2(t) + \tfrac{L_2^2}{2} ..., u_{m-1}(t) + \tfrac{L_2^{m-1}}{2}\right]; \\ L_4^k &= hf_k\left[t + h, u_0(t) + L_3^0, u_1(t) + L_3^1, u_2(t) + L_3^2 ..., u_{m-1}(t) + L_3^{m-1}\right]. \end{aligned} \tag{2.34}$$

This generalized form can also serve to solve numerically first-order coupled ODEs.

2.5.3 Numerical tools for the characterization of the dynamical state

This subsection is dedicated to present numerical tools which are used for characterizing different dynamical states of the nonlinear EMS investigated in this thesis. Among them we have the time histories diagram, phase portraits diagrams, bifurcation diagrams and Lyapunov exponent.

2.5.3.1 Time traces and phase portrait

Generally to detect dynamical regime transitions which are exhibited by a system, we start by a visual plot analysis of the computer simulation of NODEs. Attentively examine the time histories and phase portraits while Varying the parameter's values of NODEs. The chaotic behaviour is distinguished from others by its extreme irregularity.

A phase portrait of a dynamical system is a mathematical space having orthogonal coordinate directions which represent each of the variables needed to specify the instantaneous state of the system. The state of a particle moving in one dimension is specified by its position and velocity. The state of a dynamical system is represented by a point in the phase space. As the system evolves in time, it constitutes a trajectory in the phase space. Phase portraits are an invaluable tool in studying dynamical systems. They consist of a plot of typical trajectories in the state space. This reveals informations such as whether an attractor, a limit cycle is present for the chosen parameter's value. However, the drawback of this computational tool is that it can be hard to distinguish the quasi-periodicity and chaos phenomena by using the phase portrait diagram. The dynamical behaviors of the devices mathematically represented by ordinary differential equations in chapter III are illustrated using numerical simulation to present Time-histories and phase portraits.

2.5.3.2 Bifurcation diagram

The bifurcation diagram is another mean of the detection of dynamical states. Bifurcation diagram gives precise informations on the behaviors of a dynamical system when the parameters of the mathematical model are varied. A bifurcation can also be defined as the event in which one of the properties of a dynamical system changes qualitatively when a control parameter of the system is varied. Points on the diagram that represent change in the behaviour are called bifurcation points [98]. This diagram is very important for the study of the route to chaos. But the Achilles heel of this method is the confusion

between the quasi-periodicity and chaos phenomena. We can identify various routes to chaos taken by dynamical systems. The most common are: the period doubling route, the quasi-periodic route, and intermittency route. The most reliable indicator of chaos phenomenon is the maximum one-dimensional Lyapunov exponent.

2.5.3.3 Lyapunov exponent

Lyapunov exponent are the most accurate tools for characterizing chaotic and periodic states of a dynamical system. Lyapunov exponents describe the rate of divergence or convergence of nearby trajectories on to the attractor in different directions in phase space. It gives a measure of the sensitive dependence upon initial conditions which is a characteristic of chaotic system. The Lyapunov exponent expresses the convergence (when negative) or divergence (when positive) of nearby trajectories. Therefore, a state of the system is said to be chaotic if the Lyapunov exponent is positive (which corresponds, in the bifurcation diagram, to a cloud of points). The state of the system is said to be periodic if the exponent is negative (this corresponds, to a curve lines in the bifurcation diagram). The case corresponds to the quasi-periodic state of the system. The maximum one-dimensional Lyapunov exponent is defined as:

$$\lambda_{\max} = \lim_{t \to +\infty} \left\{ \left(\frac{1}{t} \right) \ln \left[D\left(t\right) \right] \right\}, \tag{2.35}$$

with

$$D\left(t\right) = \sqrt{\delta_1^2 + \delta_2^2 + \delta_3^2} \tag{2.36}$$

where $D\left(t\right)$ is the distance between neighbouring trajectories. It is computed from the variationally equations obtained by perturbing the solutions of equations as follows: $x \to x + \delta_1$, $y \to y + \delta_2$, $\dot{y} \to \dot{y} + \delta_3$.

2.6 Experimental procedure

2.6.1 Materials

The proposed materials relating to the construction of the electromechanical device use a DC motor, a rod and permanent magnets. One end of the rod is welded to the motor shaft and the other is fitted with a magnet. This magnet interacts with a set of magnets arranged along a circle and creating repulsive forces. For experiments, the magnetic field was measured by a teslameter. The DC motor comes from recycled objects, more specifically printers. Figure 2.3 below shows some examples of materials used for this thesis work.

Other equipments were used to power the device and measure physical quantities such as the angle and the rotational velocity of the arm (See figure 2.4). We can mention among others:

- a RIGOL generator of type DG812 with two channels, of bandwidth 10 MHz ;
- an accelerometer MPU 6050;
- an ARDUINO UNO microcontroller.

Figure 2.3: *Some materials used: (a) DC motor; (b) Neodymium magnets; (c) teslameter.*

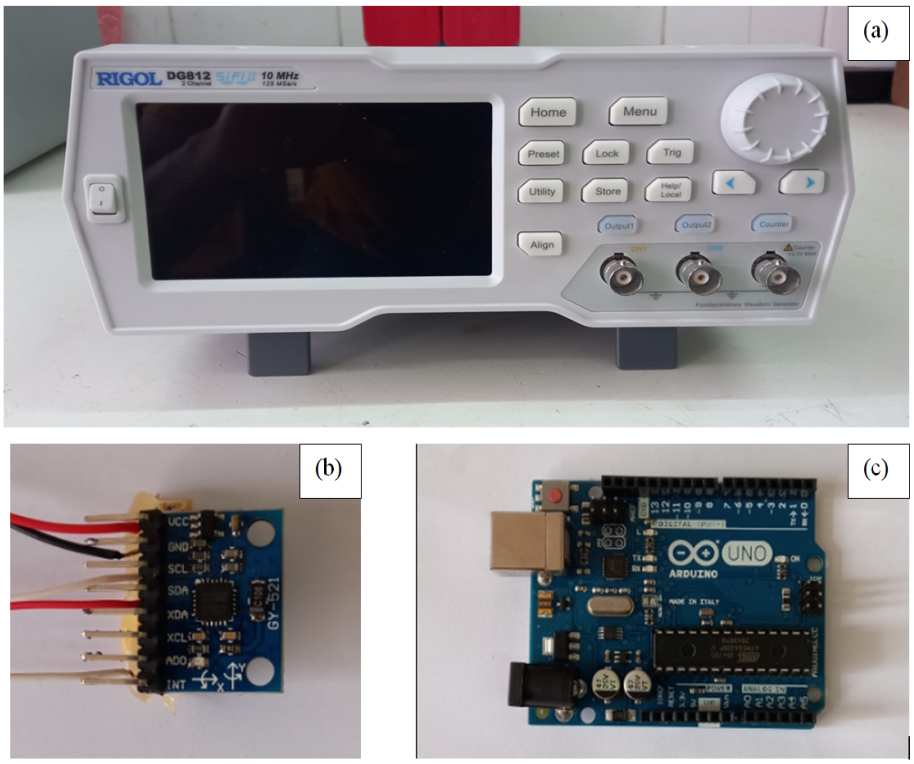

Figure 2.4: *(a) Generator; (b) accelerometer MPU 6050; (c) ARDUINO UNO microcontroller.*

2.6.2 Measuring the angular displacement and the velocity

The MPU6050 module consists of a temperature sensor and two micro-electromechanical sensors: a gyroscope and an accelerometer to measure accelerations in space. To measure the angle and the rotational velocity, we attach an MPU6050 module to the free end of the rod. The integrated gyroscope captures the different angles and rotational velocities as the arm moves over the time. These physical quantities are converted into an electrical signal which is sent to an ARDUINO UNO microcontroller and then stored in a computer.

2.6.3 Data analysis

Measurements should be made to register the data needed to draw meaningful conclusions from the system under test. These data are used to draw time-histories and phase portraits in order to have a deep analysis of the investigated system and make a comparison with results of numerical simulations.

2.7 Conclusion

The aim of this chapter was to present the physical descriptions of the models on the one hand and on the other hand, the mathematical, numerical simulation and experimental methods employed to study the dynamics of the physical systems proposed in this thesis. Mathematical formalisms and numerical methods used to solve the differential equations have been given. Then the numerical methods for the simulation of ODEs of first-order and m-order were presented. Finally, we presented experimental procedure. All of these methods will be used in Chapter III which is devoted to the presentation of the main results of this thesis.

CHAPTER III

RESULTS AND DISCUSSION

3.1 Introduction

This chapter is devoted to the results and discussion on the work carried out in this thesis. It is therefore organized as follows. Section 3.2 presents the electromechanical device with two magnets. Its mathematical equations are studied numerically. The attention is focussed on condition for complete rotation of the arm and types of dynamics that the system can exhibit when its parameters change. In section 3.3, the second model with several magnets placed periodically along a circle is also analyzed. The oscillatory states and chaos are investigated. The experimental part of this thesis is displayed in section 3.4. In section 3.5, we end this chapter by a conclusion.

3.2 Electromechanical device with two magnets

3.2.1 Potential energy and equilibrium points

This subsection is devoted to the presentation of the different potential curves depending on the pair of parameters ϕ and δ. The potential energy associated with equation (2.3) is:

$$U(\theta) = \gamma \left[\frac{1}{[\,1+\delta^2-2\delta\cos(\theta+\phi)]^{\frac{1}{2}}} + \frac{1}{[\,1+\delta^2-2\delta\cos(\theta-\phi)]^{\frac{1}{2}}} \right]. \tag{3.1}$$

Using the Taylor expansion formula, the potential energy can be approximated by the following expression:

$$U(\theta) = \frac{\gamma}{\delta_1}\left[2 + \frac{A}{2}\left(2\cos(\theta)\cos(\phi)\right) + \frac{3A^2}{8}\left(1+\cos(2\phi)\cos(2\theta)\right)\right], \tag{3.2}$$

where $\delta_1 = \sqrt{1+\delta^2}$ and $A = \frac{2\delta}{\delta_1^2}$.

The derivative of Eq. (3.2) is:

$$\frac{dU}{d\theta} = \frac{\gamma}{\delta_1}\left[-A\cos(\phi)\sin(\theta) - \frac{3A^2}{4}\cos(2\phi)\sin(2\theta)\right]. \tag{3.3}$$

By looking at the zeros of the derivative of the potential (eq. (3.3)), one finds the following equilibrium points:

$$\begin{cases} \theta_1 = 0 \\ \theta_2 = \pi \end{cases}. \tag{3.4}$$

Let us calculate the second derivative of the potential at the points $\theta = 0$ and $\theta = \pi$. One obtains:

$$\frac{d^2U}{d\theta^2}(0) = \frac{2\gamma\delta}{\left(1+\delta^2-2\delta\cos(\phi)\right)^{\frac{3}{2}}}\left[\frac{3\delta\sin^2(\phi)}{\left(1+\delta^2-2\delta\cos(\phi)\right)} - \cos(\phi)\right], \tag{3.5}$$

$$\frac{d^2U}{d\theta^2}(\pi) = \frac{2\gamma\delta}{\left(1+\delta^2+2\delta\cos(\phi)\right)^{\frac{3}{2}}}\left[\frac{3\delta\sin^2(\phi)}{\left(1+\delta^2+2\delta\cos(\phi)\right)} + \cos(\phi)\right]. \tag{3.6}$$

A point is said to be stable if the second derivative is positive. Otherwise, it is unstable. From equation (3.5), one finds that depending on the $(\delta;\phi)$, $\theta = 0$ can be stable or unstable. It is stable (respectively unstable) under the following respective conditions:

$$\frac{3\delta\sin^2(\phi)}{\left(1+\delta^2-2\delta\cos(\phi)\right)} < \cos(\phi), \tag{3.7}$$

$$\frac{3\delta\sin^2(\phi)}{\left(1+\delta^2-2\delta\cos(\phi)\right)} > \cos(\phi). \tag{3.8}$$

From equation (3.6), it appears that the point $\theta = \pi$ is unconditionally stable since the second derivative of the potential is positive. Figure 3.1 shows the potential energy configurations over two periods for two couples of parameters: $\left(\delta = 0.1; \phi = \frac{3\pi}{8}\right)$ and $\left(\delta = 0.9; \phi = \frac{\pi}{8}\right)$. These pairs of parameters meet the criteria (3.7) and (3.8) respectively. According to these shapes, the potential is $2\pi-$periodic with the angular displacement. In the first configuration (figure 3.1 a), the potential presents two equilibrium points: one unstable ($\theta = 0$) and one stable ($\theta = \pi$) (modulo 2π). The second configuration (figure 3.1 b) shows four equilibrium points, among which two are stable ($\theta = 0$ and $\theta = \pi$) and two unstable at magnets positions ($\theta = -\phi$ and $\theta = \phi$).

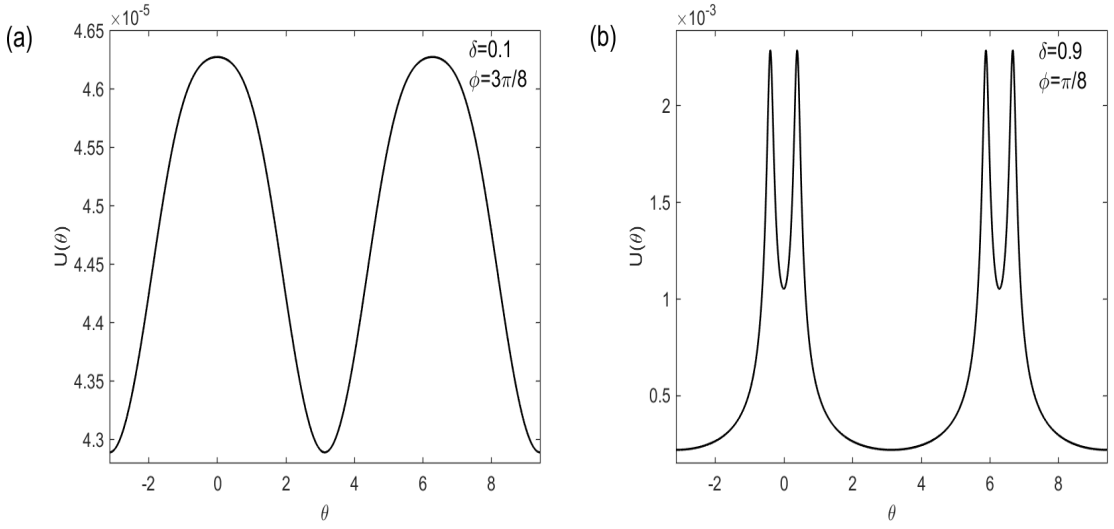

Figure 3.1: *Different configurations of the potential energy.*

3.2.2 Response of the system under DC voltage source

The forced response of system described in the previous subsection is considered in this part of thesis. We present and discuss the results on the condition for which the arm can mitigate the potential barrier and undergoes large amplitude motion leading to complete rotation and dynamical behaviors carried out previously. The dynamical behavior of the electromechanical devices is focussed on. Global analyses of different kinds of response are

found using standard methods (performed via the phase portrait, the bifurcations diagram and the largest Lyapunov exponent representations). A direct numerical simulation of the equations of motions of the system is compared with the analytical treatment. The nonlinearity has been shown to give rise to various interesting and complex dynamics such as chaos.

For small values of the parameter the interactions between the magnets are weak, the dynamical behavior is less complex. Consequently, for the rest of the work, we consider the case where is high. Specifically, we use the couple $\left(\delta = 0.9; \phi = \frac{\pi}{8}\right)$ whose potential shape is presented in figure 3.1(b).

Two sub-configurations of the potential are taken into account: The first for which the motion is around its stable focus $\theta = 0$ and the second, around its stable focus $\theta = \pi$. We carry out the numerical simulation with the initial condition $x = 0$; $y = 0$; $\dot{y} = 0$, in the first case and $x = 0$; $y = 0.5$; $\dot{y} = 0$, for the second. The fourth order Runge-Kutta method is used to solve the differential Eqs. (2.6) and (2.7). The condition for complete rotation is written as follows:

$$y_{\max} > 1, \tag{3.9}$$

with the parameters used here, the critical value above which complete rotation takes place is $E_c = 4.71077\text{x}10^{-2}$ for the first configuration and $E_c = 7.5\text{x}10^{-4}$ for the second configuration.

Figures 3.2 and 3.3 present the time-histories of the current, angular displacement and rotational velocity for the two configurations when the DC voltage is lower than the critical value E_C. Figure 3.3 indicates that the current, angular displacement and rotational velocity oscillate and then stabilize at the dimensionless values $x = 0.266$; $y = 0.041$; $\dot{y} = 0$ respectively. In Figure 3.4, as above, we observe that the current, angular displacement and rotational velocity oscillate and then stabilize at the dimensionless values $x = 4.188 * 10^{-3}$; $y = 0.0$; $\dot{y} = 0$. This highlights the fact that these points represent the new equilibrium positions in the presence of the DC voltage.

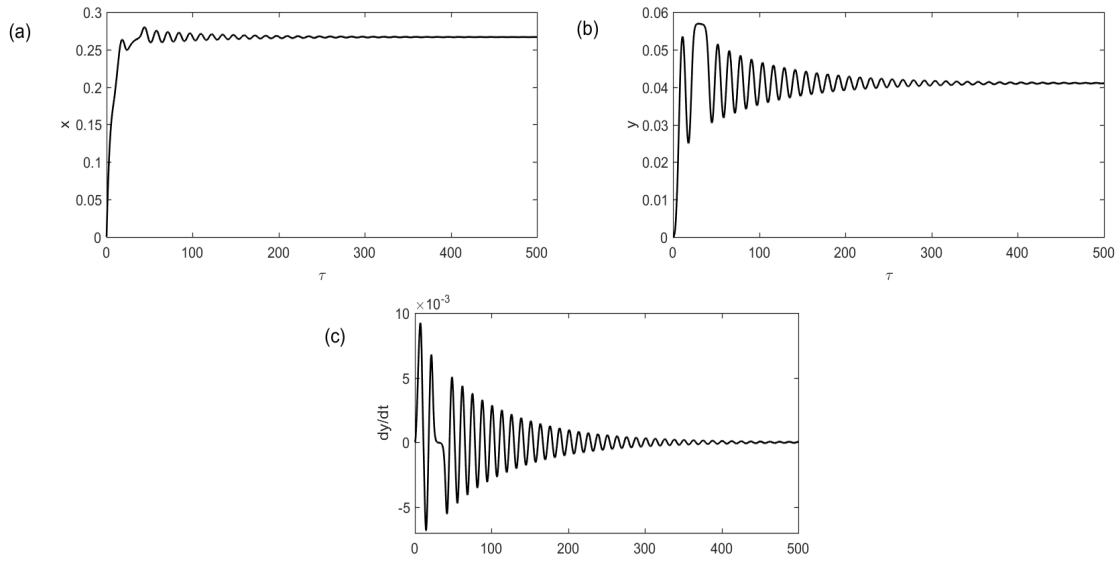

Figure 3.2: *Time histories of the current (a), angular displacement (b) and rotational velocity (c) for sub-configuration of stable equilibrium point* $\theta = 0$ *when the arm cannot perform complete rotation for* $E = 4.71076 * 10^{-2}$.

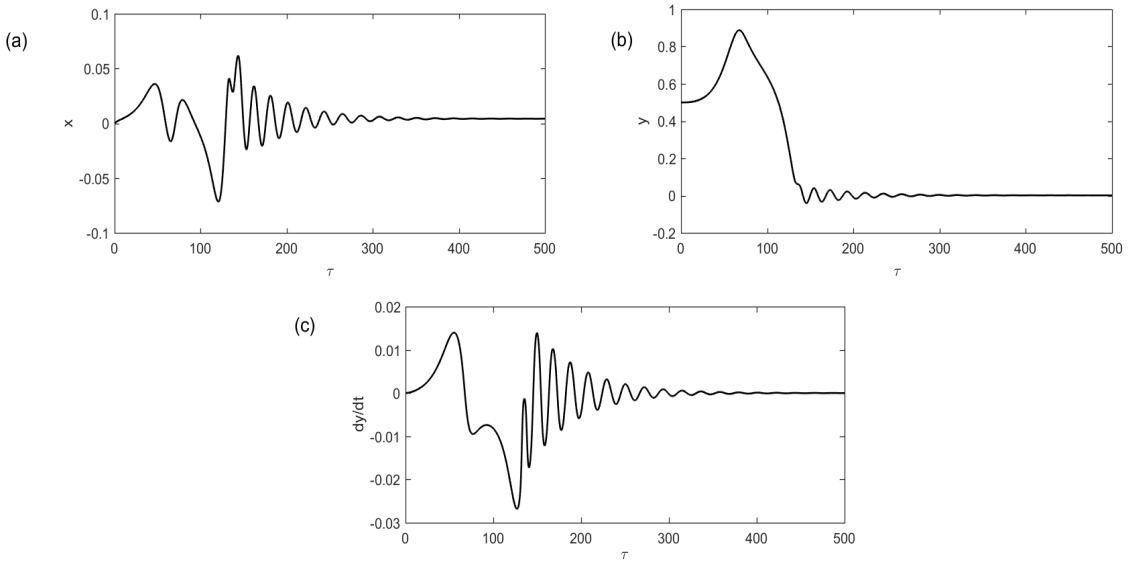

Figure 3.3: *Time histories of the current (a), angular displacement (b) and rotational velocity (c) for sub-configuration of stable equilibrium point* $\theta = \pi$ *when the device cannot perform complete rotation for* $E = 7.4 * 10^{-4}$.

The dynamical response of the system is also explored when the DC voltage is higher than the critical value E_C . Figure 3.4 presents the angular displacement and rotational velocity for dimensionless voltage equal to $E = 4.71077\text{x}10^{-2}$. The current oscillates around the equilibrium point $x = 0.266$, the angular displacement increases with the time. While the angular velocity starts to increase and then oscillates around a fixed value. Figure 3.5 shows that the current oscillates around the equilibrium value $x = 4.188\text{x}10^{-3}$, and the angular displacement first increases slightly, then decreases after some time and finally increases to large values. The angular velocity oscillates around a constant value different to zero. Due to the nonlinearity, it is seen that the angular displacement curves presents small amplitude ripples due to the oscillating behavior of the rotation velocity.

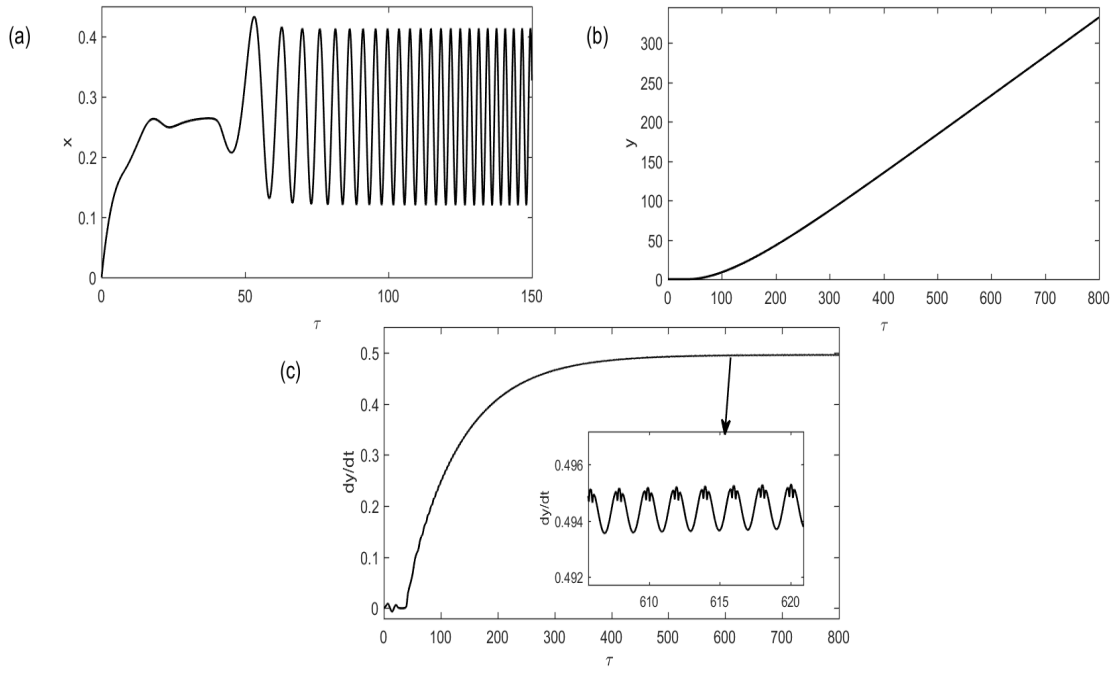

Figure 3.4: *Time histories of the current (a), angular displacement (b) and rotational velocity (c) for sub-configuration of stable equilibrium point* $\theta = 0$ *when the arm performs complete rotation for* $E = 4.71077 * 10^{-2}$.

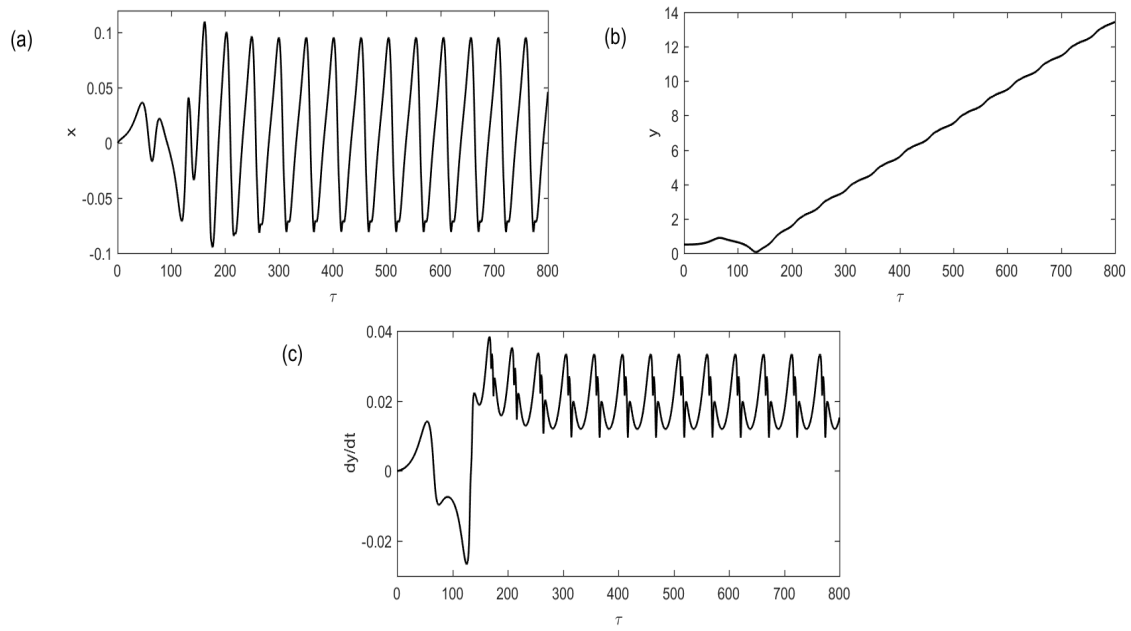

Figure 3.5: *Time histories of the current (a), angular displacement (b) and rotational velocity (c) for sub-configuration of stable equilibrium point $\theta = \pi$ when the arm performs complete rotation for $E = 7.9{*}10^{-4}$.*

3.2.3 Response of the system under AC voltage source

3.2.3.1 Linear oscillations around stable equilibrium points

We first look for the amplitudes of linear oscillations around the equilibrium points $\theta = 0$ and $\theta = \pi$. For the oscillations around the stable equilibrium point $\theta = 0$ we take $\cos(\theta) = 1$ and the nonlinear function given by Eq.(2.4) can be linearized using the Taylor expansion formula and thus gives:

$$f(\theta) = c\theta, \tag{3.10}$$

with

$$c = \frac{2\delta}{(1+\delta^2-2\delta\cos(\phi))^{\frac{3}{2}}}\left[\frac{3\delta\sin^2(\phi)}{(1+\delta^2-2\delta\cos(\phi))} - \cos(\phi)\right].$$

Eqs. (2.6) and (2.7) can thus be written as:

$$\ddot{y} + \lambda_m \dot{y} + \gamma c \theta_0 y = \varepsilon_m x, \tag{3.11}$$

$$\dot{x} + \lambda_e x + \varepsilon_e \dot{y} = E \sin(\Omega\tau). \tag{3.12}$$

The harmonic balance method is used to solve Eqs. (3.11) and (3.12). We find the sinusoidal approximations of the electrical current and angular displacement. So, the expressions of the electrical current and the angular displacement can be written as:

$$x = A_1 \cos(\Omega\tau) + A_2 \sin(\Omega\tau), \tag{3.13}$$

$$y = B_1 \cos(\Omega\tau) + B_2 \sin(\Omega\tau). \tag{3.14}$$

Let us set $A = \sqrt{A_1^2 + A_2^2}$ and $B = \sqrt{B_1^2 + B_2^2}$ the maximal amplitude of current and the maximal amplitude of the mechanical displacement. Inserting Eqs. (3.13) and (3.14) into Eqs. (3.11) and (3.12) and after some mathematical manipulations, one obtains that A and B are given as follows:

$$B = \frac{\varepsilon_m E}{\sqrt{\left[-\Omega\left(-\Omega^2 + \gamma c\right) - \lambda_e \lambda_m \Omega - \varepsilon_e \varepsilon_m \Omega\right]^2 + \left[\lambda_e\left(-\Omega^2 + \gamma c\right) - \Omega^2 \lambda_m\right]^2}}, \tag{3.15}$$

$$A = \frac{\sqrt{\left[\left(-\Omega^2 + \gamma c\right)^2 + \lambda_m^2 \Omega^2\right]}}{\varepsilon_m} B. \tag{3.16}$$

Figures 3.6 (a) and (b) show both the amplitude response of the mechanical part and electrical part. The amplitude of the current displays two peaks: an antiresonant peak and a resonant peak, while the mechanical displacement presents a resonant behavior.

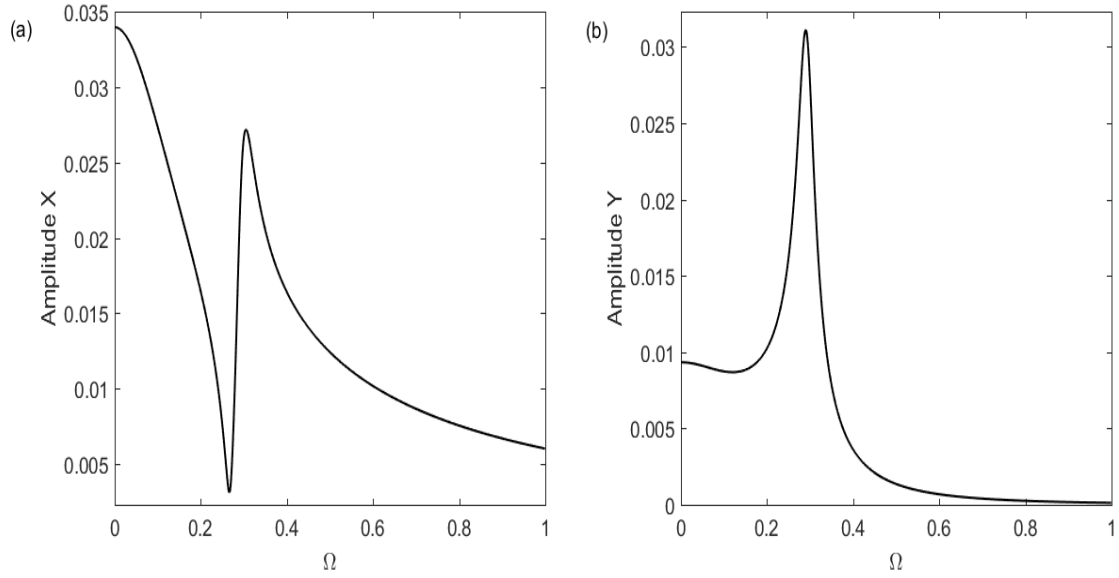

Figure 3.6: *(a) Amplitude of the current x and (b) amplitude of angle y versus the parameter* Ω *around stable equilibrium point* $\theta = 0$ *for* $E = 6.10^{-3}$.

For oscillations around $\theta = \pi$, we assume that $\theta = \pi + \alpha$ where α is very small compared to π and $\cos(\theta) = -1$. The linearization of the nonlinear function gives:

$$f(\theta) = c_1(\theta - \pi), \tag{3.17}$$

where

$c_1 = \frac{2\delta}{(1+\delta^2+2\delta\cos(\phi))^{\frac{3}{2}}}\left[\frac{3\delta\sin^2(\phi)}{(1+\delta^2+2\delta\cos(\phi))} + \cos(\phi)\right]$.

Eqs. (2.6) and (2.7) thus become:

$$\ddot{\zeta} + \lambda_m\dot{\zeta} + \gamma c_1\theta_0\zeta = \varepsilon_m x, \tag{3.18}$$

$$\dot{x} + \lambda_e x - \varepsilon_e\dot{\zeta} = E\sin(\Omega\tau), \tag{3.19}$$

where $\zeta = \frac{\alpha}{\theta_0}$

The expressions of the electrical current and of the angular displacement can be written as:

$$x = C_1\cos(\Omega\tau) + C_2\sin(\Omega\tau), \tag{3.20}$$

$$\zeta = D_1 \cos(\Omega\tau) + D_2 \sin(\Omega\tau). \tag{3.21}$$

The amplitude of the current and that of the mechanical displacement are given as:

$$D = \frac{\varepsilon_m E}{\sqrt{\left[-\Omega\left(-\Omega^2 + \gamma c_1\right) - \lambda_e \lambda_m \Omega + \varepsilon_e \varepsilon_m \Omega\right]^2 + \left[\lambda_e\left(-\Omega^2 + \gamma c_1\right) - \Omega^2 \lambda_m\right]^2}}, \tag{3.22}$$

$$C = \frac{\sqrt{\left[\left(-\Omega^2 + \gamma c_1\right)^2 + \lambda_m^2 \Omega^2\right]}}{\varepsilon_m} D. \tag{3.23}$$

where $C = \sqrt{C_1^2 + C_2^2}$ and $D = \sqrt{D_1^2 + D_2^2}$.

As shown in Figures 3.7 (a) and (b), the amplitude of the current presents two peaks: an antiresonant peak and a resonant one, while the amplitude of angular displacement decreases when the frequency increases.

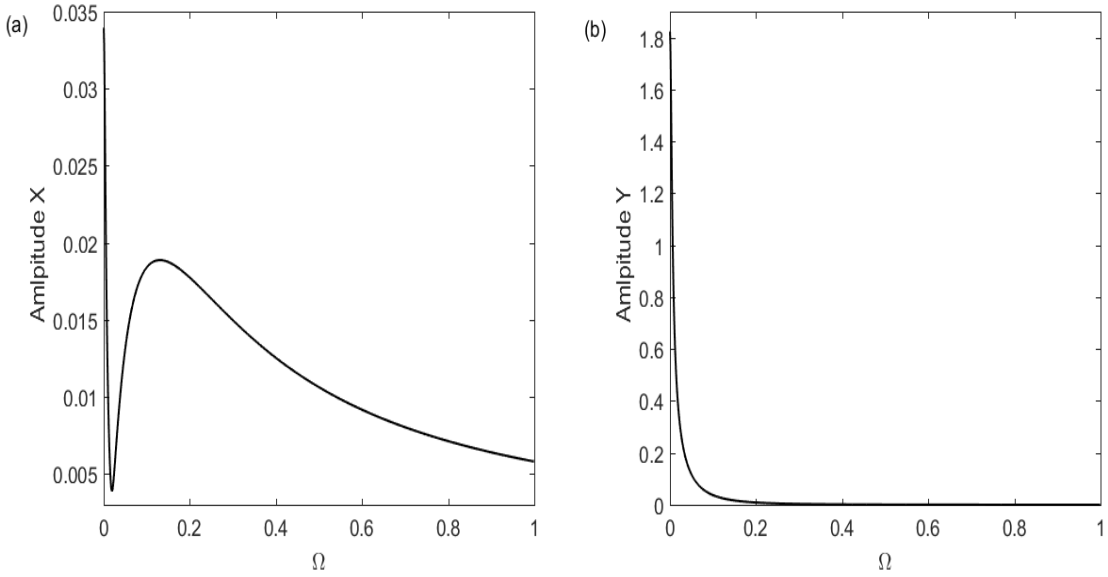

Figure 3.7: *(a) Amplitude of current x and (b) amplitude of angle y versus the parameter* Ω *around stable equilibrium point* $\theta = \pi$ *for* $E = 6.10^{-3}$.

3.2.3.2 Conditions for complete rotation of the arm

Another point to study is the condition for complete rotation when the electromechanical system is powered by a sinusoidal voltage. The same criterion (Eq.3.9) is considered.

Figure 3.8 displays E_C versus Ω for the two configurations. The domain located below each curve is where the dimensionless amplitude of vibration of the mechanical arm is less than 1 (meaning no complete rotation). Complete rotations are observed for values of E above the curves. It is found that E_C increases with the frequency. It is also observed that when the arm moves from the equilibrium point $\theta = 0$, more energy is needed to make the arm undergoes complete rotation.

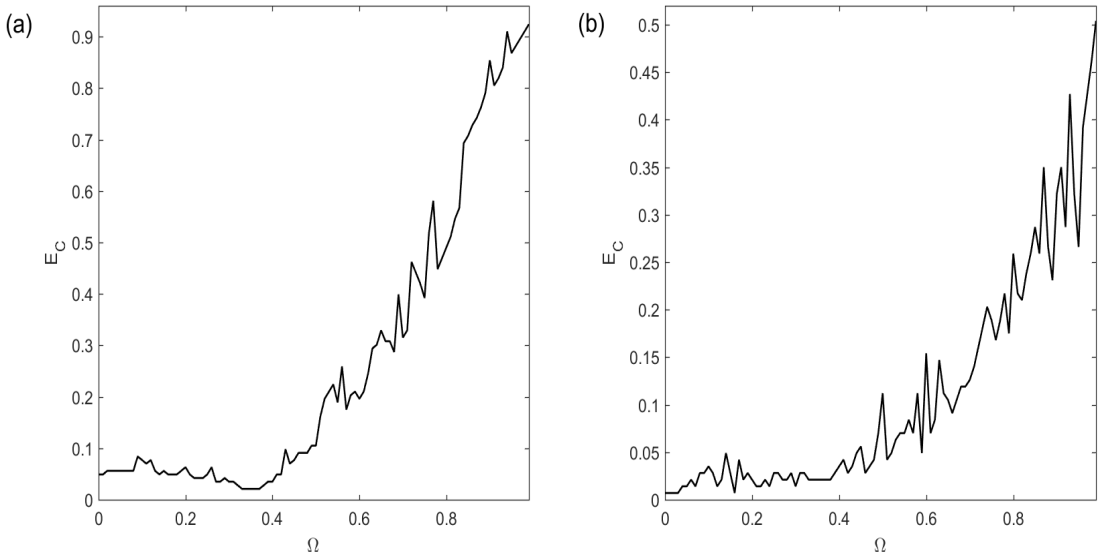

Figure 3.8: *Numerical boundary criterion for complete rotation for the arm starting at the equilibrium angle $\theta = 0$ (a) and equilibrium angle $\theta = \pi$ (b)*

Figure 3.9 (b) presents the time history of the angular displacement for the amplitude of vibration less than 1 for the sub-configuration of stable equilibrium point at $\theta = 0$. The arm oscillates with a perfect sinusoidal shape around the equilibrium position. For the sub-configuration of stable equilibrium point at $\theta = \pi$, we have also plotted in Figure 3.11 (b) the response of mechanical part. As in Figure 3.9 (b), it shows sinusoidal shape around 0 with amplitude less than one (1) turn.

Figure 3.10 (b) shows the time history of the angular displacement for the sub-configuration of stable equilibrium point $\theta = 0$ for the amplitude of sinusoidal voltage higher than the critical value. One observes that the mechanical arm presents sinusoidal

oscillations in this case with amplitude of 23 turns. This means that the arm rotates 23 turns in the forward direction; then turns back to the stable position and continues in the reverse side till 23 turns before returning back and so on. The same work has been done for the other sub-configuration, it is found that the arm performs sinusoidal oscillations with amplitude of 25 turns (see Figure 3.12 (b)).

Figure 3.9 (a), 3.10 (a), 3.11 (a) and 3.12 (a) display the response of the electrical part of the system. These curves show that the current x oscillates like the angular displacement y.

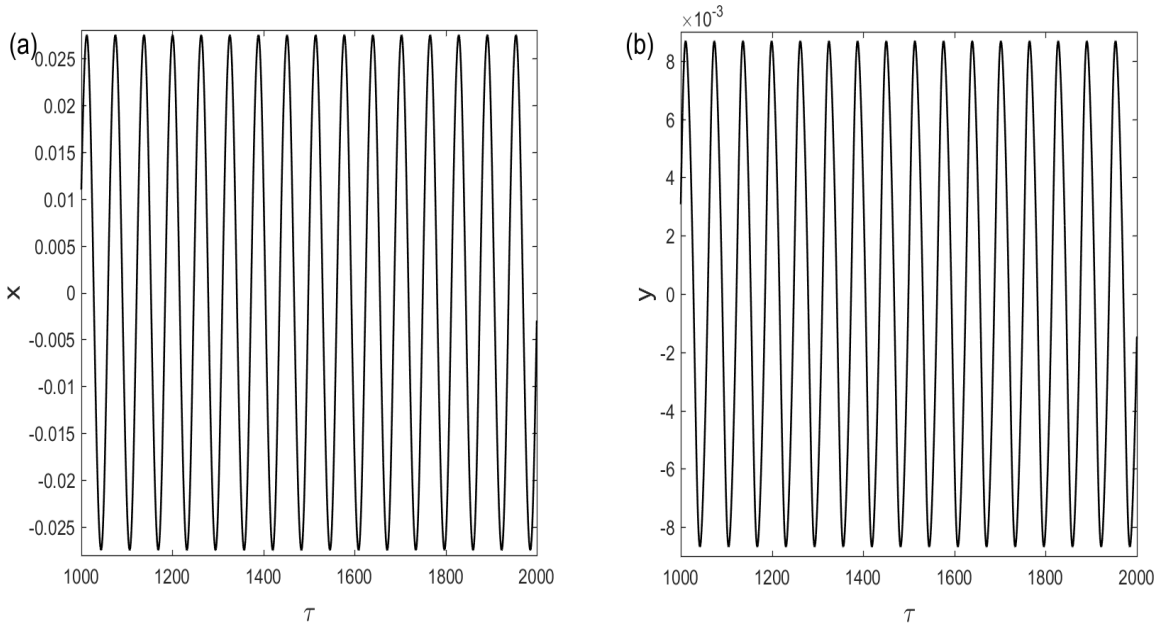

Figure 3.9: *Times histories of the current (graph (a)) and of the angular displacement (graph (b)) for the sub-configuration of stable equilibrium point at* $\theta = 0$. *(with* $\Omega = 0.1$ *and* $E = 6\text{x}10^{-3}$.*)*

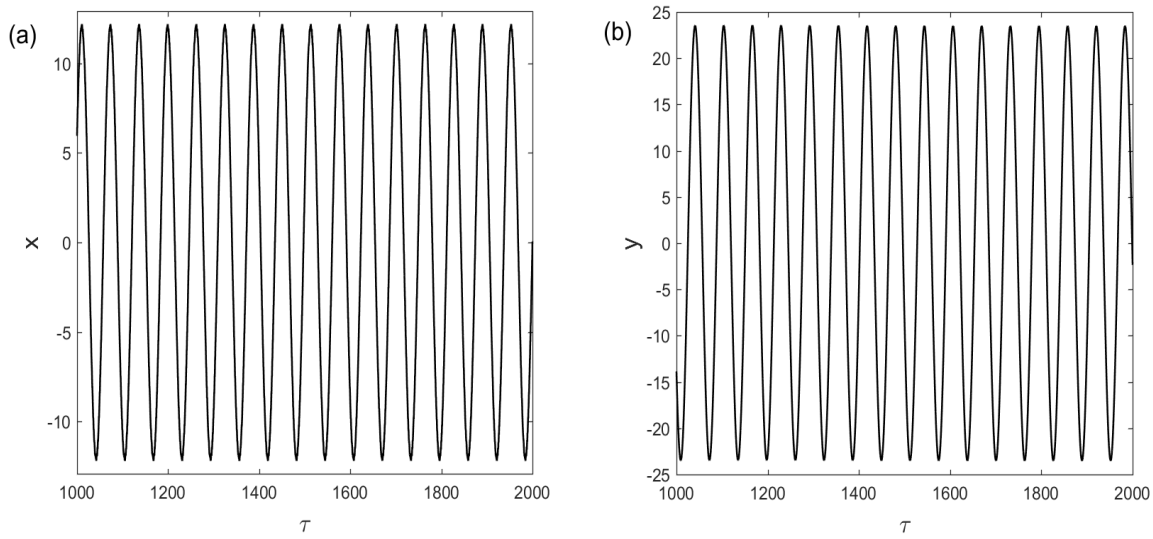

Figure 3.10: *Times histories of the current (graph (a)) and of the angular displacement (graph (b)) for the sub-configuration of stable equilibrium point at* $\theta = 0$. *(with* $\Omega = 0.1$ *and* $E = 2.45$.*)*

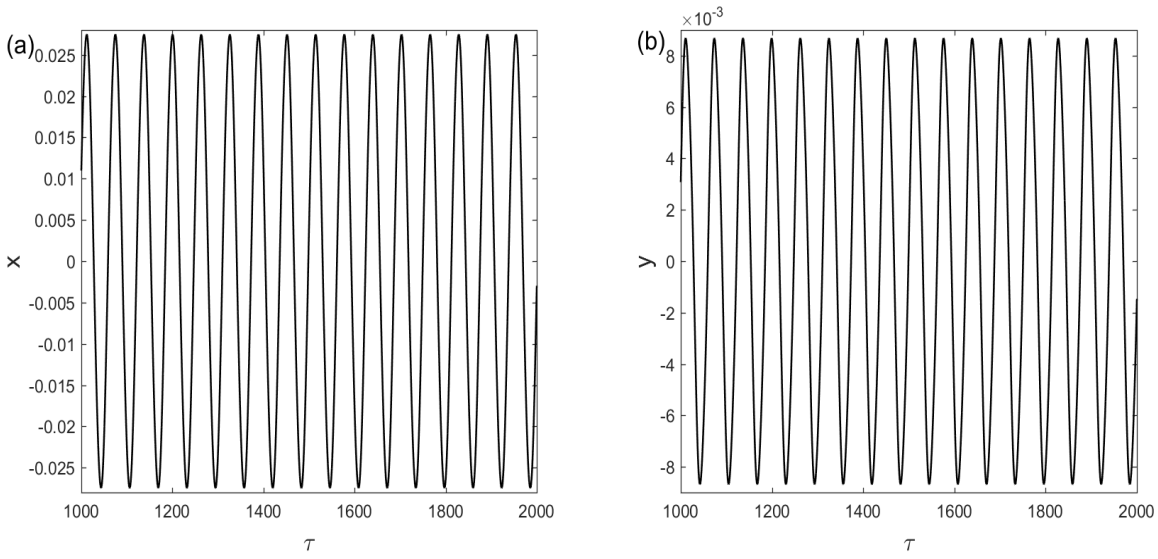

Figure 3.11: *Times histories of the current (graph (a)) and of the angular displacement (graph (b)) for the sub-configuration of stable equilibrium point at* $\theta = \pi$. *(with* $\Omega = 0.1$ *and* $E = 6\text{x}10^{-3}$.*)*

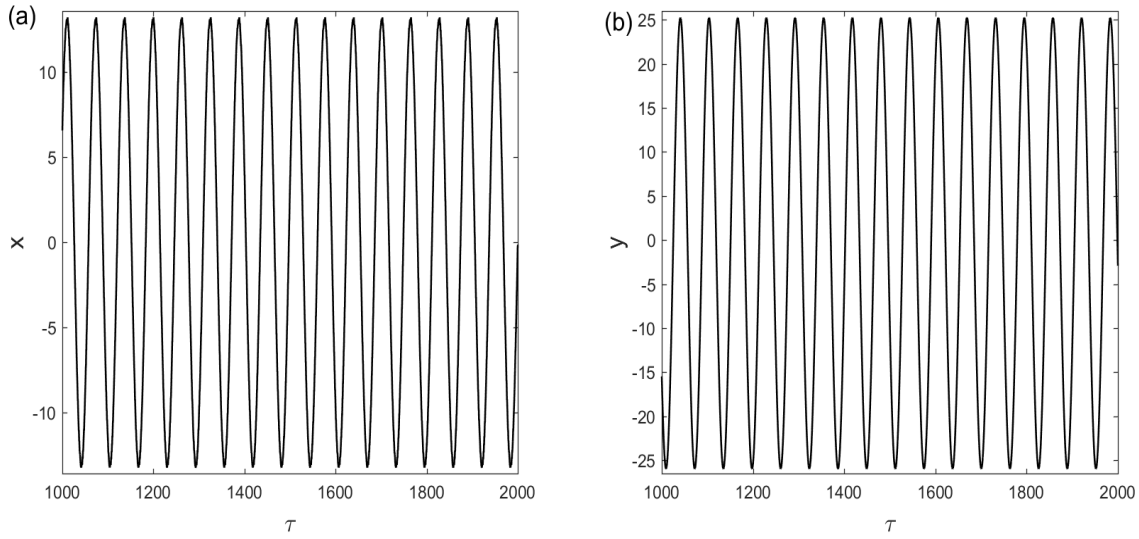

Figure 3.12: *Times histories of the current (graph (a)) and of the angular displacement (graph (b)) for the sub-configuration of stable equilibrium point at* $\theta = 0$. *(with* $\Omega = 0.1$ *and* $E = 2.67$.*)*

3.2.3.3 Bifurcations diagrams

In order to fully characterize the dynamical behavior of the system, bifurcation diagrams have been obtained from the numerical simulation taking the amplitude of the sinusoidal excitation as the control parameter. Considering $\theta = 0$ as the initial condition, the bifurcation diagram is presented in Figure 3.13 along with the largest Lyapunov exponent, while in Figure 3.14, examples of time traces and phase portraits are also represent. It is found that the system moves from regular (periodic oscillation to chaotic dynamics). From the variation of the Lyapunov exponent, one finds that the system is very sensitive to the variation of the voltage amplitude since points of positive Lyapunov exponent alternate erratically with points of negative Lyapunov exponent in some ranges of the sinusoidal voltage amplitude.

Figure 3.14 (a) and (b) also present two examples of time history of the angular displacement, one for periodic oscillations and the other one for chaotic oscillations. Figure 3.14 (c) and (d) display the corresponding phase portraits.

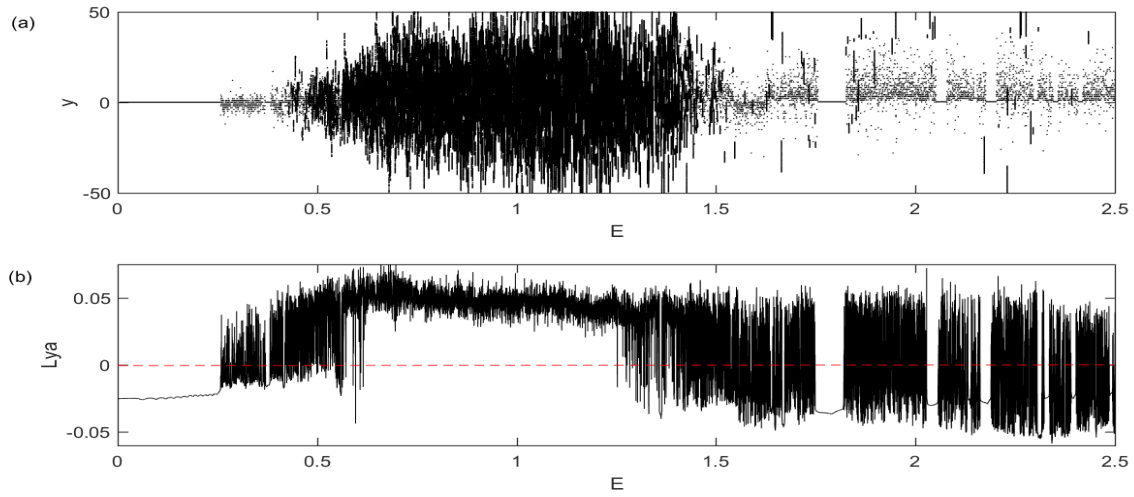

Figure 3.13: *(a) Bifurcation diagram, (b) Lyapunov exponent versus the amplitude E for the sub-configuration of stable equilibrium point $\theta = 0$ with $\Omega = 0.66$.*

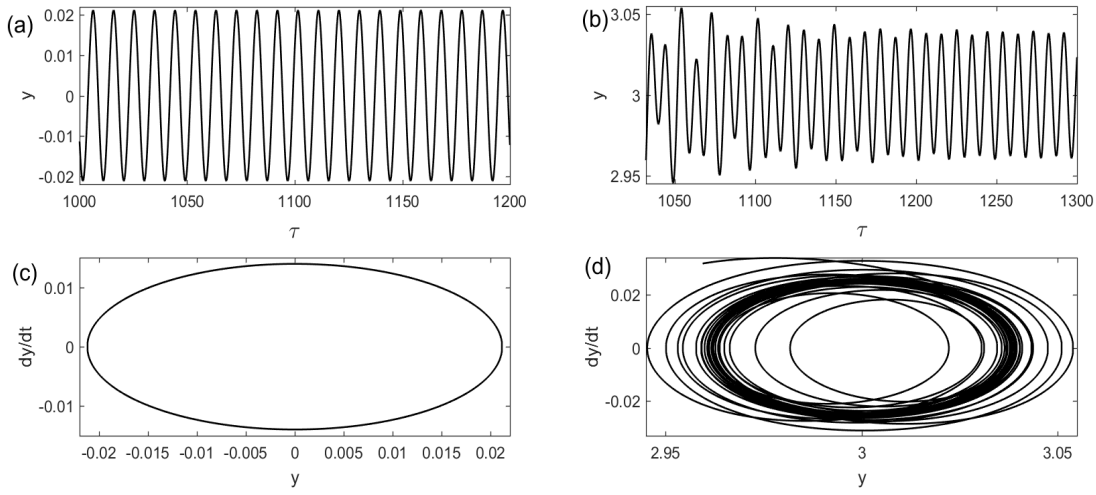

Figure 3.14: *Times histories and corresponding phase portraits of the angular displacement showing periodic motion (graphs (a) and (c)) with $E = 0.25$, chaotic oscillations (graphs (b) and (d)) with $E = 0.42$ for $\Omega = 0.66$, for the sub-configuration of stable equilibrium point $\theta = 0$.*

To more characterize the system, we have also obtained the bifurcation diagram for the sub-configuration where the stable equilibrium point is $\theta = \pi$. This is presented in Figure 3.15, which looks similar to Figure 3.13. Here, the chaotic behavior occurs for smaller values of the voltage amplitude. Figures 3.16 (a) and (b) show time-histories while Figures 3.16 (c) and (d) present the corresponding phase portrait of the angular displacement for different values of E. These curves present respectively periodic and chaotic behaviors. Because of the fact the angular displacement is not bounded, but decreases with chaotic ripples (figure 3.16 (d)), the phase portrait looks different to what is always observed. This is specific for this system since for some values of the parameters, the angular displacement y makes more than one turn before returning back while the angular velocity dy/dt oscillate around 0. This specific shape is also visible in Figure 3.18 (b).

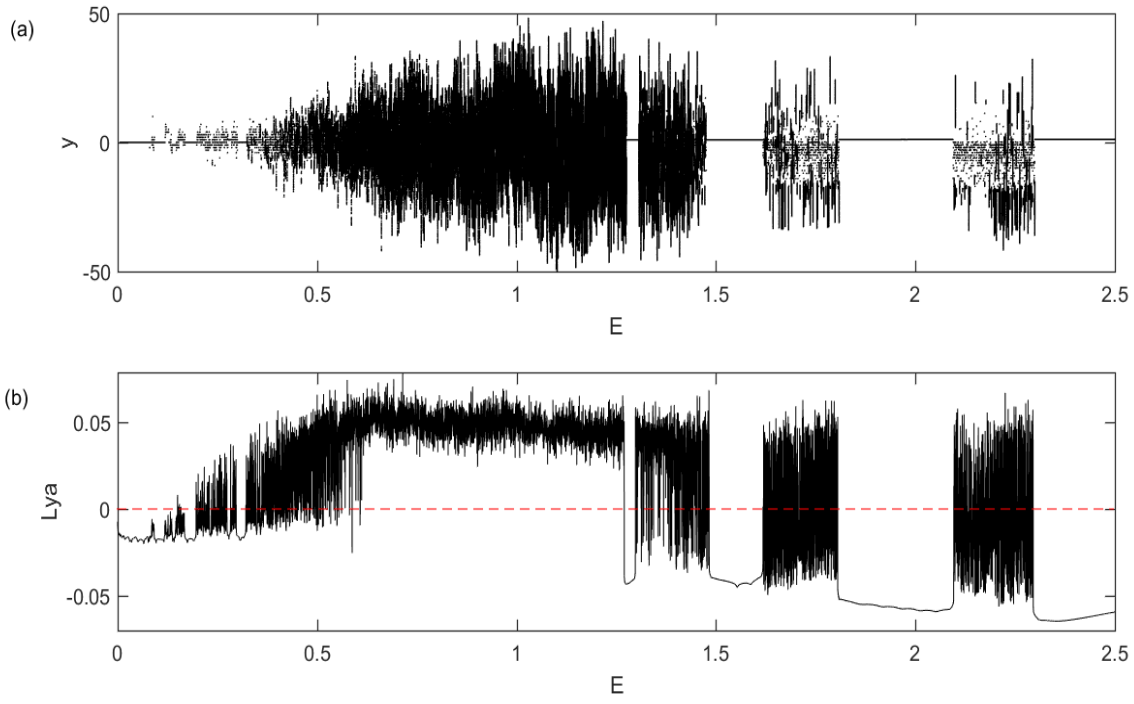

Figure 3.15: *(a) Bifurcation diagram, (b) Lyapunov exponent versus the amplitude E for the sub-configuration of stable equilibrium point $\theta = \pi$ with $\Omega = 0.66$.*

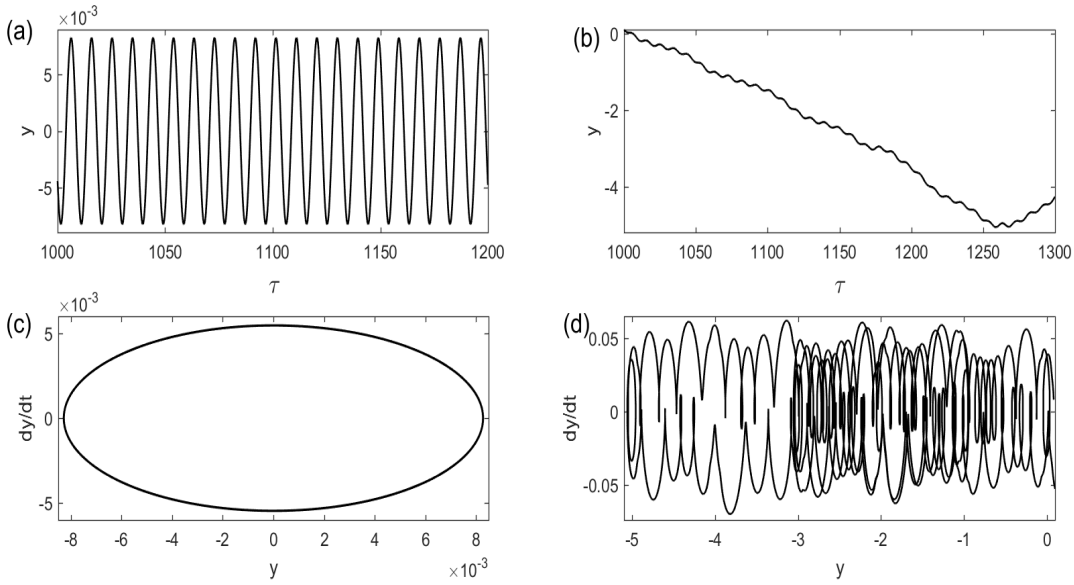

Figure 3.16: *Times histories and corresponding phase portraits of the angular displacement showing periodic motion (graphs (a) and (c)) with* $E = 0.10$ *, chaotic oscillations (graphs (b) and (d)) with* $E = 0.66$ *for* $\Omega = 0.66$*, for the sub-configuration of stable equilibrium point* $\theta = \pi$*.*

We have also plotted the bifurcation diagram versus the frequency. An example is presented in Figure 3.17 when the motion starts at $\theta = 0$. One finds that periodic motion of the system starts when $\Omega = 0.01$ and continues until 0.231. For the frequency between 0.231 and 0.408, the system response exhibits an alternation of periodic and chaotic behaviors (see the phase portraits of Figure 3.18). As the excitation frequency increases, the system undergoes periodic oscillations.

The same analysis is done for the sub-configuration where the motion starts at $\theta = \pi$. In this case, the system response presents an alternation of periodic and chaotic behaviors when Ω lies between 0.01 and 0.439 and is periodic until $\Omega = 1$ (see Figures 3.19 and 3.20).

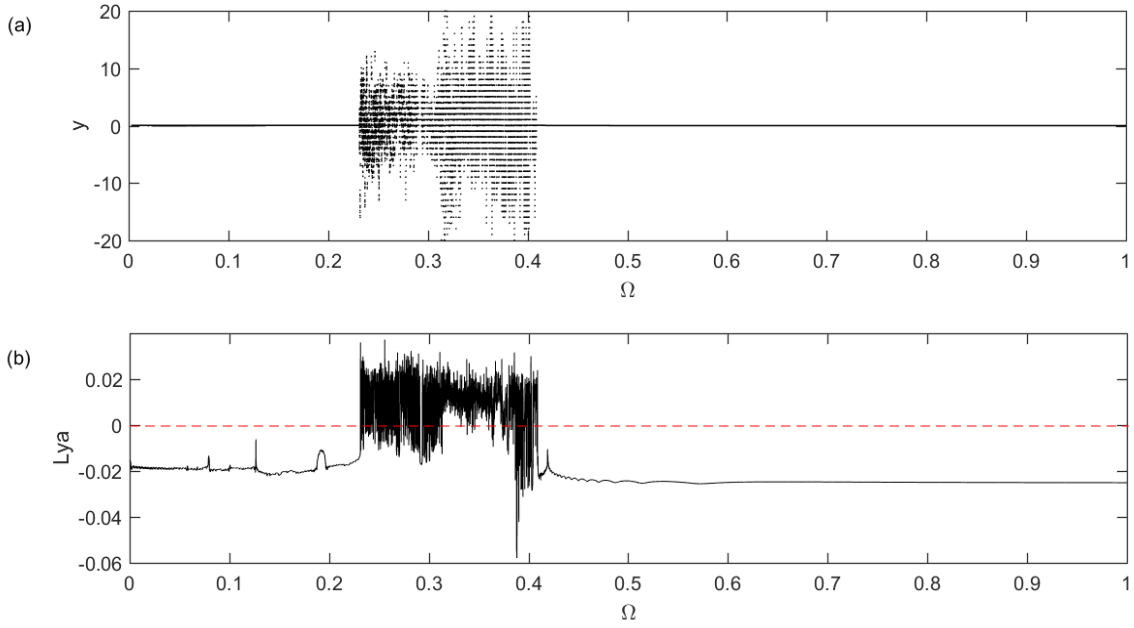

Figure 3.17: *(a) Bifurcation diagram, (b) Lyapunov exponent versus the frequency* Ω *for the sub-configuration of stable equilibrium point* $\theta = 0$ *with* $E = 4.10^{-2}$

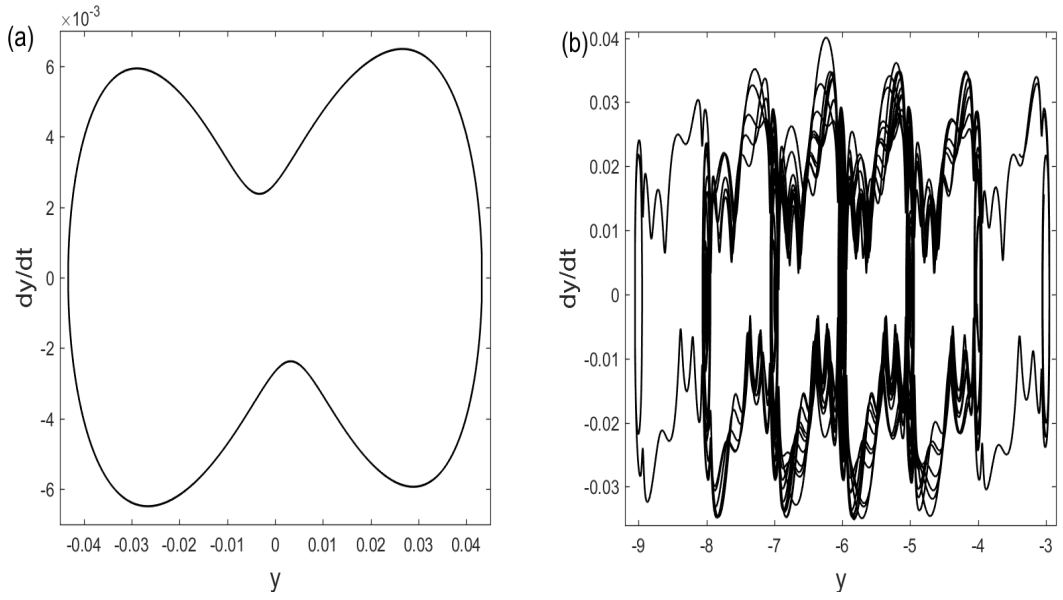

Figure 3.18: *Phase portrait of the angular displacement (graph (a) with* $\Omega = 0.15$ *and (b) with* $\Omega = 0.35$ *).*

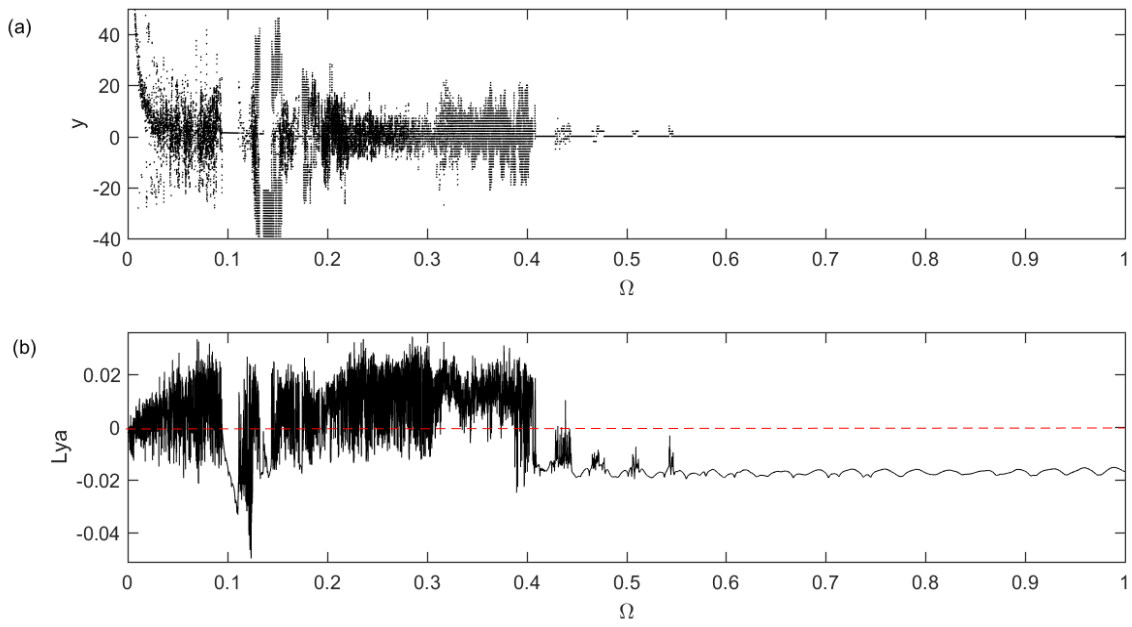

Figure 3.19: *(a) Bifurcation diagram, (b) Lyapunov exponent versus the frequency* Ω *for the sub-configuration of stable equilibrium point* $\theta = \pi$ *with* $E = 4.10^{-2}$

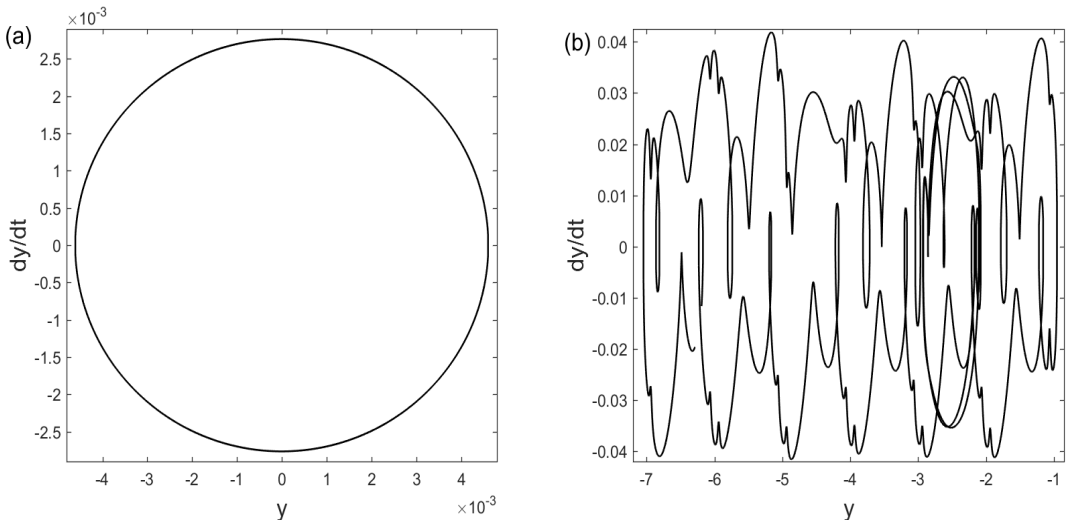

Figure 3.20: *Phase portrait of the angular displacement (graph (a) with* $\Omega = 0.6$ *and (b) with* $\Omega = 0.2$ *).*

3.3 Case of the system with several magnets arranged periodically along a circle

3.3.1 Potential energy

The potential energy associated with the system of equation (2.14) is:

$$U = \gamma \sum_{k=0}^{N-1} \frac{1}{\left[1 + \delta^2 - 2\delta\cos(\theta - 2k\phi)\right]^{\frac{1}{2}}}. \tag{3.24}$$

We present some potential curves for different values of the parameter and the number of magnets N (see Figure 3.21). These curves have been plotted for one period ($y = 1$), and for $N = 2$ magnets, and $N = 5$ magnets. It shows two wells for $N = 2$ and five wells for $N = 5$. The stable equilibrium points are between two consecutive magnets. We also notice that the depth of the wells increases with the parameter δ.

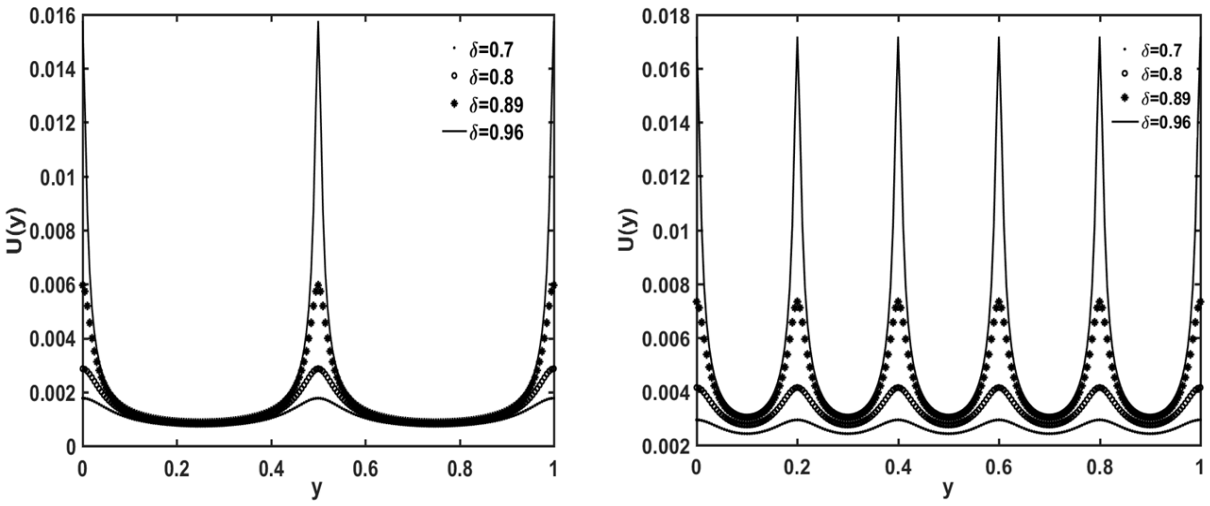

(a) (b)

Figure 3.21: *Potential energy of the system versus the angular displacement: (a) for $N = 2$ magnets and (b) for $N = 5$ magnets.*

3.3.2 Critical values of DC voltage case

As in the case of two magnets, we are also looking for the condition for which the arm can mitigate the potential barrier and undergoes large amplitude motion leading for instance a complete rotation. For this purpose, we look for the critical value E_C of the external amplitude voltage above which complete rotation takes place. Two different forms of input signal have been considered: DC and AC voltage sources. The condition given by Eq. 3.9 is also used.

3.3.2.1 Effect of the dimensionless length δ

Figure 3.22 presents the critical voltage values versus the dimensionless length for $N = 2$ magnets (solid line) and $N = 5$ magnets (dotted line). One finds that E_C increases with the arm length. In the interval $[0; 0.27]$, one needs the same energy to perform a complete rotation for both numbers of magnets. But in the interval $[0.27; 0.88]$, more energy is required for two magnets while for the interval $[0.88; 0.96]$, less energy is required for two magnets than for 5 magnets.

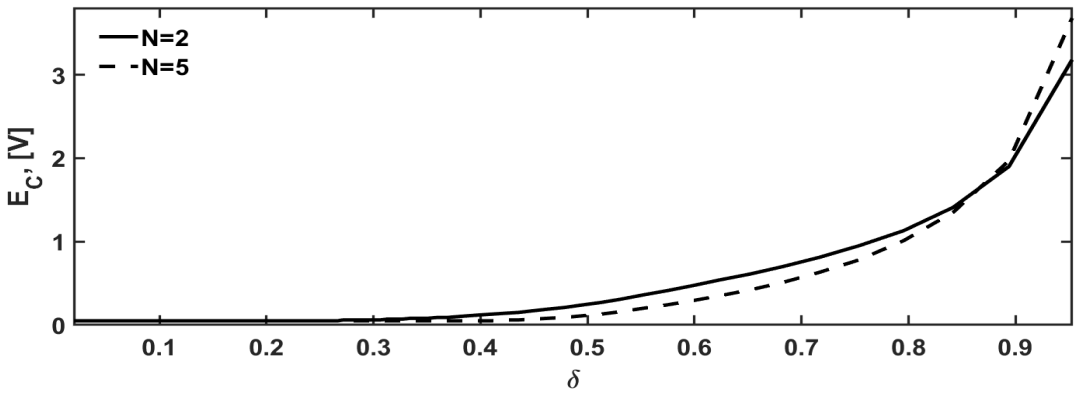

Figure 3.22: *Numerical boundary criterion for complete rotation versus the parameter δ.*

3.3.2.2 Effect of the number of magnets N

We have also analysed the effects of the number of magnets on the critical voltage. As shown in Figure 3.23, the voltage required to make a complete rotation is larger for

$\delta = 0.96$ than for $\delta = 0.80$. This is due to the fact that for large values of δ, the repulsive forces are more accentuated and therefore more energy is needed to perform a full turn. In addition, for $\delta = 0.80$, we note a decrease of this voltage with the number of magnets while for $\delta = 0.96$, it increases until reaching a maximum value at $N = 5$ then decreases with N.

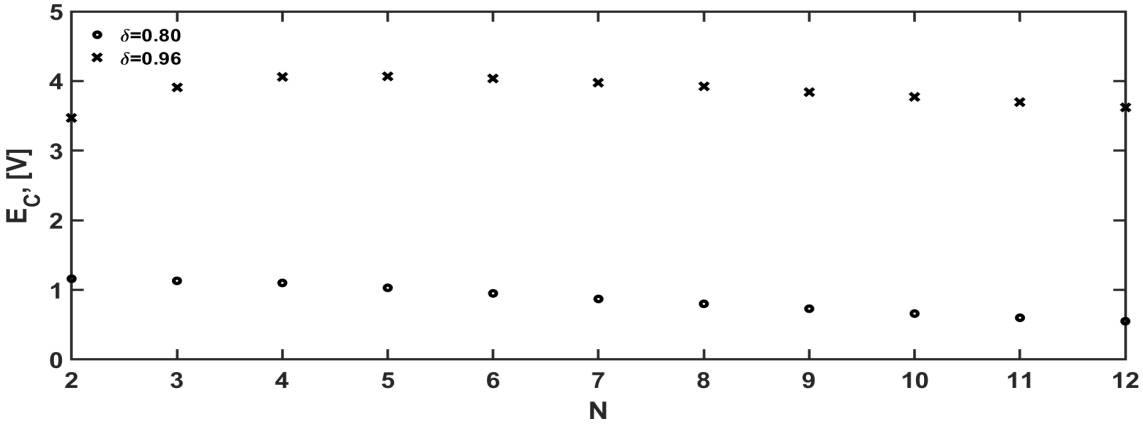

Figure 3.23: *Numerical boundary criterion for complete rotation versus the parameter N*

When complete rotation takes place, the arm rotation velocity shows a sort of NT-periodic oscillations where N is the number of magnets (see Figure 3.24). This reflects the different accelerations produced by the repulsion created by the fixed magnets as they approach the magnet attached to the arm end.

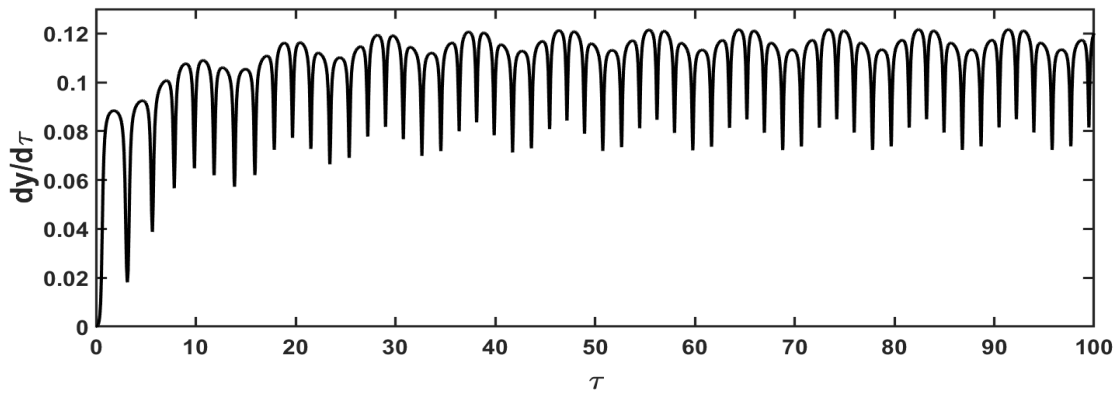

Figure 3.24: *Time-histories of the rotational velocity for $N = 5$ magnets, $\delta = 0.96$ when the arm performs complete rotation for $E = 4.5\,V$*

3.3.3 Critical values in AC voltage case

This subsection is devoted to find the condition for complete rotation when the electromechanical system is powered by a sinusoidal voltage.

3.3.3.1 Critical values versus the frequency of external generator

In Figure 3.25, the critical values of the amplitude of the sinusoidal voltage is plotted versus its frequency for 2 and 5 magnets. When the frequency lies between $0.1\,Hz$ and $0.6\,Hz$, the critical values are the same. But, much more voltage amplitude is needed in the range $0.6\,Hz$ to 2.2 for $N = 5$ magnets than for $N = 2$ magnets. As the excitation frequency is increased more, the critical voltage amplitude is less for $N = 5$ magnets than for $N = 2$ magnets.

In order to confirm the curves displayed in Figure 3.26, the time-histories of the angular displacement of the arm have been presented for two points belonging to the two regions separated by the curve (case for $N = 2$ magnets). The arm angular displacement presents oscillations with amplitude less than 1 for the region under the curve and greater than 1 for the region above the curve.

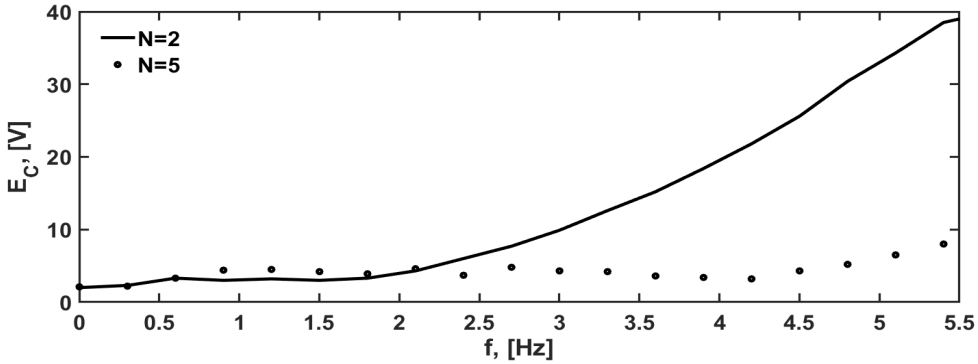

Figure 3.25: *Critical value of the sinusoidal voltage amplitude for complete rotation versus the frequency of the generator.*

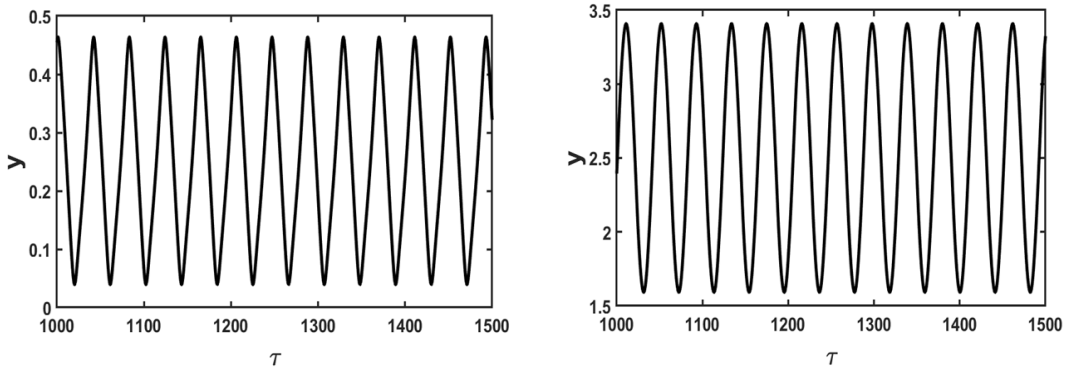

Figure 3.26: *Time-histories of the angular displacement for N=2 magnets. (a) for an input voltage lower than the critical value* $(Em = 4.5\,V)$ *and (b) for an input voltage higher than the critical value* $(Em = 5\,V)$ *and for* $f = 1.2\,Hz$.

3.3.3.2 Critical values versus the dimensionless length δ

Figure 3.27 presents the critical value of the sinusoidal voltage amplitude when the arm length varies. One finds the same critical values for the dimensionless length belonging to the interval $[0; 0.55]$ for two and five magnets. But, in the range $[0.55; 0.98]$, one obtains an alternation between the two curves. Furthermore, abrupt drops are observed at $\delta = 0.53$ for $N = 2$ and at $\delta = 0.61$ for $N = 5$. This can be justified by the presence of several resonance peaks in the system for large values of δ as it can be seen in Figure 3.28 which presents the oscillation amplitude versus the frequency.

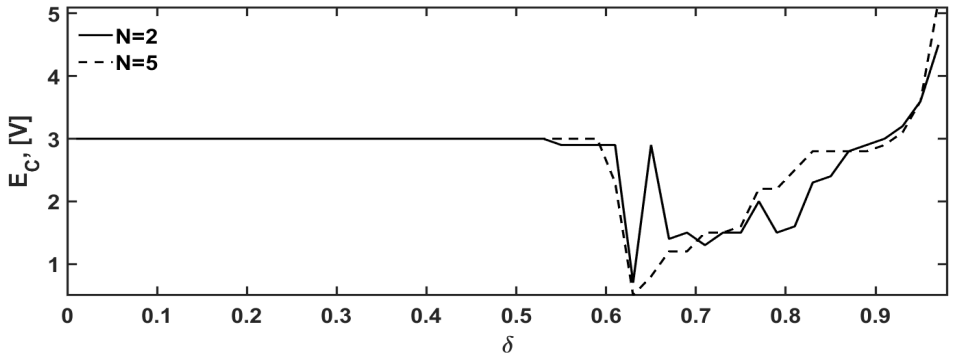

Figure 3.27: *Critical value of the amplitude of the sinusoidal voltage for complete rotation versus the parameter* δ.

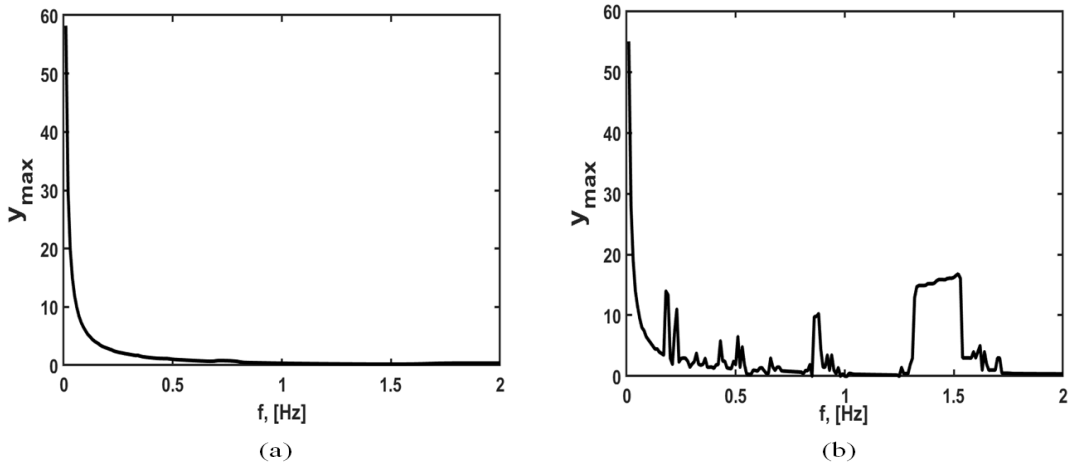

Figure 3.28: *Maximum amplitude of the rotation angle versus the frequency of the sinusoidal voltage for $E = 3V$. (a) for $\delta = 0.3$ and (b) for $\delta = 0.8$.*

3.3.3.3. Critical amplitude of voltage versus the number of magnets

As in the case of DC current, the critical voltages are higher for $\delta = 0.96$. For $\delta = 0.96$, this critical voltages are constant as the number of magnets varies while for $\delta = 0.80$, it increases and reaches a maximum at $N = 6$. Then, it decreases to reach its minimum at $N = 9$. Thereafter, it takes another relative maximal value at $N = 10$ and then decreases with the number of magnets (see Figure 3.29).

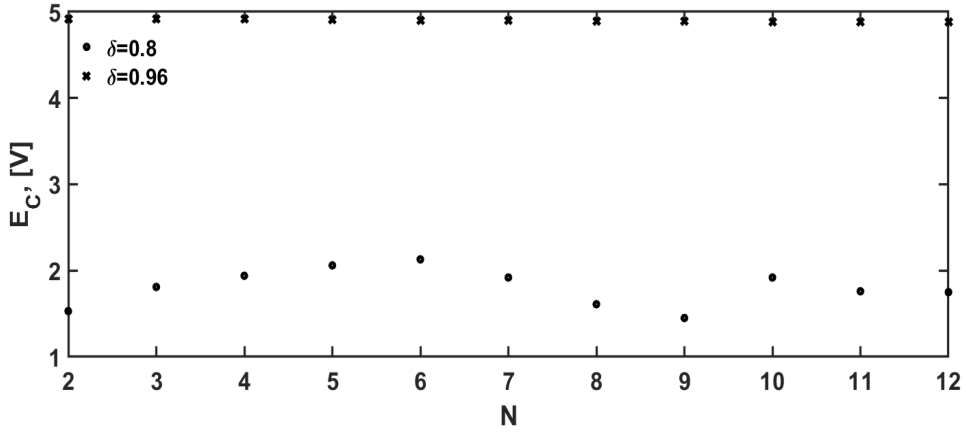

Figure 3.29: *Critical value of the amplitude of the sinusoidal voltage for complete rotation versus the number of magnets N.*

3.3.4 Bifurcation diagrams and Lyapunov exponents

In this part, one analyses the behavior of the electromechanical system considering the amplitude and the frequency of the external excitation as control parameters. For this purpose, the bifurcation diagram and corresponding Lyapunov exponent are employed.

3.3.4.1. Bifurcation diagrams in case of DC voltage source

Figure 3.30 shows that by varying the value of the DC voltage, two types of behaviors occur. The first one corresponds to the state where there is no oscillation or no motion. After a transient motion, the system evolves to a fixed state where the current and angular velocity are equal to 0 while the angular displacement attains a fixed value depending on the initial conditions. The second type of motion corresponds to the state where the angular displacement increases continuously as a function of time while the angular velocity oscillates around a fixed non null value. The transition between these two dynamics is observed at $E = 1.98\,V$ for $N = 2$ magnets and at $E = 2.07\,V$ for $N = 5$ magnets. These values represent the critical voltages for complete rotation at the corresponding numbers of magnets.

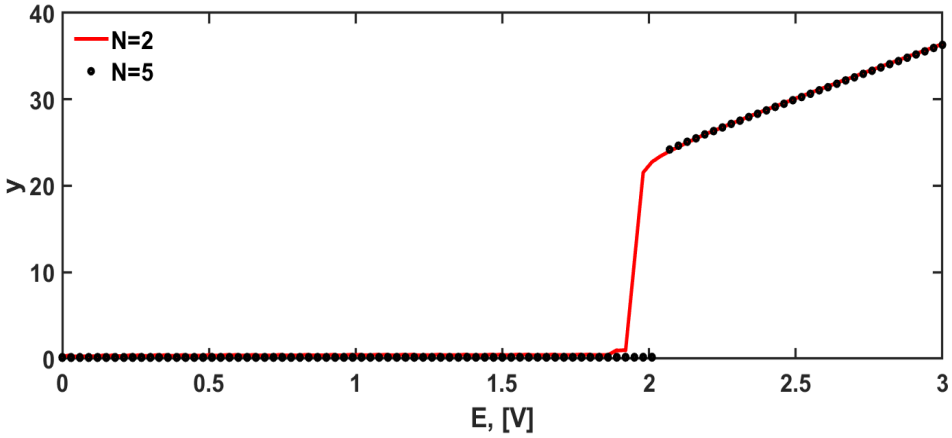

Figure 3.30: *Bifurcation diagram versus the DC voltage E when there are two magnets (full line) and five magnets (line with large dots).*

3.3.4.2. Bifurcation diagrams in case of AC voltage source

a) Bifurcation diagram versus the amplitude Em of the AC voltage

First, we have plotted the bifurcation diagram of the mechanical displacement y versus the amplitude E_m of the sinusoidal voltage source for $f = 1.2\,Hz$. The diagram for $N = 2$ magnets is presented in Figure 3.31(a) while Figure 3.31 (b) presents the corresponding Lyapunov exponent. Periodic motion starts when $Em = 0.1\,V$ and continues until $2.9\,V$. With the amplitude between 2.9 and $5.8\,V$, the system response exhibits an alternation of periodic and chaotic motions. The system response comes into a periodic motion when the amplitude lies between 5.8 and $7.2\,V$, and returns to an alternation of periodic and chaotic motions when $7.8V \leq E_m \leq 8.2V$. As the excitation amplitude increases further, the system undergoes periodic oscillation. Some examples of phase portraits are plotted in Figure 3.32.

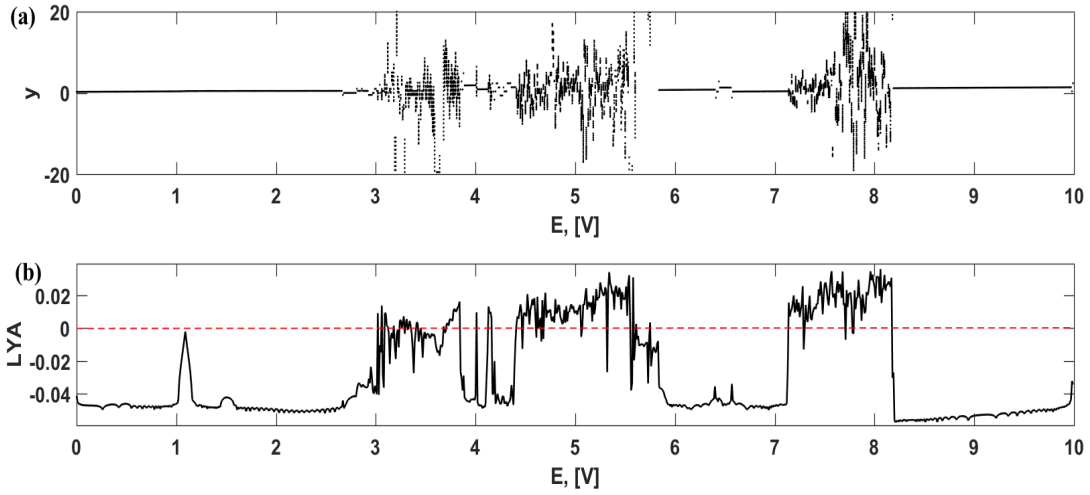

Figure 3.31: *(a) Bifurcation diagram and (b) variation of the Lyapunov exponent, both as function of the amplitude of the external generator E_m for $f = 1.2\,Hz$ and $N = 2$ magnets.*

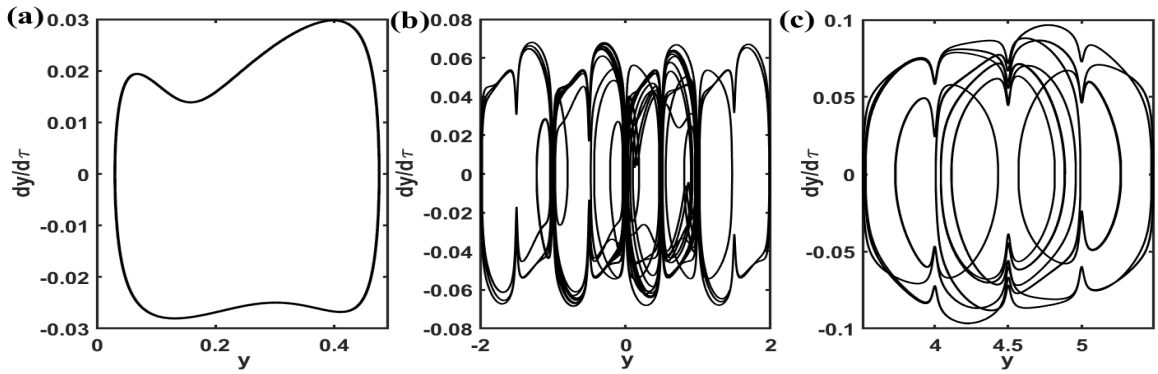

Figure 3.32: *Phase portraits of the mechanical subsystem when* $f = 1.2\,Hz$ *and* $N = 2$ *magnets; (a)* $E_m = 2.0\,V$*, (b)* $E_m = 3.1\,V$ *and (c)* $E_m = 5.0\,V$*.*

For $N = 5$ magnets, the dynamical response is almost the same (see Figure 3.33). But here, chaos occurs for higher values of the voltage amplitude.

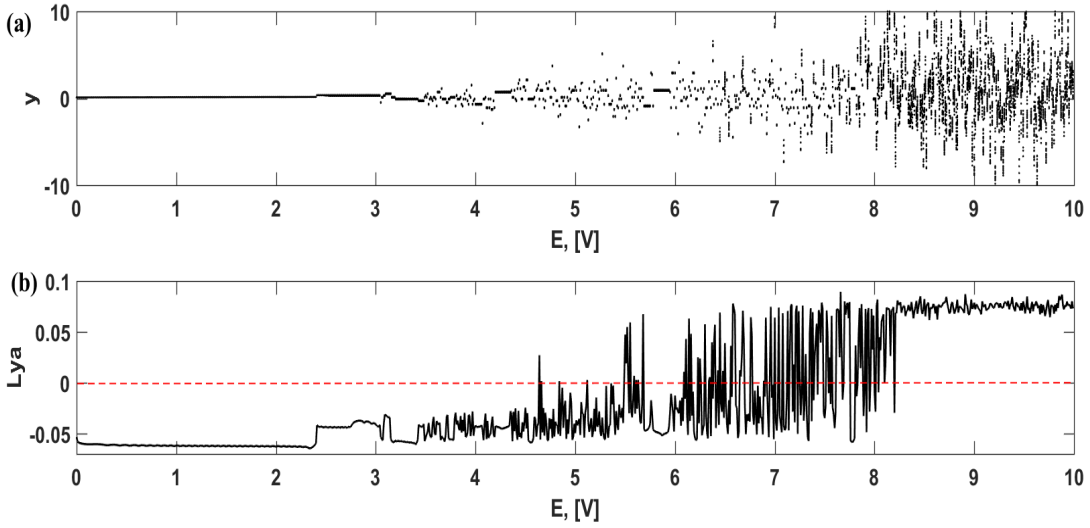

Figure 3.33: *(a) Bifurcation diagram and (b) variation of the Lyapunov exponent, both as function of the amplitude of the external generator* E_m *for* $f = 1.2\,Hz$ *and* $N = 5$ *magnets.*

b) Bifurcation diagram versus the frequency f of the AC voltage

Now considering the frequency as the control parameter, the amplitude of the external source is kept constant at $E_m = 5.0\,V$. Figure 3.34 presents the bifurcation diagram of

the arm displacement y for $N = 2$ magnets for $0.1Hz \leq f \leq 5Hz$. Periodic and chaotic oscillations are also present as the frequency varies. As in the case of the bifurcation diagram versus the voltage amplitude, the chaotic behaviour, for $N = 5$ magnets, starts a for higher value of the frequency (Fig. 3.35).

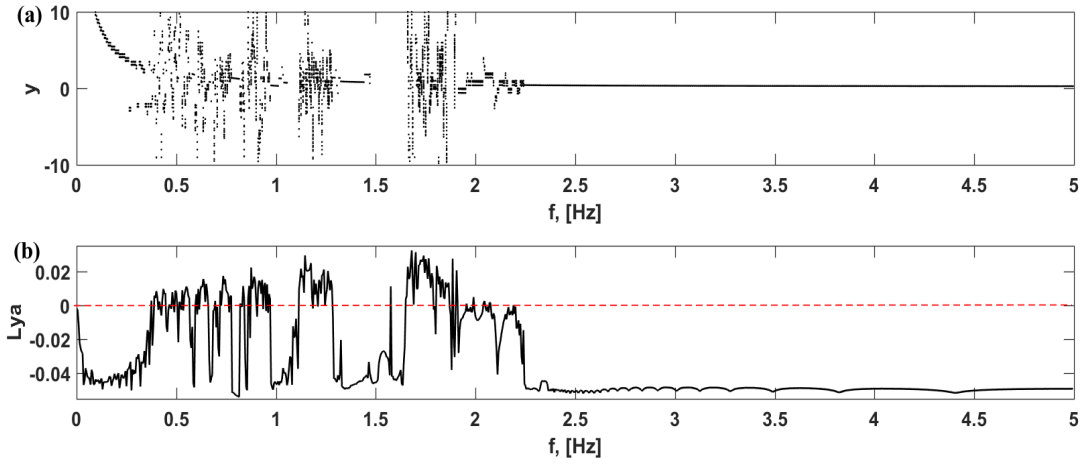

Figure 3.34: *(a) Bifurcation diagram and (b) the corresponding Lyapunov exponent as function of the excitation frequency f for $E_m = 5.0\,V$ and $N = 2$ magnets.*

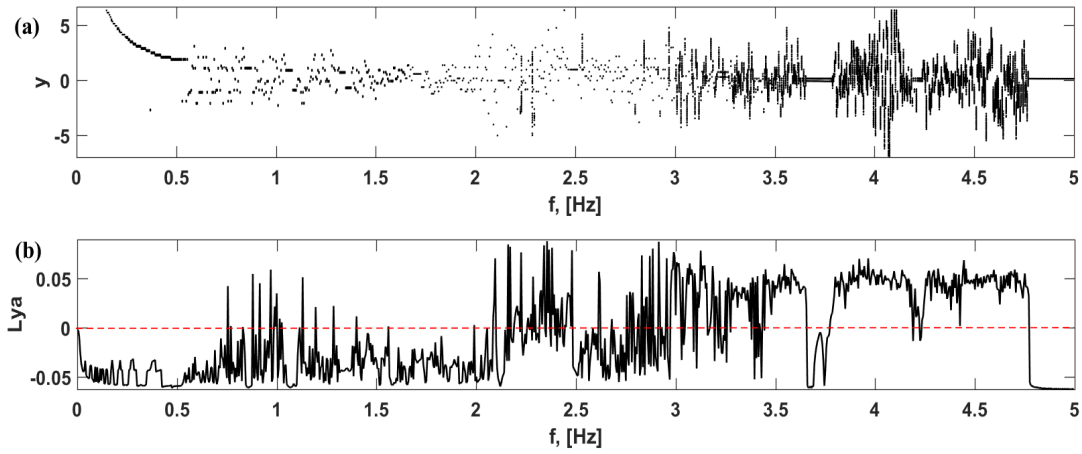

Figure 3.35: *(a) Bifurcation diagram and (b) the corresponding Lyapunov exponent as function of the excitation frequency f for $E_m = 5.0\,V$ and $N = 5$ magnets.*

3.4 Experiment

3.4.1 Experimental setup

In This subsection, we describe the series of experimental tests that were performed to validate the results obtained from numerical simulation. The value $\delta = 0.83$ is used. It corresponds to the arm length $l = 9.3\,cm$ which is used later for the experimental investigation. The other values of parameters are given in table 2.2. Figure 3.36 displays the experimental setup of the physical model described and studied theoretically in the previous sections. A voltage generator powers a low-power DC motor. The motor shaft supports a rigid iron rod which moves in the horizontal plane. The results of the experiment are presented only in the case of the system powered by the low frequency generator.

At the end of the arm, a neodymium magnet is fixed and interacts with two other magnets symmetrically positioned on a circle. The time, the angle and the angular velocity are recorded in the computer using an accelerometer MPU 6050 through an ARDUINO UNO microcontroller.

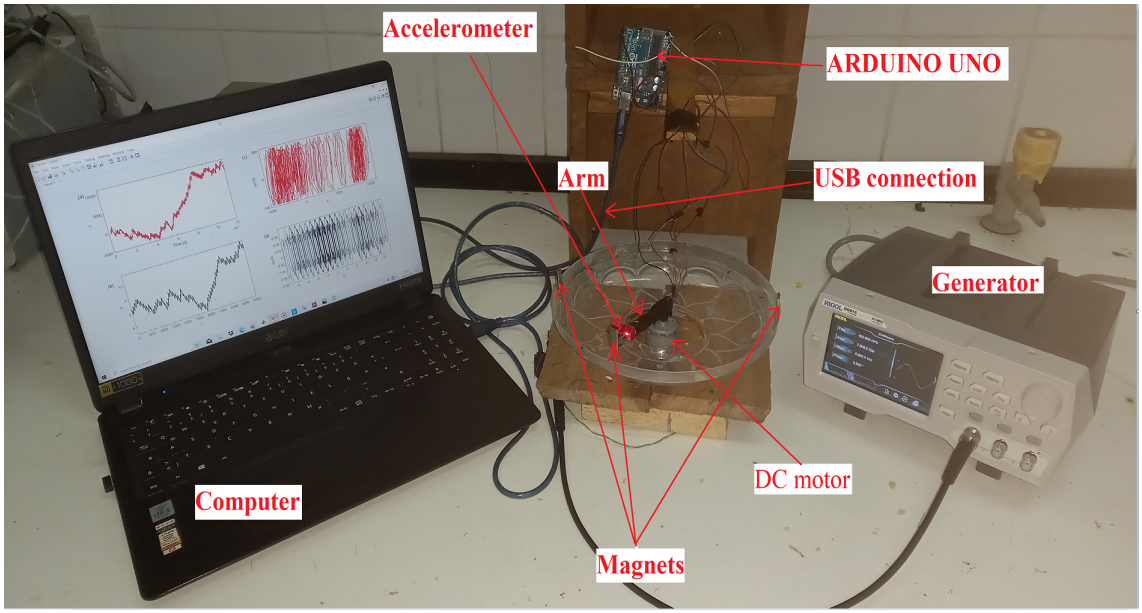

Figure 3.36: *Experimental setup.*

3.4.2 Experimental versus numerical results

Figure 3.37 compares the experimental and numerical results in terms of time-histories and phase portraits when the amplitude of the external excitation is $E_m = 1.92\,V$ and the frequency is $f = 1.2\,Hz$. As it appears, the system leads to regular dynamics. The coincidence of the numerical and experimental results is clearly visible. The same agreement is visible in Figures 3.38 and 3.39 where chaotic behaviors are presented. Let us however mention that the agreement here should be understood considering the shapes of the responses instead of considering the amplitudes of the responses since some differences are observed because of the difficulty of measuring the exact values of the physical parameters.

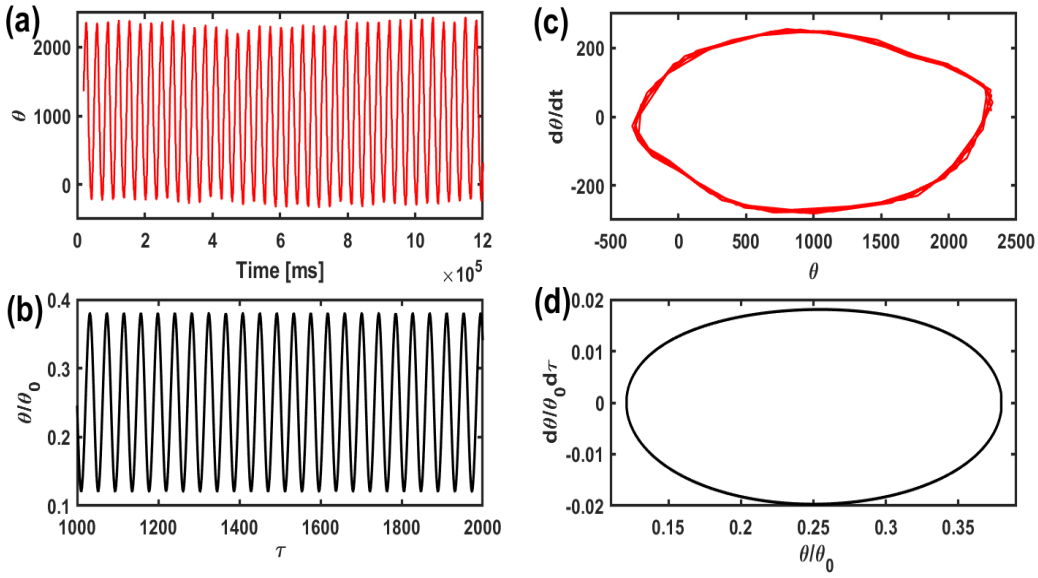

Figure 3.37: *Time-histories of the mechanical response and phase portraits (a), (c) experimentally obtained and (b), (d) numerical simulation results for* $E_m = 1.92\,V$, $f = 1.2\,Hz$ *and* $N = 2$ *magnets.*

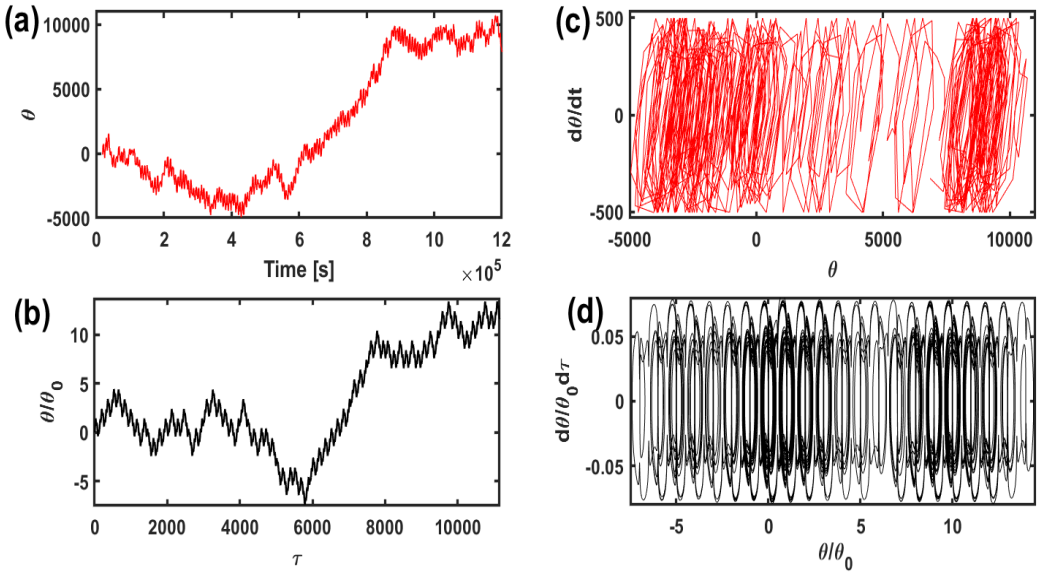

Figure 3.38: *Time-histories of the mechanical response and phase portraits (a), (c) experimentally obtained and (b), (d) numerical simulation results for* $E_m = 4.0\,V$, $f = 1.2\,Hz$ *and* $N = 2$ *magnets.*

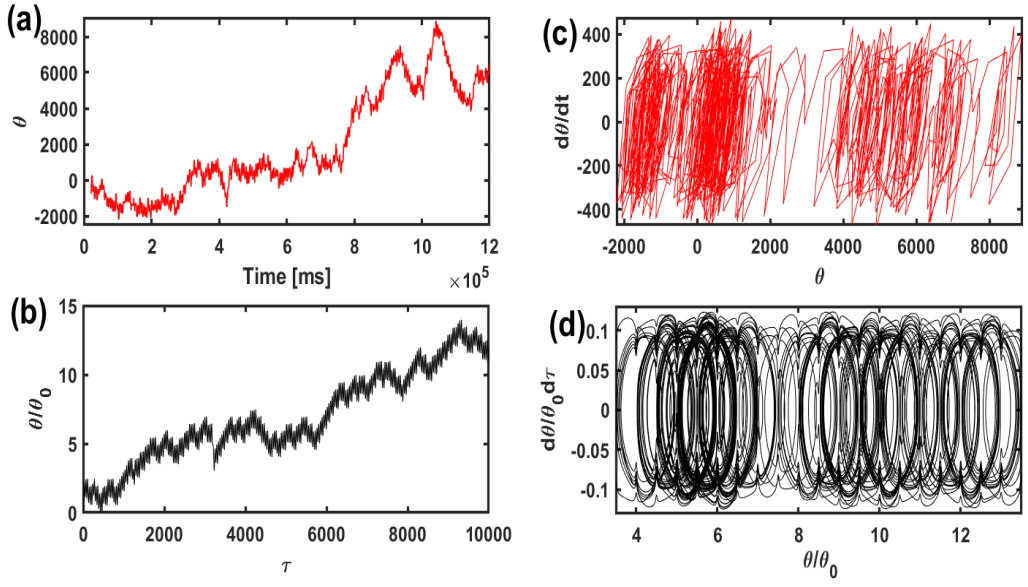

Figure 3.39: *Time-histories of the mechanical response and phase portraits (a), (c) experimentally obtained and (b), (d) numerical simulation results for* $E_m = 7.2\,V$, $f = 1.2\,Hz$ *and* $N = 2$ *magnets.*

3.5 Conclusion

In this chapter we have presented and discussed the results obtained in the thesis. The magnetic potential energy curves were presented. The electrical subsystem is powered by two forms of input signal: DC and AC voltage sources. For each case, we determine the condition for complete rotation of the mechanical arm versus the parameters of the system. Finally, the regions of chaotic and periodic motions were obtained though the bifurcation diagrams and the corresponding Lyapunov exponent. The theoretical results have been confirmed by an experiment conducted on a set-up constructed in the laboratory.

GENERAL CONCLUSION

This thesis was focused on the study of the dynamics of rotating electromechanical systems immersed in a potential generated by permanent magnets. Two models have been explored: the first, in which the arm with a magnet at the free end moves in the potential created by two permanent magnets and a second where the arm (possessing a magnet at the free end) moves in a magnetic field generated by several magnets arranged along a circle. To achieve this, we used mathematical, numerical and experimental tools. Here are the main results.

We have first investigated the dynamics of an electromechanical system consisting of a DC motor arm within a circular periodic potential created by three permanent magnets. Two configurations of the circular potential appear when one varies the positions of the magnets and the length of the DC motor-arm. Two different forms of input signal are used: DC and AC voltage sources. For each case, conditions under which the mechanical arm can perform a complete rotation are obtained. Under the DC voltage excitation, the arm oscillates and then stabilizes at an equilibrium position for a DC voltage lower than a critical value E_C. When the DC voltage is higher than the critical value , the arm performs large amplitude motions (complete rotation). Submitted to an AC voltage with amplitude lower than a critical value, the mechanical arm exhibits sinusoidal oscillations around the equilibrium position 0 with amplitude less than one turn. Angular oscillations with amplitude greater than one turn are observed when the voltage amplitude is higher than the critical value. Bifurcation diagrams show that the simple system can enter chaotic

behaviour with the angular oscillations amplitude varying erratically from small to high values.

Secondly, we have considered the dynamical behaviour of the rotating arm of an electromechanical system subjected to the action of circularly placed magnets. The magnetic torques arise from permanent magnets mounted at the free end of the arm and along a circle. The magnetic potential energy curves were presented displaying the number of wells equivalent to the number of magnets. The critical voltage for which the mechanical arm undergoes a complete rotation was also determined for the DC and AC input voltages. The results have shown that, for a DC voltage lower than the critical value, the mechanical arm undergoes damped oscillations and then stabilizes at an equilibrium position. When the voltage is above the critical value, the arm displacement increases continuously with time (performing complete rotation) while the angular velocity oscillates showing frequency proportional to the number of magnets. When the motor is powered by a sinusoidal voltage, the arm displays angular oscillations with amplitude larger than one turn for large values of the voltage amplitude. The regions of chaotic and periodic motions were obtained though the bifurcation diagrams and the corresponding Lyapunov exponent.

Finally, the second model studied above was produced and processed experimentally in the laboratory. The test has been done with two fixed neodymium magnets which are symmetrically positioned on a circle and interact with another magnet placed at the free end of the arm. A voltage generator powers a low-power DC motor. The time, the angle and the angular velocity are recorded in the computer using an accelerometer MPU 6050 through an ARDUINO UNO microcontroller. Chaotic and periodic dynamics are detected experimentally and confirmed numerically.

These dynamical behaviors can find applications in engineering, e.g. sieves in which chaos motion could enhance the dispersion of particles and avoid stagnation and formation

of aggregates. The device can also give some idea on how to optimize the operation of home appliances such as those used for mixing various food components. The second model considered in this work can also be used to mechanically study some phenomena encountered in condensed matter physics such as a particle moving in a periodic potential with variable shape and in the study of the resistively capacitance shunted Josephson junctions [99].

Despite the results obtained in this thesis, other points of interest will be investigated in the future to complement results. For instance, the electromechanical systems can be used as pendulum energy harvester and the nonlinearity introduced by magnets can be help to design devices with powerful energy recovery. In another way, we will use other types of input signals (square wave signals, pulsed signals, ect.) to study the behavior of the device. Finally, we will analyze the performance of mixers based on the rotational arm with magnetic interactions.

APPENDICES

APPENDIX A: Magnetic torques and corresponding potential for the system with two magnets

In this appendix, we give some intermediate steps for obtaining equations (2.4), (3.1) and (3.2).

Repulsive magnetic forces $\overrightarrow{F}_{A/M}$ and $\overrightarrow{F}_{B/M}$ are given by following expressions:

$$\overrightarrow{F}_{A/M} = \frac{\mu_0 q_1 q_2}{4\pi} \frac{\overrightarrow{AM}}{\left\|\overrightarrow{AM}\right\|^3},$$

$$\overrightarrow{F}_{B/M} = \frac{\mu_0 q_1 q_2}{4\pi} \frac{\overrightarrow{BM}}{\left\|\overrightarrow{BM}\right\|^3},$$

in polar coordinates one finds:

$$\overrightarrow{OA} = R\cos(\theta+\phi)\overrightarrow{e}_r - R\sin(\theta+\phi)\overrightarrow{e}_\theta,$$

$$\overrightarrow{AM} = (l - R\cos(\theta+\phi))\overrightarrow{e}_r + (R\sin(\theta+\phi))\overrightarrow{e}_\theta,$$

$$\overrightarrow{OB} = R\cos(\theta-\phi)\overrightarrow{e}_r - R\sin(\theta-\phi)\overrightarrow{e}_\theta,$$

$\overrightarrow{BM} = (l - R\cos(\theta - \phi))\overrightarrow{e}_r + (R\sin(\theta - \phi))\overrightarrow{e}_\theta.$

Thus:

$\vec{F}_{A/M} = \frac{\mu_0 q_1 q_2}{4\pi} \frac{(l - R\cos(\theta+\phi))\overrightarrow{e}_r + (R\sin(\theta+\phi))\overrightarrow{e}_\theta}{[l^2+R^2-2lR\cos(\theta+\phi)]^{\frac{3}{2}}},$

$\overrightarrow{F}_{B/M} = \frac{\mu_0 q_1 q_2}{4\pi} \frac{(l - R\cos(\theta-\phi))\overrightarrow{e}_r + (R\sin(\theta-\phi))\overrightarrow{e}_\theta}{[l^2+R^2-2lR\cos(\theta-\phi)]^{\frac{3}{2}}}.$

Mechanical torques due to magnetic forces have the following mathematical expressions:

$\overrightarrow{\Gamma}_{A/M} = \overrightarrow{OM} \wedge \overrightarrow{F}_{A/M}$ and $\overrightarrow{\Gamma}_{B/M} = \overrightarrow{OM} \wedge \overrightarrow{F}_{B/M}$

where $\wedge$ is the cross product. We obtain the following expressions:

$\overrightarrow{\Gamma}_{A/M} = \frac{\mu_0 q_1 q_2}{4\pi} \frac{lR\sin(\theta+\phi)\overrightarrow{k}}{[l^2+R^2-2lR\cos(\theta+\phi)]^{\frac{3}{2}}},$

$\overrightarrow{\Gamma}_{B/M} = \frac{\mu_0 q_1 q_2}{4\pi} \frac{lR\sin(\theta-\phi)\overrightarrow{k}}{[l^2+R^2-2lR\cos(\theta-\phi)]^{\frac{3}{2}}}.$

The total magnetic torque is:

$\overrightarrow{\Gamma}_M = -\frac{\mu_0 q_1 q_2}{4\pi R} f(\theta)\overrightarrow{k}$

with

$f(\theta) = -\frac{\delta\sin(\theta+\phi)}{[1+\delta^2-2\delta\cos(\theta+\phi)]^{\frac{3}{2}}} - \frac{\delta\sin(\theta-\phi)}{[1+\delta^2-2\delta\cos(\theta-\phi)]^{\frac{3}{2}}}.$

By the integration of this relation, the magnetic potential is:

$$U = \gamma \left[\frac{1}{[1+\delta^2-2\delta\cos(\theta+\phi)]^{\frac{1}{2}}} + \frac{1}{[1+\delta^2-2\delta\cos(\theta-\phi)]^{\frac{1}{2}}} \right].$$

with

$$\gamma = \frac{\mu_0 q_1 q_2}{4\pi R}.$$

If one sets

$$\delta_1 = \sqrt{1+\delta^2} \text{ and } A = \frac{2\delta}{\delta_1^2},$$

the magnetic potential can be write as follow:

$$U = \frac{\gamma}{\delta_1} \left[(1 - A\cos(\theta+\phi))^{-\frac{1}{2}} + (1 - A\cos(\theta-\phi))^{-\frac{1}{2}} \right]$$

Using the Taylor series expansion at order 2, we obtain the following expression:

$$U = \frac{\gamma}{\delta_1} \left[\left(1 + \frac{A}{2}\cos(\theta+\phi) + \frac{3A^2}{8}\cos^2(\theta+\phi)\right) + \left(1 + \frac{A}{2}\cos(\theta-\phi) + \frac{3A^2}{8}\cos^2(\theta-\phi)\right) \right],$$

$$U = \frac{\gamma}{\delta_1} \left[2 + \frac{A}{2}\left(\cos(\theta+\phi) + \cos(\theta-\phi)\right) + \frac{3A^2}{8}\left(\cos^2(\theta+\phi) + \cos^2(\theta-\phi)\right) \right]$$

furthermore,

$$U = \frac{\gamma}{\delta_1} \left[2 + \frac{3A^2}{8} + A\cos(\theta)\cos(\phi) + \frac{3A^2}{8}\cos(2\theta)\cos(2\phi) \right]$$

The derivative of this equation is :

$$\frac{dU}{d\theta} = \frac{\gamma}{\delta_1}\left[-A\cos(\phi)\sin(\theta) - \frac{3A^2}{4}\cos(2\phi)\sin(2\theta)\right]$$

By looking at zeros of the derivative of the potential, one finds the following equations of equilibrium points:

$$\begin{cases} \sin(\theta) = 0 \\ \sin(2\theta) = 0 \end{cases}$$

thus

$$\begin{cases} \theta = 0 \\ \theta = \pi \end{cases}$$

APPENDIX B: Magnetic torques and corresponding potential for the system with several magnets

In this appendix, one presents the derivation of equations (2.12), (3.24).

The magnetic force exerted by the k-th magnet on the arm is given by the following relation:

$$\overrightarrow{F}_{M_k/M} = \frac{\mu_0 q_1 q_2}{4\pi} \frac{\overrightarrow{M_k M}}{\left\|\overrightarrow{M_k M}\right\|^3},$$

The total magnetic force is:

$$\vec{F} = \sum_{k=0}^{N-1} \vec{F}_{M_k/M}$$

But we have:

$$\overrightarrow{OM_k} = R\cos(\theta - 2k\phi)\overrightarrow{e}_r - R\sin(\theta - 2k\phi)\overrightarrow{e}_\theta,$$

$$\overrightarrow{M_k M} = (l - R\cos(\theta - 2k\phi))\,\vec{e}_r + R\sin(\theta - 2k\phi)\vec{e}_\theta.$$

We then obtain :

$$\overrightarrow{F}_{M_k/M} = \frac{\mu_0 q_1 q_2}{4\pi} \frac{(l - R\cos(\theta - 2k\phi))\vec{e}_r + R\sin(\theta - 2k\phi)\vec{e}_\theta}{[l^2 + R^2 - 2lR\cos(\theta - 2k\phi))]^{\frac{3}{2}}},$$

The total magnetic torque generated by all the several magnets is:

$$\overrightarrow{\Gamma}_M = \sum_{K=0}^{N-1} \overrightarrow{\Gamma}_{M_k/M}$$

with :

$$\overrightarrow{\Gamma}_{M_k/M} = \frac{\mu_0 q_1 q_2}{4\pi R} \frac{\delta \sin(\theta - 2k\phi)}{[1+\delta^2 - 2\delta\cos(\theta-2k\phi)]^{\frac{3}{2}}} \overrightarrow{k}$$

By the integration of relation, the magnetic potential is:

$$U = \gamma \sum_{k=0}^{N-1} \frac{1}{[1+\delta^2 - 2\delta\cos(\theta-2k\phi)]^{\frac{1}{2}}}$$

Bibliography

Bibliography

[1] H. Meriem, K. Bouchra, (2015). Simulation D'un Electro-aimant. *Master thesis, Laboratoire des Matériaux électrotechniques, Université Kasdi Merbah Ouargla, Algérie.*

[2] K. Polczynski, A. Wijata, J. Awrejcewicz, G. Wasilewski, (2019). Numerical and experimental study of dynamics of two pendulums under a magnetic field. *J. Systems and Control Engineering* 233:441-453.

[3] R. Kepinski, J. Awrejcewicz, D. Lewandowski, J. Gajek, (2015). Experimental investigations of stability in a hybrid stepper motor. *Adv. Intell. Syst. Comput.* 317: 81-90.

[4] J. Gajek, J. Awrejcewicz, (2018). Mathematical models and nonlinear dynamics of a linear electromagnetic motor. *Nonlinear Dyn.* 94:377-396.

[5] D.D. Kozanecka, (2012). Theoretical and experimental investigations of dynamics of the flexible rotor with an additional active magnetic bearing. *in: R. Sehgal (Ed.), Perform. Eval. Bear., InTech, Rijeka,* pp. 163-192.

[6] H. Bleuler, M. Cole, P. Keogh, (2009). Magnetic bearings: theory, design, and application to rotating machinery. *Berlin: Springer.*

[7] F. Sun, K. Oka, (2011). Feasibility analysis of two iron balls-simultaneous suspension using flux path control mechanism. *J Syst. Des. Dyn.* 5:1155-1166.

[8] B. Yan, H. Ma, C. Zhao, C. Wu, K. Wang, P. Wang, (2018). A vari-stiffness nonlinear isolator with magnetic effects: Theoretical modeling and experimental verification. *International Journal of Mechanical Sciences* 148:745-55.

[9] Q. Li, Y. Zhu, D. Xu, J. Hu, W. Min, L. Pang, (2013). A negative stiffness vibration isolator using magnetic spring combined with rubber membrane. *Journal of Mechanical Science and Technology* 27:813-24.

[10] D. Ning, H. Du, S. Sun, M. Zheng, W. Li, N. Zhang, Z. Jia, (2020). An electromagnetic variable stiffness device for semiactive seat suspension vibration control. *IEEE Transactions on Industrial Electronics* 67:6773-84.

[11] S. Yuan, Y. Sun, J. Zhao, K. Meng, M. Wang, H. Pu, Y. Peng, J. Luo, S. Xie, (2020). A tunable quasi-zero stiffness isolator based on a linear electromagnetic spring. *Journal of Sound and Vibration* 482:115449-12.

[12] M. Bednarek, D. Lewandowski, K. Polczynski, J. Awrejcewicz, (2021). On the active damping of vibrations using electromagnetic spring. *Mechanics Based Design of Structures and Machines* 49:1131-1144.

[13] M. Przybylska, W. Szuminski, (2013). Non-integrability of flail triple pendulum. *Chaos Solitons Fractals* 53:60-74.

[14] Y. Chen, X. Wu, Z. Liu, (2009). Global chaos synchronization of electro-mechanical gyrostat systems via variable substitution control. *Chaos Solitons Fractals* 42:1197-205.

[15] D. Sequeira, J. Little, B.P. Mann, (2019). Investigating threshold escape behaviour for the gimballed horizontal pendulum system. *J. Sound Vib.* 450:47-60.

[16] M.F.P. Polo, M.P. Molina, J.G. Chica, (2009). Chaotic dynamic and control for micro-electro-mechanical systems of massive storage with harmonic base excitation. *Chaos Solitons Fractals* 39:1356-70.

[17] G. Meng, W. Zhang, H. Huang, H.G. Li, Chen D, (2009). Micro-rotor dynamics for micro-electro-mechanical systems (MEMS). *Chaos Solitons Fractals* 40:538-62.

[18] M.E. Semenov, A. M. Solovyov, P.A. Meleshenko, (2021). Stabilization of the coupled inverted pendula: from discrete to continuous case. *J. Vib. Control* 27:1-2.

[19] D. Belato, H.I. Weber, J.M. Balthazar, D.T. Mook, (2001). Chaotic vibrations of a nonideal electro-mechanical system. *Int. J. Solid Struct.* 38:1699-1706.

[20] F.H.I. Pereira-Pinto, A.M. Ferreira, M.A. Savi, (2004). Chaos control in a nonlinear pendulum using a semi-continuous method. *Chaos Solitons Fractals* 22:653-668.

[21] J. Awrejcewicz, B. Supel, C.H. Lamarque, G. Kudra, G. Wasilewski, P. Olejnik, (2008). Numerical and experimental study of regular and chaotic motion of triple physical pendulum. *Int. J. Bifurc. Chaos* 18:2883-2915.

[22] A.S. de Paula, M.A. Savi, (2009). Controlling chaos in a nonlinear pendulum using an extended time-delayed feedback control method. *Chaos Solitons Fractals* 42:2981-2988.

[23] R.H. Avanço, H.A. Navarro, R.M.L.R.F. Brasil, J.M. Balthazar, (2014). Nonlinear dynamics of a pendulum excited by a crank-shaft-slider mechanism. *Vol. 4B Dyn. Vib. Control ASME,* Dynamics, Vibration and Control, Montreal, Quebec, Canada.

[24] M. Kazmierczak, G. Kudra, J. Awrejcewicz, G.Wasilewski, (2015). Numerical and experimental investigation of bifurcational dynamics of an electromechanical system consisting of a physical pendulum and DC motor. *Dyn. Syst. - Math. Numer.Approaches, TU of Lodz* pp.579-590.

[25] M. Kazmierczak, G. Kudra, J. Awrejcewicz, G. Wasilewski, (2015). Mathematical modelling, numerical simulations and experimental verification of bifurcation dynamics of a pendulum driven by a dc motor. *Eur. J. Phys.* 36:55028.

[26] R. Tsapla Fotsa, P. Woafo, (2016). Chaos in a new bistable rotating electromechanical system. *Chaos Solitons Fractals* 93:48-57.

[27] B. Nana, S.B. Yamgoué, R. Tchitnga, P. Woafo, (2017). Dynamics of a pendulum driven by a DC motor and magnetically controlled. *Chaos Solit. Fractals* 104:18-27.

[28] B. Nana, S.B. Yamgoué, R. Tchitnga, P. Woafo, (2018). Nonlinear dynamics of a sinusoidally driven lever in repulsive magnetic fields. *Nonlinear Dyn.* 91:55-66.

[29] A. Fradkov, B. Andrievsky, K . Boykov, (2005). Control of the coupled double pendulums system. *Mechatronics* 15:1289-1303.

[30] M.O. Donnagain, O. Rasskazov, (2006). Numerical modelling of an iron pendulum in a magnetic field. *Physica B* 372:37-39.

[31] N. Han, Q. Cao, (2016). Global bifurcations of a rotating pendulum with irrational nonlinearity. *Commun. Nonlinear Sci. Numer. Simulat.* 36:431-445.

[32] J. Bethenod, (1938). Sur l'entretien du mouvement d'un pendule au moyen d'un courant alternatif de fréquence élevée par rapport à sa fréquence propre. *Comptes Rendus Hebd, Des Séances l'Académie Des Sci.* 207:847-849.

[33] H.P. Knauss, P.R. Zilsel, (1951). Magnetically maintained pendulum. *Am. J. Phys.* 19:318-320.

[34] Y. Kraftmakher, (2009). Demonstrations with a magnetically controlled pendulum. *Am. J. Phys.* 78:532-535.

[35] Y. Kraftmakher, (2007). Experiments with a magnetically controlled pendulum. *Eur. J. Phys.* 28:1007-1020.

[36] M. Wojna, A. Wijata, G. Wasilewski, J. Awrejcewicz, (2018). Numerical and experimental study of a double physical pendulum with magnetic interaction. *J. Sound Vib.* 430:214-230.

[37] K. Polczyński, A. Wijata, J. Awrejcewicz, G. Wasilewski, (2019). Numerical and experimental study of dynamics of two pendulums under a magnetic field. *Proc. Inst. Mech. Eng. Part I J. Syst. Control Eng.* 233:441-453.

[38] K. Polczyński, A. Wijata, G. Wasilewski, G. Kudra, J. Awrejcewicz, (2020). Modelling and analysis of bifurcation dynamics of two coupled pendulums with a magnetic forcing. *in: I. Kovacic, S. Lenci (Eds.), IUTAM Symp. Exploit. Nonlinear Dyn. Eng. Syst., Springer International Publishing, Cham,* pp. 213-223.

[39] F.C. Moon, J. Cusumano, P.J. Holmes (1987). Evidence for homoclinic orbitd as a precursor to chaos in magnetic pendulum. *Physica 24D* 383-390.

[40] G. Wasilewski, G. Kudra, J. Awrejcewicz, M. Kaźmierczak, M. Tyborowski, (2015). Experimental and numerical investigations of a pendulum driven by a low-powered DC motor, in: J. Awrejcewicz, M. Kaźmierczak, P. Olejnik, J. Mrozowski *(eds.) Dynamical Systems-Mathematical and Numerical Approaches, TU of Lodz, Lodz.* pp. 579-590.

[41] P.C. Tesso W., R. Kouam Tagne, P. Woafo, (2022). Energy harvesting from a micro-system with circular bistable potential due to magnets. *Int. J. Bifurc. Chaos* 32:2250039.

[42] G.T. Oumbé Tékam, C.A. Kitio Kwuimy, P. Woafo, (2011). Analysis of tristable energy harvesting system having fractional order viscoelastic material. *Chaos* 25:013112.

[43] R. Kumar, S. Gupta, S.F. Ali, (2019). Energy harvesting from chaos in base excited double pendulum. *Mech. Syst. Signal Process* 124:49-64.

[44] P.V. Malaji, M.I. Friswell, S. Adhikari, G. Litak, (2020). Enhancement of harvesting capability of coupled nonlinear energy harvesters through high energy orbits. *AIP Adv.* 10:085315.

[45] P.V. Malaji, S.F. Ali, (2018). Analysis and experiment of magneto-mechanically coupled harvesters.*Mech. Syst. Signal Process* 108:304-316.

[46] "http://galileoandeinstein.physics.virginia.edu/more_stuff/E&M_Hist.html."

[47] "https://courses.lumenlearning.com/boundless-physics/chapter/magnetism-and-magnetic-fields."

[48] "https://www.aps.org/publications/apsnews/200807/physicshistory.cfm."

[49] "https://infos.clients.teching.com, "électroaimants pour systémes électromécaniques", techniques de l'ingénieur, paris (2015).

[50] S. F. S. Ferreir, (2016). Electromagnetic study of a variable inductor controlled by a DC current. *Universidada de Coimbra,* pp. 14-20.

[51] J. Maxwell (1891). A Treatise on Electricity and Magnetism. *Oxford University Press reprint 3rd edn (1998).*

[52] T. Weiland (1996). Time domain electromagnetic field computation with finite difference methods. *Internat. J. Numer. Modelling* 9:295-319.

[53] O. Farsund, B.U. Felderhof, (1996). Force, torque and absorbed energy for a body of arbitrary shape and constitution in an electromagnetic radiation field. *physica A, Statistical Mechanics and its applications* 227:1-2

[54] A. Kovetz, (2000). Electromagnetic theory. *Oxford University Press.*

[55] A. Sihvola, S. Tretyakov, (2008). Comments on boundary problems and electromagnetic constitutive parameters. *Optik* 119:247-249.

[56] B. Yaaqoub, B. Houmame, (2018). Modèles analytiques pour modéliser les dispositifs de positionnement en lévitation. *Master thesis, Faculté de Sciences et de Technologie, Université Mohamed Seddik Ben Yahia, Jijel, Algérie.*

[57] "https://www.pinterest.de/pin/63261569737776585/nic=1."

[58] H. Allag, (2010). Modèles et Calcul des Systèmes de Suspension Magnétique Passive : Développements et Calculs Analytiques en 2D et 3D des Interactions entre Aimants Permanents. *Thèse de Doctorat, Université de Constantine.*

[59] H. Allag, J. P. Yonnet, (2008). 3D analytical Calculation of Interactions Between Perpendiculary Magnetized Magnets. *European Magnetic Sensors and Actuators Conference.*

[60] N. Bencheikh, (2006). Conception et réalisation d'un convoyeur électromagnétique planaire miniature. *Thèse de Doctorat de l'Université de Technologie de Compiègne.*

[61] K. Halbach, (1985). Applications of permanent magnets in accelerators and electron storage rings.*Journal of Applied Physics* 57:3605.

[62] H. Kube, V. Zoeppig, R Hermann, A Hoffmann, E Kallenbach, (2000). Electromagnetic mini-actuators using thin magnetic layers. *Smart material structure* 9:p.336-342.

[63] M.G. Lee, S.Q. Lee, D.G. Gweon, (2004). Analysis of Halbach magnet array and its application to linear motor. *Mechatronics* 14:115-128.

[64] J.M.M. Rovers, J.W. Jansen, E.A. Lomonova, (2010). Analytical calculation of the force between a rectangular coiland a cuboidal permanent magnet. *IEEE Trans. Magn.* 46:1656-1659.

[65] J. Topfer, B. Pawlowski, H Beer, K Plotner, P, Hofmann, J Herrfurth, (2004). Multipole magnetization of NdFeB magnets for magnetic micro-actuators and its chracherisation with a magnetic field mapping device. *Journal of magnetic and magnetic materials* 270:124-129.

[66] "https: //images.app.goo.gl/jvXi5riFpguThJfd7"

[67] "https: //images.app.goo.gl/tUgCW9KRkuubbiv5"

[68] "https: //dewwol.com/20-uses-of-magnets/"

[69] "https: // sciencing.com/use-magnets-daily-life-8056272.html"

[70] "https://www.twinkl.com/homework-help/science-homework-help/magnets-facts-for-kids/ what-are-some-everyday-uses-of-magnets"

[71] A. Nalin, Chaturvedi, Taeyoung Lee, M. Leok, N.H. McClamroch (2011). Nonlinear Dynamics of the 3D Pendulum. *J Nonlinear Sci.* 21:3-32.

[72] Khalid El Rifai, G. Haller, A.N. Bajaj (2007). Global dynamics of an autoparametric spring-mass-pendulum system. *Nonlinear Dyn.* 49:105-116.

[73] X.Chen, Z. Jing, X. Fu (2015). Chaos control in a pendulum system with excitations, Discret Contin. *Dyn. Syst.-B* 20:373-383.

[74] D. Komali, D. Smritilekha, B. Prabha, V.V.S. Sasank, (2020). Enhancement for the position of inverted pendulum using linear quadratic regulator based fuzzy system. *Eur. J. Mol. Clin. Med.* 7(4):757-765.

[75] M.C. Nuci, (2017). The nonlinear pendulum always oscillates. *J.Nonlinear Math.Phys.* 24:1146-156.

[76] C.A. Kitio Kwuimy, C. Nataraj, M. Belhaq, (2012). Chaos in a Magnetic Pendulum Subjected to Tilted Excitation and Parametric Damping. *Mathematical Problems in Engineering* 5:546364.

[77] H.F. Olson, (1957). *Acoustical Engineering. Van Nostrand, Princeton.*

[78] M. Soutif, (1970). *Vibrations, Propagations et Diffusions. Dunod, Paris.*

[79] J. Granier, (1936). *Les Systemes Oscillants. Dunod, Paris.*

[80] J. Thurin, (1971). *Les systemes Asservis. Eyrolles, Paris.*

[81] A. Preumont, (2006). *Mechatronics: Dynamics of Electromechanical and Piezoelectric Systems. Springer, Netherlands.*

[82] V.Y. Taffoti Yolong (2009). Dynamics of Network of Nonlinear Electromechanical Systems with Rigid and Flexible Arms. *Ph.D. Thesis, Faculty of Science, University of Yaounde 1, Cameroon.*

[83] J.L. Sudworth, (2011). Sodium/nickel chloride (Zebra) battery. *Journal of Power Sources* 100:149-163.

[84] "https: //images.app.goo.gl/a1BLcYjfgDgbYRWi9"

[85] J.B. Mogo, (20110). Modelling and dynamics of pendulum arms of electromechanical robots. *Ph.D. Thesis, Faculty of Science, University of Yaounde 1, Cameroon.*

[86] A.M. Tusset, V. Piccirillo, A.M. Bueno, J.M. Balthazar, D. Sado, J.L.P. Felix, R.M.L.R Brsil, (2015). Chaos control and sensitivity analysis of a double arm exciyed by RLC circuit base nonlinear shaker. *Journal of Vibration and Control* 257:754-760.

[87] C.A. Kitio Kwuimy, P. Woafo, (2008). Dynamics, chaos and synchronization of self-sustained electromechanical systems with clamped-free flexible arm. *Nonl. Dynamics* 53:201-203.

[88] I. Kemajou, B. Nana, P. Woafo, (2022). Dynamics of the electromechanical sieve with hysteretic iron-core inductor. *Nonlinear Dyn* 1-19.

[89] C.A. Kitio Kwuimy, P. Woafo, (2010). Experimental bifurcations and chaos in a modified self-sustained macro electromechanical system. *Journal of Sound and Vibration* 329:3137-3148.

[90] Z. Xizhe, I. Sajid, Z. Yanhe, L. Xinyu, Z. Jie, (2017). Applications of chaotic dynamics in robotics. *Int. J. Adv. Robot. Syst.* 13:1-7.

[91] R.K. Ana, M.B. José, L.P. Jorge, R.C. Fàbio, (2010). The nonlinear dynamics of a vibrating systemmodeled by an inverted pendulum, with an electrodynamics shaker. *In Conference on Dynamics, Control and Their Applications, Brazil.*

[92] K. Polczyński, S. Skurativskyi, M. Bednarek, J. Awrejcewicz, (2021). Nonlinear oscillations of coupled pendulums subjected to an external magnetic stimulus. *Mech. Syst. Signal Process.* 154:107560.

[93] A. Wijata, K. Polczyński, J. Awrejcewicz, (2021). Theoretical and numerical analysis of regular one-side oscillations in a single pendulum system driven by a magnetic field. *Mech. Syst. Signal Process.* 150:107229.

[94] S. Skurativskyi, K. Polczyński, M. Wojna, J. Awrejcewicz, (2022). Quantifying periodic, multi-periodic, hidden and unstable regimes of a magnetic pendulum via semi-analytical, numerical and experimental methods. *J. Sound Vib.* 524:116710.

[95] R. Tsapla Fotsa, (2018). Rotating electromechanical systems with bistable potential, hysteretic iron-core inductor and delay. *Ph.D. Thesis, Faculty of Science, University of Yaounde 1, Cameroon.*

[96] C. Hayashi, (1964). *Nonlinear Oscillations in Physical Systems. New York : McGraw-Hill 392.*

[97] A.H. Nayfeh, D.T. Mook, (1979). *Nonlinear oscillations. Wiley.*

[98] D.E. McCumber, (1968). Effect of ac impedance on dc voltage-current characteristics of superconductor weak-link junctions. *J. Applied Physics* 39:3113-3118.

[99] G. Chen, D. Lai, (1998). Feedback anticontrol of discrete chaos. *Int. J. Bifurcat. Chaos* 8:1585-1590.

List of publications

1. Publications of the thesis

1- **R. Kouam Tagne**, P. Woafo, J. Awrejcewicz, (2023). Dynamics of the rotating arm of an electromechanical system subjected to the action of circularly placed magnets: numerical study and experiment. *Int. J. Bifurc. Chaos* 33:2350052.

2- **R.F. Kouam Tagne**, R. Tsapla Fotsa, P. Woafo, (2021). Dynamics of a DC motor-driving arm with a circular periodic potential and DC/AC voltage input. *Int. J. Bifurc. Chaos* 31:2150178.

2. Other publication

1- P.C. Tesso W., **R. Kouam Tagne**, P. Woafo, (2022). Energy harvesting from a microsystem with circular bistable potential due to magnets. *Int. J. Bifurc. Chaos* 32:2250039.